Title

Technical Assistance from Lawrence Berkeley National Laboratory and National Energy Technology Laboratory to Elko Heat Company and the City of Wells, Nevada

Authors

Spycher, N

McKoy, ML

Ayling, B

et al.

Publication Date

2018-03-30

DOI

10.18141/1430193

Peer reviewed

NETL
NATIONAL ENERGY TECHNOLOGY LABORATORY

GREAT BASIN CENTER FOR Geothermal Energy

Nevada Bureau of Mines and Geology

BERKELEY LAB

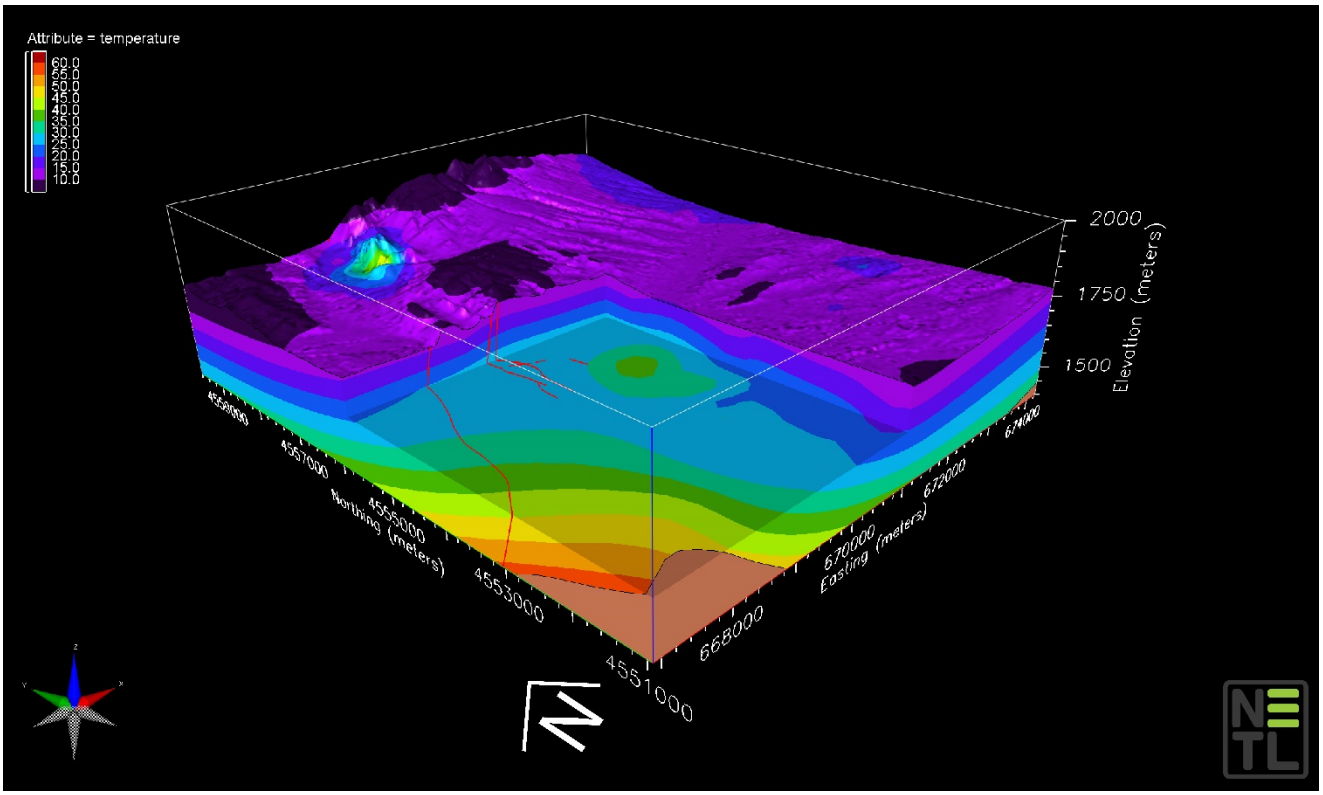

Small Business Vouchers Pilot:

Technical Assistance from Lawrence Berkeley National Laboratory and National Energy Technology Laboratory to Elko Heat Company and the City of Wells, Nevada

30 March 2018

Office of Energy Efficiency & Renewable Energy

U.S. DEPARTMENT OF ENERGY | NATIONAL ENERGY TECHNOLOGY LABORATORY

BERKELEY LAB

NETL-TRS-7-2018

LBNL-2001126

Disclaimer

Cover Illustration: *Temperature model with cutaway, carved to 1580 meter elevation to show temperature variation at depth in vicinity of City of Wells, Nevada.*

Suggested Citation: Spycher, N.; McKoy, M. L.; Ayling, B.; Bill, M.; Bosshardt, K.; Cameron, E.; Creason, C. G.; DiGiulio, J.; Dobson, P.; Justman, D.; Hammack, R.; McKoy, M.; Miller, R.; Mark-Moser, M.; Rackley, I.; Rose, K.; Siler, D.; Supp, J.; Veloski, G.; Zehner, R.; Zuza, A. *Small Business Vouchers Pilot: Technical Assistance from Lawrence Berkeley National Laboratory and National Energy Technology Laboratory to Elko Heat Company and the City of Wells, Nevada*; NETL-TRS-7-2018; NETL Technical Report Series; U.S. Department of Energy, National Energy Technology Laboratory: Morgantown, WV, 2018; p 196. DOI: 10.18141/1430193.

An electronic version of this report can be found at:

http://netl.doe.gov/research/on-site-research/publications/featured-technical-reports

https://edx.netl.doe.gov/dataset/small-business-vouchers-pilot-technical-assistance-from-lbnl-netl-to-elko-and-wells-nevada

https://edx.netl.doe.gov/dataset/small-business-vouchers-pilot-technical-assistance-from-lbnl-netl-to-elko-and-wells-nevada/resource_download/2c6aac65-690d-4619-8818-428e3a19051b

Technical Assistance from Lawrence Berkeley National Laboratory and National Energy Technology Laboratory to Elko Heat Company and the City of Wells, Nevada

Project PI's:

Nicolas Spycher[1], Mark McKoy[2]

Team Members (alphabetical order):

Bridget Ayling[3,8], Markus Bill[1], Kelby Bosshardt[4], Emily Cameron[2], C. Gabriel Creason[2], Jennifer DiGiulio[2], Patrick Dobson[1], Devin Justman[2], Richard Hammack[2], Mark McKoy[2], Roy Miller[2], MacKenzie Mark-Moser[2], Ira Rackley[5], Kelly Rose[2], Drew Siler[1], Nicolas Spycher[1], Jolene Supp[6], Garret Veloski[2], Richard Zehner[7], Andrew Zuza[8]

DOE Project Manager:

Josh Mengers[9]

[1] Lawrence Berkeley National Laboratory
[2] Research & Innovation Center, National Energy Technology Laboratory
[3] Great Basin Center for Geothermal Energy, University of Nevada Reno
[4] Better City, Ogden, Utah
[5] Elko Heat Company, Inc.
[6] City of Wells, Nevada
[7] Lumos & Associates, Inc.
[8] Nevada Bureau of Mines and Geology, University of Nevada Reno
[9] Geothermal Technologies Office, U.S. Dept. of Energy

NETL-TRS-7-2018

30 March 2018

NETL & LBNL Contacts:

Nicolas F. Spycher & Mark L. McKoy, Principal Investigators

Patrick Dobson & Kelly Rose, Technical Portfolio Leads

Bryan Morreale, Executive Director, Research & Innovation Center, NETL

Jens Birkholzer, Division Director, Energy Geoscience Division, LBNL

This page intentionally left blank.

Table of Contents

Table of Contents (cont.)

List of Figures

List of Figures (cont.)

List of Tables

This page intentionally left blank.

Acronyms, Abbreviations, and Symbols

Term	Description
Al	Aluminum
ArcGIS	Archival Geographic Information System
B	Boron
C	Carbon
°C	Celsius
Ca	Calcium
Cl	Chlorine
cm	centimeters
CO_2	Carbon dioxide
Cs	Cesium
CSIL	Cumulative Spatial Impact Layers
δ	Delta - Isotope concentration reported in “per mil” relative to a standard
DC	Direct Current
DEM	Digital Elevation Model
DIC	Dissolved inorganic carbon
DOE	U.S. Department of Energy
E	East
EDX	Energy Data eXchange
EHC	Elko Heat Company
EMI	Electromagnetic Induction
ESRI	Environmental Systems Research Institute, Inc.
°F	Fahrenheit
FEMA	Federal Emergency Management Agency
ft	feet
Ge	Germanium
GeoT	Geo-thermometer software
GIS	Geographic Information System
gpm	gallons per minute
GPS	Global Positioning System
H	Hydrogen
HCO_3	Bicarbonate
Hz	Hertz
ICP-MS	Inductively Coupled Plasma – Mass Spectrometry
IHS	Information Handling Services (HIS Markit), Inc.
InSAR	Interferometric Synthetic Aperture Radar
IP	Induced polarization
K	Potassium
km	kilometers
L	liter
LBNL	Lawrence Berkeley National Laboratory
Li	Lithium
LiDAR	“Light raDAR” airborne laser scanner surveys
m	meters
MASL	Meters above sea level
mg	milligram
Mg	Magnesium

Acronyms, Abbreviations, Symbols (cont.)

Term	Description
mi	miles
mL	milliliter
MPa	MegaPascals
Mw	Seismic moment earthquake magnitude from low-frequency seismic data
N	North
Na	Sodium
NAD	North American Datum (83)
NBMG	Nevada Bureau of Mines and Geology
NDWR	Nevada Division of Water Resources
NETL	National Energy Technology Laboratory
O	Oxygen
PCA	Principal Component Analysis
psi	pounds per square inch
Rb	Rubidium
S	South
SBV	Small Business Vouchers Program
$S_{h\,max}$	Maximum horizontal stress component
$S_{h\,min}$	Minimum horizontal stress component
Si	Silicon
SOZ	Southern Outflow Zone
S_v	Vertical stress component
UNR	University of Nevada, Reno
USGS	United States Geological Survey
UTM	Universal Transverse Mercator coordinate system
W	West
WAAS	Wide Area Augmentation System
ZGC	Zehner Geologic Consulting, LLC

Acknowledgments

This work was completed as part of Lawrence Berkeley National Laboratory (LBNL) and National Energy Technology Laboratory (NETL) research for the U.S. Department of Energy's (DOE) Small Business Vouchers Pilot Program, Round 2, under DOE's Office of Energy Efficiency and Renewable Energy. The authors wish to acknowledge Josh Mengers (DOE Geothermal Technologies Office, Small Business Vouchers Pilot Program) and Arlene Anderson (DOE Geothermal Technologies Office, Deep Direct Use Program Manager) for programmatic guidance, direction, and financial support; Jimmy Thornton for waiver of NETL's Research & Innovation Center overhead fees; Jolene Supp (City Manager, City of Wells, NV) for supporting this project through many means, including drilling four shallow exploratory wells, additional Geoprobe tests for shallow temperatures, and funding background studies of geothermal prospects; Better City of Ogdon, Utah for participation; Nevada Bureau of Mines and Geology (NBMG) for geologic mapping, data on wells, publications, and permissions to reproduce certain illustrations; the Federal Emergency Management Agency (FEMA) for LiDAR data; and all the land owners near the City of Wells who provided permissions and helpful information that made this study possible.

The authors also wish to acknowledge Professor Paul Jewell for sharing unpublished water chemistry data; Dr. Wenming Dong for chemical analyses of water samples; and Dr. Harpreet Singh and David Rampton for assistance with interpretation of electric logs from exploration well GEO#4.

This page intentionally left blank.

EXECUTIVE SUMMARY

Warm waters in several domestic and municipal water wells in and around the City of Wells, Nevada, along with several hot springs a few kilometers away, suggest economical geothermal resources that could meet residential and commercial space heating demands, perhaps even geothermal electricity generation. To date, only a few low-temperature, single-user space heating applications have been developed. Under the U.S. Department of Energy's Small Business Vouchers Pilot (SBV) Program, research teams from Lawrence Berkeley National Laboratory (LBNL) and the National Energy Technology Laboratory (NETL), in collaboration with the University of Nevada, Reno (UNR), Better Cities, and Lumos & Associates, advised the Elko Heat Company and the City of Wells in their recent drilling of a shallow geothermal gradient well, based on new field work along with a compilation and review of existing geologic, geochemical, geothermal, and geophysical data for this area. New field data include ground temperature measurements with shallow 2-meter probes and with Geoprobe holes penetrating to depths of 5 to 9 meters, new geochemical analysis of springs and wells, revision of geologic maps through geologic and structural mapping, and shallow direct current resistivity and electromagnetic induction surveys. All 51 datasets collected and created throughout the project were cataloged and categorized according to their metadata and attributes, and compiled into a data catalog and ESRI ArcGIS geodatabase and map package, all of which are available as shared, public resources through NETL's Energy Data eXchange (EDX)[1]. Once assembled, 11 surface- and subsurface- spatial-datasets were incorporated into NETL's Cumulative Spatial Impact Layers (CSIL) tool, and imported into EarthVision, a 3-dimensional visualization software, to demonstrate regions of high-data density, construct an interpolated temperature model, and identify favorable locations to drill a geothermal exploration well. Anomalously high temperatures (≥43°C) at shallow depths (5 to 9 m) were found along the north floodplain margin of the Humboldt River, northwest of the City of Wells and coinciding with the possible intersection of N-S and E-W faults. While no subsurface waters have been analyzed in this anomaly, water samples from springs and wells to the east and west of this zone were found to display differing chemical and isotopic characteristics, suggesting two different deep circulations on either side of the shallow anomaly that could provide shallow hydrothermal flow: outflow from the hot spring system northwest of the City, and outflow from a blind system further east following the regional hydraulic gradient. Maximum temperatures at depth for the two fluid types as estimated by multicomponent geothermometry are ~180°C for the hot spring system and ~150°C east of the shallow temperature anomaly. The drilling of four temperature gradient wells (GEO#1 -- GEO#4) within and near the shallow temperature anomaly failed to encounter a useful resource, but other shallow prospects and deeper resource prospects remain untested.

[1] EDX is connected through OpenEI.net to the U.S. DOE Geothermal Technology Office's Geothermal Data Repository (GDR) such that Elko project's datasets can be accessed from GDR.

1. INTRODUCTION

1.1 BACKGROUND

Elko Heat Company (EHC) was formed in 1979 as a municipally owned entity in response to a United States Department of Energy (DOE) program opportunity notice to promote the use of geothermal resources. Now EHC is a privately held utility that has provided geothermal heat through a district heating system to the central business district of Elko, Nevada, a geothermal industrial park, and adjoining residential areas (Bloomquist, 2004). The City of Wells reached out to Elko Heat Company for assistance in determining economic opportunities using geothermal heat nearby.

Supported by the 1979 DOE program opportunity, EHC drilled a well into a hot artesian aquifer that lies beneath the cold-water aquifer of the Humboldt River. The well has an artesian flow with a capacity of up to 1,000 gallons per minute (gpm) with a static pressure head of 49 psi. The artesian flow from the well has been controlled during the 35 years of operations to meet operational and seasonal needs fluctuating between 200 to 450 gpm, with the higher flows during the winter heating season. The temperature and static head has remained constant during the operational period.

1.2 PURPOSE

The City of Wells, Nevada has hot springs, thermal wells and a geologic setting conducive to hosting a viable geothermal resource. Under the DOE Small Business Vouchers (SBV) Pilot Program, the objective of this project is to identify a source of geothermal fluids ≥ 66°C (150°F for district heating, in lieu of electricity currently used for heating systems, which would result in cost savings and reduce greenhouse gas emissions. Research teams from Lawrence Berkeley National Laboratory (LBNL) and the National Energy Technology Laboratory (NETL), in collaboration with the University of Nevada Reno (UNR), worked closely with the Elko Heat Company and the City of Wells to improve the current understanding of the geothermal system(s) around Wells with the goal of determining an optimal location for a geothermal exploration well and assess the economic viability of installing a production well at this location for district heating and other direct use applications.

2. APPROACH

This study involved the review of existing, and collection of new, geologic, structural, geochemical and geophysical data to refine the Wells geothermal resource models originally developed by Jewell (1982) and Jewell et al. (1994). A multipronged approach was implemented, consisting of the following broad tasks:

Task 1: Collection and synthesis of existing geologic, geochemical, geophysical, and hydrologic data for the Wells area. This task built upon the work of Rick Zehner, a consulting geologist for Elko Heat Company, who developed a synthesis of many of the earlier studies of the area (Zehner, 2016; Appendix A). New web and literature searches were also conducted, revealing several additional geochemical and geophysical studies completed in the region. These data were collected and incorporated into a data catalog and GIS database (Sections 4 & 6, Appendix I), and used to identify data gaps and inform new field surveys.

Task 2: Review and analysis of geochemical data from wells and springs to assess the origins and deep temperatures of fluids. Various analytical methods were applied to assess the origin and types of geothermal fluids in the vicinity of Wells, including geochemical data from wells and springs as reported by Jewell (1982), Jewell et al. (1994), and Sladek (2011), unpublished data from Jewell, and new data collected as part of this study (Section 5.3.1, Appendices F & G). These analyses included a range of traditional graphical methods as well as newer statistical methods such as Principal Component Analysis. Mixing relationships and deep geothermal reservoir temperatures were also assessed using LBNL's multicomponent geothermometry code, GeoT, and classical geothermometers.

Task 3: Development of a structural model for the Wells geothermal system. The locations of both the up-flow zones and outflow pathways in geothermal systems are highly dependent on structure and geology in the subsurface. Sladek (2011) noted that temperature changes of up to 9°C were observed for some features following the 2008 Wells Mw 6.0 earthquake, highlighting the control that structural features have on fluid flow within the geothermal system. Two models have been proposed that could explain the spring distribution and shallow temperatures in and around the City of Wells: 1) geothermal fluid up-flow beneath the fault-controlled warm springs to the northwest of town, along with outflow in the shallow subsurface towards the town of Wells, and 2) a separate up flow zone to the south of or beneath the town of Wells (Figure 2-1). An evaluation using available data including geologic maps and airborne laser scanner surveys of topography ("LiDAR") and new surveys (Task 4, below) were conducted to further consider these models.

Task 4. Collection of additional field data to better characterize the Wells geothermal system. Based on the analysis of existing data for the area, additional field surveys (Section 5) were executed to better constrain the Wells geothermal system. These included:

- 2-meter temperature measurements (Section 5.1.1)
- Geoprobe temperature measurements (Section 5.1.2)
- Geologic and structural mapping survey (Section 5.2.1)
- Sampling and chemical/isotopic analysis of springs and wells (Section 5.3)
- EMI and resistivity surveys (Section 5.4)

These investigations were conducted in the area between the Threemile hot springs to the northwest of the City of Wells and the warm wells in town.

Task 5. Development of a conceptual geologic model for the Wells geothermal system. This task involved integrating relevant datasets (historical and new) into EarthVision, a software package used for analysis, visualization, and 2- and 3-dimensional modeling of spatially referenced data (Section 7.2). The completed model was used to visualize geologic and geothermal trends in the subsurface, identify regions of highest density and/or quality data, and inform decision-making on optimal location(s) for a geothermal exploration well. Results of the various activities under these tasks are presented below in separate sections, followed by conclusions and recommendations for further work and potential drilling locations.

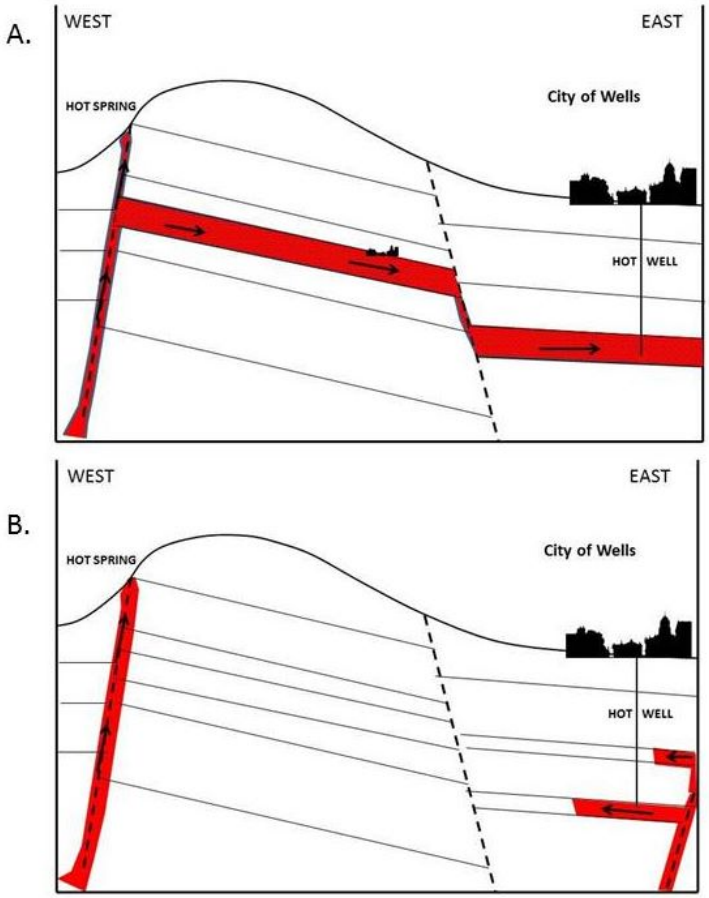

Figure 2-1: Two conceptual models for up-flow zones feeding hot springs and warm wells around the City of Wells, Nevada (Zehner, 2016; Appendix A).

3. GEOLOGIC SETTING

3.1 SURFACE GEOLOGY

The City of Wells lies in the Basin and Range Province in northeast Nevada. The geology of the study area is dominated by outcrops of Paleozoic rocks in the Ruby, Snake, and Humboldt Mountains and lower density deposits (mostly Miocene sediments and tuffs) in the Elko Basin to the west and Town Creek Flat Basin to the northeast (Ponce et al., 2011). Accommodating these basins is the pre-Cenozoic basement, which deepens to over 5 km in the Elko Basin, shallows significantly eastward toward Wells, deepens to about 1.8 km to the northeast in the Town Creek Flat Basin, and outcrops in the surrounding mountain ranges (Ponce et al., 2011) (Figure 3-1).

Previous geologic maps completed near Wells and the surrounding regions include those of Garside (1968), Jewell (1982), Thorman et al. (2010), and Henry and Thorman (2011). The north-trending Snake Mountains are located to the northwest of Wells. The Cenozoic (Miocene) Threemile Spring volcanic and sedimentary rocks are dominant in the southern portion of this range (Garside, 1968), and these strata are observed unconformably overlying the Mississippian Melandco sandstone (Henry and Thorman, 2011). Along the Snake Mountains, sedimentary rock layers are tilted moderately to the east as evidenced by ~25° east-dipping strata just to the northwest of Wells, presumably due to north-northeast-striking west-dipping normal faults along the western boundary of the range. Quaternary normal faults observed along the western flank of the Snake Mountains and within the Town Creek Flat Basin are predominately west-dipping, but older variably dipping faults have been reported along the eastern flank of the Snake Mountains (Jewell, 1982; Thorman et al., 2010; Ramelli and DePolo, 2011) (Figure 3-1).

Due to relatively poor exposures in hills around Wells, the best observations of the local stratigraphy come from cuttings from the Dalton well, which is located within the study area (Figure 3-1) (Jewell, 1982). A stratigraphic column from this well is presented in Figure 3-2, which drilled through >1 km of Miocene strata. The overall lithology consists of siltstone, tuffaceous siltstone, sandstone, and conglomerate. The conglomerate clasts are volcanics, quartzite, siltstone, and chert cobbles that are poorly sorted. The top ~75 m of the stratigraphy logged in the Dalton well is tuffaceous siltstone, which is underlain by ~50 m of siltstone and ~100 m of conglomerate (Jewell, 1982). Alternating gravelly sandstone and siltstone layers make up the remaining ~650 m of the well. Additionally, geophysical logs from the Dalton well show high porosity zones (as interpreted from density logs) and bottom-hole temperatures exceeding 113°C (235°F) at a depth of approximately 1285 m.

Silicification within the Threemile Spring unit occurs along the western side of the range-bounding normal fault (Jewell, 1982) and is most obvious within one (or several) cobble conglomerate unit(s) (Zehner, 2016). Of note, Zehner (2017a; Appendix B) points out that fault-related silicification is not evident near faults mapped by Jewell (1982) close to the area where a 2-meter shallow temperature survey revealed anomalously high temperatures (Section 5.1.1; Figure 3-1). Rather, silicification appears to be confined to the cobble conglomerate unit. Zehner (2017a; Appendix B) concludes that geothermal fluids likely flowed up along the western range-bounding normal fault and outflowed along the east-southeast-dipping conglomerate strata (model A discussed previously in Task 3 of Section 2). The exact path of these fluids is not known, but these observations highlight that past and present geothermal fluid flow may be controlled by the geometries of the dipping Miocene unit, the west-dipping normal faults, and any silicified structures.

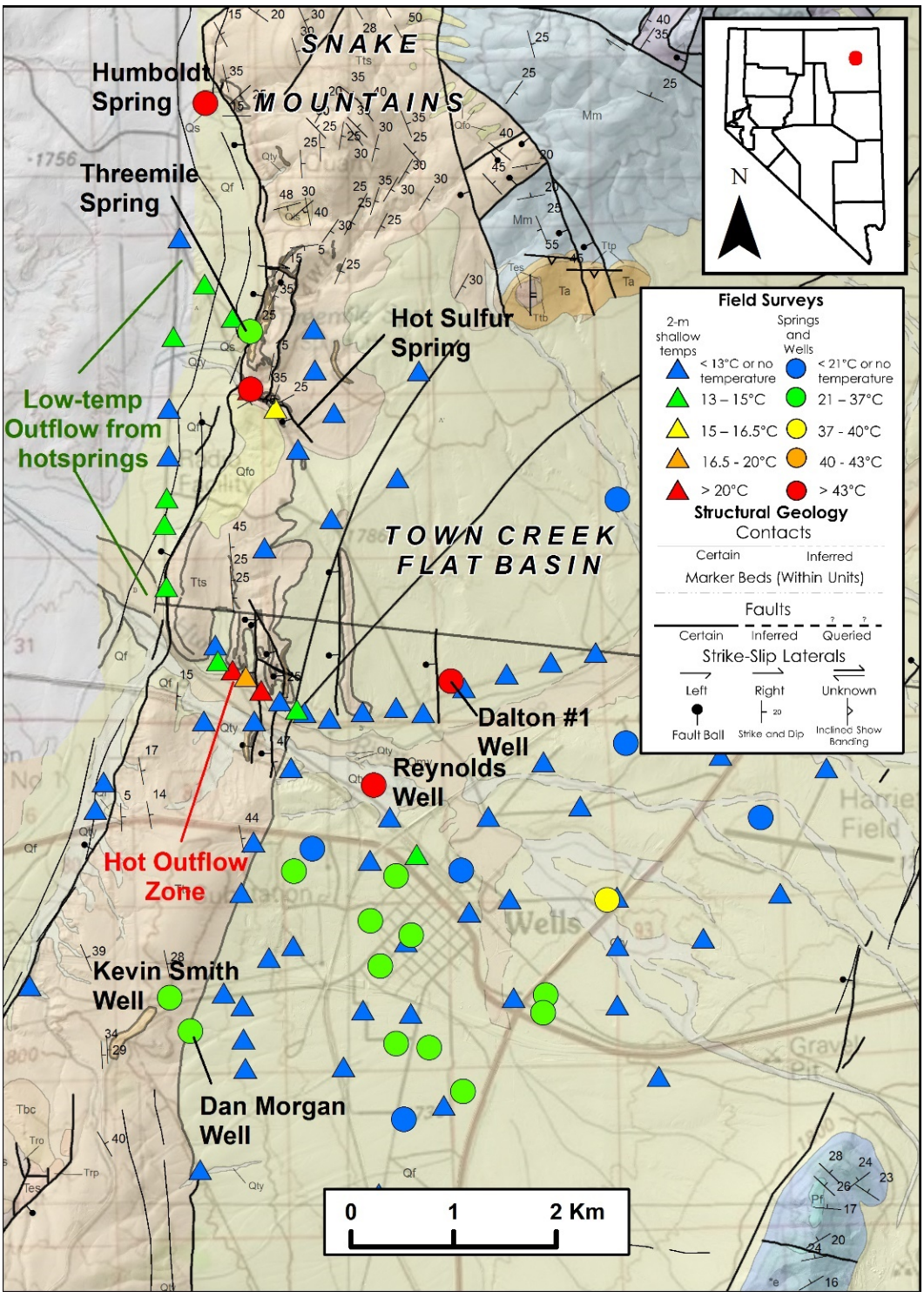

Figure 3-1: Map of the southern Snake Mountains showing local geology (Henry and Thorman, 2011), locations of well and springs and their temperatures (Jewell, 1982; Zehner, 2016, Appendix A), and inferred geothermal outflow zones. Inset shows the location of Wells, Nevada.

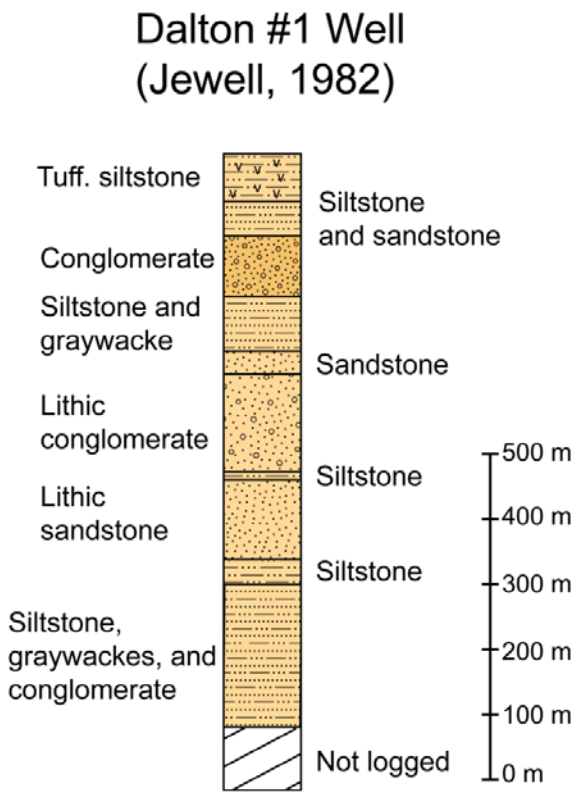

Figure 3-2: Sketch of the Dalton well stratigraphy as described in Jewell (1982). See Figure 3-1 for location.

3.2 2008 EARTHQUAKE INFORMATION

In February 2008, a magnitude 6.0 earthquake occurred 9 km northeast of the town at a hypocenter depth of about 8 km (Smith et al., 2011; Sladek, 2011; Henry and Colgan, 2011). Published information on the earthquake indicates the main shock slippage occurred on a fault dipping 55^{o} SE, with a strike of N40E locally (Smith et al., 2011). The initial rupture's maximum displacement is estimated to be about 86 cm near the middle of the rupture surface, which approximates a circle of radius 4 km (about 8 km diameter across the initial rupture surface), centered at a depth estimated as 8 km (Ibid). At distances more than 80 km from the epicenter, Hammond et al. (2011) estimated displacements exceed 1 mm.

While faults mapped at the land surface did not have noticeable movement, temperatures of water in wells and springs in the vicinity (including in and around the town of Wells) reportedly had temporary temperature increases varying up to 9^{o}C, including at the Reynolds Ranch well and Ray Reynolds well, after the earthquake (Sladek, 2011). Some water wells experienced a temporary reduction in the clarity of the water produced, and several water wells ceased to be serviceable and are thought to have suffered broken casings during the earthquake (Ibid.). These observations occurring within four weeks after the earthquake strongly suggest that wells and springs in and near the town of Wells have immediate hydraulic connection to faults that

experienced at least small amounts of slippage. In other words, the wells and springs are served at least locally by faults and fractures that are open and permeable to water.

Henry and Colgan (2011), Smith et al. (2011), and Thorman and Brooks (2011) determined the 2008 earthquake fault is part of a more recent set of faults that steeply dip to the east, rather than to the west as observed with the faults that typically bound the basins and mountain ranges. They consider these east-dipping normal faults to be more recent than the west-dipping faults and more active presently. Most aftershocks associated with the 2008 earthquake clustered along a fault surface northeast of the town of Wells. Most occurred at depths between 2 km and 11 km, but a few were shallower. The southward extent of the aftershocks ends in the vicinity of the hypothetical "Wells Fault" (Thorman and Brooks, 2011; Figure 3-3), leading to suggestions that the "Wells Fault" relieved stresses along the southern end of the aftershock zone. With the additional information from the aftershocks, seismologists have projected the earthquake fault towards the ground surface along the western margin of Town Creek Flat, northwest and north of the town of Wells and north of the Humboldt River (Smith et al., 2011; Thorman and Brooks, 2011; Figures 3-4, 3-5, 3-6). Thorman and Brooks (2011), among others, speculate that the earthquake fault is a northern extension of the Clover Hill Fault, which marks the western side of the basin to the west and south of town. No land surface ruptures, cracks or slippage have been noticed in this area.

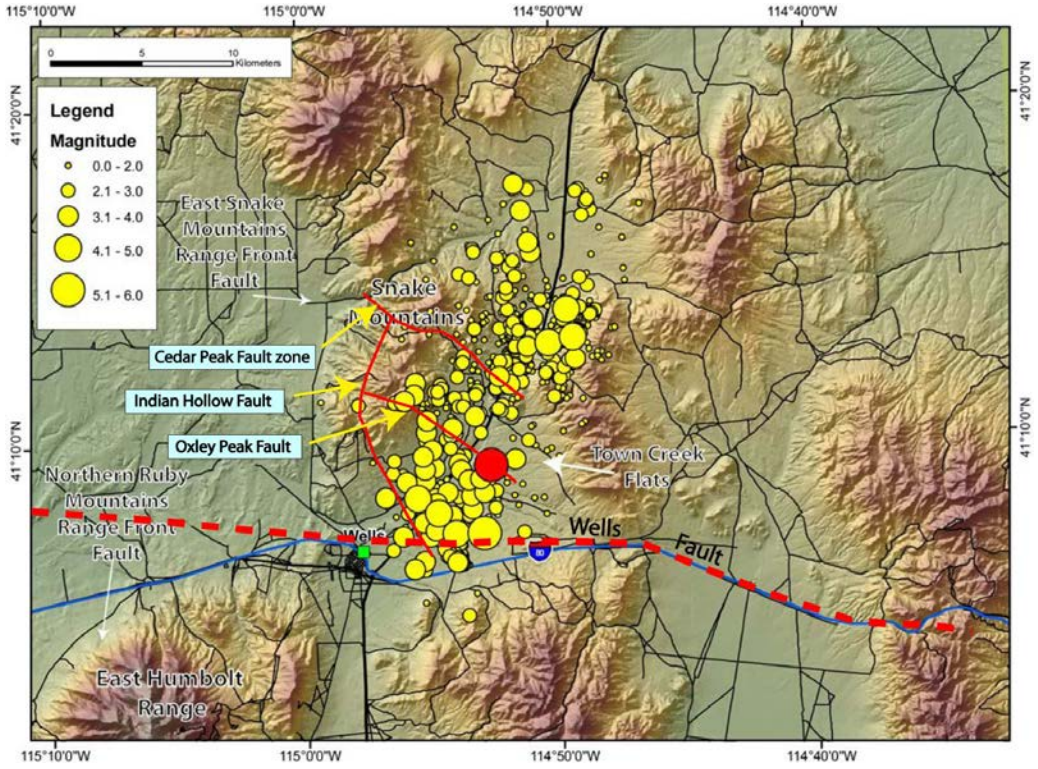

Figure 3-3: Map showing superposition of the hypothetical "Wells Fault" and three northwest trending high-angle faults of Thorman and others (2003) on the HypoDD relocations of the 2008 earthquake events, as published by Smith et al., 2011. Reproduced from Thorman and Brooks, 2011, as modified from Smith et al., 2011, with permission of Nevada Bureau of Mines and Geology, University of Nevada, Reno.

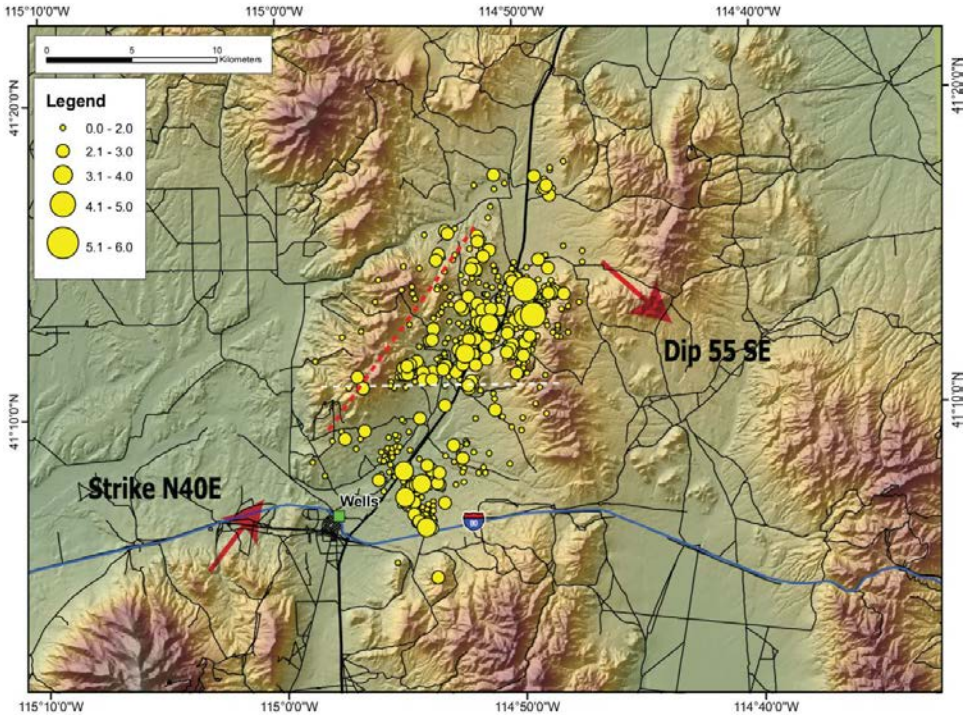

Figure 3-4: Map showing HypoDD relocations of aftershocks occurring after installation of portable instruments (until Oct. 18, 2008). The surface projection of the 2008 earthquake fault is indicated by a red dotted line. An aeromagnetic structure identified by Ponce et al. (2011) is indicated by the while dashed line. Reproduced from Smith et al., 2011, with permission of Nevada Bureau of Mines and Geology, University of Nevada, Reno.

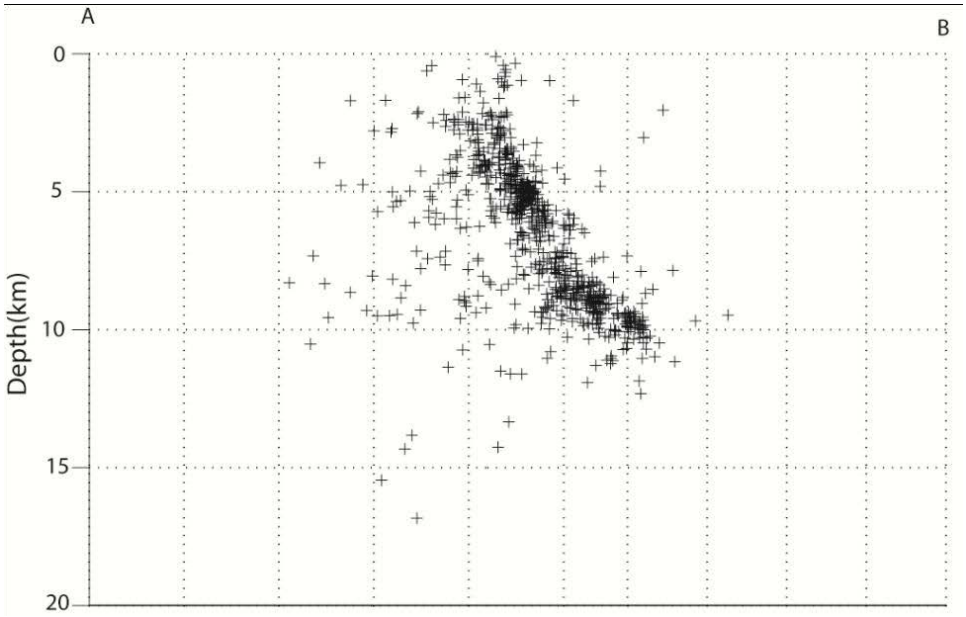

Figure 3-5: Plot of aftershock locations versus depth along a cross-section view looking N40E. Reproduced from Smith et al., 2011, with permission of Nevada Bureau of Mines and Geology, University of Nevada, Reno.

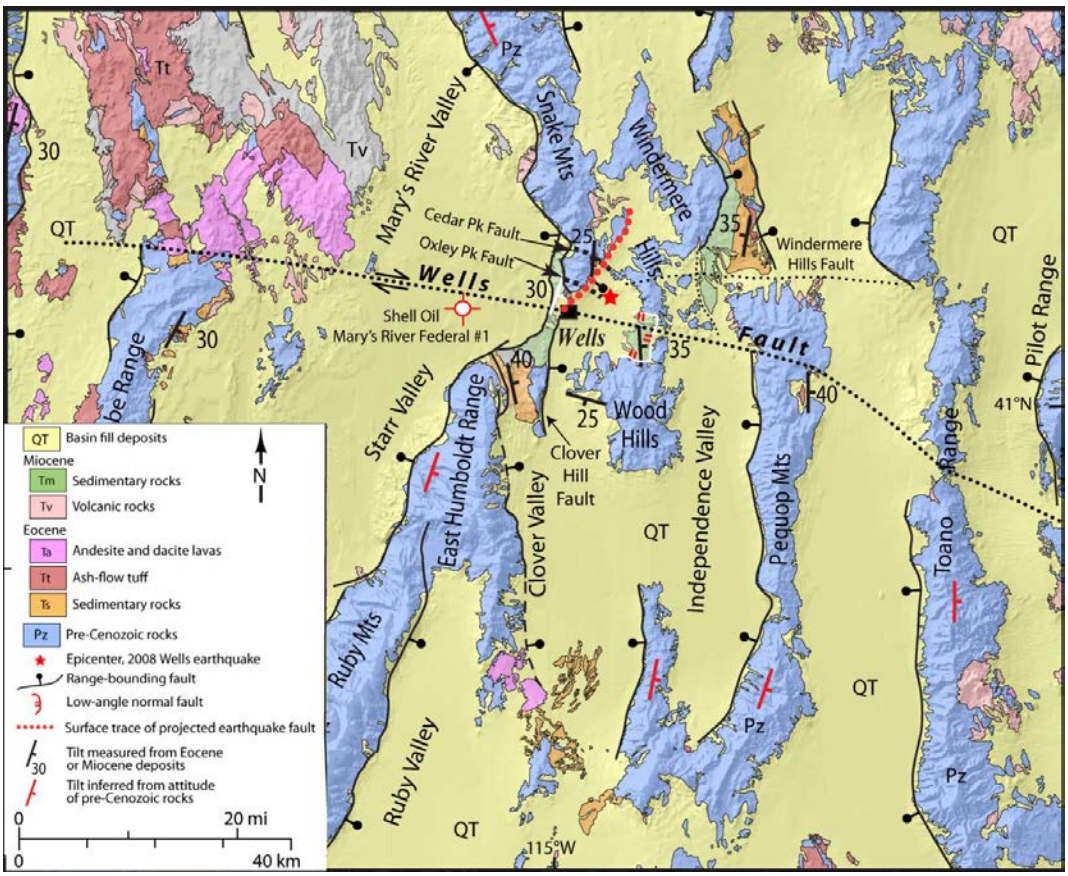

Figure 3-6: Location map showing the 2008 earthquake epicenter (red star) and a projected surface trace of the earthquake fault (dotted red line). Reproduced from Thorman and Brooks, 2011, as modified from Henry and Colgan, 2011, with permission of Nevada Bureau of Mines and Geology, University of Nevada, Reno.

A comparison of pre- and post-earthquake InSAR images by Bell (2011) reveals a land surface depression caused by the earthquake, with the depression's center located at the epicenter of the earthquake. The area of land surface depression extends southwest to the town of Wells and westwards to the western margin of Town Creek Flat. The depression is asymmetric with a steeper limb on the western side, where the earthquake fault accommodated substantial discrete slippage. A reasonable interpretation of Bell's Figure (Figure 3-7) would suggest, among other things, the 2008 earthquake propagated up through competent rock, probably including the Miocene sediments, to the upper surface of the competent rocks; but the surface colluvium apparently obscured the rupture at the land surface. Further interpreting this image, there is a single fault or narrow fault zone with displacements ranging up to 7 cm (or more) north of town.

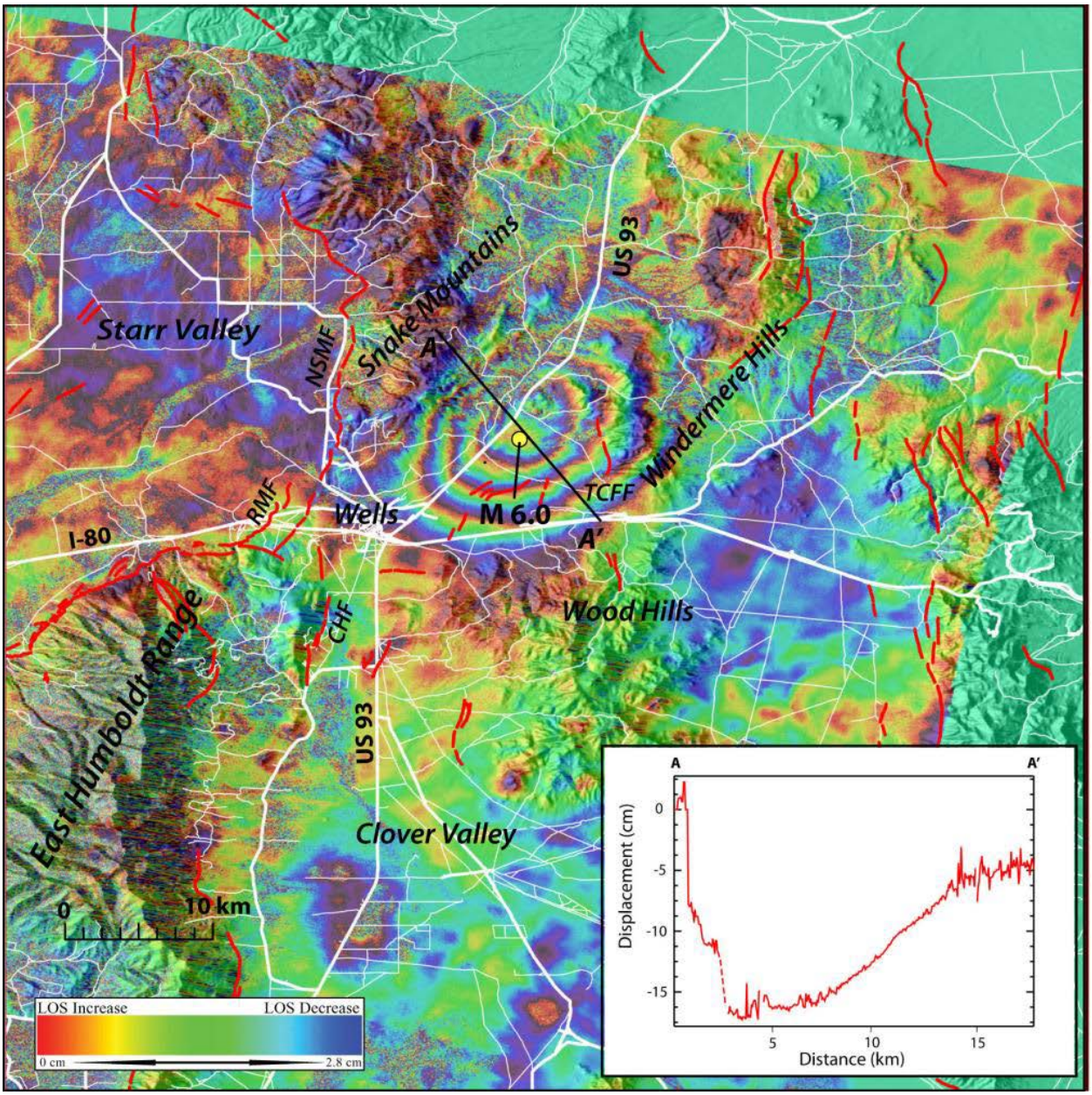

Figure 3-7: Ground surface deformation as indicated by an interferogram made from two Envisat images, one before the 2008 earthquake and one after (Aug. 13, 2007 and May 19, 2008). Each color cycle around the earthquake epicenter represents 2.8 cm radar line of sight change in position. Ground subsidence is indicated across a 20 km (SW to NE) ellipsoidal area, with a maximum of 15 cm of subsidence indicated at the center. Quaternary fault traces from U.S. Geological Survey (2006) shown in red; CHF, Clover Hill Fault; NSMF, northern Snake Mountains fault; RMF, Ruby Mountain fault; TCFF, Town Creek Flat fault. Reproduced from Bell, 2011, with permission of Nevada Bureau of Mines and Geology, University of Nevada, Reno.

4. REVIEW AND COMPILATION OF OTHER EXISTING DATA

As mentioned in previous sections, several relevant local and regional studies were completed prior to this effort. All previously existing surface and subsurface datasets in the vicinity of the Wells, Nevada were collected and cataloged. Datasets were identified through literature and web searches, and the majority of relevant resources came from the Nevada Bureau of Mines and Geology, Nevada Division of Water Resources (NDWR), and United States Geological Survey (USGS), and previous geologic and geothermal exploration projects (Jewell 1982, 1994). Datasets were grouped into five categories: Topography and administrative boundaries, geologic and structural data, geochemical data, geothermal data, and geophysical data. A detailed catalog (described more in Section 6.1; Appendix I) was compiled to organize the datasets.

4.1 TOPOGRAPHY AND ADMINISTRATIVE BOUNDARIES

Relevant administrative boundaries include the City of Wells, Elko County, and the state of Nevada (ESRI, 2017). These boundaries helped to define a study area extent for the 3-dimensional geologic model and uncertainty analyses (Section 7.2). Topographic datasets include the high resolution (1 m) LiDAR ("Light Detecting and Ranging") Digital Elevation Model (DEM) from the Federal Emergency Management Agency (FEMA), which was used to create a hillshade (hypothetical sun illumination) representation of the surface. Both the DEM and hillshade datasets are helpful in constraining the geologic architecture of the study area by assisting in identifying key geologic structural features, selecting potential geophysical survey sites, and determining well surface locations in three dimensions.

4.2 GEOLOGIC AND STRUCTURAL DATA

Additional geologic and structural data around the City of Wells and the surrounding area has been collected since Jewell's (1982) study. Detailed geologic maps with geospatial data (Henry and Thorman, 2011) and cross sections (Zuza, 2017; see Section 5.2) describe the surface sediments, rock formations, faults and other structural attributes. To better constrain and asses the stratigraphic framework of the study area, lithologic logs from water wells (NDWR) were obtained for further interpretation and analysis (See Section 5.2.6; Appendix E). Areal aquifer extents and ground-water depths were collected (USGS, 2005; Lopes et al., 2006) to better understand the presence and potential extent of ground water, particularly thermal waters. To further define local geologic structure, faults and other structural data were supplemented from Jewell (1982), Dohrenwend (2012), and Henry and Thorman (2011). Regional sediment thicknesses were constrained from depth to basement estimates (Ponce and Damar, 2017).

The geologic and structural datasets described here comprise the foundation of the 3-dimensional geologic model. They provide the geologic architecture of major surface and subsurface structures and identify regions containing data and knowledge gaps.

4.3 GEOCHEMICAL DATA

Existing geochemical analyses of water samples from springs (hot and cold) and wells around the City of Wells were compiled from a review of available published papers and reports, including those of Garside and Schilling (1979), Garside (1994), Jewell (1982), Jewell et al. (1994), Jewell (personal communication), Sladek et al. (2011), Zehner et al. (2006), and Zehner (2016). Data from the Nevada Bureau of Mines and Geology (NBMG) were also included. Sampling locations (coordinates) for these data were established from information gathered from

each author's maps, tables, and/or comments. In many cases the same analyses from given springs or wells were reported by more than one author. In some cases, the different authors reported the same analysis using a different name or location. In such cases reported analyses were consolidated and assigned one unique name, ID number, and location. The resulting geochemical data are presented in Appendix F. These data were reviewed and compared with newly collected data, then subjected to various geochemical data analysis methods as discussed further in Section 5.3.

4.4 GEOTHERMAL DATA

Geothermal temperature measurements were acquired from wells, springs, and other ground water sources (NBMG, NDWR; Zehner, 2006, 2017a, -b). Where depth information was available, geothermal gradients were calculated to determine temperature at specific depths. **These gradients should be considered with caution given mixing of cooler, shallow ground water with hotter, deeper ground water in the shallow subsurface, or the possible presence of shallow geothermal outflow plumes with cooler temperatures below.** The most reliable temperature data was compiled and included in the 3D geologic model and uncertainty analyses (Section 7.2). These datasets and analyses are key for identifying potential hydrothermal flow pathways and reservoirs as well as highlighting data gaps.

4.5 GEOPHYSICAL DATA

Collected geophysical datasets highlight major geologic and structural changes in the subsurface to help prioritize areas for geothermal exploration. This includes earthquakes (USGS) in and around the City of Wells, specifically the 2008 earthquake swarm which delineates previously unmapped faults (Ramelli and DePolo, 2011). Subsurface stress data (Heidbach et al., 2008) and calculated fault attributes such as dip, slip, and dilation (See Section 7.1) were used to help infer fault permeability in the area. Additionally, physical properties of subsurface lithologies were obtained through downhole geophysical logs (gamma ray, resistivity, acoustic, neutron, etc.) from oil and gas wells in the area (IHS, Figure 4-1; Table 4-1). Each of these geophysical datasets plays an important role in constraining the 3-dimensional geologic and structural framework of the area of interest, and assists in identifying potential hydrothermal flow pathways.

Table 4-1: Wells containing geophysical logs in study area.

Well Name	API Number	Surface Elevation (m)	Total Depth (m)	BHT* (°C)	Log Type**									
					GR	C	R	SP	N	BD	CNP	CFDP	M	A
Wilkins Ranch	27007050070000	1,706	2,565	112	X		X	X	X					
Howell	27007050570000	1,678	2,656	126	X	X	X	X			X	X	X	X
Dalton	27007052100000	1,710	1,282	113	X	X	X			X			X	
Marys River Federal 1	27007052110000	1,682	1,682	-									X	
AZL-Superior	27007052120000	1,676	3,566	-										
Marys River Federal 2	27007052210000	1,754	2,734	169	X	X		X			X	X	X	X
Farnes 1	27007052370000	1,758	686	-										
Farnes 2	27007052390000	1,547	335	-										
Texxon 1	27007052400000	1,757	366	22	X	X	X	X			X	X		X

*BHT – bottom-hole temperature
**GR – gamma ray, C – caliper, R – resistivity, SP – spontaneous potential, N – neutron, BD – bulk density, CNP – compensated neutron porosity, CFDP – compensated formation density porosity, M – mud, A – acoustic (sonic)

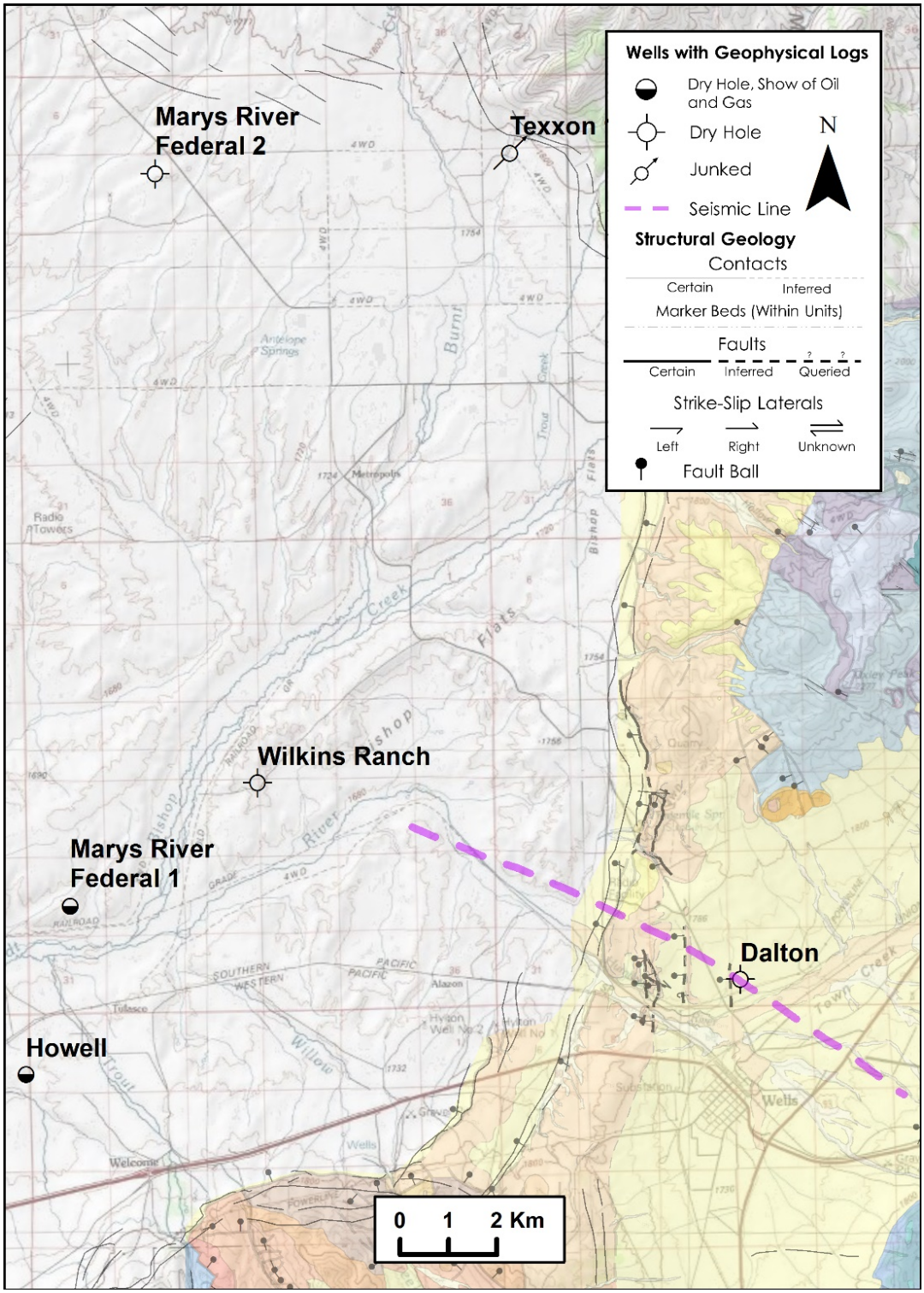

Figure 4-1: Overview map showing locations of deep wells near Wells, Nevada. Table 4-1 summarizes basic information about these wells, and what types of geophysical logs were collected within each wellbore.

5. FIELD DATA COLLECTION AND INTERPRETATION

5.1 TEMPERATURE SURVEYS

5.1.1 2-m Shallow Temperature Survey

In November, 2016 the City of Wells, Nevada commissioned Zehner Geologic Consulting, LLC (ZGC) to perform a shallow, 2-meter temperature survey in the area around Wells, following recommendations from an earlier desktop study compiled by Geothermal Development Associates (Zehner, 2016; Appendix A). Results from this temperature survey were submitted in January 2017 to Elko Heat Company and the City of Wells in an unpublished report included in Appendix B (Zehner, 2017a).

In this survey, temperatures were measured at 1.0, 1.5, and 2.0 m below ground level at 73 sites across the project area. Temperatures at 14 of the sites were measured at or above background levels (13.0°C, or 55.4°F). Indications of weak, western-directed thermal outflow were detected in sites adjacent to the Snake Mountains range front in the vicinity of known, but unnamed, hot springs. Two sites east of the range front near Sulphur Hot spring indicate that thermal up-flow is occurring along structures inboard of the range front. The most interesting discovery from this survey was the identification of a strong thermal anomaly (Figure 5-1) near the northern edge of the Humboldt River floodplain, due south of Sulphur Hot spring. The anomaly, labeled the Southern Outflow Zone in Figure 5-1, is ~600 meters long with temperatures reaching 24.5°C (76.1°F) at 2-m depth.

5.1.2 Geoprobe Surveys

A direct-push Geoprobe survey was conducted in April 2017 along the ~600 m long thermal anomaly identified by the shallow temperature survey (Section 5.1.1; Figure 5-1). The Geoprobe was chosen as an inexpensive verification method to measure temperatures and obtain water samples at greater depths. Results from this survey were submitted in May 2017 to Elko Heat Company and the City of Wells in an unpublished report included in Appendix C (Zehner, 2017b).

Zehner (2017b) oversaw the Geoprobe survey at a location approximately 2-3 km (1.2-1.9 miles) northwest of the City of Wells (Figure 5-1). The surveyor made eight un-cased holes ranging from 5 to 9 m (17- 30 ft) in depth. The locations of the holes were designed to explore the thermal anomaly labeled as the “Southern Outflow Zone” on Figure 5-1. Measured bottom-hole temperatures were between 32.2° and 45.4° C (~90°-114° F), indicative of a high geothermal gradient. This gradient is interpreted by Zehner (2017b) to indicate the presence of geothermal fluids at shallow depths. The circulation of these hot fluids could result either from up-flow along the fault mapped by Jewell (1982) and confirmed by new mapping (Section 5.2.1), a south-directed outflow zone from the unnamed hot springs to the north, or some combination of the two. However, no ground water was actually detected in the Geoprobe holes.

Subsequent to the April 2017 survey, the City of Wells commissioned five additional Geoprobe holes, which were made August 14, 2017 on the south side of the Humboldt River, to the southwest and southeast of the hottest thermal anomaly and along Metropolis Road. The locations of these measurements are also shown in Figure 5-1. A report was not produced specifically for these Geoprobe investigations. The western hole (WGP-09) had a temperature of 21°C (69.8°F) at a depth of 8.2 m (27 ft). The next three holes further east (WGP-10, -11, -12)

had a bottom hole temperature of about 29°C (84°F) at depths of 8.4 to 9.4 m (27.5 to 31 ft). The eastern most hole (WGP-13) had a temperature of 33°C (91.6°F) at 8.5 m (28 ft). (J. Supp, email on Aug. 16, 2017).

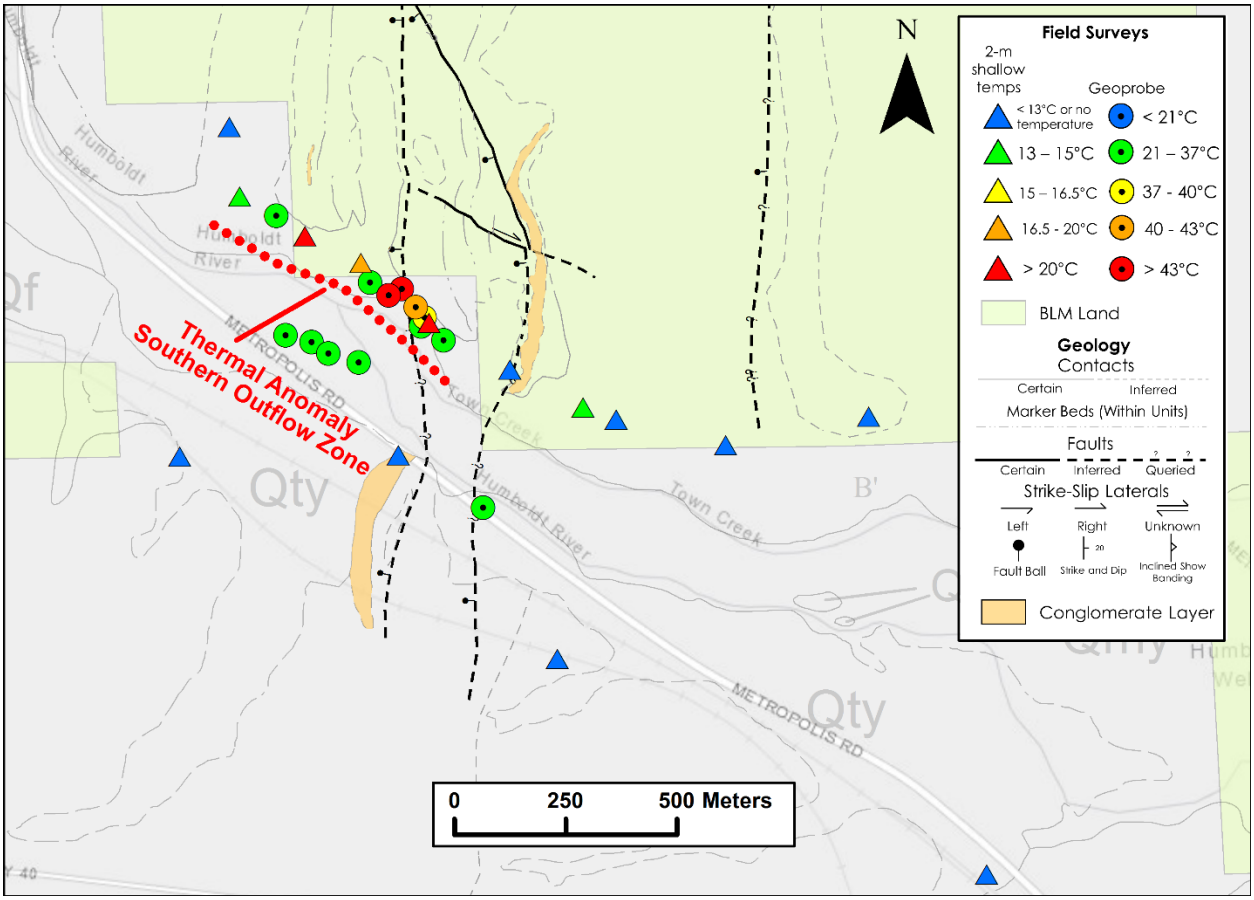

Figure 5-1: Close-up view of the thermal anomaly adjacent to the Humboldt River, showing results of the 2-meter shallow temperature survey (triangles; Zehner, 2017a) and Geoprobe survey (circles; Zehner, 2017b). Temperatures are indicated by color in the legend. Conglomerate layer from Zuza (2017).

5.2 GEOLOGIC AND STRUCTURAL SURVEY

5.2.1 Geologic and Structural Mapping

Geologic and structural mapping was required to constrain the nature of the Southern Outflow Zone (SOZ) and better understand the overall structural geometries of the potential geothermal system around Wells, Nevada. Andrew Zuza, Assistant Professor and Structural Geologist at the Nevada Bureau of Mines and Geology at the University of Nevada, Reno, was contracted in April 2017 to map geologic features around the study area, building on previous work by Jewell (1982), Thorman et al. (2010), and Henry and Thorman (2011). The mapped area spans ~80 km^2, and extends from the Humboldt Hot springs in the north to the Kevin Smith and Dan

Morgan wells in the south. It is bounded to the east by the City of Wells, and to the north and west by the low foothills of the southern Snake Mountains. Rock exposures are generally poor in the study area as most of the Miocene strata are poorly consolidated sediments susceptible to weathering and erosion. However, the more resistant rocks did crop out and were able to be mapped. A condensed version of the Zuza (2017) geologic map is presented in Figure 5-2, and the full-scale map is provided in Appendix D.

There were three primary objectives for detailed mapping:

(1) **Determine the nature and orientation of faults.** In general, Quaternary faults in the Wells area are west dipping, but previous mapping identified some east-dipping normal faults (Jewell, 1982). The east-dipping faults identified in Jewell (1982) were verified in the field and mapped. Understanding the attitudes and kinematics of local and regional faults is necessary for reconstructing subsurface geometries and determining possible fluid-flow pathways and barriers.

(2) **Thoroughly assess attitude of the Miocene Threemile Spring unit.** This is especially helpful in determining whether thermal waters could be flowing within specific stratigraphic intervals, such as a porous conglomerate bed. Furthermore, exposure of strata is poor in the southern Snake Mountains, so reliable bedding observations are particularly important.

(3) **Investigate nature of silicification within strata and along fault surfaces.** The presence of silicification can indicate past hydrothermal flow and provide clues about current flow pathways. In addition, cross cutting relationships between older and younger silicified features (layers, bedding, and fault surfaces) should be established, as these features can redirect flow in the subsurface.

5.2.2 Lithologic Units

All strata exposed in the study area are Cenozoic or younger in age and include Miocene volcanic and sedimentary strata and Quaternary alluvium. The low-lying foothills of the Snake Mountain range are comprised of the Miocene Threemile Spring unit (Thorman et al., 2010), which consists predominately of siltstone, tuffaceous siltstone, sandstone, and conglomerate (Figures 5-3, 5-4) and is part of the broader Humboldt Formation. Drill core data from the Dalton well in the eastern study area demonstrates that the Threemile Spring unit is locally >1 km thick (Figure 5-3) (Jewell, 1982; Thorman et al., 2010). The lower portion of the Threemile Spring unit consists of tan to buff colored fluvial and lacustrine siltstone, sandstone, and conglomerate, which contains clasts ~3 cm in diameter. The uppermost portion of the Dalton well consists of a thick conglomerate layer, interbedded with sandstone and siltstone. The conglomerate consists of subrounded clasts, up to 10 cm in diameter, of rhyolite, basalt, quartzite, chert, and shale, and is mapped as a distinct marker unit within the Miocene strata (Figure 5-2). The most complete surface exposure of the Threemile Spring unit is a railroad cut west of the City of Wells.

Quaternary deposits unconformably overlie the Miocene strata, but were not mapped in detail in Jewell (1982), Thorman et al. (2010), or Henry and Thorman (2011). The mapping completed in our study includes Quaternary divisions for active tributary and medial stream deposits (Qty and Qmy), alluvial fan deposits (Qf), spring deposits (Qs), landslide deposits (Qls), and older alluvial surfaces (Qfo) (Figure 5-2).

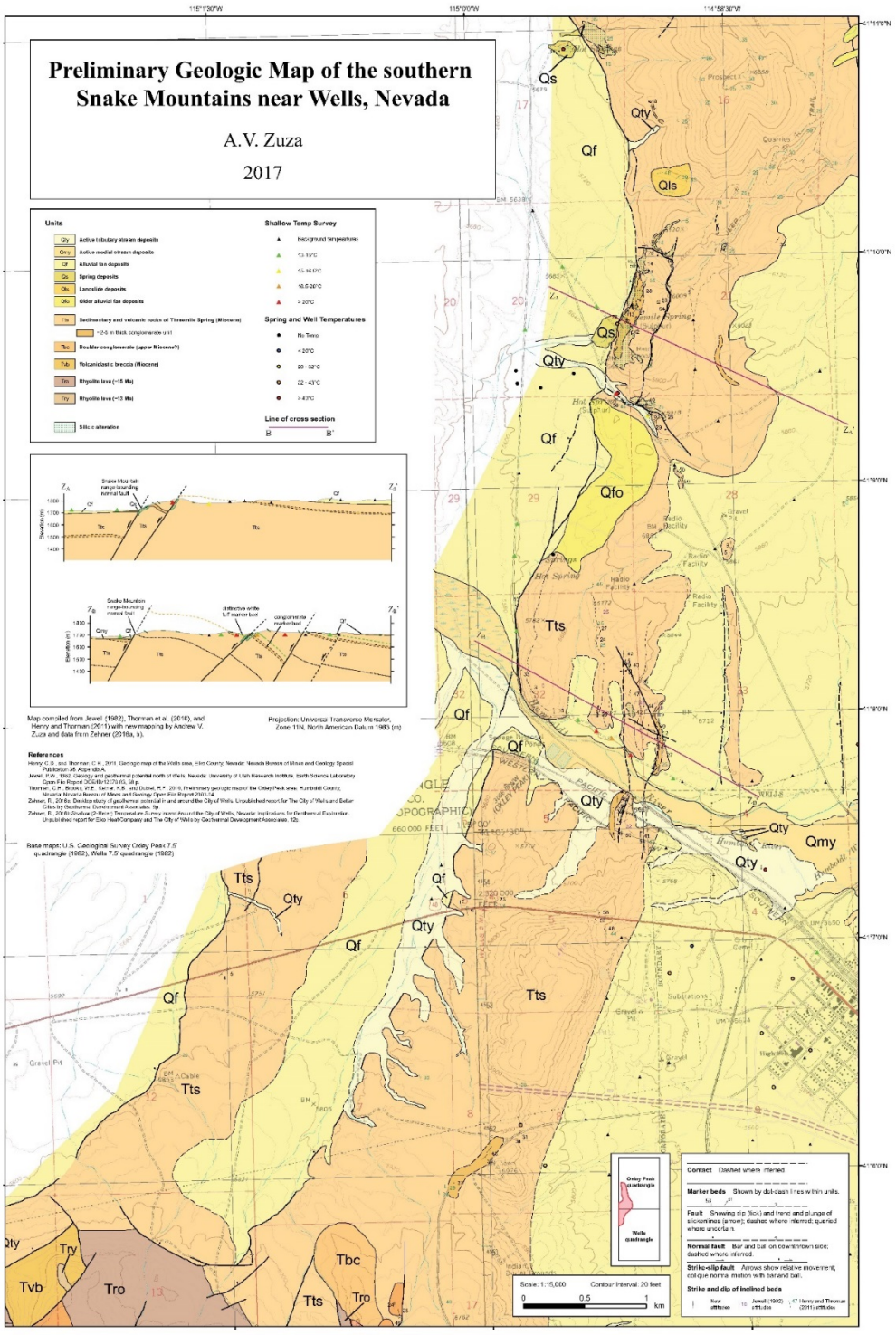

Figure 5-2: Preliminary geologic map and cross sections of the southern Snake Mountains near Wells, Nevada, based on new field observations and a compilation of Jewell (1982), Thorman et al. (2010), and Henry and Thorman (2011). The full-sized map and cross sections are provided in Appendix D.

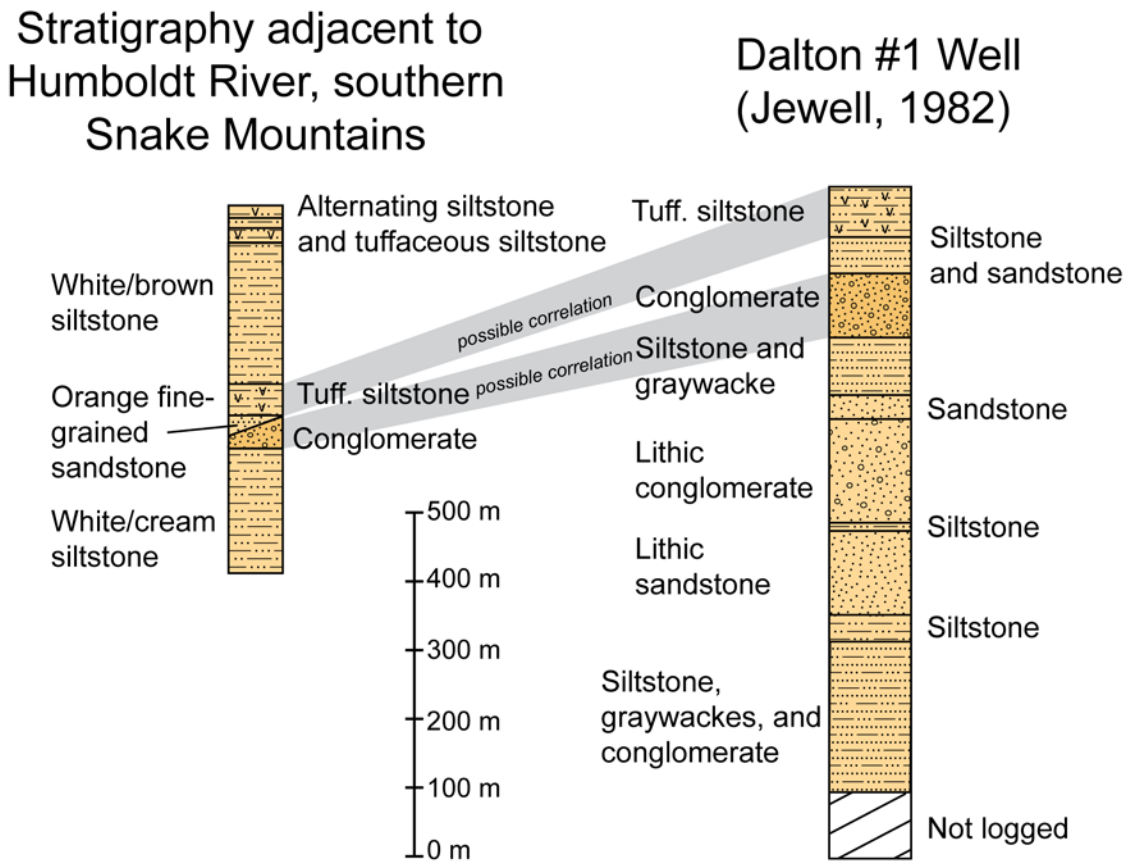

Figure 5-3: Sketch of the Dalton well stratigraphy, as described in Jewell (1982), compared against field observations of the local stratigraphy developed in this study. See Figure 3-1 for the location of the Dalton well.

5.2.3 Dominant Structures

Almost all bedding observations show a north strike (~0-10°E) and east dip (~10-40°) (Figure 5-5). Shallowly dipping beds (<10°) show more dip-direction variability, presumably in part because the near horizontal poorly lithified beds are either folded or slump locally.

There are two dominant orientations to the mapped fractures and joint sets: (1) north-northeast-striking and steeply dipping (~70°E or W) and (2) west-northwest striking and moderately dipping (~50-60°N or S). Many of the faults have ~10-50-cm-thick fault-breccia zones, which are often silicified. Most of the mapped faults (19 of 24 fault measurements; Figure 5-2) strike north (345-010°) and dip west (60-70°) (Figure 5-5). The three exceptions that dip to the east may be explained as conjugate faults to the west-dipping normal faults. Slickenlines on observed fault surfaces rake ~80-90°, suggesting primarily dip-slip motion. Due to the orientation of the faults, bedding, and slickenlines, the majority of mapped faults are interpreted to be dip-slip normal faults with the hanging wall located on the west side of the fault (Figure 5-2). Field relationships suggest that the slip displacement of each of these faults is ~10 to 100 meters. Range-bounding faults on the western flank of the Snake Mountains show geomorphic evidence

for late Quaternary activity (de Polo, 2008; Ramelli and de Polo, 2011). Timing of distributed faulting within the range is not well constrained, but because many of these faults control topography and local drainage patterns, their latest motion may have been in the Quaternary.

The southernmost west-northwest-striking fault, located just north of the Humboldt River (Figure 5-2) has apparent right-lateral separation. A north-striking normal fault and the conglomerate marker horizon are offset right-laterally, although there were no slickenline observations to constrain any dip-slip component. Near the Hot Sulphur Spring, a west-northwest striking normal fault shows primarily dip-slip normal faulting based on slickenline observations. The hanging wall is on the south side of the fault, and this fault appears to truncate a north-striking normal fault to the north. Just to the north of Threemile Spring, there is a west-northwest-striking fault where oblique right-lateral normal faulting is observed. Note that a north-striking normal fault crosscuts this west-striking oblique normal fault (Figure 5-2).

Some north-striking normal faults are mapped with inferred links between the north and south sides of the Humboldt River. However, this is an interpretation based on the fault's projections along strike, and the faults may link differently than is shown in Figure 5-2. Conversely, some of the mapped faults were inferred entirely by topographic breaks and north-trending drainages, especially in the eastern portion of the map area where outcrop is exceptionally poor. It is possible that these faults do not exist, but their spacing in relation to the other faults makes their existence plausible.

In addition to many large faults, there are also numerous minor normal faults with <0.5 m offset observed in the field area (Figure 5-2). These faults were not mapped in detail by Zuza (2017).

Throughout the map area, the tuffaceous siltstones are commonly cream-white in color, friable, and susceptible to weathering (Figure 5-4), resulting in the rounded hills with poor rock-exposure northwest of Wells. However, in altered zones, which were mapped with a green stippled pattern in Figures 5-2, 5-4, the tuffaceous siltstones are green-yellow in color, silicified, and more resistant to weathering. The mapped conglomerate unit is observed in both silicified and non-silicified states, although it is more commonly found in a silicified state, suggesting that it has had silica-rich fluids flowing through it in the past. As noted above, many of the brecciated fault zones are also strongly silicified (Figure 5-4). In the hills north of the Humboldt River, calcite veins crosscut bedding parallel to the local north-striking, west-dipping normal faults (Figure 5-4). This area is brecciated and beds are variably silicified, indicating a complex history of silica- and calcite-rich fluids flowing through the region.

Both the hot springs and evidence of alteration concentrate around the mapped faults in the area (Figure 5-2). Of note, the most intense alteration and the location of Hot Sulphur Spring appear to be located around complex faulting zones where north-striking and west-northwest-striking faults crosscut each other and interact. Although the west-northwest-striking faults appear to be minor relative to the north-striking normal faults, the Humboldt River parallels these west-northwest-striking faults in this mapping region, possibly indicating that its course through these hills was controlled by a west-northwest fault. The inferred Wells Fault (Thorman and Ketner, 1979) has a similar orientation, and has been schematically drawn across this region (Henry and Thorman, 2011).

5.2.4 Cross Section Discussion

Two cross sections, Z_A-Z_A' and Z_B-Z_B', based on the geologic mapping are shown in Figure 5-2 and Appendix D. These sections were drafted perpendicular to the north-striking normal faults, and primarily convey the tiling of strata due to the west-dipping normal faults. In these cross sections, it is assumed that the observed sequence of conglomerate overlain by siltstone rocks and a stratigraphically higher tuffaceous marker bed is correlative (Figure 5-2). This is a significant limitation of the cross sections, and without detailed stratigraphic analyses and/or drill core data, this correlation cannot be verified.

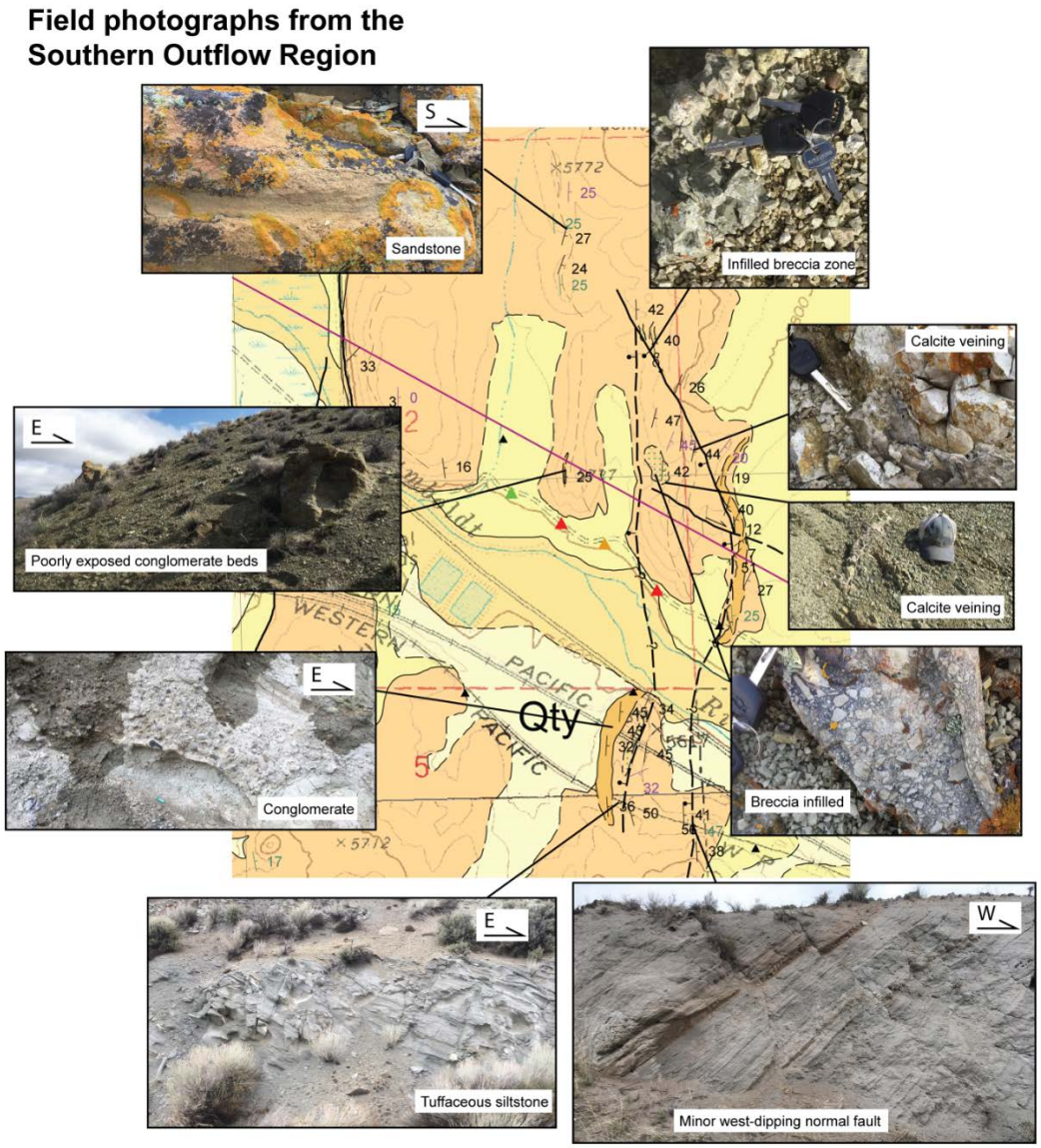

Figure 5-4: Zoomed-in geologic map from the Southern Outflow Zone (SOZ) around the Humboldt River (cropped from Figure 5-2) showing field photographs of important geologic observations.

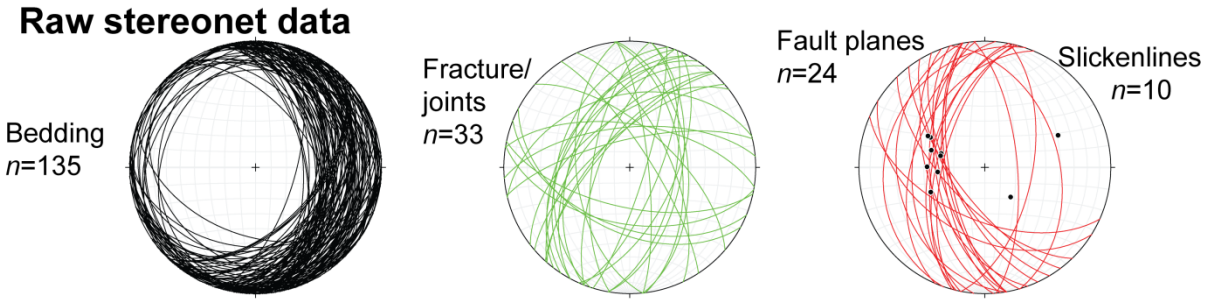

Figure 5-5: Stereonet plots of structural data from the mapping area in Figure 5-2, including bedding joint/fractures, fault planes, and slickenlines.

5.2.5 Other Field Observations

Cross sections Z_A-Z_A' and Z_B-Z_B' convey the inferred slip magnitude of observed normal faults by assuming that the conglomerate-tuff sequence aligned prior to faulting. Bedding observations were projected to the cross-section line, and used to construct the fold geometries (Figure 5-5). Faults were assumed to be planar at depth. In section Z_B-Z_B' (Figure 5-2), the easternmost beds were drafted so that they intersect the Dalton well data, and the siltstone, tuff, and conglomerate units align with the well observations (Jewell, 1982; Figure 5-3). Maximum observed normal-fault offset is ~300 m, on the western range-bounding faults, while some of the minor faults show tens of meters of fault offset. Using a line-length restoration, the regional extension accommodated via normal faulting results in low minimum extension magnitudes of 216 m (9% extensional strain) and 218 m (9% extensional strain) for sections Z_A-Z_A' and Z_B-Z_B' respectively. The similarity between these strain values -- from different sections across the same normal-fault system -- adds confidence to the cross section models.

5.2.6 Geologic Interpretation of NDWR Water Wells

There are 59 historic well logs collected from the Nevada Department of Water Resources (NDWR) access database. For each well log, information was compiled about surface location and elevation, drilled depth, perforated intervals, water level, and measured water temperatures. The logs usually indicate the driller's interpretation of lithology (i.e., rock type) and unit thicknesses. Each well containing lithologic logs (54 in total) was graphically illustrated in Adobe Illustrator CC6 and exported as a jpeg image for use in subsequent subsurface interpretations (Appendix E). Graphically illustrating the lithologic logs frequently required further geologic interpretation. For example, a unit described as "loam," "sand," or "hard rock" in the lithologic log was displayed as "top soil," "sandstone," or "basement" in the graphical illustration.

To further constrain and assess the stratigraphic framework of the study area, the graphically illustrated lithologic logs were used to construct four cross sections crisscrossing the southeast region of study area: A-A', B-B', C-C', and D-D' (Figure 5-6; Appendix E). Rather than follow a straight-line transect, each cross section follows a zigzag path, chosen to maximize the number of lithologic logs in the cross sections. Lithologic logs were selected for inclusion in cross sections based on one or more of the following criteria: depth (>25 m), water level information, measured water temperatures, and the presence of conglomerate and/or basement lithologic

units. In some instances, the cross sections transect a fault (or inferred fault). This information is also displayed on the cross sections.

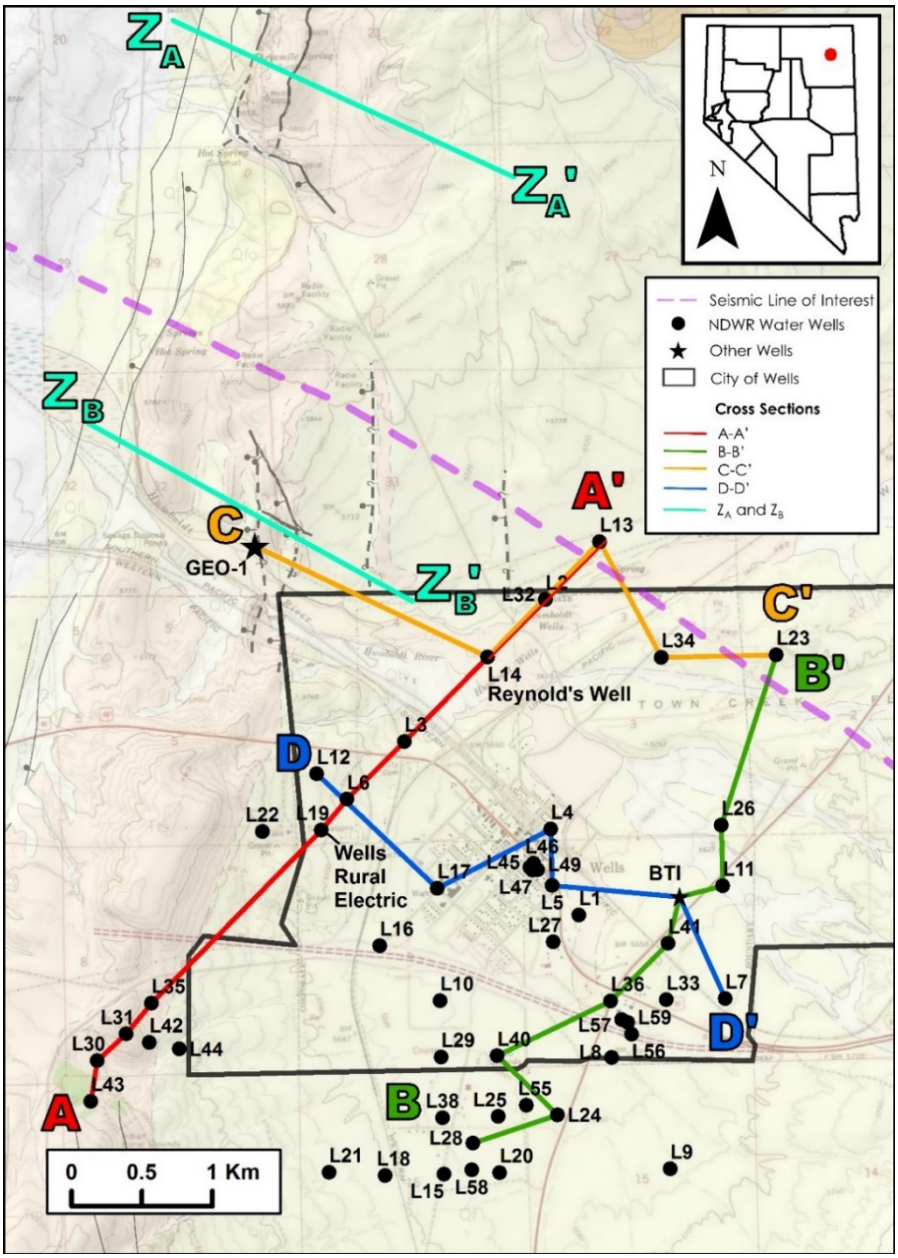

Figure 5-6: Locations of cross sections constructed for this study. Cross sections A-A' (red), B-B' (green), C-C' (orange), and D-D' (dark blue) were constructed using graphically illustrated lithologic logs from NDWR water wells. Two-dimensional (2D) cross section profiles can be viewed in Appendix E. Cross sections Z_A-Z_A' and Z_B-Z_B' (light blue) were prepared by Zuza (2017; Appendix D). The dashed purple line represents the 2D seismic track purchased for this study (Section 5.5). The black polygon shows Wells city limits. Faults are shown in black and black dashed lines, with hanging wall indicated by ball and stick symbol. Geologic base map from Zuza (2017) and Henry and Thorman (2011).

5.3 GEOCHEMICAL SAMPLING AND ANALYSIS

To complement historical water chemistry data compiled from existing sources (Appendix F), water samples were collected from springs and wells for chemical and isotopic analyses. The sampling locations and types are listed in Table 5-1 and shown on Figure 5-7, and chemical analyses are provided in Appendix G.

A field sampling survey was conducted by LBNL and UNR in April 2017, covering an area from Humboldt Springs in the north, to Railroad Spring located south of Wells. During this time, 7 city wells, 6 private wells, and 6 springs were sampled (Table 5-1) for general chemical and carbon (C), oxygen (O), and hydrogen (H) stable isotopic compositions. These samples were collected and preserved as described in Section 5.3.1. Five more grab samples were collected by the City of Wells in June 2017 at 3 wells and one hot spring. It was noted that Hot Sulfur Spring is no longer active, but Threemile Spring has increased its flow (Bottari, personal comm.).

In August 2017, 11 more grab samples were collected from ground-water seeps near the thermal anomaly and within the floodplain of the Humboldt River to the northwest of Wells. Two other grab samples from the Humboldt River were also collected in October 2017. All samples collected after April 2017, were analyzed only for their isotopic composition (C, O, H).

5.3.1 Sampling and Analytical Methods

Samples collected in April 2017 were collected either directly from sampling ports on well heads or using a peristaltic pump. Prior to sampling, field pH, electrical conductivity, and temperature were monitored until stabilized. All samples were collected using a syringe with in-line 0.2 micron filters, minimizing contact with air. Samples collected for analysis of metals by ICP-MS were collected in SARSTEDT 15 mL screw cap tubes with conical base; prior to sampling, ultra-pure HNO_3 was introduced into these vials in a quantity sufficient to keep the pH of the sampled fluid below 2. Samples for anion analysis by IC were collected in 2.0 mL clean Eppy centrifuge tubes, without headspace. Samples for TIC-TOC infrared analyses (total inorganic and total organic carbon) were collected in 40 mL VWR(R) TraceClean vials without headspace. Samples for O and H isotopic analyses were collected in 10 mL glass screw-cap bottles. Samples for dissolved inorganic carbon (DIC) and C isotopes were collected in evacuated 60 mL serum bottles.

5.3.2 Geochemical Data Processing

Both the newly acquired and previously collected geochemical data were processed to provide insights on the origin of sampled waters and geothermal reservoir temperatures. This included traditional graphical analyses, correlation plots, principal component analysis (PCA), the application of various classical chemical geothermometers, and multicomponent geothermometry computations. The results of these investigations are summarized in the next sections.

Table 5-1: Location and types of water samples collected for chemical and isotopic analysis. Figure 5-7 shows locations on a topographic map. (Coordinates are UTM Zone 11T)

ID	Name	Type	Date Sampled	Easting (m)	Northing (m)	Temp (°C)	(°F)
1	Rural Electric	City Well	4/26/2017	670402	4553365	34.6	94.3
2	Well #2	City Well	4/26/2017	670152	4552927	29.0	84.2
3	Well #6	City Well	4/26/2017	670727	4551696	26.0	78.8
4	Golf Course Well	City Well	4/26/2017	670407	4551729	23.3	73.9
5	Well #7	City Well	4/26/2017	669770	4551534	20.9	69.6
6	Well #5	City Well	4/26/2017	673571	4553291	25.4	77.7
7	Airport Well	City Well	4/26/2017	674053	4553531	13.5	56.3
8	Reynolds Well	Private Well	4/26/2017	670179	4554259	41.0	105.8
9	Arnold Merrill Well	Private Well	4/27/2017	672254	4552864	20.1	68.2
10	BTI Well	Private Well	4/27/2017	671971	4552744	30.5	86.9
11	Dan Morgan Well	Private Well	4/27/2017	668388	4551882	32.0	89.6
12	Reynolds House	Private Well	4/28/2017	671043	4551274	17.7	63.9
13	Bottari Well	Private Well	4/28/2017	668587	4558251	21.4	70.5
14	Threemile spg	Spring	4/27/2017	668990	4558659	41.6	106.9
15	Humboldt spg (lower)	Spring	4/27/2017	668512	4560914	53.0	127.4
16	Humboldt spg (upper)	Spring	4/27/2017	668692	4561041	44.9	112.8
17	Spring (NID 20)	Spring	4/28/2017	669320	4549216	16.2	61.2
18	Railroad Spg	Spring	4/28/2017	668782	4548025	23.7	74.7
19	"Last" Spring***	Spring	4/28/2017	668174	4556142	15.0	59.0
20	Twelve-mile spg (hot)*	Spring	June 2017	671949	4567732		
21	Twelve-mile spg (colder)*	Spring	June 2017	671949	4567732		
22	Trap Range Well*	Private Well	June 2017	673574**	4554566**		
23	Windmill Well*	Private Well	8/30/2017	670805	4557233		
24	Ritchie's Well*	Private Well	8/30/2017	670777	4554896		
25	Seep 1*	Seep/spring	August 2017	669562	4554634	17.0	62.6
26	Seep 2*	Seep/spring	August 2017	669515	4554624	13.5	56.3
27	Seep 3*	Seep/spring	August 2017	669499	4554658	17.2	63.0
28	Seep 4*	Seep/spring	August 2017	669472	4554688		
29	Seep 5*	Seep/spring	August 2017	669377	4554761	22.6	72.7
30	Seep 6*	Seep/spring	August 2017	669245	4554807	18.0	64.4
31	Seep 7*	Seep/spring	August 2017	669410	4554775	15.9	60.6
32	Seep 8*	Seep/spring	August 2017	669451	4554785		
33	Seep 9*	Seep/spring	August 2017	669328	4554851	15.4	59.7
34	Seep 10*	Seep/spring	August 2017	669240	4554871	16.4	61.5
35	Seep 11*	Seep/spring	August 2017	669260	4554901	16.4	61.5
36	E_Fork Humboldt River a*	River	10/1/2017	668167	4555708	8.2	46.8
37	E_Fork Humboldt River b*	River	10/1/2017	668167	4555708	8.2	46.8

* Samples 36 and 37 are duplicate grab samples collected in soda bottles – isotopic analyses only
**Approximate, from Google Earth general location
*** Arbitrary name chosen for this study

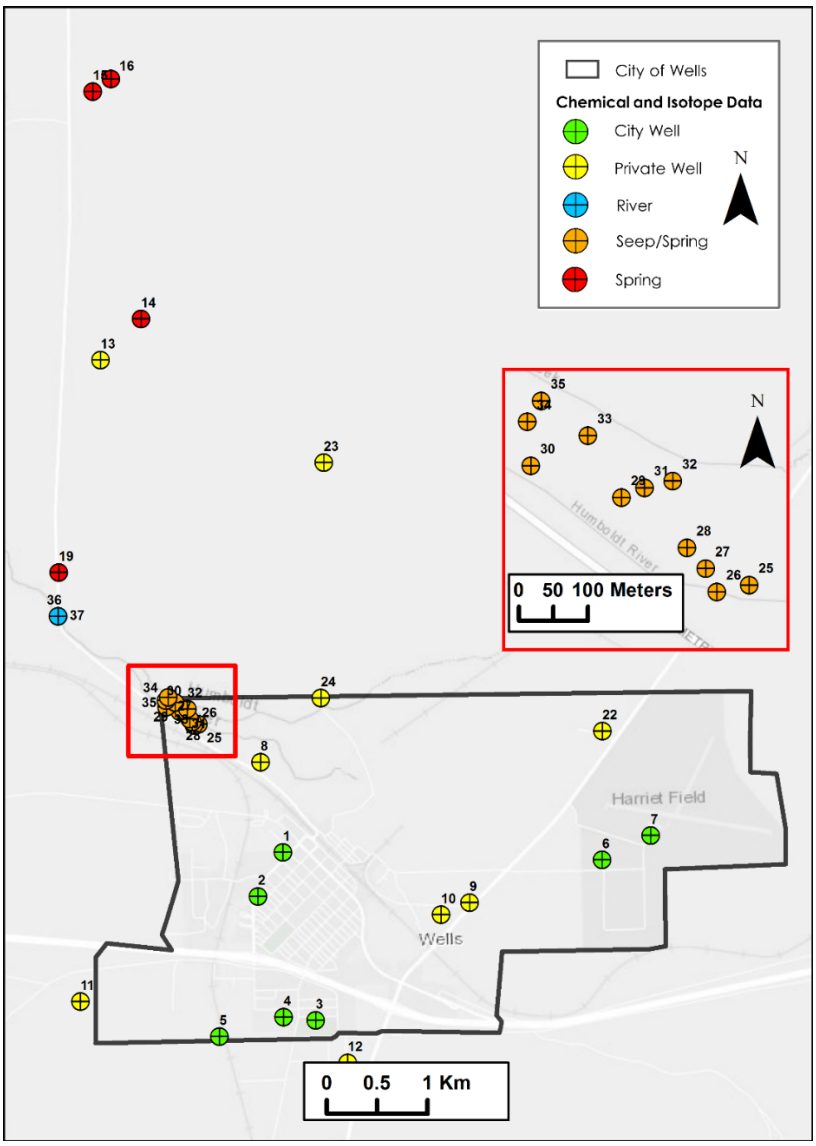

Figure 5-7: Location of water samples collected for chemical and isotopic analysis. The sample numbers correspond to those shown in Table 5-1. Note that three samples fall outside the map: Railroad Spring (#18) is located about 4 km south of Wells, around a km west of Old Clover Valley Road; and Twelve-mile hot spring (#20 and #21) is located about 20 km north of Wells along Bishop Creek.

5.3.3 Common Dissolved Ions and Trace Metals

In general, the new analytical results (Appendix G) are consistent with the previously reported data (Appendix F). Thermal waters in the vicinity of Wells can be characterized as sodium-bicarbonate waters with low chloride concentrations typically between about 10 and 40 mg/L. Waters with the highest total dissolved solids (around 2000 mg/L, primarily as bicarbonate with up to about 400 mg/L sodium) occur at Threemile and Humboldt hot springs, where thermal waters are found to also have the highest temperatures (between about 40 and 60°C) compared to

other sampled waters in the Wells area. Colder waters typically have higher proportions of calcium and magnesium (up to about equal proportions with sodium on an equivalent basis), and lower chloride concentrations. A few samples from the Humboldt River collected in October 2017 (#36 and #37, Appendix G) and one sample collected by Jewell et al. (1994) near that river (#51 in Appendix F) showed significantly higher chloride concentrations (> 100 ppm) attributed to evaporative concentrations along the non-perennial river.

Previous analyses using Piper diagrams suggested that mixing occurs between cold waters in the Wells area and the hot spring waters from Threemile and Humboldt hot springs to the northwest of the city (Jewell et al., 1994; Zehner 2016a) and explained the composition of waters at intermediate temperatures found in the Reynolds (#8), BTI (#10) and Rural Electric (#1). While such a mixing trend could be implied by looking only at major chemical parameters on a Piper diagram (Figure 5-8), a closer examination of all geochemical data, including trace metal and isotopic analyses not previously available, together with more detailed correlation analyses, show that waters along, and to the west of, the western Snake Mountain range-bounding fault have distinct chemical signatures from waters east of this boundary.

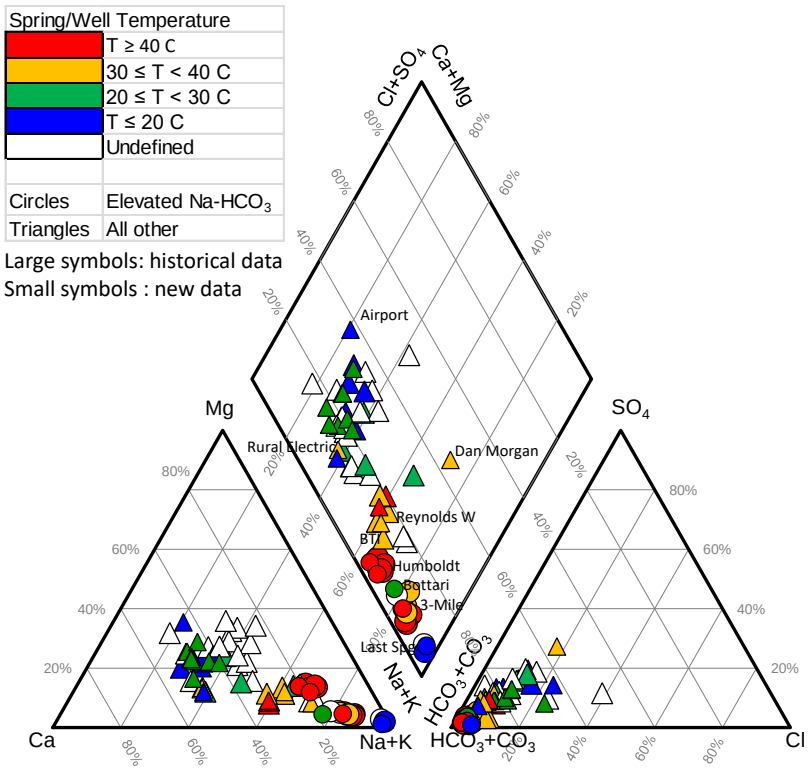

Figure 5-8: Piper diagram showing new (small symbols) and previous analyses (large symbols) of thermal and non-thermal waters in the vicinity of Wells. A close examination of these data reveals two groups of waters: those with elevated sodium and bicarbonate (high Na and HCO_3, shown with circles), and those with lower concentrations of these solutes (shown with triangles), with each group displaying its own separate mixing trend rather than one global mixing trend for all waters. Symbol colors indicate temperature as shown on the legend.

Indeed, the waters west of the fault show remarkably higher concentrations of sodium and bicarbonate when compared to the other waters (Figure 5-9). These include samples from the hot springs (#14, Threemile; #15 and #16, Humboldt), a sample from the Bottari well down-gradient and west of the hot springs (#13), and a cold spring sample collected one to two miles south-southwest of the hot springs at locations near the Snake Mountain range-bounding fault (#19, Last Spring). All historical data from these areas show the same trend of elevated sodium and bicarbonate concentrations compared to other waters sampled east of the range-bounding fault (Figure 5-9). These two distinct groups are hereafter referred to as the "Northwest Group" (elevated sodium and bicarbonate) and the "East" Group (lower sodium and bicarbonate than the Northwest Group).

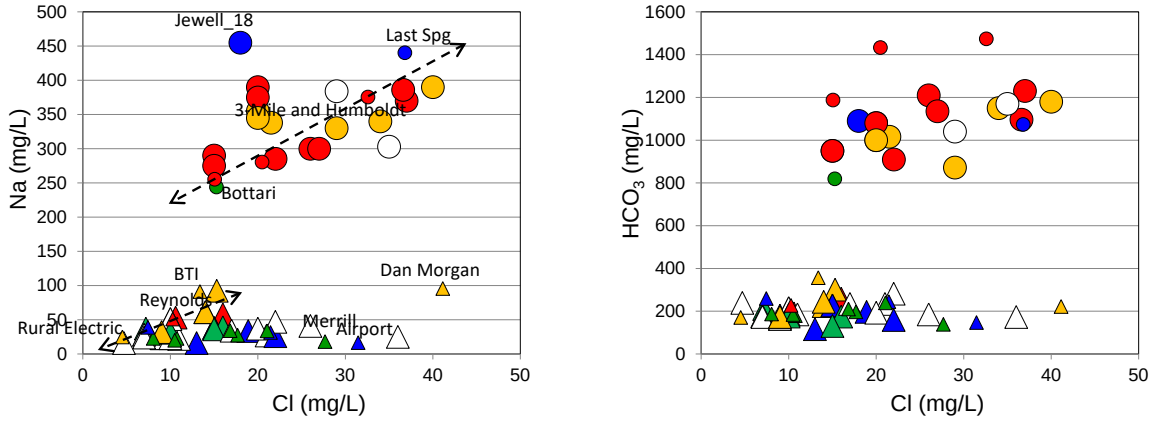

Figure 5-9: Plots of sodium (left) and bicarbonate (right) versus chloride concentrations using new (small symbols) and previous analyses (large symbols) of thermal and non-thermal waters in the vicinity of Wells. These plots show two distinct groups of waters: elevated Na and HCO_3 (shown with circles), and lower Na and HCO_3 (shown with triangles). Each group displays its own variability and/or mixing trend (dashed arrows). Symbols colors indicate temperature as shown on the legend of Figure 5-8.

Figure 5-9 also shows that the Dan Morgan well (#11 on Figure 5-7, located to the southwest of town) plots somewhat apart from the rest of the East Group waters, suggesting it may be tapping waters from a different zone than the rest of the East Group waters. This well also plots apart from other East Group waters on many of the diagrams discussed below.

The distinction between the Northwest and East groups of waters is also clear when looking at the concentration of other elements such as boron (B), lithium (Li), cesium (Cs), and germanium (Ge) (Figure 5-10). Boron and lithium are typically enriched in thermal waters, although elevated concentrations of these elements can also be found in evaporites and related saline waters. Cesium is often associated with felsic intrusives, and has a strong affinity to bind with clay minerals and for this reason it is often depleted in waters from clay-rich sedimentary rocks. Germanium has been found enriched in some hot springs; it is typically enriched in sulfide deposits and depleted in carbonate rocks; it displays a silicon-like behavior in water, with Ge/Si ratios typically higher in thermal waters than surface waters. The fact that these elements show a significant enrichment in waters from the Northwest Group compared to the East Group, and significantly higher Ge/Si ratios, in addition to elevated bicarbonate concentrations, could point

to an origin that is associated with deeper carbonate and/or igneous rocks, in contrast with shallower clay-rich continental deposits. An origin from deep rocks is also consistent with the association of hot springs with a range-bounding fault. In contrast, waters from the East Group could have been depleted in lithium and cesium while interacting with more clay-rich sedimentary rocks and also be depleted in boron and germanium because of a shallower, cooler origin or a greater distance from a deep source. A plot of cesium versus rubidium (Rb), which is another trace element taken up in clays, tends to support this hypothesis (Figure 5-11).

Another useful graphical analysis of these waters is the Giggenbach ternary plot of lithium, chloride and boron concentrations (Figure 5-12). This plot further shows the evolution of water compositions from more igneous waters enriched in B and Li at Humboldt and Threemile Springs to more chloride-rich waters at the Airport well. Interestingly, on this plot, the BTI well falls closer to the Northwest Group waters than either the Reynolds or Rural Electric wells.

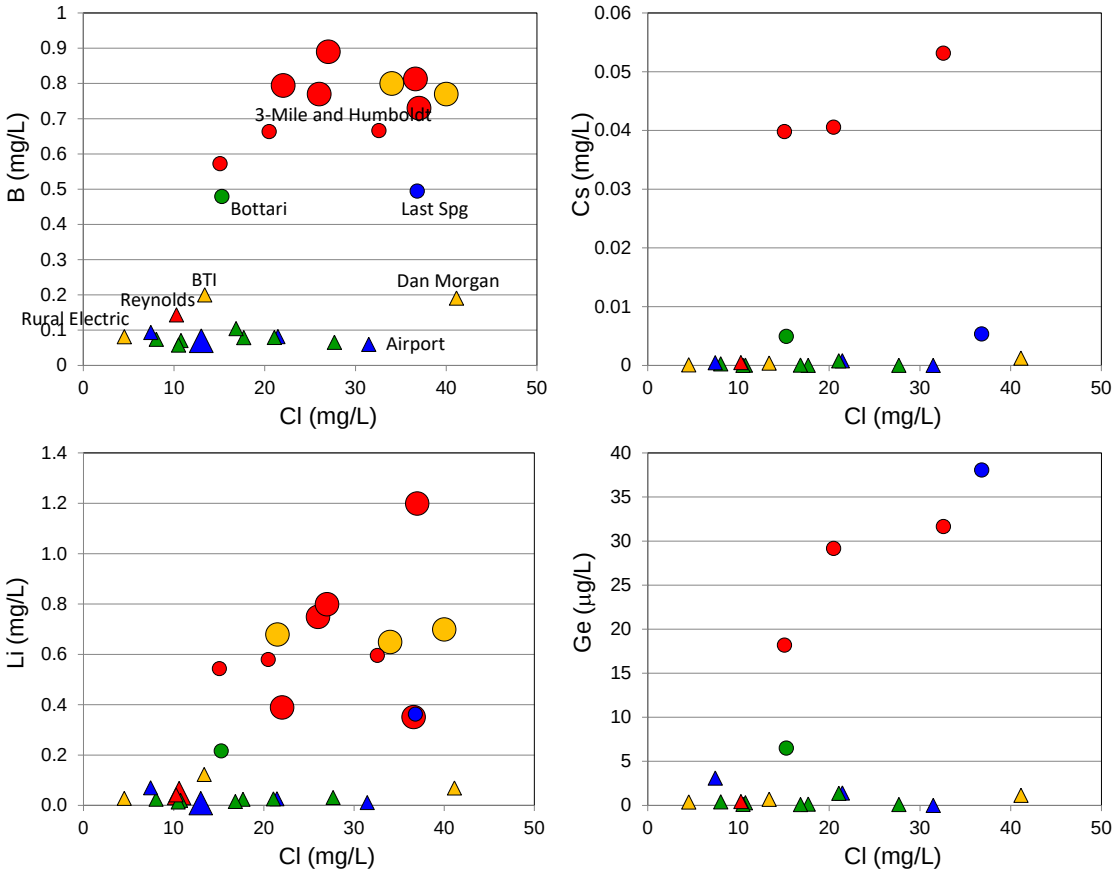

Figure 5-10: Correlations of various trace elements with chloride concentrations clearly show the distinct compositions of waters from the Northwest Group (circles) and East Group (triangles). Symbols colors indicate temperature as shown on the legend of Figure 5-8.

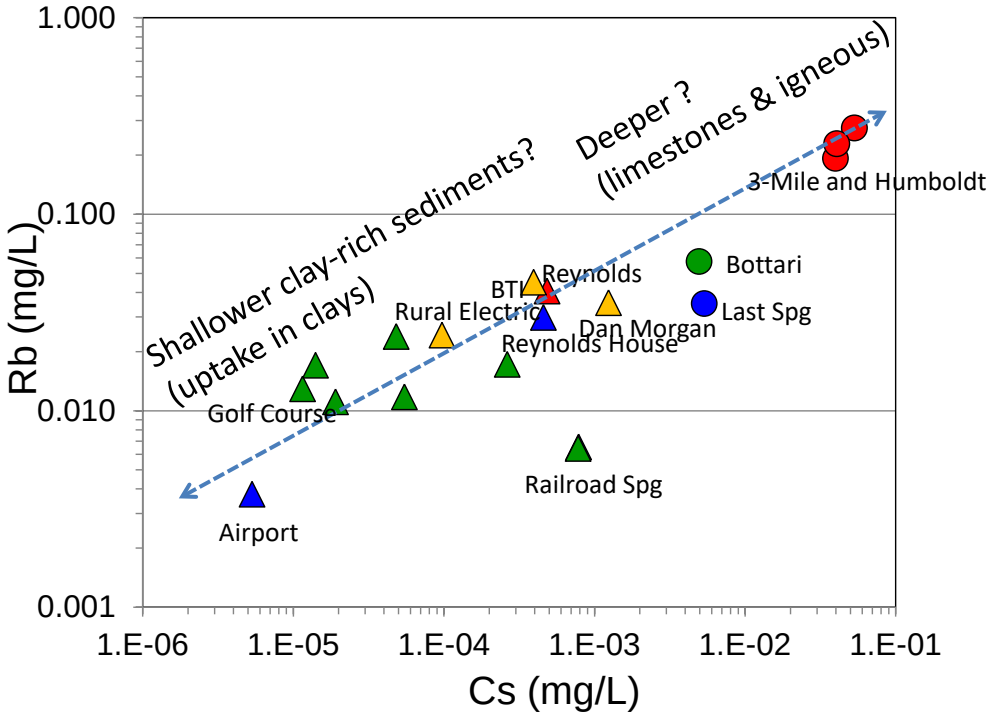

Figure 5-11: Correlation plot of rubidium versus cesium concentrations showing distinct compositions of waters from the Northwest Group (circles) and East Group (triangles). Symbols colors indicate temperature as shown on the legend of Figure 5-8.

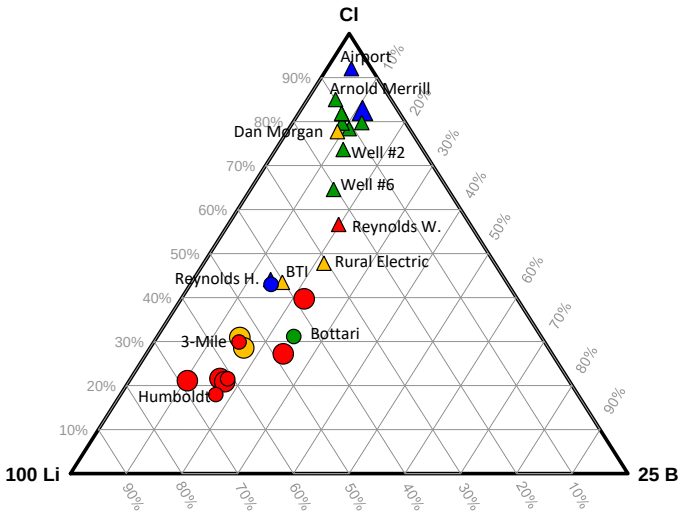

Figure 5-12: Giggenbach ternary plot of lithium (Li), boron (B), and chloride (Cl) concentrations showing the distinct compositions of waters from the Northwest Group (circles) and East Group (triangles). Symbols colors indicate temperature as shown on the legend of Figure 5-8.

Excluding the Dan Morgan well located to the southwest of town, waters sampled in the Rural Electric, Reynolds, and BTI wells had the highest temperatures in the East Group, with the Reynolds well the hottest (Table 5-1). On the log of the Reynolds well, a sharp increase in temperature was recorded from the depth of 111 m (starting with a 9-m-layer of volcanic conglomerate rock) to the well total depth of 165 m (Appendix E, L14 or Reynolds Well lithologic log); the perforated interval was not recorded, but the depth of the seal was recorded at 18 m. Thus, it is presumed this well was perforated from about 18 to 165 m. The log of the Rural Electric well shows a perforated interval between a depth of 145 m and total depth of 236 m, with a conglomerate layer starting at ~50 m depth (Appendix E, L19 or Rural Electric lithologic log). The log of the BTI well shows a perforated interval between 0 and 15m, and another perforated interval between ~228 and ~258 m. No lithology was logged for the upper perforated interval, and the lower perforated interval begins in a clay-rich conglomerate layer before intersecting siltstone and gravelly sandstone layers a greater depth (Appendix E, BTI lithologic log). The stratigraphic horizons between the other wells do not appear to correlate, although the lack of geologic detail in the logs makes any correlation difficult. Nevertheless, there appears to be a more or less linear relationship between these wells on the Piper diagram and concentration plots versus chloride, as shown in Figures 5-8, 5-9. The increasing chloride concentrations in these wells, however, do not follow a clear trend with temperature. This may be because the spread in temperature between these wells (only about 10°C) is too small to establish a clear trend. It should also be noted that water from the BTI well was sampled from a pipe connected to this well but with an outlet located more than 30 m away from the well head. Therefore, measured temperatures for this well are likely to be lower than actual temperatures at the well head.

When looking at the East Group waters as a whole, without the Dan Morgan well, there appears to be some inverse correlation of chloride with temperature (Figure 5-9, left, triangles only). This could be explained if thermal waters mixed with cooler, more saline, shallow ground water, which would be consistent with the significantly higher chloride concentrations measured in the Humboldt River than in the thermal waters. Therefore, progressive mixing of thermal waters originating in the area of the Reynolds and Rural Electric wells with a more saline and colder component from the East could conceivably explain the eastward trend of higher chloride concentrations but lower temperatures in some (but not all) samples of the East Group waters. These trends are consistent with shallow ground water flowing in a general western direction (as reported by Jewell et al., 1994) but are far from uniform. In fact, elevated temperatures measured in the BTI well located on the east side of town suggest that waters from this well could have as much, or possibly more, of a thermal component than the Reynolds well. The Giggenbach ternary diagram shown in Figure 5-12 and isotopic trends discussed below seem to confirm this hypothesis.

In contrast to the East Group, chloride concentrations tend to increase with temperature in many samples from the Northwest Group, although this trend is far from clear (Figure 5-13, left, circles). For both groups of waters, however, bicarbonate concentrations more clearly increase with temperature, with each group displaying its own trend (Figure 5-13, right).

The distinction between the Northwest and East groups of waters is also noticeable when looking at the concentration of other elements such as boron (B) and lithium (Li) as a function of temperature (Figure 5-14).

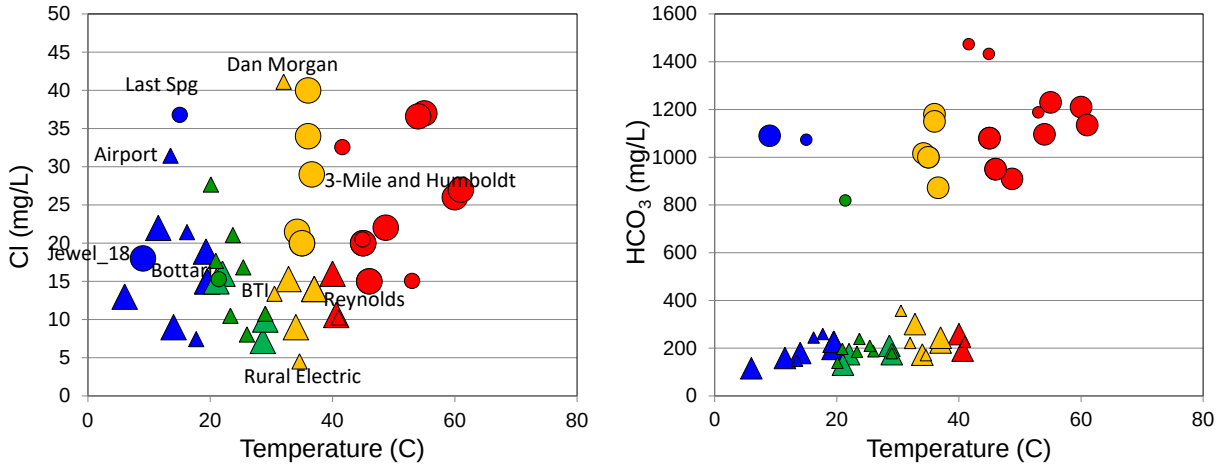

Figure 5-13: Plots of chloride (left) and bicarbonate concentrations (right) versus sampling temperature showing the distinct compositions of waters from the Northwest Group (circles) and East Group (triangles). Symbols colors indicate temperature as shown on the legend of Figure 5-8.

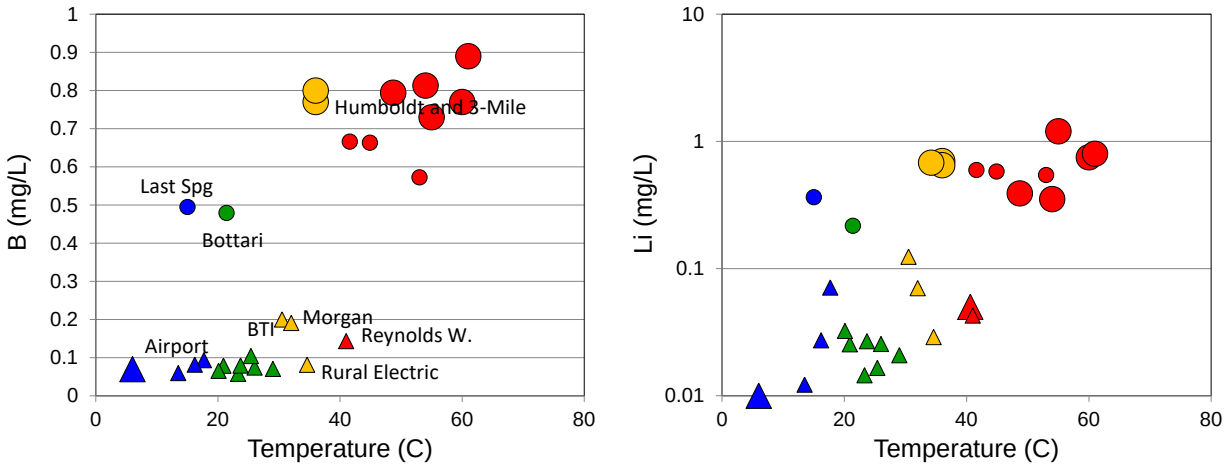

Figure 5-14: Plots of boron (left) and lithium concentrations (right) versus sampling temperature, showing the distinct compositions of waters from the Northwest Group (circles) and East Group (triangles). Symbols colors indicate temperature as shown on the legend of Figure 5-8.

Principal Component Analysis (PCA) was conducted to further investigate differences and potential relationships between the chemical compositions of the Northwest and East groups of waters, using the full suite of newly analyzed waters, including all trace elements. These analyses confirm the distinct chemical signatures between the Northwest and East groups of waters (Figure 5-15), and the strong correlation between bicarbonate (HCO_3), sodium (Na), boron (B), lithium (Li), cesium (Cs) and germanium (Ge) in the Northwest Group.

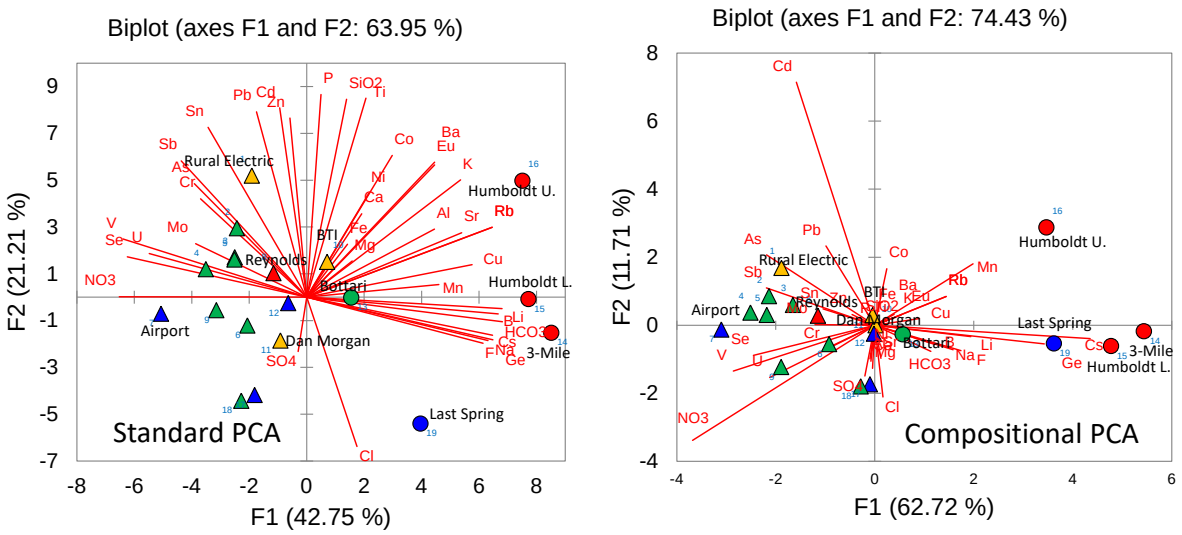

Figure 5-15: PCA biplots of the newly collected water chemistry data. Symbol colors indicate temperature as shown on the legend of Figure 5-8. The high bicarbonate waters (circles) plot separately from the other waters (triangles) in both the standard and compositional biplot. On such plots, lines (rays) are shown for each analyte, and symbols for each sampled location; rays that point toward symbols and/or plot within the same general region as symbols indicate that common factors can explain the variability of these analytes in the samples. Also, angles between rays are inversely proportional to correlation (i.e., the smaller the angle, the better the correlation).

Whether the thermal component in the East Group waters actually originates from the hot spring area is a question that is difficult to answer with certainty, although the clear separation and discontinuity in chemical compositions between waters of the Northwest and East Groups suggests that it is not likely. Rather, it would seem more conceivable that the thermal component in the East Group waters originate from one or more deep seated fault zones in basement rocks further east where the sedimentary cover is thicker (or where waters travel a longer distance in sedimentary units) than in the hot spring area. This would correspond to a conceptual model similar to that illustrated in Figure 2-1, lower diagram. Unfortunately, the lack of data on the depth of water production zones and/or the large perforated intervals in many wells precludes a thorough analysis of spatial concentration trends. However, it is interesting that even without depth-resolved data, isotopic trends for these waters show well-defined and remarkably different trends in the Northwest and East Groups, as discussed further below.

5.3.4 Isotopic Geochemistry

Isotopic analyses of hydrogen (H) and oxygen (O) isotopes in all sampled waters are shown in Figure 5-16. As seen with the general chemistry data, the isotopic compositions of the Northwest and East Groups of waters follow different linear trends. Waters from the East Group fall more-or-less aligned with, or close to, the line established for local meteoric waters in a climatic environment similar to that of Wells (data from Rightmire and Lewis, 1987, for rain in Idaho Falls, the closest location for which such data were found). It is interesting that data for Twelvemile hot springs, 12 miles north of Wells, also fall within the range of isotopic

compositions of East Group waters, suggesting an origin from recharge of rainfall for all these waters.

In contrast, waters from the Northwest Group are isotopically shifted to higher $\delta^{18}O$ values (Figure 5-16). Such a shift in waters in the Great Basin has been considered a possible indication of Pleistocene-age waters (Smith, 2002), which would imply a deeper origin for these waters than waters of the East Group. The shifted isotopic compositions for the Northwest Group waters also follow the arid meteoric water line defined by Welch and Preissler (1986) for an arid climate (Brady Hot springs area, Nevada) similar to that around Wells, although it is unclear how this line was defined by these authors. The composition of the seeps (points #25 to #35 in Table 5-1) appear to follow an evaporation trend from the line defining the East Group waters. This is consistent with the fact that these surface seeps were sampled during summer when surface evaporation is high. As would be expected, the trend of seeps also aligns with the Humboldt River samples, which showed high chloride concentrations (118 mg/L) compared to the rest of the sampled waters.

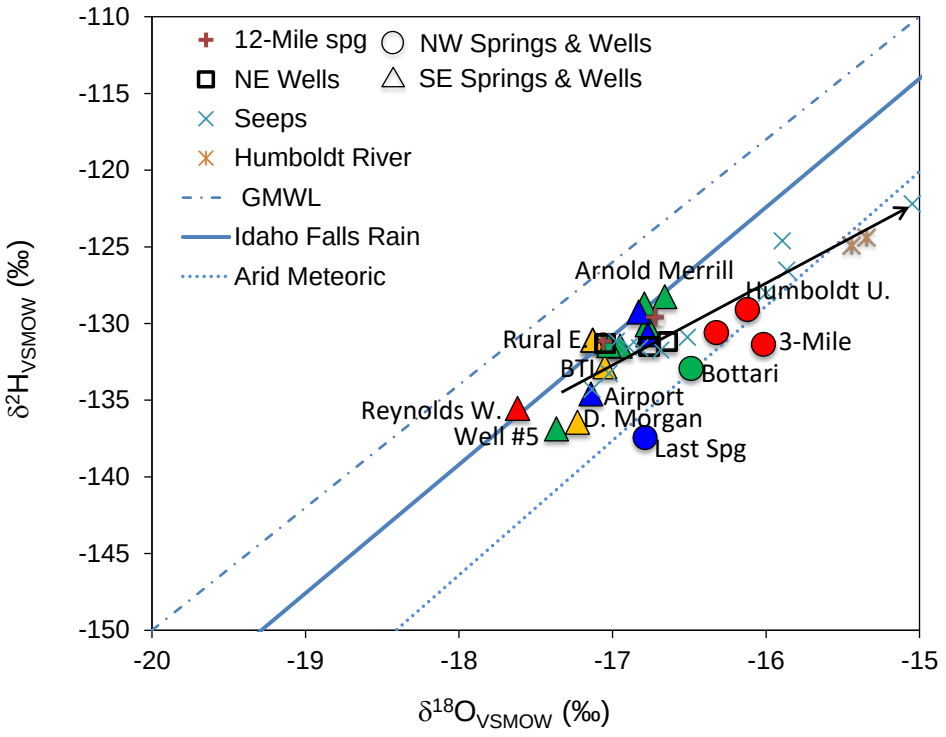

Figure 5-16: Plot of hydrogen versus oxygen isotopic compositions, showing distinct trends of waters from the Northwest Group (circles) and East Group (triangles and squares). Points shown as NE Wells in the legend (squares) correspond to the Richie's, Trap Range, and Windmill wells. Points shown as Seeps in the legend correspond to seeps 1-11 in Table 5-1; these seeps follow an evaporation pattern (arrow) and increasing chloride concentrations. Symbol colors indicate temperature as shown on the legend of Figure 5-8. GMWL stands for Global Meteoric Water Line. The line for Idaho Falls Rain is from Rightmire and Lewis (1987), and the Arid Meteoric line is from Welch and Preissler (1986).

The carbon isotopic composition, when plotted against dissolved inorganic carbon (DIC) concentrations (in this case essentially bicarbonate) show distinct trends for the Northwest and East Groups of waters (Figure 5-17). The $\delta^{13}C$ values are higher and DIC concentrations more elevated in the Humboldt and Threemile hot springs, which could reflect dissolution of deep Paleozoic limestones and/or metamorphosed carbonates at depth. The trend of decreasing DIC values and slightly increasing $\delta^{13}C$ values away from the hot springs could be compatible with progressive degassing of CO_2 from these waters as they outflow away from the range-bounding fault towards the Bottari well. In contrast, the much lower $\delta^{13}C$ values and lower DIC concentrations that define the trend of the East Group waters could imply waters associated with biogenically derived CO_2, at the lower end of the trend, mixing with degassed waters originating from a source similar to the NW Group waters. Because the BTI well plots closer to the hypothetical mixing point (where the dashed line on Figure 5-17 would intersect), but is located much farther east of the hot spring area than the Reynolds or Rural Electric wells, we conclude that the thermal component of the East Group waters is not likely to originate from waters feeding the hot springs. Rather, East Group waters likely originate from fluids that initially follow a similar chemical evolution as the hot spring fluids at depth, but at a different location further east along one or more concealed faults. These fluids would then migrate through clay-rich sediments, lose their deeper trace element signature, degas and mix with shallower ground waters.

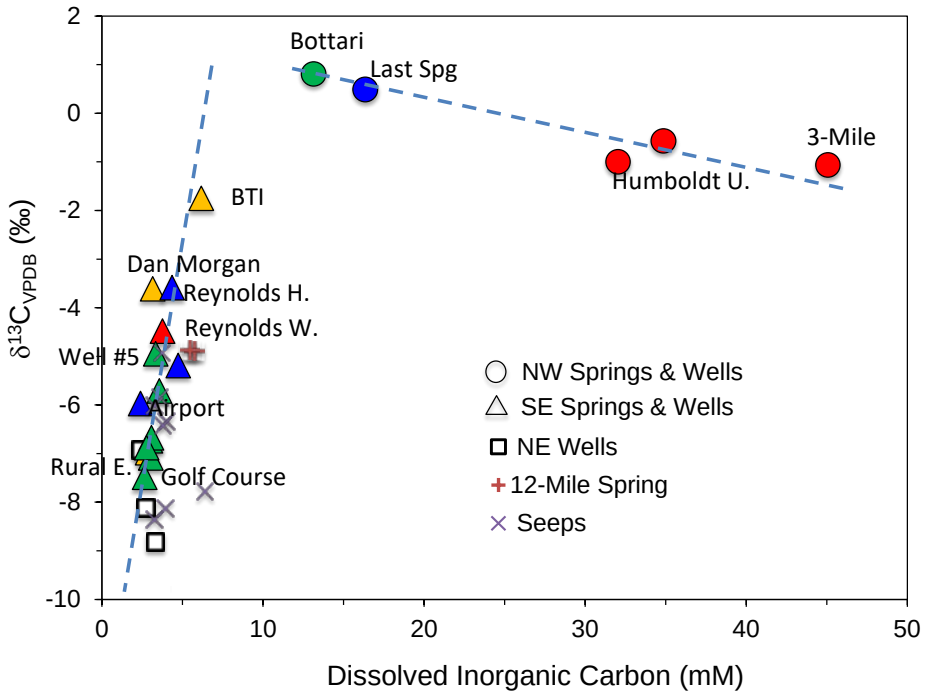

Figure 5-17: Plot of carbon isotopic composition versus dissolved inorganic carbon, showing distinct trends of waters from the Northwest Group (circles) and East Group (triangles and squares). Points shown as NE Wells in the legend (squares) correspond to the Richie's, Trap Range, and Windmill wells. Points shown as Seeps in the legend correspond to seeps 1-11 in Table 5-1. Symbol colors indicate temperature as shown on the legend of Figure 5-8.

5.3.5 Geothermometry

Reservoir temperatures were estimated using various solute geothermometry approaches with chemical analyses from previous studies and new samples. Because new and previously reported chemical analyses were found to be fairly consistent, we report here only on results of the new data.

Classical geothermometers yield very inconsistent results with both the sampled thermal and cold waters (Figure 5-18). This is typically observed with waters from the Basin and Range province because of ambient re-equilibration, equilibration with minerals different from those on which classical geothermometers are based, and/or dissolution of salts in the shallow subsurface that mask the chemical signature of deep reservoirs (e.g., Peiffer et al., 2014). Dilution with cold ground water also affects the results of classical geothermometers that do not rely on a straight ratio of chemical elements, as is the case with the silica, K/Mg and Na-K-Ca geothermometers. For waters with discharge temperatures above 30°C (Figure 5-18, top), the highest temperatures were obtained with the Na/K geothermometer (at ~ 230°C and above) and lowest temperatures with the K/Mg geothermometer (below 100°C). With waters colder than 30°C (Figure 5-18, bottom), calculated temperatures were even lower except for higher and unrealistic Na/K temperatures. None of these calculated temperatures should be considered reliable. The silica-quartz temperatures of the thermal waters fall for the most part between 120 and 140°C; these values apply to undiluted waters and would be higher if mixing occurred with cold ground waters of lower silica concentrations.

The Giggenbach ternary Na-K-Mg geothermometer is useful to assess the degree of equilibrium within a geothermal reservoir, by simultaneously looking at the temperatures calculated with the Na/K and K/Mg geothermometers. This geothermometer shows that samples from the hot springs (Threemile and Humboldt) yield consistent Na/K temperatures around 230°C, but fall far from the line defining "equilibrated" waters (i.e., defining consistent Na/K and K/Mg temperatures) (Figure 5-19). Samples from other waters fall even farther away from that line, except for the cold samples from the Northwest Group (Last Spring, and another sample collected by Jewell in the same area) which may have partially re-equilibrated at temperatures around 110°C or less (Figure 5-19). All samples can be considered "immature" waters, for which the application of classical geothermometers is not recommended.

Multicomponent geothermometry computations using the iGeoT software (LBNL: https://eesa.lbl.gov/technology/geot/; Spycher et al., 2014) were carried out to try narrowing the range of estimated reservoir temperatures. This method relies on the full analyses of water samples and allows for the reconstruction of deep water compositions to account for effects of mixing, degassing, or reactions that are not necessarily those on which classical geothermometers are based. The iGeoT software relies on computed saturation indices of alteration minerals that constrain the composition of deep geothermal waters. These minerals typically are not known, and because results can differ depending on the choice of minerals selected for the computations, this method is not without uncertainty. Nevertheless, the iGeoT method involves a numerical optimization scheme that can be used to narrow down the list of conceivable minerals for temperature determinations, and also to compute unknowns such as the fraction of exsolved gas (mostly CO_2) and amount of dilution that could have affected the thermal waters on their way to the ground surface.

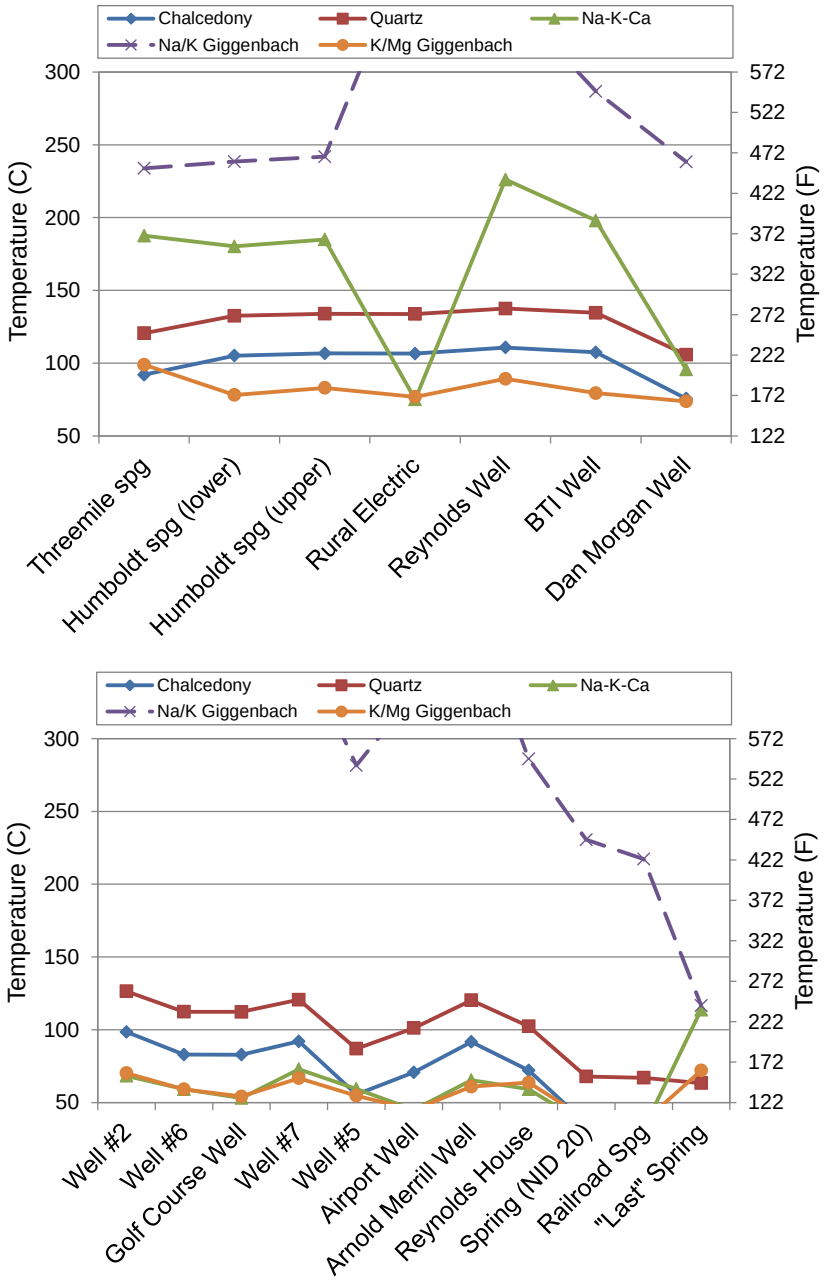

Figure 5-18: Reservoir temperatures predicted using traditional geothermometers (Na-K-Ca, Fournier and Truesdell, 1973; Na-K and K/Mg, Giggenbach, 1988; chalcedony, Fournier, 1977; quartz, Fournier and Potter, 1982) for thermal waters with discharge temperatures greater than 30°C (top) and other colder waters (bottom). These geothermometers yield highly inconsistent results and are most likely not suitable for these waters.

This method was applied to samples from Threemile and Humboldt hot springs (sample #14 and #15, respectively), and from the BTI and Reynolds thermal water wells (samples #10 and #8, respectively). With the hot springs samples, convergence to a narrowly defined reservoir

temperature could only be achieved by maintaining waters at equilibrium with quartz and calcite during the computation. Using only a few additional minerals (kaolinite, K-feldspar, and montmorillonite), measured Al and Mg concentrations, and solving for a dilution factor and fraction of exsolved gas, excellent fits were obtained around temperatures of 180°C. These calculations for the hot spring waters yielded essentially no dilution and small amounts of degassing (Figure 5-20, top). With more minerals, a good clustering of saturation indices could be achieved around temperatures of 200-220°C but yielding larger dilution factors around 2.0 that may be less probable for the hot springs.

For the Reynolds and BTI wells, similar computations yielded somewhat lower temperatures in the 160°C range (Figure 5-20, bottom) but larger dilution factors near 1.5. Because the composition of waters at these wells is more dilute than the hot springs, dilution in this case is more conceivable. As for the hot spring waters, computations using more minerals yielded higher temperatures in the 200-220°C range and higher dilution factors, although with a broader cluster of mineral saturation indices.

Overall, it was difficult with all waters to obtain a narrow cluster of mineral saturation indices. Because higher temperatures could be computed with higher dilution factors (but worse clustering), and because measured Al concentrations could be too low if Al dropped from solution upon cooling, which would result in underestimated temperatures, the temperatures shown by the clustering of mineral saturation indices on Figure 5-20 are likely to be minimum temperatures.

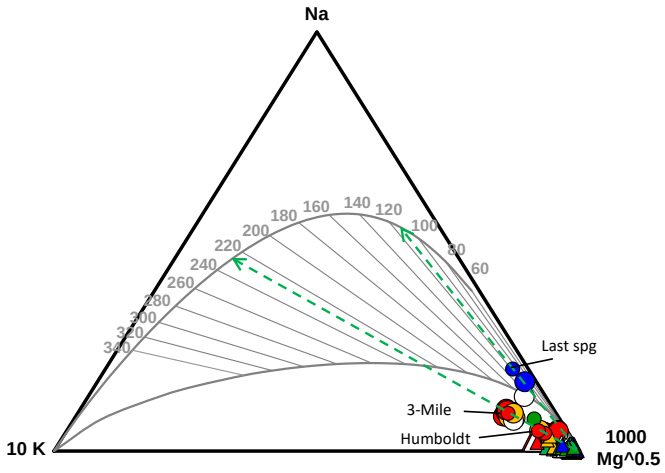

Figure 5-19: Na-K-Mg ternary geothermometer (Giggenbach, 1988) showing waters from the Northwest Group (circles) and East Group (triangles and squares). The dashed arrows indicate the range of Na/K temperatures (in degrees C) of the Northwest Group waters. The line with temperature labels defines "mature" waters for which the Na/K and K/Mg geothermometers would yield identical temperatures. All samples fall significantly away from this line, implying "immature" waters to which these geothermometers are likely not applicable. Symbol colors indicate discharge temperature as shown on the legend of Figure 5-8.

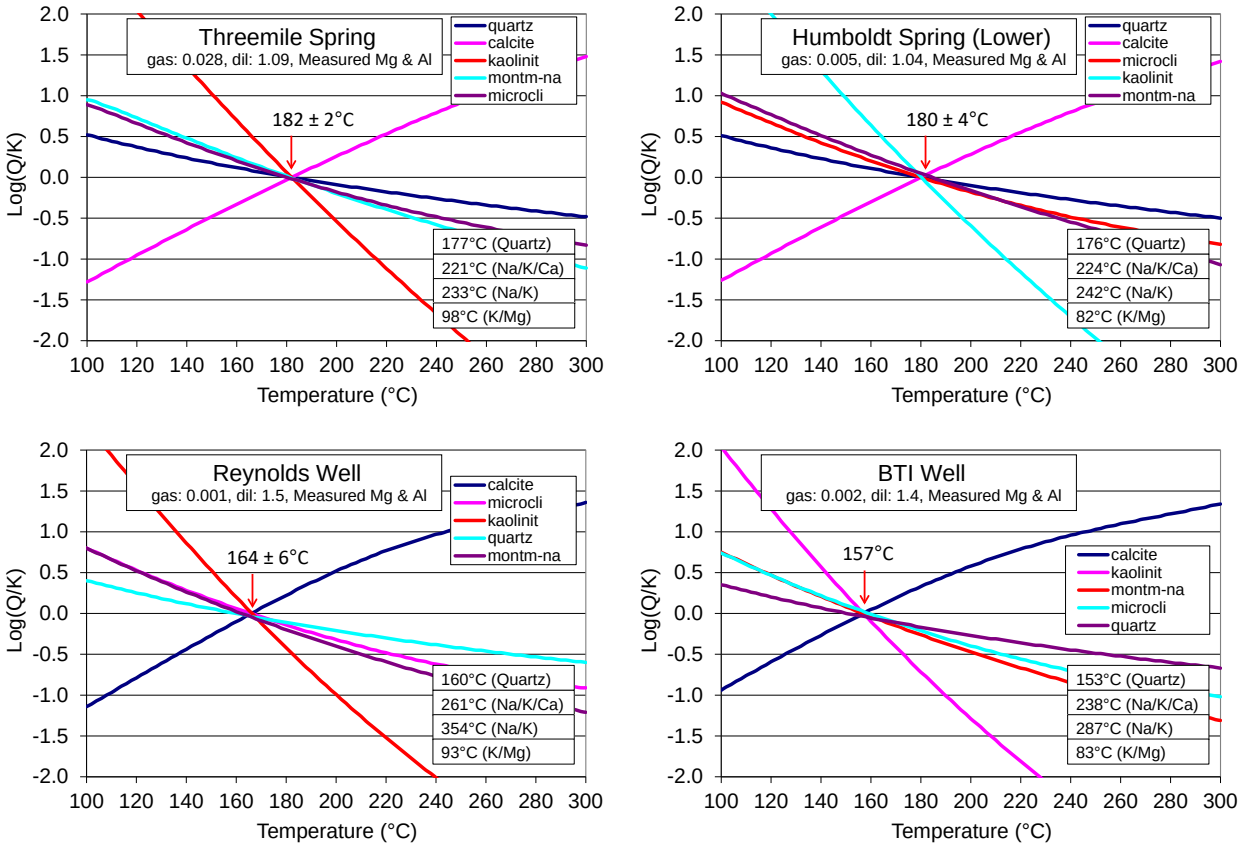

Figure 5-20: Computed mineral saturation indices (Log(Q/K)) as a function of temperature. Equilibrium temperatures are shown at Log(Q/K) = 0. The gas fraction ("gas") and dilution factor ("dil") estimated by numerical optimization are shown below each title. Results of classical geothermometers using the reconstructed water composition (undiluted and with re-dissolved gas) are also shown.

5.4 ELECTROMAGNETIC INDUCTION (EMI) AND DIRECT CURRENT (DC) RESISTIVITY SURVEYS

Two complementary, near-surface geophysical methods (electromagnetic induction and direct current resistivity) were used to explore the shallow subsurface in the Wells study area. In July 2017, an electromagnetic induction (EMI) survey was deployed to determine the near-surface apparent conductivity of a geothermally promising subset of the study area, located in the headwaters of the Humboldt River. The site is located in an area bounded by Old Metropolis Road to the north, and Metropolis Road to the south, and is referred to hereinafter as the "Metropolis Road Site" (Figure 5-21). A second EMI survey (not shown in this report) was performed in proximity to Threemile Spring as a test of the electrical conductivity of hydrothermal waters. Both survey locations were selected due to the presence of anomalously high temperatures measured in the Geoprobe survey and the prospects of hydrothermal outflow features (Section 5.1.2).

In September 2017, three direct current (DC) resistivity surveys were used to probe to a greater depth than the EMI survey, and to provide the distribution of resistivity $\left(\frac{1}{conductivity}\right)$ with respect to depth. The DC resistivity profiles were acquired on the north side of the Humboldt River within an area of high conductivity identified by the EMI survey (Figure 5-21). Each DC resistivity survey had a different electrode spacing and different array configuration. The motivation for completing the EMI and DC resistivity surveys was to:

1. Explore and map anomalous conductive features related to the accumulations of solutes in the near-surface, possibly related to waters of geothermal origin.
2. Determine the apparent conductivity of saturated soils from a nearby hot spring area.
3. Find possible correlations between other direct physical measurements, such as temperature, and the apparent conductivity measurements derived through geophysical methods.
4. Find any possible correlations and supporting evidence for features depicted on geologic maps based upon the apparent conductivity mapping results.
5. Generate 2-dimensional models of the subsurface depicting resistivity $\left(\frac{1}{conductivity}\right)$ as a function of depth to better characterize geologic strata, zones of saturation, and possible faults.

The overall objective for the geophysical mapping was to obtain additional information that would be used in combination with other field observations to help identify a favorable location for siting a geothermal exploration well.

5.4.1 EMI Field Survey

A Geophex GEM-2 broadband inductive conductivity instrument (Won et al., 1996) was used to perform a walking EMI survey at the Metropolis Road Site. The GEM-2 uses a primary coil to transmit a time-varying magnetic field into the ground (a multiplexed signal composite of five frequencies including 450 Hz, 1530 Hz, 5310 Hz, 18330 Hz, and 63030 Hz), which, in turn, induces electrical currents (eddy currents) to flow in subsurface conductors. Subsurface electrical currents create a secondary magnetic field (phase shifted 90° to 180° from the primary magnetic field) that is detected by the GEM-2 receiver coil and has an intensity directly proportional to soil conductivity. A third "bucking coil" removes any direct coupling between the primary signal and the receiver. The ratio of GEM-2 receiver /transmitter coil's magnetic field strengths are directly proportional to the apparent or bulk conductivity of the soil reported in milli-Siemens per meter. The instrument was oriented in a horizontal coplanar coil geometry, resulting in a vertical dipole mode of operation. The instrument was factory serviced and calibrated 2 weeks prior to the Wells geothermal field investigation.

A serpentine survey course was completed, having a nominal line spacing of 30 m, using a custom software application composed by NETL. Survey guidance (also a custom application) was provided by a track-up, GPS-linked, moving map vector representation of the survey course.

Data from the GEM-2 was transmitted via Bluetooth™ wireless communication at 10 Hz and recorded to file on a tablet PC. A dedicated WAAS-enabled, GPS receiver was mounted to the GEM-2 and linked to the data acquisition system, providing location and timestamp information for each measurement. GEM-2 data was collected in 18 sessions at the Metropolis Road Site,

totaling 176,570 data soundings. Each measurement contains easting (x), northing (y), elevation, time, and in-phase and quadrature field components for a total of 14 channels per record. The GEM-2 data acquisition application, WinGEM2 (Geophex, Ltd., 2008), automatically synchronizes recorded measurements to GPS time. No appreciable lag was expected in the data because the GPS antenna was mounted on the instrument, and the average survey speed was 0.9 m/s. A GEM-2 drift check was performed before and after each survey by collecting data with the instrument stationary for ~2-3 minutes in an area away from conductive materials. The test detects signal drift due to temperature variation and battery drain, and provides a means to correct datasets for these types of aberrations.

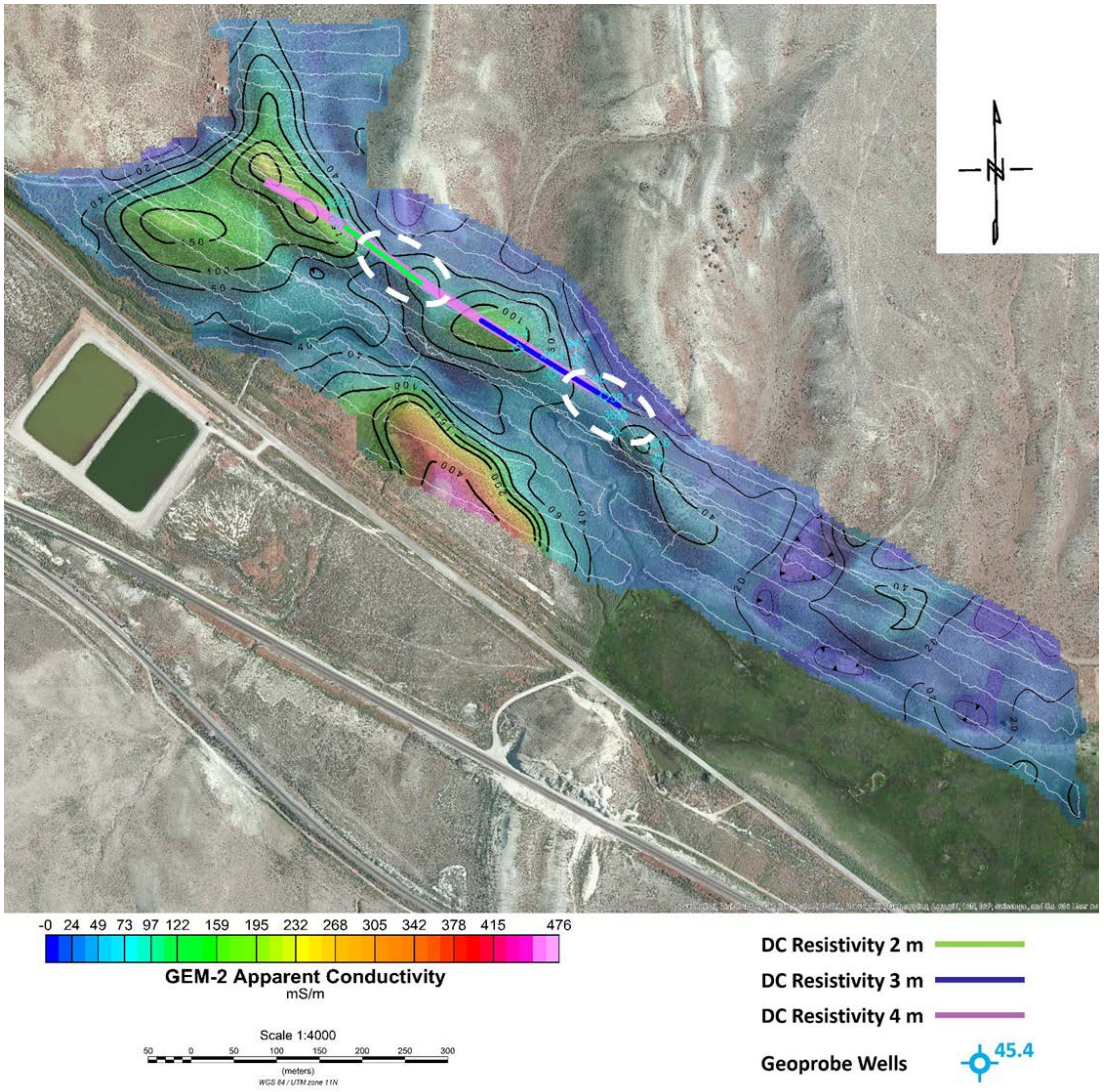

Figure 5-21: Color-scale, near-surface EMI (GEM-2 apparent conductivity) map of the Metropolis Road Site. Colored lines show the locations of 2-m, 3-m, and 4-m DC resistivity surveys in green, blue, and magenta, respectively. Dashed white ovals depict areas with shallow geothermal potential based on results of the EMI and DC resistivity surveys and soil temperature measurements.

The GEM-2 raw data was processed using a custom NETL application that calls CONDSUS.exe, an embedded application (Huang et al., 2000; 2001) to convert low-induction number, and frequency domain EMI data, from parts per million to apparent conductivity units that were stored in an ASCII comma-separated-values format for import into Geosoft Oasis Montaj Software. Geosoft was used to process the data to generate grids and contour maps depicting apparent conductivity at discrete frequencies.

Exploration depth for the GEM-2 instrument is approximated using skin depth (D). Skin depth is a complex relationship dependent on frequency (f), dipole moment (μ), and soil conductivity (σ) (Figure 5-22). In general, the greatest exploration depth is achieved when soil conductivity is low and when energy from lower frequencies is used.

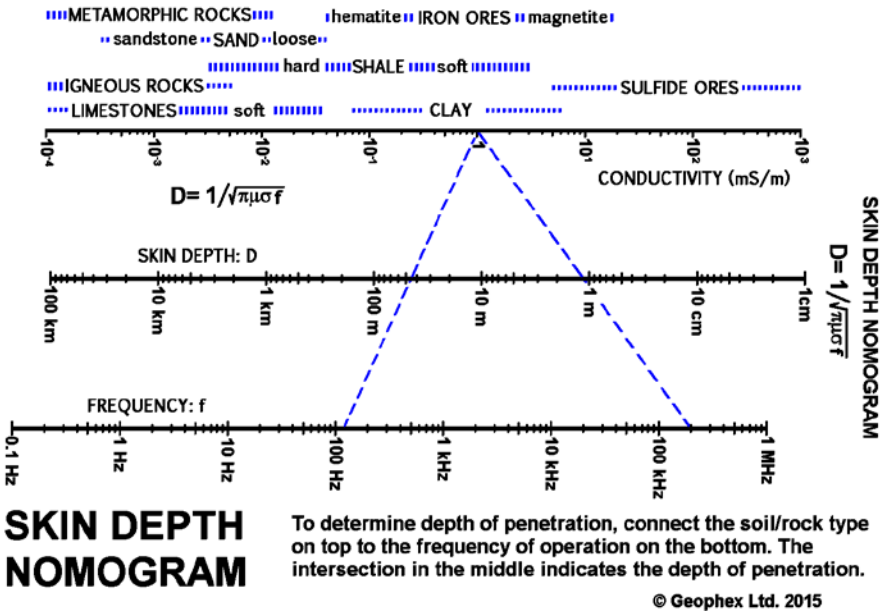

Figure 5-22: Skin depth nomogram diagram for estimating exploration depths for the Geophex GEM-2 instrument.

5.4.1.1 EMI Survey Results

The GEM-2 survey of the study area (Figure 5-21) found conductive areas that spatially correspond to upper terraces with sparse vegetation on both sides of the Humboldt River. The evaporative concentration of salts within the vadose zone could explain the high conductivity and the inhibition of plant growth observed along these upper terraces. Because the highest conductivity was found where small valleys open into the broader Humboldt River valley from the south (highest conductivity) and north, solutes dissolved in the alluvial flow or ephemeral streams emerging from small valleys may be the source of salts in the terraces. Low-lying terraces, the riparian zone, and the Humboldt River channel were less conductive and supported dense vegetation. Salts were likely washed from soil in these areas by ground water flow in the alluvial aquifer and by seasonal flooding of the Humboldt River. The least conductive areas were found where the survey intersected the ends of ridges - dry areas with thin soil and shallow bedrock.

Geothermal prospecting using GEM-2 surveys may involve looking for low conductivity areas along the upper terraces that typically exhibit high conductivity. The rationale is that a geothermal water source for district heating would require significant flow; a flow that would flush salts from soils contacted by the geothermal water, making these areas less conductive. Geothermal flows emerging in areas along the Humboldt River channel and floodplain would likely not be detected because these areas typically exhibit low conductivity and would present no contrast to geothermal waters with low conductivity. Using this rationale as a guide for geothermal prospecting, two areas of low conductivity were identified as geothermal targets along an elongated area of high conductivity (Figure 5-21, white dashed circles) on the north side of the Humboldt River.

5.4.2 DC Resistivity Field Survey

DC resistivity surveys were performed using the SuperSting R8 IP, an 8-channel earth resistivity and IP instrument (Advanced Geosciences, Inc., 2009). For this study, the R8 instrument was operated in resistivity mode using a 56-electrode array deployed along a linear profile with uniform electrode spacings. Initially, a long (444-m) profile was acquired with 4-m electrode spacing to obtain the greatest depth of investigation (≤ 50-m depth). Subsequently, shorter segments of interest from the 4-m survey were further investigated using deployments with 2-m and 3-m electrode spacing to obtain more detailed, but shallower, profiles. For the 2-m deployment only, electrode interrogation used dipole-dipole, Schlumberger, and Wenner array geometries. Surveys with 3-m and 4-m electrode spacing used dipole-dipole array geometry with the roll along of multiple, 8-electrode segments.

Data from each DC resistivity profile were downloaded and inverted using AGI EarthImager 2D software to obtain resistivity/depth modeled sections that can show subsurface geological features having sufficiently contrasting electrical resistivity. Prior to inversion, statistical processing was used to identify and remove noisy data that often are the result of poor contact between the electrodes and ground (high contact resistance; >2000 ohms). The edges of inverted resistivity sections commonly contain artifacts from the inversion; a blanking function in EarthImager is used to remove these areas so inherent processing artifacts are not a source of misinterpretation.

The first DC resistivity profile was run in a west-east direction (roughly parallel to the Old Metropolis Road) starting at 668667E, 4555468 N and ending at location 669041 E, 4555229 N. The terrain was nearly level along the profile ranging between 1704 and 1707 m MASL. A dipole-dipole survey geometry (Figures 5-23, 5-24) with 4-m electrode spacing was used for this profile because dipole-dipole surveys provide good resolution of vertically-oriented features, acceptable depths of exploration, and short survey times. The initial deployment was 220-m long, and eight electrode segments (each totaling 32 m) were rolled along for 7 iterations, traversing some 444-m total distance from the survey origin (Figure 5-21, magenta line).

A second 2-meter DC resistivity profile (Figure 5-21, green line) was acquired after repositioning and centering the 56-electrode array over a group of anomalously conductive features observed about 20 m below the surface in the resistivity profile from the initial survey. The 2-m electrode spacing was used to obtain a total profile length of 110 m, originating at 668755 E, 4555416 N and ending at location 666844 E, 4555350 N. No “roll along” profile extensions were run. The 2-m (versus 4-m) array was employed to improve the horizontal

resolution of features. Three different array geometries: Dipole-dipole, Wenner, and Schlumberger were used for this profile.

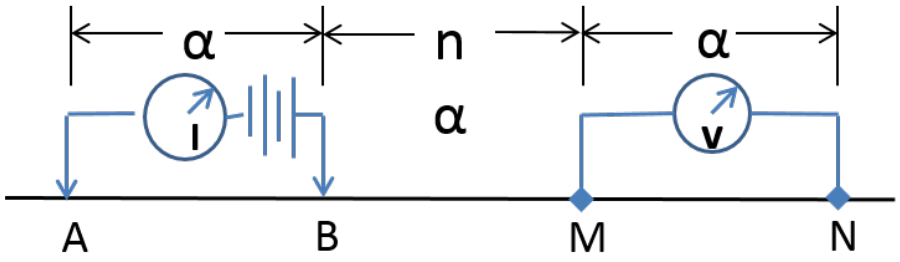

Figure 5-23: Dipole-dipole electrode configuration. The dipole electrodes are spaced equidistant while the spacing between electrode pairs is an integer multiple of the electrode spacing.

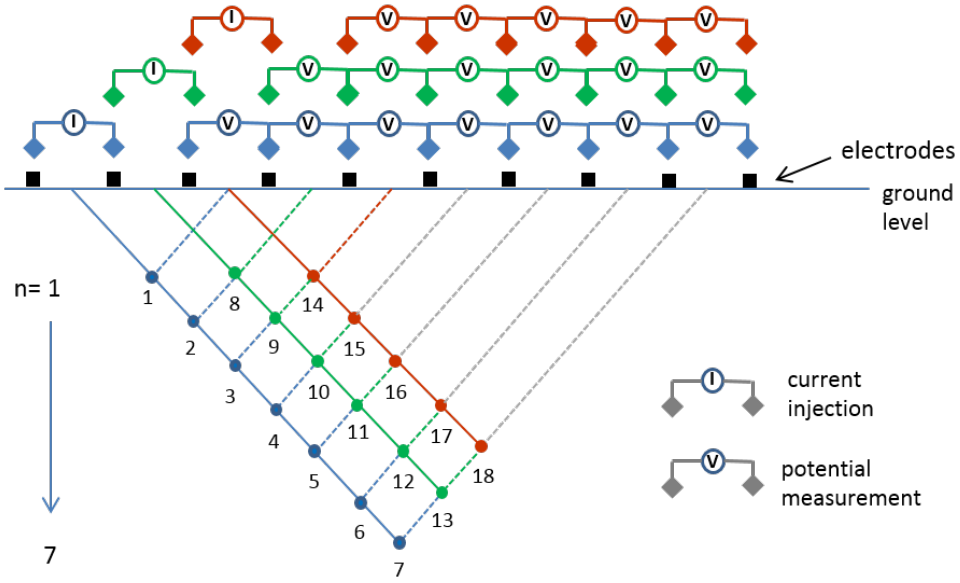

Figure 5-24: DC resistivity survey profile schematic showing 3 iterations of dipole-dipole geometry data acquisition sequencing.

A third, 3-meter, DC resistivity profile (Figure 5-21, blue line) was acquired by centering the 56-electrode array over a narrow and prominent vertically-oriented, resistive feature observed at about 354 m along the resistivity profile from the initial survey. The objective of the third DC resistivity survey was to provide a more detailed image of the deep, resistive feature and to achieve a better understanding of its origin. The third DC resistivity profile employed a dipole-dipole array with 3-m electrode spacing, and was approximately 189 m in length, including a single roll-along consisting of 8 electrodes (24 m). It originated at 668914 E, 4555307 N and ended at location 669076 E, 4555207 N.

5.4.2.1 DC Resistivity Survey Results – 4-m Electrode Spacing

The resistivity/depth model in Figure 5-25, depicts a near-surface zone of low resistivity (high conductivity), approximately 4-m thick that is present in the intervals: 0 - 134 m and 168 – 348 m. This agrees with the location of conductive areas in the EMI conductivity map (Figure 5-21) and is interpreted to represent the evaporative concentration of salts in the vadose zone. Beneath the near-surface conductive layer is a resistive layer of varying thickness (typically 2 to 4-m thick) that is present across the 444-m-long profile. Beneath the resistive layer is a discontinuous conductive layer that is notable for its extremely low resistivity in certain areas that suggest a porous material containing highly conductive pore fluids (brine) or perhaps low porosity clay-rich material with brackish pore water. A highly resistive body can be seen in the lower portion of the 4-m resistivity/depth model that is presumed to be bedrock. The inferred bedrock surface is denoted by a dashed black line in Figure 5-26.

5.4.2.2 DC Resistivity Survey Results – 2-m Electrode Spacing

A DC resistivity survey 110 m in length with 2-m electrode spacing was conducted over a body of extremely low resistivity (high conductivity) identified between 13- and 25-m depth in the 4-m resistivity profile (Figure 5-25, black dashed box). This profile was centered over a conductive body of interest and was interrogated using dipole-dipole, Schlumberger, and Wenner array geometries. All array geometries showed a discontinuous, highly conductive layer beneath a continuous, resistive layer and provided more detail to the findings of the original 4-m resistivity survey. Because the depth of investigation was decreased using 2-m electrode spacing (versus 4-m electrode spacing), the interpreted bedrock surface was not observed.

5.4.2.3 DC Resistivity Survey Results – 3-m Electrode Spacing

A DC resistivity survey 189 m in length with 3-m electrode spacing (Figure 5-26) was conducted over an area containing an unusually shaped, resistive pinnacle in the 4-m resistivity profile that was interpreted to be a bedrock high. Because the resistive pinnacle was near the edge of the resistivity profile, an area prone to modeling artifacts, a second, more detailed resistivity profile that extended beyond the pinnacle was needed to show that it was real. Because of the reduced depth of investigation, the subsequent resistivity survey with 3-m electrode spacing only showed the top of the resistive pinnacle, but confirmed that it was not a modeling artifact. Surficial geologic mapping by Zuza (2017) (Appendix D, this report) inferred a normal fault at the approximate location of the resistive pinnacle (interpreted bedrock pinnacle). A normal fault at this location is consistent with the bedrock high inferred from the resistivity profile obtained at 4-m-electrode spacing (see dashed fault, Figure 5-25). The 3-m resistivity profile shows areas of very low resistivity (high conductivity) above and on each side of the resistive pinnacle. Like other highly conductive areas at this depth to the west, these areas could represent porous material containing highly conductive pore fluids (brine) or perhaps a low porosity clay-rich material with brackish pore water.

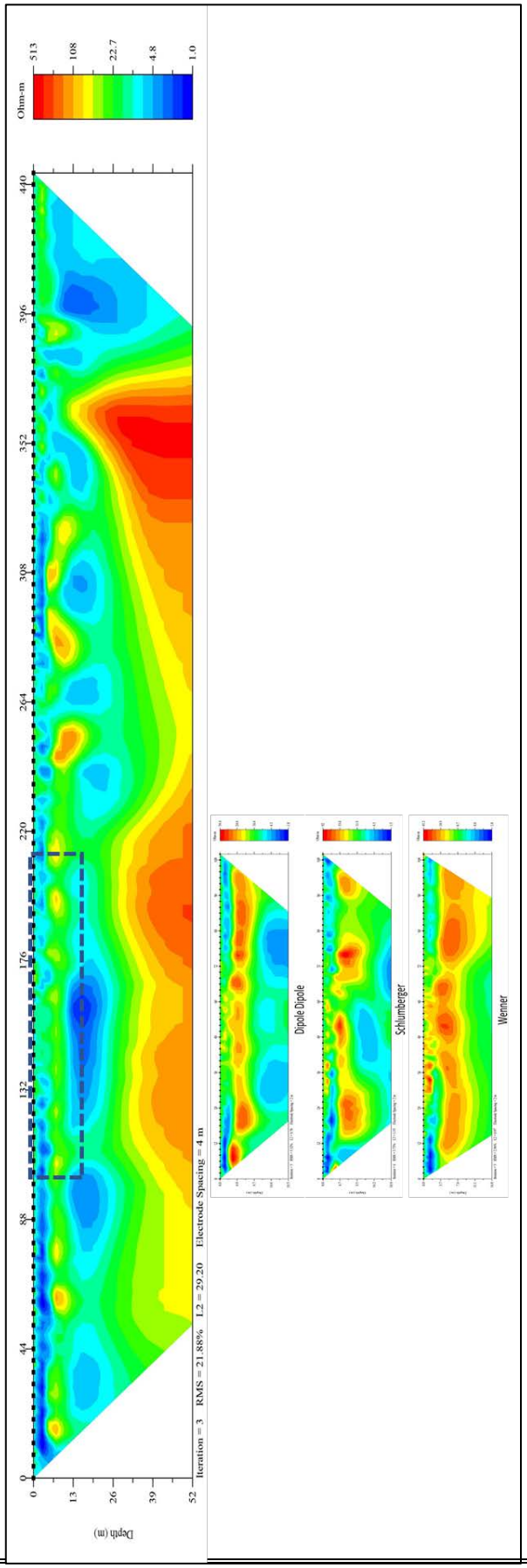

Figure 5-25: DC resistivity profile collected at 4-m electrode spacing using dipole-dipole array. Shorter DC resistivity profiles were acquired at 2-m electrode spacing using either a dipole-dipole array, a Schlumberger array, or a Wenner array. The approximate area of the 2-m profiles are shown as a dashed rectangle on the 4-m array. Note that the depth of exploration and resistivity color scale is different for each array type and each electrode spacing.

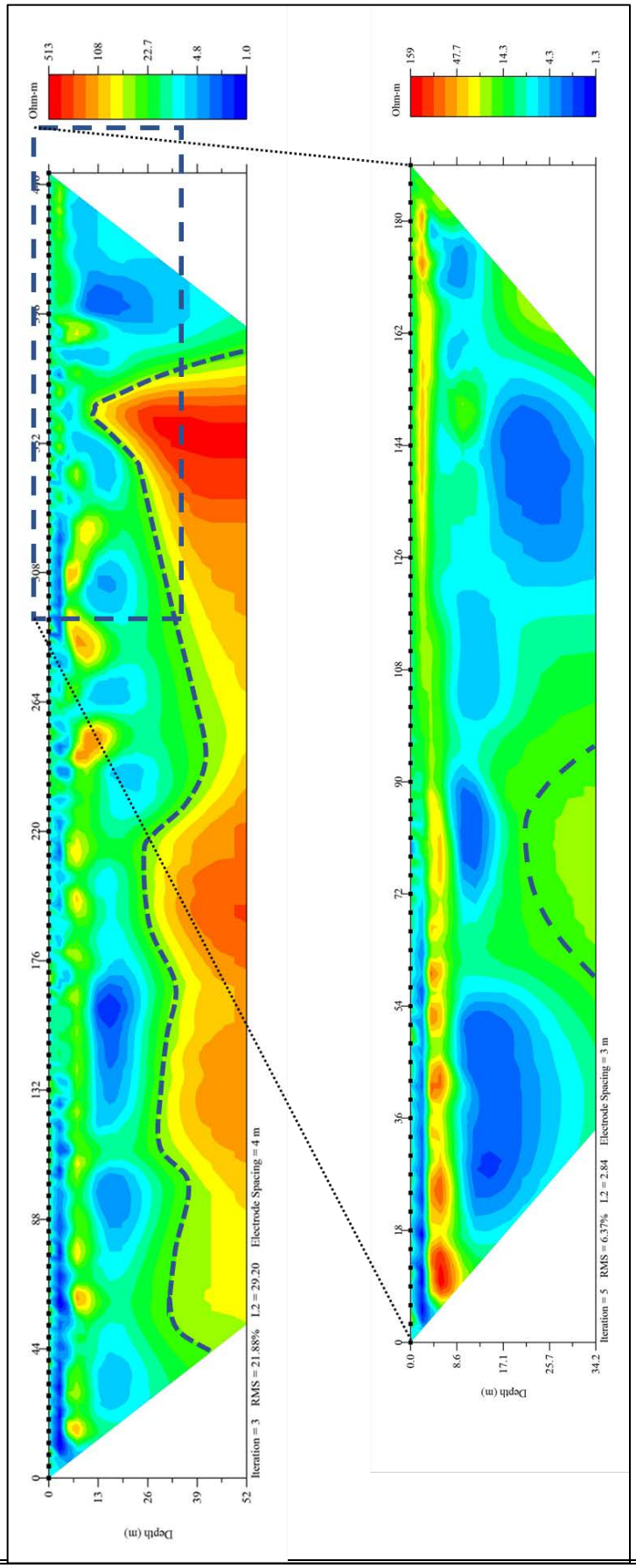

Figure 5-26. DC resistivity profile collected at 4-m electrode spacing using dipole-dipole array. Shorter DC resistivity profile was acquired at 3-m electrode spacing using a dipole-dipole array. The approximate area of the 3-m profile is shown as a dashed rectangle on the 4-m array profile. Note that the depth of exploration and resistivity color scale is different for each electrode spacing. A dashed line shows the interpreted top of bedrock in both profiles.

5.4.3 Geophysical Interpretations

The objective of both the EMI and DC resistivity surveys was to delineate areas where geothermal waters could be present at shallow depths (0 to 30 m). The starting hypothesis was that geothermal waters are more conductive than shallow ground water because of higher temperature and higher solute content. This hypothesis was tested by performing GEM-2 traverses across the outflow from Threemile Spring, a nearby analog for the near-surface source of geothermal water that was sought within the study area. This simple test showed that geothermal waters flowing as a perennial stream were less conductive than unwetted soils on either side of the flowing geothermal stream, an unexpected finding that changed the interpretation of EMI survey results within the study area. For arid soils where salts are evaporatively concentrated in the vadose zone, near-surface geothermal waters would likely be expressed as a low conductivity (i.e., higher resistivity) anomaly.

5.5 2-DIMENSIONAL SEISMIC REFLECTION SURVEY

About 6.2 linear miles of 2-dimensional seismic data (and sections) has been procured from Seismic Exchange, Inc. for a northwest to southeast traverse across the area of interest (see Figure 4-1). This data comes from the eastern end of seismic survey line 76-120-015. Due to the reduced number of shot and receiver pairs along the ends of seismic lines, reflectors are less clearly revealed in these portions of survey lines. Unfortunately, the eastern end of the seismic line is over the area of greatest interest, which is across Town Creek Flat, just north of the City of Wells. This situation reduces the amount of information that can be extracted from this survey line in the area of interest. The data was obtained in 1976 and reprocessed in 2014. This data is proprietary and is considered to be a trade secret of Seismic Exchange, Inc. While the seismic data is proprietary to Seismic Exchange, Inc., NETL's interpretations can be given to Elko Heating Company and the City of Wells and may be published with permissions from Seismic Exchange, Inc. Any interpretations will be released separately from this report. Efforts are in progress to reprocess the seismic data to extract useful information.

6. DATA INTEGRATION

6.1 DATA CATALOG

All 47 datasets collected and created throughout this project were cataloged and categorized according to their metadata and attributes, and compiled into a data catalog entitled, "City of Wells Geothermal Data Catalog" (Appendix I). The data catalog is shared as a public resource on NETL's Energy Data eXchange (EDX), a data-driven, web-based portal designed to encourage collaboration and science-based decision making. The data catalog primarily describes spatial datasets, and records dataset names, descriptions, categories, spatial extent, year published or created, formats, number of records, sources, citations, public availability, who acquired the dataset, and if the dataset was collected and interpreted for analysis (See Sections 5 and 7). To improve interpretability, datasets were categorized by dataset topic. Dataset topics include: topographic and administrative, geologic and structural, geothermal and geochemical, and geophysical. Dataset formats were divided into two spatial designations, either feature class (41 total) or raster (6 total). Feature classes are collections of geographic features with the same geometry type (such as point, line, or polygon), the same attributes, and the same spatial reference (ESRI). Rasters are spatial data models that define a space as an array of equally sized cells arranged in rows and columns (ESRI). These categories and formats are well suited for database integration, visualization, and analytical purposes. Key datasets compiled in the City of Wells Geothermal Data Catalog are shown in Figure 6-1.

6.2 DATABASE CREATION

Using ESRI's ArcGIS software, datasets collected were integrated into a geodatabase entitled, "City of Wells Geothermal Database". A geodatabase is a proprietary database or file structure used primarily to store, query, and manipulate spatial data (ESRI). This geodatabase contains 34 publicly available datasets but does not include the 13 private datasets listed in the data catalog. In total, there were 31 feature classes and 3 raster datasets compiled into a single geodatabase requiring 0.55 GB of memory. Using the dataset categories discussed in the previous section, feature classes were grouped into feature datasets. Feature datasets are collections of feature classes stored together that share the same spatial reference (ESRI). Although raster datasets cannot be stored in a feature dataset, they can be stored within the geodatabase. All datasets were projected to the NAD 1983 UTM Zone 11N spatial reference system. To increase the interpretability and share-ability of the data, an ArcGIS map package was created and shared on EDX, along with the geodatabase. This allows users to visualize set symbologies of key individual data layer attributes (such as well temperature or depth) without having to manually manipulate the datasets within the geodatabase.

6.3 DATA ISSUES

Each dataset was acquired in different formats, levels of completeness, and spatial reference systems. Most of the datasets collected were in a spreadsheet (.xlsx), spatial vector data (.shp or .kmz), or raster (.tiff) formats. Datasets that were collected as .xlsx or .kmz needed to be converted into .shp formats to be used in the geodatabase. All datasets were checked for the consistent spatial reference system information, duplication, and location errors before importing into the final geodatabase. For example, ground-truthing was necessary to rectify and update well locations taken from the Nevada Division of Water Resources (NDWR).

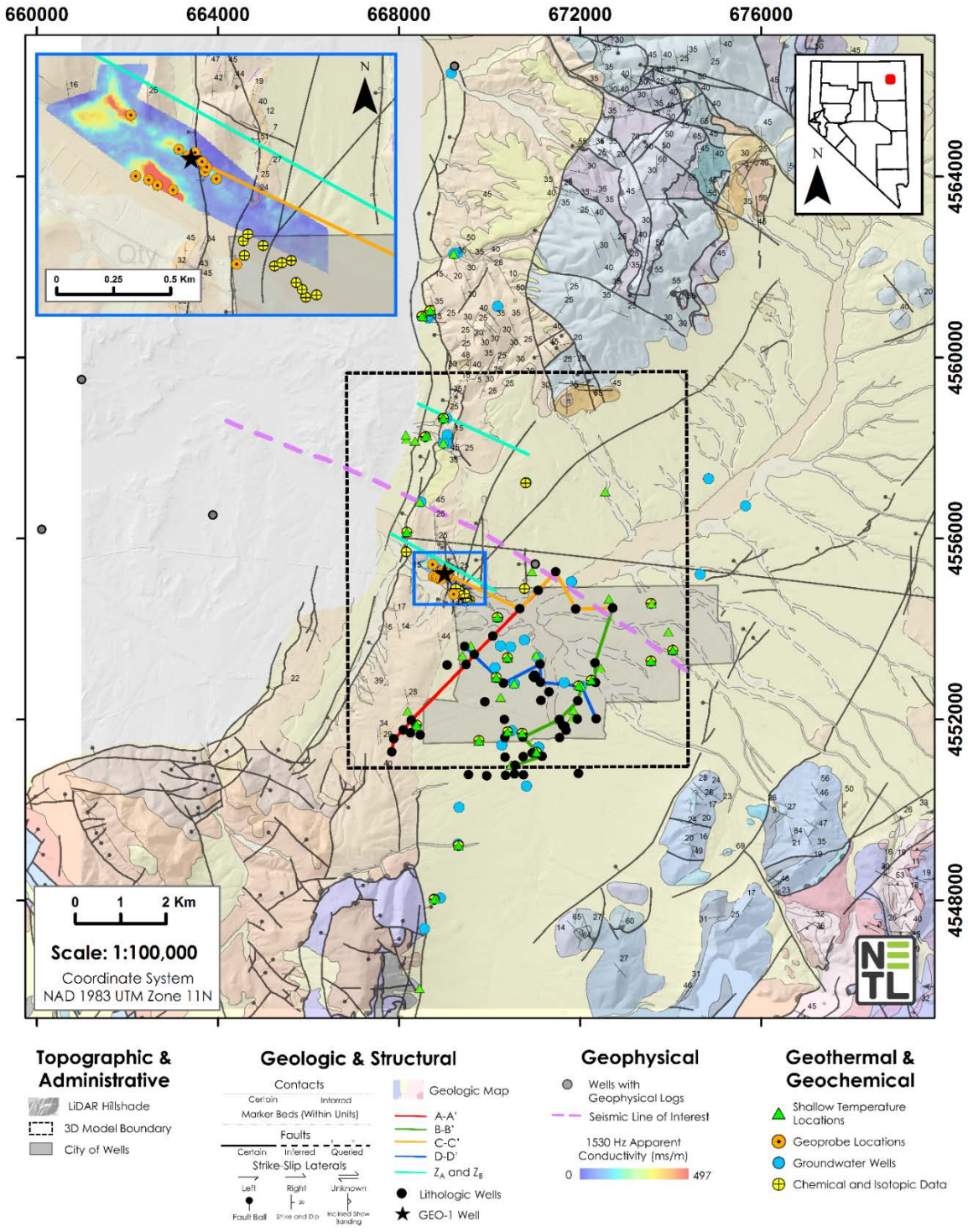

Figure 6-1: Map displaying variety of public and private datasets in the "City of Wells Geothermal Data Catalog." Datasets featured contain topographic (Miller, 2017), administrative (ESRI, 2017; NETL, 2017), geologic (Henry and Thorman, 2011; DiGiulio, 2017; Zuza, 2017; Zehner, 2017), and structural (Henry and Thorman, 2011; Zuza 2017; Jewell, 1982), geophysical (IHS, 2015; Zehner, 2017; SEI, 1976; NETL, 2017), and geothermal and geochemical (Zehner, 2017b; Spycher and Zehner, 2017; Zehner et al., 2006; Spycher, 2017) datasets.

7. DATA MODELING

7.1 STRUCTURAL MODELING

A structural analysis of slip tendency (Morris et al., 1996) and dilation tendency (Ferrill et al., 1999) was performed for the Wells study area to provide a proxy for permeability development on faults. Fault segments with a high tendency to slip and/or dilate under ambient tectonic stress conditions are likely to be very near a critically stressed state and, therefore, are likely to conduct fluid flow (Barton et al., 1995; Zoback and Townend, 2001). They are also susceptible to induced seismicity. The stress tensor (three directions and three magnitudes) used in the analysis is based on several different datasets. Estimates of stress orientations are informed by stress data for the western US as compiled from inverted earthquake focal mechanisms (Heidbach et al., 2008). A nearest-neighbor interpolation was performed on these stress directions, including the 2008 Wells earthquake data, to define representative stress directions for the Wells area (Figure 7-1). Stress magnitudes used in the analysis are based on observed relationships between stress magnitudes for normal faulting regimes throughout the Basin and Range region and on the inferred stress state under which the 2008 Wells earthquake occurred. Empirical relationships between stress magnitudes for a normal faulting regime were calculated as follows (Hickman et al., 1998; Hickman and Davatzes, 2010; Siler et al., 2016):

$$\frac{S_{h\,min}}{S_v} = 0.4 - 0.6$$

$$(S_{h\,min} + S_v)/2 \; = S_{h\,max}$$

where $S_{h\,min}$ is the minimum principal component of horizontal stress, $S_{h\,max}$ is the maximum principal component of horizontal stress, and S_v is the vertical component of stress.

If we assume that the fault upon which the 2008 earthquake occurred was critically stressed, or was very near to a critically stressed state, this information can be used to further constrain the stress magnitudes. Assuming a frictional failure criterion and a coefficient of friction equals 0.4, the following stress magnitudes satisfy both the empirical relationships above and the inferred critically stressed state of the fault upon which the 2008 earthquake occurred: $S_{h\,min}$ = 27 MPa, $S_{h\,max}$ = 43.5 MPa, and S_v = 60 MPa. These stress magnitudes used the slip and dilation tendency calculations consistent with those found at the typical geothermal system depth of ~1-2 km (e.g., Hickman et al., 1998; Hickman and Davatzes, 2010; Siler et al., 2016).

Fault segments were acquired from geologic mapping by Thorman et al. (2010) and Zuza (2017). Assumptions for these calculations include fault dips as follows: normal = 60°, strike-slip = 90 °, thrust = 30°, low-angle normal = 45°).

Under these stress conditions north-northeast striking steeply-dipping fault segments in the Wells study area have the highest dilation tendency, whereas north-northeast striking moderately-to-steeply-dipping fault segments have the highest slip tendency. A linearized Mohr-Coulomb stress analysis and failure criterion for this scenario is shown in Figure 7-2. These high slip and dilation tendency (i.e., most likely to be critically stressed) fault segments are inferred to have a relatively high likelihood of hosting geothermal fluid flow relative to segments with low slip or dilation tendency (e.g., Barton et al., 1995; Zoback and Townend, 2001).

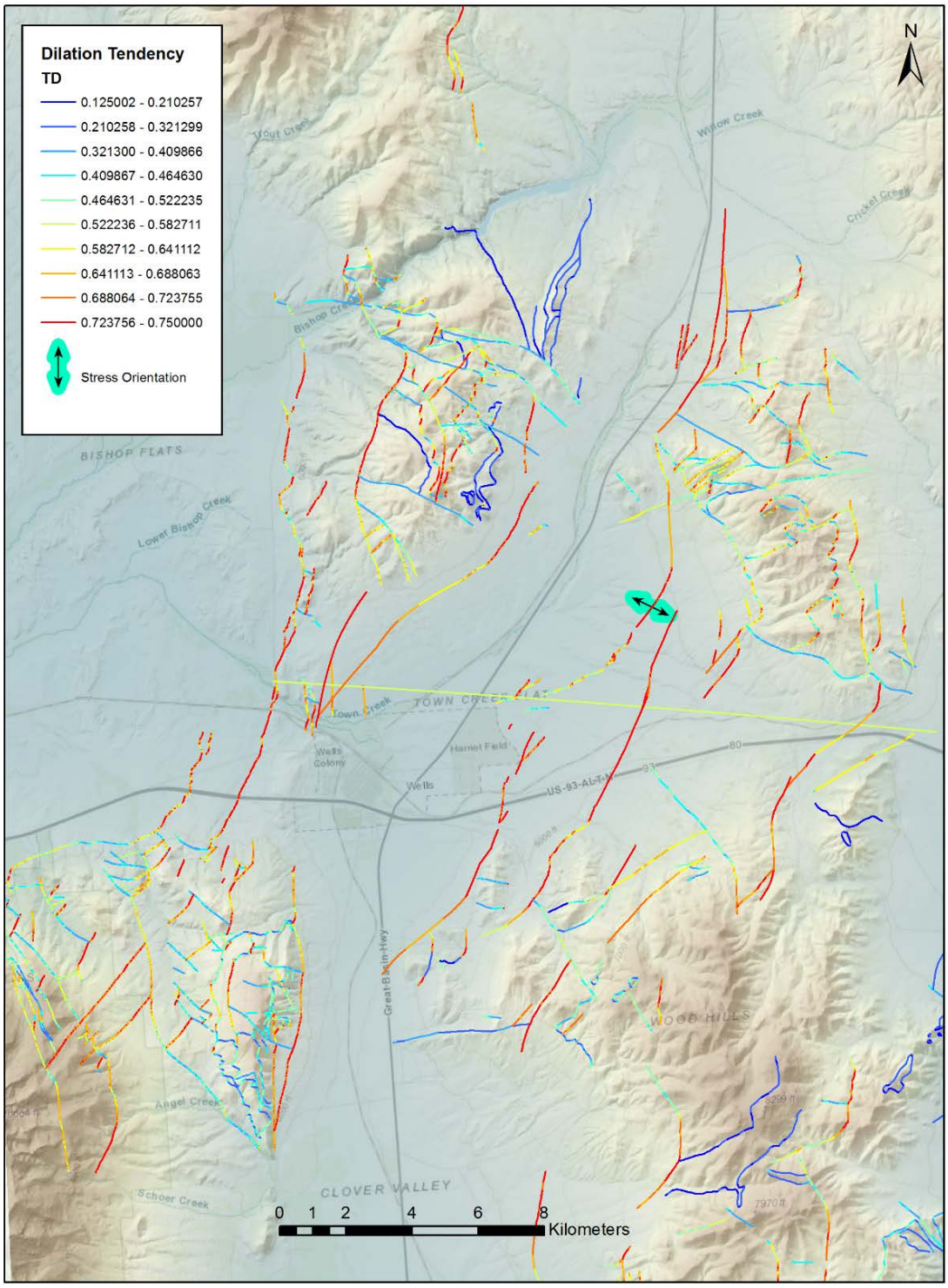
Dilation Tendency
TD
0.125002 - 0.210257
0.210258 - 0.321299
0.321300 - 0.409866
0.409867 - 0.464630
0.464631 - 0.522235
0.522236 - 0.582711
0.582712 - 0.641112
0.641113 - 0.688063
0.688064 - 0.723755
0.723756 - 0.750000
Stress Orientation
N
BISHOP FLATS
Lower Bishop Creek
Trout Creek
Willow Creek
Cricket Creek
Bishop Cr
Town Creek
TOWN CREEK FLAT
Wells Colony
Harriet Field
Wells
US-93-Alt-N
80
93
Great Basin Hwy
WOOD HILLS
Angel Creek
Schoer Creek
CLOVER VALLEY
0 1 2 4 6 8
Kilometers

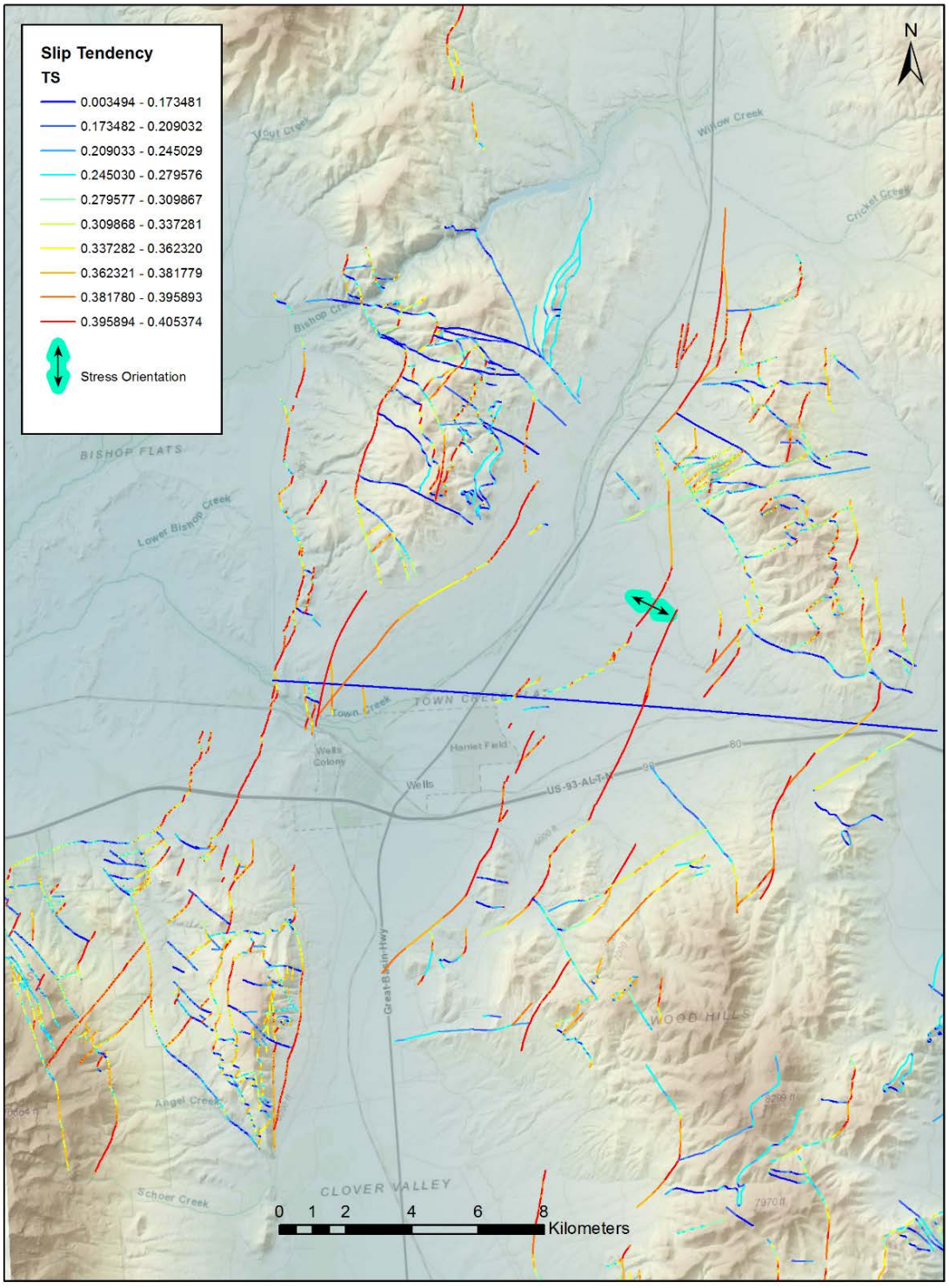

Figure 7-1: Slip tendency (top) and dilation tendency (bottom) of faults in the Wells study area. The stress orientation shown is the $S_{h\,min}$ inverted from the Wells 2008 earthquake event.

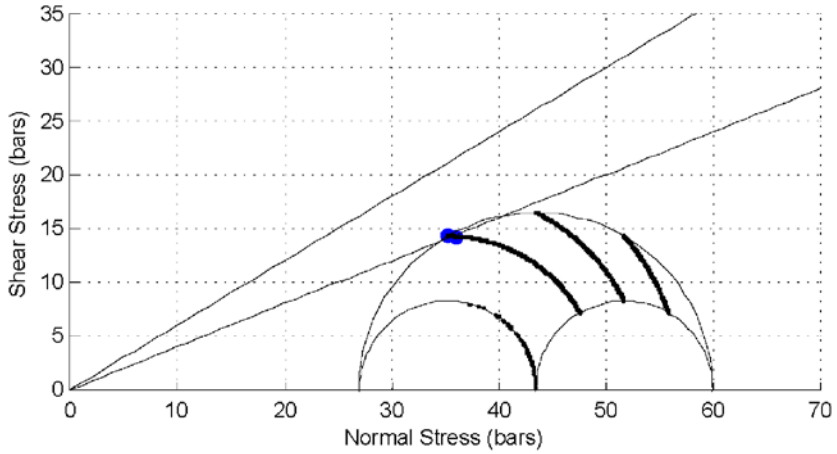

Figure 7-2: Mohr's circle for faults in the Wells study area. The failure envelope has a friction coefficient of 0.4. If it is assumed that the fault upon which the Wells earthquake occurred (blue) is critically stressed, the magnitudes of the three components of the effective stress field are $S_{h\ min}$ = 27 MPa, $S_{h\ max}$ = 43.5 MPa and S_v = 60 MPa.

7.2 NEW CONCEPTUAL GEOLOGIC MODEL

A conceptual three-dimensional geologic model was built to visualize the three-dimensional datasets in geologic context. This model was constructed using EarthVision v9.1 (Dynamic Graphics, Inc.).

7.2.1 Datasets and Methods

Initial steps to building the conceptual 3-dimensional geologic model required assembling spatial datasets from the ArcGIS map package (Section 6.2). LiDAR elevation data (1-meter resolution) was used to model accurately the topography (FEMA). All faults drawn within the study area were compared and selected by the following criteria: Confirmation across multiple datasets or recently mapped by Zuza (2017; Appendix D), USGS (2006), Thorman et al. (2010), Dohrenwend (2012), or Jewell et al. (1982). Surface geology was assessed with this method as well, primarily using maps of Zuza (2017) and Henry and Thorman (2011).

Import of datasets into the EarthVision software necessitates defining an extent and pairing spatial datasets with elevation data. The final model extent selected is 7.362 km x 8.667 km x 600 m extending from 666891 Easting, 4550933 Northing to 674237 Easting, 4559600 Northing. A 2-dimensional surface grid was constructed from the FEMA LiDAR ASTER dataset to serve as topographic control.

Various surficial images are draped over the topography in the model to provide a reference for surface and subsurface datasets. These include satellite imagery (ESRI World Imagery, 2017), the Zuza (2017) geologic map, and the 2017 electromagnetic survey results (Section 5.4.1).

Fault point locations from shapefiles were imported into EarthVision as text files. These files were edited to project a 3-dimensional fault surface based on the surface trace of the faults, nature of slip, dip angle, and dip direction using a custom MATLAB script (Appendix J). The

point data were then converted into fault planes using EarthVision's built-in 2-D gridding algorithm.

In the subsurface, correlation of lithologic units is poorly informed due to the heterogeneity of the sedimentary layers at the scale of the model; thus, no sedimentary horizons were interpolated in the model. Structural cross sections (Section 5.2.4; Appendix D) and lithologic well-logs (Section 5.2.6; Appendix E) were included in the model; however, these data serve comparative purposes only and do not constrain the temperature interpolations. Depth to pre-Cenozoic bedrock (also referred to as basement in this report) was constrained using 2-km resolution geophysical data (Ponce and Damar, 2017).

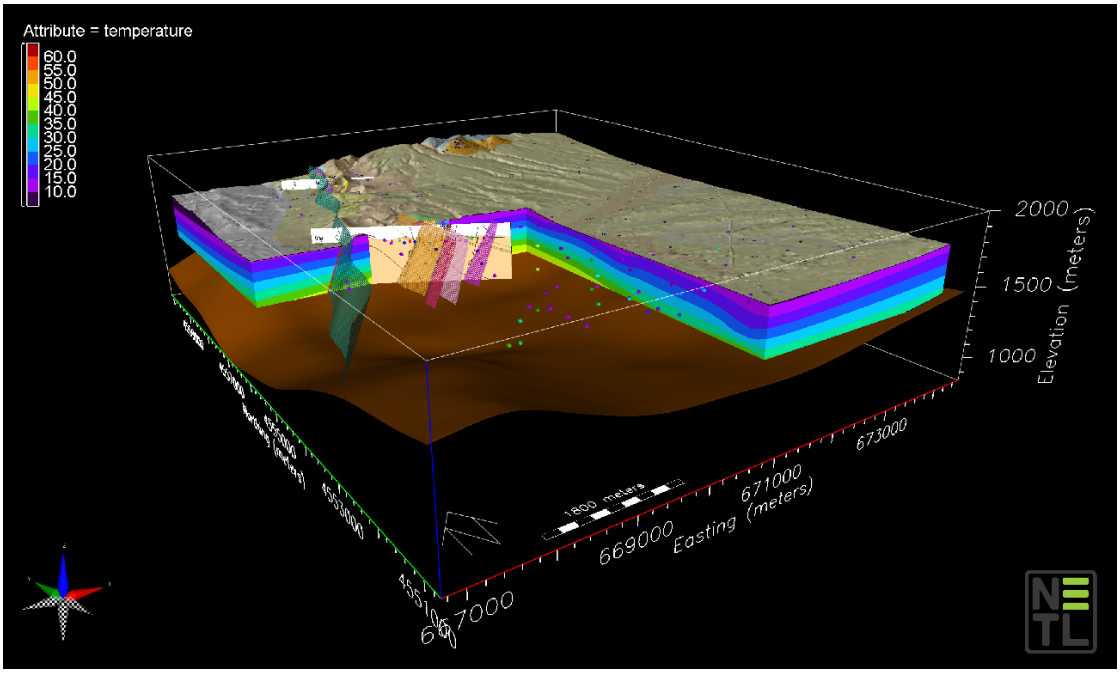

Figure 7-3: A 3-D temperature model of the City of Wells, NV region. Subsurface temperatures binned in five degree increments (e.g., 15 to 20 deg. C), ranging from red (hotter) to purple (cooler). Individual temperature data points shown as small colored boxes scattered throughout the model space, following same color scale. Fault planes (semitransparent) and structural cross section (Zuza, 2017) shown only for illustrative purposes. City of Wells surficial geology is draped on the surface of the model (Zuza, 2017). Interface between basement rock and basin sediments shown as dark brown surface (Ponce and Damar, 2017). Vertical exaggeration = 2. Refer to Figure 6-1 for temperature data locations and Figure 7-7 for uncertainty analysis.

Subsurface temperatures were modeled using the iterative "minimum tension gridding" algorithm native to EarthVision. This was achieved in several stages. First, individual temperature measurements were imported as scattered data and converted into a coarse 3-dimensional grid. Temperatures were assigned to grid nodes using an inverse-distance weighting average function. Next, several iterations were executed to calculate new temperature values for each grid node, with the neighboring nodes and scattered data informing a cubic function that assigns the new value. Once the initial set of iterations is completed for the coarse grid, temperatures are re-calculated for a new, finer-scale grid with user-defined dimensions. We chose a node spacing of 243 x 243 x 83 meters (x, y, z, respectively) based on the average

distance between nearest neighbors. Temperature measurements incorporated in the scattered data are sourced from the 2-m shallow temperature survey (Zehner, 2017a), local wells, springs, and streams (Zehner, 2006, 2017; NDWR; NBMG; LBNL) (Figure 7-3). Temperature profiles from the recent geothermal exploration wells have not been added to this data set.

7.2.2 Model Results

Three-dimensional model temperature results are shown in Figures 7-4 and 7-5. Subsurface temperatures were interpolated for areas above the geophysically-derived basement. Higher temperature anomalies among well and spring data occur in the northwest portion of the model, near Threemile Spring and in the Mary's River basin just north of Wells (Figure 7-4). A temperature trend generally increasing towards the southwest is also present. Anomalous hotspots also persist at depth (Figure 7-5). It should be noted, however, that the increasing temperature trend in the southwest region of the model is not well constrained by data.

Several additional datasets were imported into EarthVision to provide visual context and aid in the interpretation of the subsurface. These include: four of the graphically illustrated lithologic wells (Section 5.2.6) located nearest to the seismic transect, and lithologic cross sections A-A', B-B', C-C', and D-D' (Appendix E). Temperature profiles were also extracted from the model results along the lithologic cross section lines to demonstrate any correlations between the lithologic logs and temperature interpolation (Appendix E).

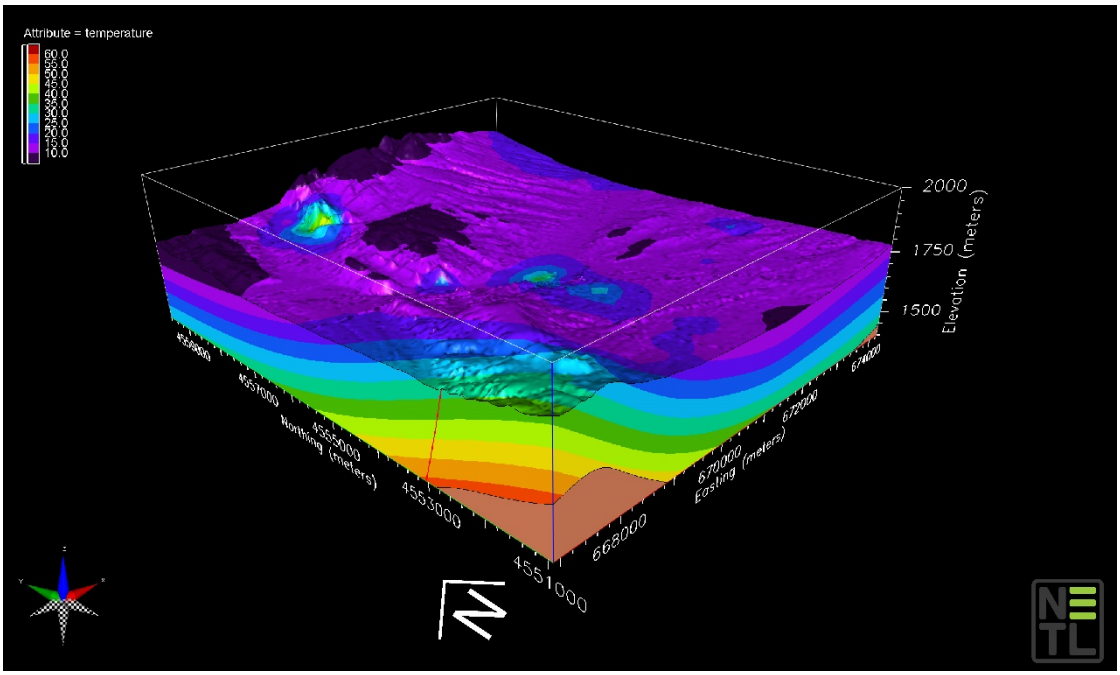

Figure 7-4: A 3-D temperature model of City of Wells, NV region, showing surficial temperature results from an oblique perspective. The pink volume in the deepest portion of the model (foreground) represents the geophysically-estimated depth to "basement rock". Red lines represent fault planes within the model. Refer to Figure 6-1 for temperature data locations and Figure 7-7 for uncertainty analysis.

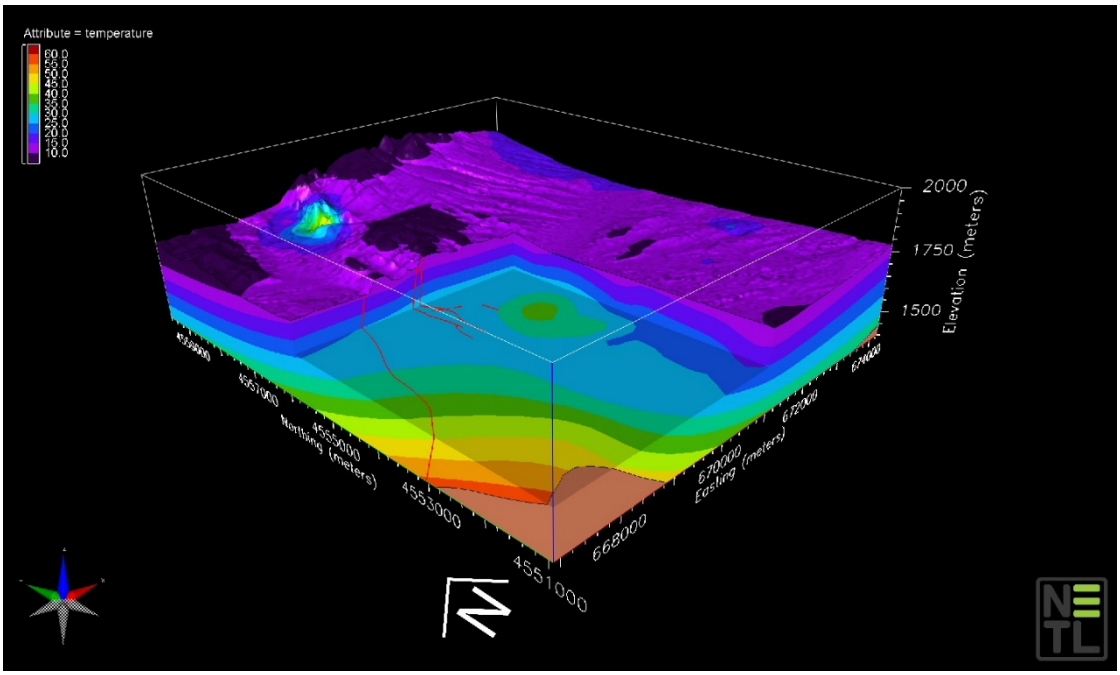

Figure 7-5: Temperature model with cutaway, carved to 1580 meter elevation to show temperature variation at depth. Same view perspective and color-scale as above. Refer to Figure 6-1 for temperature data locations and Figure 7-7 for uncertainty analysis.

7.2.3 Geologic Model Uncertainty Analyses

The temperature model depicted in Figures 7-4 and 7-5 is shown as a solid volume that does not indicate data density and thus does not communicate its quality. To better understand and visualize data density and quality, an uncertainty analysis was completed using the Cumulative Spatial Impact Layers (CSIL) geospatial tool developed by NETL (Bauer et al., 2015). This tool incorporates spatial datasets and summarizes them based on spatial overlap (presence or absence), which results in a dataset density feature layer for the area of interest. For the City of Wells geothermal investigation, a CSIL analysis was performed to represent the uncertainty of the geologic and geophysical datasets in the 3-dimensional geologic model.

Spatial datasets incorporated into this analysis are comprised of point, polyline, and polygon features representing the synthesis of 11 datasets within the 3-dimensional geologic model's areal extent. These datasets were projected into the model in UTM Zone 11N, datum NAD 1983 and include geologic cross sections, depth to Cenozoic basement, depth to ground water, elevation, conglomerate surface contact, mapped faults, wells with lithologic logs, wells and springs with temperature data, surface lithology, seismic line data, and electromagnetic and resistivity surveys (Table 7-1).

Table 7-1: Datasets evaluated using CSIL. Weight is based on coverage and resolution of subsurface information. Feature type refers to how the data is spatially represented for input into the tool – either as a point, polyline, or polygon.

Data set	Source	Rank (0.1-1)	Feature type
Geologic cross sections	Zuza, 2017	0.6	Polyline
Depth to pre-Cenozoic bedrock	Ponce and Damar, 2017	0.2	Polygon
Depth to ground water	Lopes et al., 2006	0.2	Polygon
Elevation data (LiDAR DEM)	FEMA, 2015	0.5	Polygon
Conglomerate surface contact	Zuza, 2017	0.6	Polygon
Mapped faults	Zuza, 2017; USGS	0.8	Polyline
Wells with lithologic logs	NDWR	0.8	Points
Wells and springs with temperature measurements	LBNL; NBMG; NDWR; Spycher and Zehner, 2017, 2017a	0.5	Points
Surface lithology	Henry and Thorman, 2011	0.8	Polygon
Seismic line data	SEI	0.7	Polyline
Apparent conductivity Survey (south)	NETL	0.8	Polygon

Each dataset was weighted subjectively on a relative scale from 0.1 to 1 based on data quality, resolution, and coverage of the subsurface representation. The higher the rank of the dataset, the higher the degree of certainty in its subsurface interpretation. Summed values less than 0.1 are not shown in the 3-dimensional model as those indicate areas of little or no data influencing the model. The output CSIL feature layer summarizes the presence (1) and absence (0) of each dataset or layer per grid cell and the total number (sum) of overlapping datasets per grid cell. For each grid cell, the appropriate weights are applied to each CSIL presence representation of each dataset and summed together. To determine the grid cell size of the output feature layer, an observed nearest neighbor statistical analysis was performed on the point feature layers within the model extent (area of 65.6 square kilometers) to obtain a grid cell resolution of 200.0 square meters. This step ensures that the spatial variability of all datasets are appropriately represented in the final output. A description of each dataset included in the 3-dimensional model CSIL uncertainty analysis is included below.

Datasets:

1. Geologic cross sections

   Geologic cross sections are vertical slices or sections of the subsurface that are important for understanding the 3-dimensional spatial context and organization of geologic structures and formations. Geologic cross sections prepared by Zuza (2017) were used to understand the interactions between the surface and subsurface by constraining suitable locations for geothermal exploration. The dataset was represented as polylines for evaluation in the CSIL tool and given a 0.6 weight based on recent structural field mapping (Section 5.2) and the dataset's ability to improve subsurface interpretation. This dataset was not ranked higher because the cross section lines only cover the northwest

area of the model boundary and because the subsurface geology is not well constrained (only the Dalton well provides reliable stratigraphic control in the area).

2. Depth to pre-Cenozoic basement

   Incorporating the depth to basement or bedrock in the 3-dimensional model is important for understanding the thickness and structure of the overlying sediment, which can provide implications for subsurface fluid flow. This dataset is a representation of a regional scale depth to the pre-Cenozoic basement (Ponce and Damar, 2017) and is derived from an iterative gravity inversion method. Due to the relatively coarse resolution of this dataset (4 square kilometer grid cells) compared with the areal extent of the 3-dimensional geologic model (area of 65.6 square kilometers), it is most useful as a reference layer and not for interpreting local structures. For this reason, the polygon representation of this dataset was given a 0.2 weight in the CSIL tool evaluation.

3. Depth to ground water

   This dataset represents the depth to the ground water surface as recorded between 1947 and 2004, based on a statewide water table contour dataset (Lopes et al., 2006). Although the water table surface fluctuates in depth depending on seasonal variation and weather conditions, this dataset provides a reference for where the water table surface likely resides and where it may potentially interact with local geologic structures. This dataset is also based on the extent of the state of Nevada, as compared to the much smaller areal extent of the 3-dimensional geologic model (approximately four times the area of the City of Wells). For these reasons the polygon representation of this dataset is mainly used as a reference, and given a weight of 0.2 in the CSIL evaluation.

4. Elevation data (LiDAR DEM)

   The high resolution (1 m) LiDAR DEM (FEMA, 2015) represents the land surface elevation above sea level (in meters) in the area and was overlain onto the areal extent of the 3-dimensional geologic model. This dataset provides surface elevation information that is used to make inferences about surface/subsurface structure and is important for calibrating the depth of temperature measurements and well log data. A weight of 0.5 was given to the polygon representation of this dataset in the CSIL evaluation.

5. Conglomerate surface contact

   Conglomerate is a coarse-grained sedimentary rock composed of rounded fragments within a matrix of finer grained material that is mapped on the land surface. This specific geologic unit (Zuza, 2017) is important for its inferred association with hydrothermal pathways and is key for subsurface correlation and interpretation among lithologic units. It has also helped to identify locations for geophysical surveys in this report (See Section 5.4). Although the spatial representation is only at the surface as a polygon, it was given a weight of 0.6 in the CSIL evaluation.

6. Mapped faults

   The faults used in the model extent are mapped regional faults that best represent the overall structure and incorporate attributes such as slip, dip, and, dip direction (Appendix J). These constraints are critical for understanding the presence and behavior of

subsurface fluid pathways; therefore, the weight given to this polyline dataset is 0.8 in the CSIL evaluation.

7. Wells with lithologic logs

   This point dataset represents an interpretation of driller's logs from 75 (54 within the model extent) individual wells (NDWR, IHS, Lumos & Associates) where lithologies were recorded. Although there is some uncertainty to the naming conventions/ descriptions of lithologies within the logs, they are direct descriptions of the subsurface stratigraphy. Therefore, this point dataset warrants a weight of 0.8 in the CSIL evaluation.

8. Wells and springs with temperature measurements

   The wells and springs with temperature point data come from a combination of data sources that include different temperature measurement methods for surface springs and wells at various depths. The spatial distribution of these 139 points is critical for understanding where temperature anomalies exist and how these anomalies relate to known geologic structures. This dataset also highlights areas lacking sufficient information for interpretation. For example, there is an absence of data in the northeast region of the study area, and the dataset overall only reaches a maximum depth of 305.1m below the surface. There is also a degree of uncertainty in the reliability of the temperature measurements, as methodologies were not recorded in some of the data sources. However, this dataset is necessary for understanding and creating the 3-dimensional temperature profile within the model extent so this dataset was given a weight of 0.5 in the CSIL evaluation.

9. Surface lithology

   The surface lithology dataset (Henry and Thorman, 2011) represents the mapped geologic formations that are present at the surface. The geology at the surface is critical for inferring the stratigraphic framework in the shallow subsurface and relationships with known structural features. These relationships help identify locations for further geothermal exploration and provide geologic context for potential geothermal reservoirs. This polygon dataset (Henry and Thorman, 2011) is draped onto the surface of the 3D geologic model but lacks some coverage in the northwest area of the model extent. A weight of 0.8 was given to this dataset in the CSIL evaluation.

10. Seismic line data

    This polyline dataset is a surface trace of the 2-dimensional seismic profile. The seismic data acquired (SEI) displays an approximate cross section through the strata, revealing seismic reflectors (See Section 5.5). This information is important for understanding and interpreting the stratigraphic and structural architecture within the depths of the model extent and validating other subsurface datasets such as faults and major regional structures. Although this dataset facilitates a direct interpretation of the stratigraphy, it is limited by the attenuation of the seismic signal near the ends of the seismic line and the spatial extent of the seismic line across the model area. Therefore, this dataset was given a weight ranking of 0.7 in the CSIL evaluation.

11. Electromagnetic induction survey and direct current resistivity survey

    In July 2017, apparent conductivity was mapped via two electromagnetic induction surveys (See Section 5.4). Of the two surveys, the southern survey covers a small area (represented as a polygon) in the central-western region of the model extent (Figure 7-6). This survey was incorporated into the uncertainty evaluation due to the high temperature anomaly reported (See Section 5.1) within close proximity to the City of Wells and its aid in choosing locations for drilling exploratory wells (See Section 8.1). Although this dataset only covers a small area within the model extent, its high-resolution (13.7 square kilometer grid cells) information provides more constraints to improve understanding and predictions of shallow subsurface features and their relationships with fluid flow. For this reason, this dataset was given a weight of 0.8 in the CSIL evaluation.

Figure 7-6 displays the coverage of the model datasets in 2-dimensions. Input layers to the CSIL tool are shown on the left (a), while the CSIL tool output evaluating all data sources from Table 7-1 is shown on the right (b). The CSIL analysis is bound by the areal model extent. High ranked —higher density and quality of data—regions are shown in **red**, while lower ranked regions are shown in yellow. Point and polyline data have the finest resolution of information for interpreting the subsurface, while the polygon datasets provide excellent coverage and extent of data to support interpretation. The 2-dimensional visualization of data sources, types, and resolutions communicates differences in the 3-dimensional model resolution and quality. While the geological, geophysical, and elevation data have broad extents, their resolution is coarser than that of well data, which includes rock core and wireline data. Thus, the value or resolution of those areas where only broad surveys exist displays a lower cumulative rank, while areas where additional data sources are integrated receive a higher cumulative rank. The output CSIL feature layer represents summed rank values, ranging from 0.9 to 5.0. Within the CSIL output, finer resolution data from faults, wells and springs, the seismic line, and cross sections coincide with the broad extent of the geological, geophysical, and elevation surveys to produce higher cumulative rank values locally indicating greater confidence in the 3-dimensional geologic model for those areas (Figure 7-6, right). This distribution can be seen in the northwestern section of the model extent along the cross sections and seismic line.

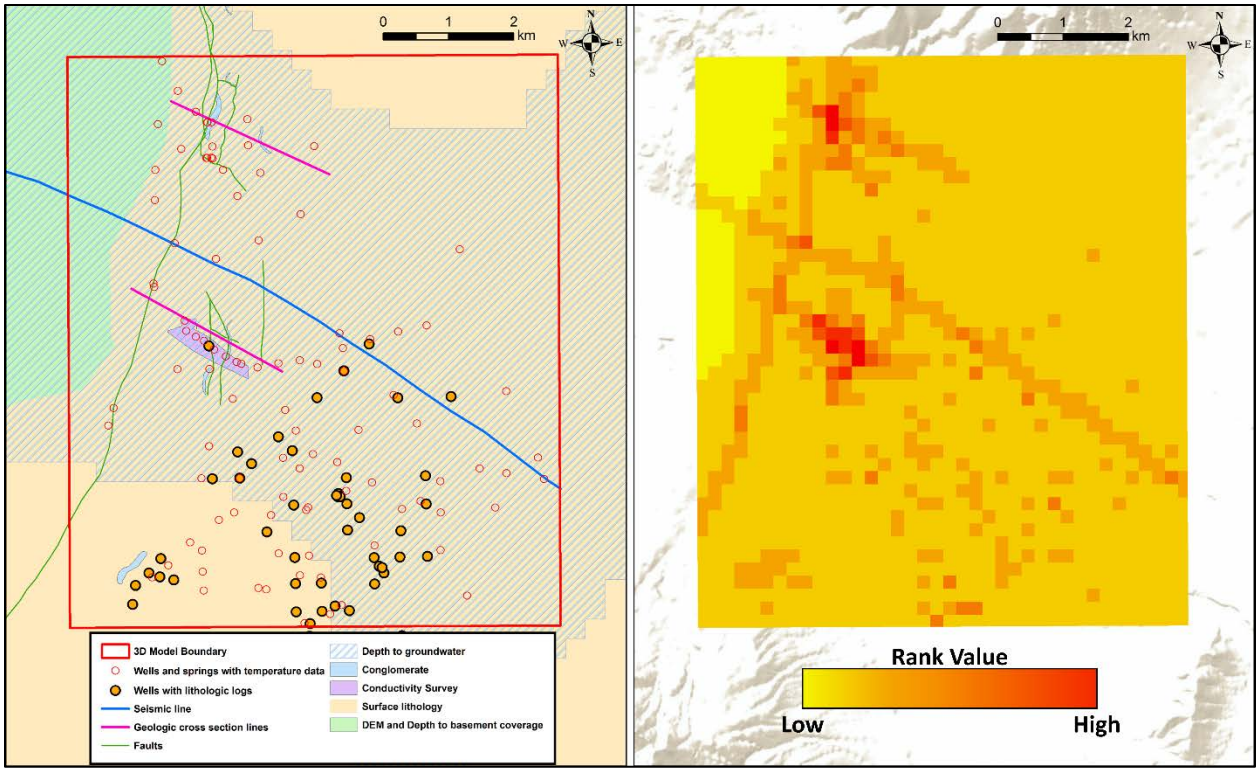

Figure 7-6: Input layers to the CSIL tool shown on the left (a), while output from CSIL tool evaluating all data sources from Table 7-1 shown on the right (b). Layers are evaluated by the CSIL tool only within the model extent. High "rank"-- density and quality of data -- is represented by red, while low rank is represented by yellow.

7.2.3.1 Three-Dimensional Temperature Model Uncertainty Analysis

Although the interpolated temperature model strikes a good balance between honoring the input data and creating a "natural" looking temperature profile with uniform grid spacing, it is important to have an estimate of the regions that are most well-constrained by the data. Thus, a 3-dimensional point density analysis was performed using the well and spring temperature data to demonstrate the uncertainty of the temperature profile calculations (Figure 7-7). To achieve this, a polygon grid representing the density of temperature points at different depths was created using ArcGIS v10.5 and interpolated and modeled in EarthVision v9.1. The 2-dimensional (or XY) dimensions of each of the grid cells were determined to be 245.83 m, based on the 3-dimensional average nearest neighbor distance between all the temperature points. The depth (or Z) dimension of each of the grid cells was based on the depth range of the dataset (403 m) and the standard deviation of depth values (80.3 m). Dividing the depth range by the standard deviation obtains a value of about five, which translates to the number of grid cells or "layers" in the Z dimension. Dividing the depth range evenly among the five "layers" yields a final Z dimension of 80.6 m. After the dimensions of these grid cells were calculated, the count of temperature points was incorporated into the polygon grid. The grid cells were then converted to points using their centroid locations and interpolated with the same "minimum tension gridding" algorithm as the temperature data. The results of this analysis indicate which areas of the temperature interpolations most well-informed and which are more distant from data.

It is important to notice that most temperature data from wells are point measurements instead of temperature profiles versus depth, so non-linear temperature profiles are not always represented accurately with the data available from most wells.

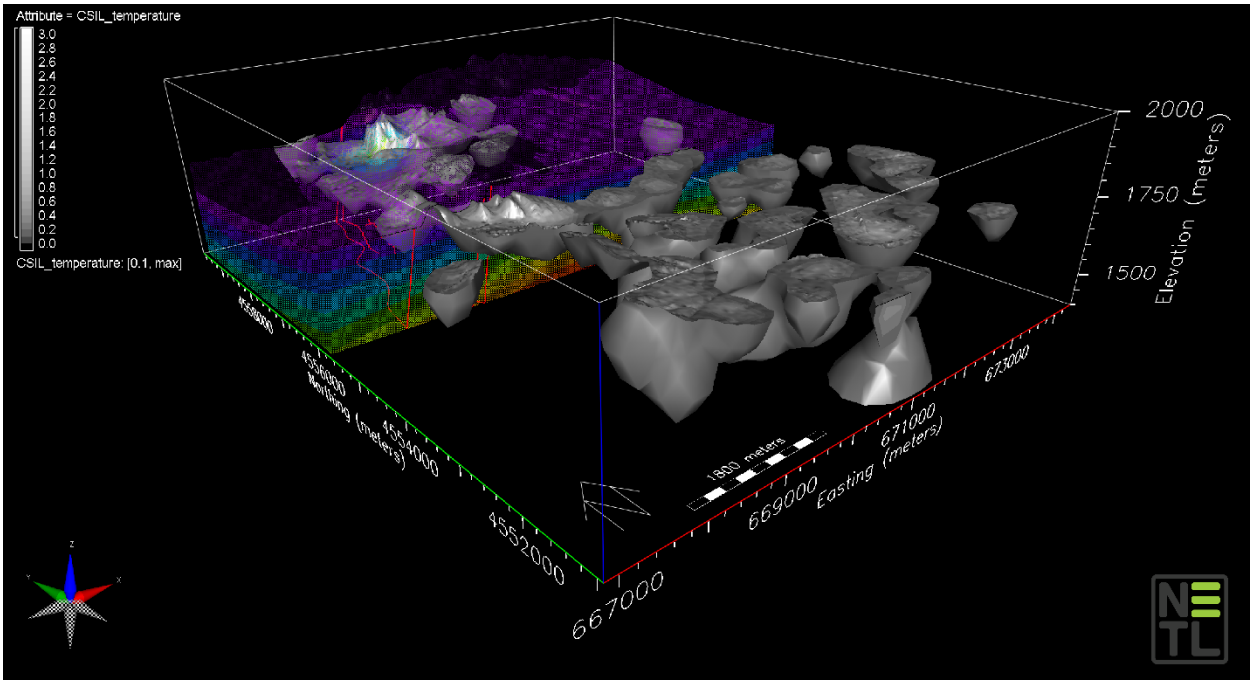

Figure 7-7: Uncertainty analysis of the interpolated temperatures showing number of data points per cell. Higher density data is represented by gray volumes within the model; area with no data (density = 0) is fully transparent. The temperature model (Section 7.2.2; Figure 7-5) is shown for reference as a semi-transparent slice along the Y-axis. Refer to Figure 6-1 for temperature data locations.

8. CONCLUSIONS AND RECOMMENDATIONS

8.1 OCTOBER 2017 EXPLORATION WELL – GEO#1

Based on recommendations from the project team, the City of Wells undertook the drilling of a geothermal exploration well near the location of the hottest shallow temperature readings, as identified by the 2-meter shallow temperature and Geoprobe surveys. Preliminary interpretation of the DC resistivity survey showed a resistive feature at a depth of ~15 m (45 ft) on the eastern end of the 3- and 4-m resistivity traverse (Figure 5-21, blue and magenta lines), which could be silicified fault material, perhaps the same fault observed above the floodplain escarpment to the north in the maps of Jewell (1982) and Zuza (2017), or other non-porous rock. Jewell (1982) and Jewell et al. (1994) noted that deep circulating waters experienced significant vertical flow in the vicinity of the Humboldt River and the City of Wells. Thus thermal waters could be moving up along the east side of the fault (the hydrologic up-gradient side), if the fault is impermeably silicified. Jewell (1982) and Jewell et al. (1994) alternatively suggested that the thermal waters may up-well along an inferred west-north-west-striking fault in the same region. The recommended location was also expected to sample shallow hydrothermal outflow from the north, especially if outflow was traveling southward toward the river by following the east-side of the fault.

The exploration borehole, named GEO#1 (shown as a black star in Figures 5-6 and 6-1), was air-rotary drilled by Rosenlund Drilling, LLC, between October 23 and November 1, 2017. The 134 m (440 ft) borehole was first advanced to 18 m (60 ft) depth, where drilling paused and steel casing was set. A layer of sand or soft sandstone was encountered between about 4 and 7.5 m (14 and 24 ft) depth. Rosenlund measured temperatures of 19° and 20°C (66° and 68°F) at 0 and 18 m, but did not measure temperature while drilling through this sandstone unit. Below, the rock was a less permeable claystone and siltstone of light color in the zone of oxidation down to about 27.5 m (90 ft) depth and mostly medium gray at greater depths. Subsequent drilling continued down to a depth of 134 m (440 ft). Cuttings were sampled and mud return temperatures were recorded as drilling progressed. Drill vibrations suggested a thin zone of fractures at a depth of 52-53 m (170-175 ft), but notable inflow of water was not detected at any depth in the borehole. Artesian conditions were not observed, and temperature measurements were substantially lower than temperatures expected based on results of the Geoprobe survey (up to 45°C). Drilling terminated at a depth of 134 m due to the absence of hot temperatures and lack of water yield. Six days after drilling ceased, a temperature log and electric log were completed in the borehole to a depth of 107 m (350 ft). Temperatures varied less than 2°C over this depth range, reaching a maximum 24.3ºC (75.8°F) at a depth of 38 m (125 ft) and gradually decreasing from there to 107 m (350 ft), where logging ceased. The electric log made of this well correlates with the resistivity estimates completed by NETL in Section 5.4.2, although it appears the more conductive zones observed in the DC resistivity surveys are due to slightly higher salinities in the claystones, rather than increased porosity and hot water. A more detailed report is found in Appendix K.

8.2 DECEMBER 2017 AND JANUARY 2018 EXPLORATION WELLS

After drilling GEO#1, the City of Wells applied its remaining exploration funds to drilling three additional test wells. Another air-rotary exploratory borehole, GEO #2, was drilled (in the same area as GEO #1, Table 8-1) to a depth of 104 m (340 ft). This borehole, completed in early

January 2018, first encountered water in a thin permeable zone at 12 m (39 ft) with maximum temperatures at 32°C (90°F) at 13 m (43 ft) depth. Circulation was lost in fractures as drilling progressed to greater depths until the borehole penetrated clays at about 100 m (328 ft) depth. No logs are available for this well. Drilling was terminated due to declining temperatures. This appears to confirm the hypothesis of quite shallow thermal outflow at this location; however, the water was neither warm enough nor in sufficient quantities for large-scale direct use applications.

A third borehole (GEO #3) was advanced to a depth of 37 m (120 ft) in late December 2017 on the Bakes junk yard parcel near Metropolis Road, but was abandoned because of flooding by low-temperature water (~20°C or 68°F), presumably from the Humboldt River. No logs are available for this well.

In early January, borehole Geo#4 was also drilled on the north margin of the Humboldt River floodplain but closer to town, between the shallow temperature anomaly and the Reynolds well (see Table 8-1 for coordinates). Total depth indicated on the log is about 215 m (704.6 ft). Resistivity logs suggest fresh water down to a depth of 50 m (165 ft) and more saline water at greater depths with salinity increasing with depth. A spontaneous potential log suggests (preliminary interpretation) more porous and permeable layers between 24 and 34 m (80 and 110 ft) depth, between 72 and 90 m (235 and 295 ft) depth, between 101 and 146 m (330 and 480 ft) depth and between about 178 and 181 m (585 and 595ft) depth. A temperature log shows increasing temperature from the surface (34°C at 5 m or 93°F at 15 ft) to about 140 m (460 ft) where the temperatures recorded reached a maximum of 38°C (100°F) and decreasing temperatures from there to the bottom of the hole (approximately 35°C or 95°F). Temperatures were re-logged in late January, with the peak temperature now at 41°C (106°F), also at a depth of 140 m, but with the temperature profile showing the same trend of temperature reversal below 140 m depth. The maximum temperature is observed near the base of a log-interpreted layer of higher permeability (101 to 146 m or 330 to 480 ft depth), which could be a location of lateral flow for warmer water. This well first hit water at 11.6 m (38 ft) depth. Circulation was lost to fractures at around 55 m (180 ft) depth, but artesian conditions were not noted by the driller.

Table 8-1: Location of new exploration boreholes and maximum recorded temperatures (not at thermal equilibrium)

Borehole	Total Depth (m)	Maximum Temperature (°C)	Latitude	Longitude
GEO #1	107	24 (at 38 m)	41.130837N	114.986470W
GEO #2	104	32 (at 13 m)	41.129851N	114.984323W
GEO #3	37	20	Not Surveyed	Not Surveyed
GEO #4	213	41 (at 140 m)	41.124066N	114.979321W

Locations of these new boreholes are given in Table 8-1. Temperatures measured in these boreholes are plotted with depth in Figure 8-1. For comparison, temperatures reported on the driller's logs of the warmest existing wells (BTI and Reynolds wells) and on the geophysical log of the Dalton #1 oil exploration well (Jewel, 1982) are also shown on Figure 8-1. Although none

of these temperatures can be considered fully equilibrated, these data suggest that one should expect finding a resource suitable for direct use at moderate depths. It should be noted that none of these boreholes were cased to total depth and all were abandoned. For this reason it was not possible to re-log temperature in these boreholes after a period of time sufficient to ensure thermal equilibrium was reached in these boreholes. Also, no water samples were collected from these boreholes before they were abandoned. Because the holes were not cased, there may be cross flow between permeable zones in the well, thus complicating interpretation of the temperature logs.

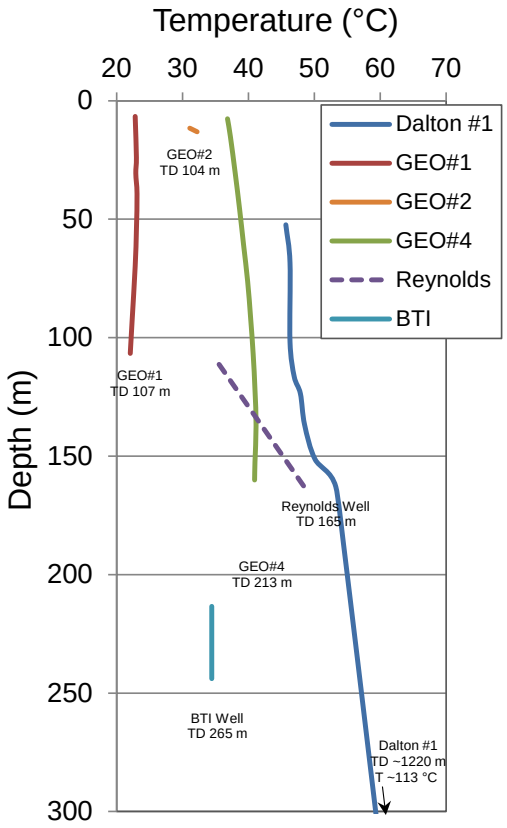

Figure 8-1: Temperatures measured in new exploratory boreholes (GEO #1, #2, and #4), existing warmest water wells (BTI and Reynolds wells), and the Dalton #1 oil exploration well (Jewell, 1982).

8.3 RECOMMENDATIONS AND RATIONALES

Geothermal features around the City of Wells make a compelling case for the availability of geothermal energy for direct use in the heating of buildings, homes, and various commercial and municipal uses. The heat likely comes from the regionally-elevated geothermal gradient, rather than from magmas recently intruded into the shallow crust of the Earth. Both conceptual models in Figure 2-1 remain under consideration; however, the geochemistry data and analysis (Section 5.3) favors the conceptual model in which thermal waters around the City of Wells originates from upwelling along a fault or fracture zone beneath the town. The thermal waters then mix variably with cold, shallow ground water and are tapped by municipal and residential facilities in

town. While future studies should continue to investigate the shallow outflow of thermal waters rising to the surface in the vicinity of the warm springs located to the northwest of Wells, future studies should also investigate deeper opportunities that may exist closer to town.

Some specific conclusions follow:

- *Geothermal upwelling is occurring along parts of the north-northeast-striking fault system on the west side of the Snake Mountains. Thermal springs and shallow temperature anomalies seem to coincide with the intersection of these faults with west-northwest-striking faults and fractures.*
- *The highest measured temperatures occur in hot springs several miles northwest of town, perhaps too far away and of insufficient flow volumes to economically pipe water to a district heating system in town. Exploration has therefore focused on areas much closer to town along the Humboldt River and adjacent to a north-northeast-striking fault system.*
- *Based on geothermometry, the estimated deep reservoir temperatures of the geothermal system(s) appear to be ~160° C (320°F), sufficient not only for district heating, but also for electricity generation. However, to obtain such temperatures, deep wells would be needed to reach this resource.*
- *A shallow thermal anomaly was identified along the north side of the Humboldt River floodplain. This area coincides with the possible intersection of north-northeast- and west-northwest-striking faults. Alternatively, this thermal anomaly could represent lateral geothermal outflow along permeable horizons within the Tertiary siltstone unit, coming from the hot springs area to the north.*
- *Different chemical and isotopic signatures were identified in thermal waters along and west of the Snake Mountains range-bounding fault (Northwest group) compared to thermal waters east of this boundary (East Group). The compositions of Northwest Group waters suggest a deeper origin, including older waters having a longer residency time, than for the East Group.*
- *Low electrical resistivity measurements in the shallow subsurface (depths < 50 m) along the northern margin of the Humboldt River floodplain northwest of town suggests the presence of either water with slightly higher salinity (which could be in low porosity rock, such as claystones and siltstones) and/or higher porosity material with warmer temperatures. While certain clays can result in lower resistivity measurements, more salinity would also need to be present in the clays to achieve the interpreted electrical conductivities.*
- *The exploratory well's temperature measurements did not reveal the expected level of locally elevated temperatures given the prior Geoprobe measured temperatures; however, the exploratory well did not measure temperatures at the exact location and depth where the Geoprobe measurements were made. Nevertheless, the discrepancy has cast some doubt on the veracity of the nearby Geoprobe temperature measurements, which were significantly higher than temperatures observed in the exploration borehole. The exploratory well also failed to locate higher porosity rock at depths drilled (other than a thin sandstone unit between 4 m and 7 m depth) and did not indicate significant up-flow (artesian conditions) of thermal waters on the hydrologically up-gradient side of the north-northeast-striking fault or along a hypothesized west-northwest-striking fault.*

The most likely scenario is that geothermal fluids are traveling laterally along the sandstone unit. The more electrically conductive rock at depth appears to be clay-rich rock, apparently with slightly higher salinities (although this was not tested), rather than the sought-after higher porosity rock encompassing warmer waters.

We present below several recommendations for continued exploration of both shallow hydrothermal outflow areas and deeper geothermal prospects. These shallow hydrothermal outflows are natural flows of water, which likely circulated to depths of 1 to 2 km along faults and fracture systems, fed by infiltrating water in the Snake Mountains and carrying heat up and into flow pathways at shallow depths (typically less than 150 m depth). In contrast, deep geothermal prospects exist wherever sufficiently hot rock is found at depth, often without significant quantities of fluids and permeability. Where permeable rock layers and fractures exist in these deeper, hotter rocks, existing flow pathways can be used to mine heat, typically with one or more pairs of wells through which circulation is created. The Dalton well's logs suggest temperatures are sufficient for the intended purposes and porosity exists at depths of perhaps 915 m or more.

Site-Wide Investigations:

- *A gravity survey with close-spaced (250 m) sample points over a region extending from the City of Wells to at least 12 km north, 8 km south, 8 km west, and 6 km east could better constrain deep subsurface architecture, including locations of major fault displacements and igneous intrusions. Further consideration of existing information on deep subsurface features (e.g., 2-D seismic survey, Section 5.5) should support the delineation of the area for a new gravity survey.*
- *Soil CO_2 flux measurements covering an area from the hot springs to the east across major north-south faults, the thermal anomaly identified during this study, and the area south of this anomaly and the Humboldt River, including Angel Road and structures near the Dan Morgan and Kevin Smith wells. The alternative is to obtain more shallow (2-meter depth) temperature measurements.*
- *A magneto-telluric (MT or CS-AMT) survey of close-spaced sample points across the existing geothermal focus area, and surrounding areas where hydrologic information would be of use, could further indicate zones of shallow outflow and possibly deeper zones of hydrothermal circulations, faults and other permeable zones.*

Shallow Hydrothermal Outflow Areas:

- *Additional shallow temperature surveys around the thermal anomaly. This should include:*
  - *a) 2-meter survey in hills immediately north of the thermal anomaly.*
  - *b) Additional Geoprobe holes.*
  - *c) Several shallow (<30m deep) boreholes or auger holes at select locations along the northern margin of the floodplain of the Humboldt River through the previously identified thermal anomaly area to gather additional temperature measurements, water chemistry and stable isotope samples, and well-yield (or permeability) measurements. Further probing of this prospect area seems prudent given the low costs of the probing. Additionally, if identified, resource located here would be inexpensive to develop. Priority should be given to locations where the EMI survey*

shows low electrical conductivity (which could distinguish the presence of less saline thermal waters from more saline surface and shallow ground water) and/or elevated CO_2 flux measurements.

- *Shallow temperature measurements along the dry bed of the Humboldt River, or in the river flow during low flow conditions, to further search for upwelling thermal water beneath the river. Downstream from the City of Wells and to the Snake Mountain Fault, thermal waters could be upwelling along north-south faults, along the intersection of permeable strata with the river and active stream alluvium, or along the "Wells Fault". This theory has scarcely been investigated.*

Deeper Geothermal Prospects:

- *Deeper Permeable Strata: The Dalton well, as described by Jewell (1982) and Jewell et al. (1994) indicates a substratum of the Humboldt Formation that has high porosity (as interpreted from density logs) and suitable temperatures (exceeding 88°C, 190°F) at a depth of nearly 915 m. The high porosity signature likely indicates relatively high permeability. Strata of interest appear to be permeable sandstones interbedded with shale layers, with a sequence thickness of about 91 m and a relatively high thermal conductivity (as indicated by the temperature log). These strata should be given prime consideration for further prospecting, given the useful attributes indicated and the possibility for exploitation of the heat resource via a pair of 1000 m deep wells for heat mining (i.e., the circulation of water between a pair of deep wells, one for injection and the other for production, to extract heat from the intervening rock). The lateral extent of the target strata is of interest for determining the placement of wells for long-term heat mining. Further determination of deep in-situ principal stress directions (via well- or core-derived data) would be helpful for planning a heat-mining project, as the in situ stresses control the orientation of induced hydraulic fractures and affect the characteristics of natural fractures.*
  - *Dalton Well – should be investigated for potential re-entry and use in logging and permeability testing. If plugged, depending on the type of plug it may be possible to drill through the plug and perforate the casing to test strata of interest. Some useful logging tools (e.g., gamma ray spectra logging, density logging, temperature logging) can be used in cased sections of a well, and more tools (e.g., formation micro-resistivity logging) are available for uncased sections of the well. Perforation of casing (if existing) in the high-porosity stratum at a depth near 1000 m and permeability and pressure testing of this stratum would support decisions on potential use of this stratum for heat mining.*
  - *New Seismic Reflection Data – At least one 2-dimensional seismic line oriented perpendicular to the existing seismic survey line could be procured to further support identification and delineation of deep prospects. The idea is to get information on basin geometry in the north-south direction to help with planning for deeper prospects, and to search for the "Wells Fault" or any other cross-strike discontinuities in this area. This is assuming that we will be successful in reprocessing and interpreting the seismic survey line previously purchased.*
  - *Additional geothermal gradient wells that can facilitate measurement of the gradients below the depths at which shallow cold water flows interrupt the deeper*

thermal gradient profiles. It would be most helpful to also get careful static water table measurements at different depths as the well is drilled, deeper water samples (for chemistry and isotope analyses) and logs of the strata in these wells (driller's log, geologist's interpretive log, gamma ray log, spontaneous potential log, and resistivity logs).

- *Deep Active Fault Zones: Several observed or inferred faults have been indicated by the 2008 earthquake and aftershocks as being active and, therefore, permeable. These are located north of town (including where higher temperatures have been observed). Some of these faults may be encountered by drilling at acceptable depths (perhaps as little as 1000 m) and could either yield a suitable flowing well or could be suitable for heat mining via a pair of wells. Among the potential targets: the east dipping fault causing the 2008 earthquake, three steeply dipping faults trending northwest to southeast, and the "Wells Fault". There are likely other fault zones at acceptable depths for drilling that may be detected with the 2008 earthquake aftershock data, seismic reflection data, and future passive seismic monitoring. These prospects should be investigated further. In particular, the 3D earth modeling done for this report could be supplemented with 2008 Earthquake aftershock hypocenters in an effort to locate additional active faults and fracture zones.*
    - *Continuing Seismograph Monitoring – low magnitude natural seismicity can indicate zones of permeable fractures. At oil and natural gas prospects, these zones are now being detected and even mapped through sensitive seismograph monitoring over long periods of time (months). This technique should be considered for prospecting in natural fracture zones near town through deployment of several portable seismographs.*

The acquisition of seismic data, as described above, could help locate fault zones at depth that could be permeable targets for either thermal water extraction or heat mining.

Additional Needs:

To facilitate further decision-making on deeper exploration, it would be most helpful to prepare a basic techno-economic analysis of a proposed district heating system, including an analysis of heat demand or market potential, surface equipment and piping costs, and a few options for hypothetical wells drilled to different depths.

9. REFERENCES

Barton, C.A., Zoback, M.D., and Moos, D., 1995. Fluid flow along potentially active faults in crystalline rock. *Geology*, v. 23, p. 23–27. https://doi.org/10.1130/0091-7613(1995)023<0683

Bauer, J. R., Nelson, J., Romeo, L., Eynard, J., Sim, L., Halama, J., Rose, K., and Graham, J., 2015. *A spatio-temporal approach to analyze broad risks and potential impacts associated with uncontrolled hydrocarbon release events in the offshore Gulf of Mexico*. NETL-TRS-2-2015; EPAct Technical Report Series; U.S. Department of Energy, National Energy Technology Laboratory, Morgantown, WV, 2015, p 60.

Bell, J.W., 2011. Interferometric synthetic aperture radar map of the 2008 Wells earthquake. *In:* DePolo, C.M., and LaPointe, D.D., editors, 2011, The 21 February 2008 M_w 6.0 Wells, Nevada earthquake—a compendium of earthquake-related investigations prepared by the University of Nevada, Reno [online version]: Nevada Bureau of Mines and Geology Special Publication 36, Appendix B, p. 479.

Bloomquist, R.G., 2004. Elko Heat Company District Heating System – A case study. *GeoHeat Center Bulletin*, June 2004, p. 7-10.

Coolbaugh, M.F., Sladek, C., Faulds, J.E., Zehner, R.E., and Oppliger, G.L., 2007. Use of rapid temperature measurements at a 2-meter depth to augment deeper temperature gradient drilling: Proceedings, 32nd Workshop on Geothermal Reservoir Engineering, Stanford University, Stanford, CA, Jan. 22-24, 2007, p. 109-116.

dePolo, C.M., 2008, Quaternary fault map of Nevada. Nevada Bureau of Mines and Geology Map 167, 1:1,000,000 scale.

EarthImager 2D Version 2.4.0, 2009. Resistivity and IP inversion software manual. Advanced Geosciences, Inc., Austin TX.

Ferrill, D.A., Winterle, J., Wittmeyer, G., Sims, D., Colton, S., Armstrong, A., Horowitz, A.S., Meyers, W.B., and Simons, F.F., 1999. Stressed rock strains groundwater at Yucca Mountain, Nevada. *GSA Today* v. 9, p. 2–9.

Garside, L.J., 1968. Geology of the Bishop Creek area, Elko County, Nevada: unpublished Master's thesis, University of Nevada, Reno.

Garside, L.J., 1994. Nevada low-temperature geothermal resource assessment: 1994. Final Report prepared for the Oregon Institute of Technology Geoheat Center. Nevada Bureau of Mines and Geology. DOE/ID/13223-75.

Heidbach, O., Tingay, M., Barth, A., Reinecker, J., Kurfeß, D., and Müller, B., 2008. The world stress database release 2008. sdf. https://doi.org/doi:10.1594/GFZ.WSM.Rel2008

Henry, C.D., and Colgan, J.P., 2011. The regional structural setting of the 2008 Wells earthquake and Town Creek Flat Basin — Implications for the Wells earthquake fault and adjacent structures. *In:* dePolo, C.M., and LaPointe, D.D., editors, 2011, The 21 February 2008 M_w 6.0 Wells, Nevada earthquake—a compendium of earthquake-related investigations prepared by the University of Nevada, Reno [online version]. Nevada Bureau of Mines and Geology Special Publication 36, pp. 53-64.

Henry, C.D., and Thorman, C.H., 2011, Geologic map of the Wells area, Elko County, Nevada. *In:* dePolo, C.M., and LaPointe, D.D., editors, 2011, The 21 February 2008 M_w 6.0 Wells, Nevada earthquake—a compendium of earthquake-related investigations prepared by the University of Nevada, Reno [online version]. Nevada Bureau of Mines and Geology Special Publication 36, Appendix A.

Hickman, S., Zoback, M.D., Benoit, W.R., 1998. Tectonic controls on reservoir permeability in the Dixie Valley, Nevada, geothermal field. Proceedings, Twenty-Third Workshop on Geothermal Reservoir Engineering, Stanford University. p. 291–298.

Hickman, S.H., and Davatzes, N.C., 2010. In-situ stress and fracture characterization for planning of an EGS stimulation in the Desert Peak Geothermal Field, Nevada. Proceedings, Thirty-Fifth Workshop on Geothermal Reservoir Engineering, Stanford University. 13 p..

http://earthquakes.usgs.gov/regional/qfaults.

Huang, H., and Won, I.J., 2000. Conductivity and susceptibility mapping using broadband electromagnetic sensors. *Journal of Environmental and Engineering Geophysics*, v. 5, n. 4, p. 31-41.

Huang, H., and Won, I.J., 2001. Conductivity and susceptibility mapping using broadband electromagnetic sensors. Presented at The International Symposium on the Application of Geophysics to Engineering and Environmental Problems, March 4-7, 2001, Denver, Colorado (Proceedings on CD).

Jewell, P.W., 1982. Geology and geothermal potential north of Wells, Nevada. University of Utah Research Institute, Earth Science Laboratory Open File Report DOE/ID/12079-83, 38 p.

Jewell, P.W., Rahn, T.A., and Bowman, J.R., 1994. Hydrology and chemistry of thermal waters near Wells, Nevada. *Ground Water*, v. 32, n. 4, p. 657-665.

Lopes, T.J., Buto, S.G., Smith, J.L., and Welborn, T.L., 2006. Water-table levels and gradients, Nevada, 1947–2004. U.S. Geological Survey Scientific Investigations Report: 2006-5100, 35 p., 3 pls.

Morris, A., Ferrill, D.A., and Henderson, D.B., 1996. Slip-tendency analysis and fault reactivation. *Geology*, v. 24, p. 275–278.

Peiffer, L., Wanner, C., Spycher, N., Sonnenthal, E., Kennedy, B.M., and Iovenitti, J., 2014. Optimized multicomponent vs. classical geothermometry: Insights from modeling studies at the Dixie Valley geothermal area. Geothermics, v. 51, p. 154-169.

Ponce, D.A., and Damar, N.A., 2017. Depth to pre-Cenozoic bedrock in northern Nevada. U.S. Geological Survey data release, https://doi.org/10.5066/F75B01DD.

Ponce, D.A., Watt, J.T., and Bouligand, C., 2011. Geophysical setting of the February 21, 2008 Mw 6.0 Wells earthquake, Nevada, Implications for earthquake hazards. *In:* dePolo, C.M., and LaPointe, D.D., editors, 2011, The 21 February 2008 M_w 6.0 Wells, Nevada earthquake—a compendium of earthquake-related investigations prepared by the University of Nevada, Reno [online version]. Nevada Bureau of Mines and Geology Special Publication 36, pp. 89-100.

Ramelli, A. R., and dePolo, C. M. (2011). Quaternary faults in the 2008 Wells earthquake area. *In:* dePolo, C.M., and LaPointe, D.D., editors, 2011, The 21 February 2008 M_w 6.0 Wells, Nevada earthquake—a compendium of earthquake-related investigations prepared by the University of Nevada, Reno [online version]. Nevada Bureau of Mines and Geology Special Publication 36, pp. 79-88.

Ramelli, A.R., and dePolo, C.M., 2011. Quaternary faults in the 2008 Wells earthquake area. *In:* dePolo, C.M., and LaPointe, D.D., editors, 2011, The 21 February 2008 M_w 6.0 Wells, Nevada earthquake—a compendium of earthquake-related investigations prepared by the University of Nevada, Reno [online version]. Nevada Bureau of Mines and Geology Special Publication 36, pp. 79-88.

Siler, D.L., Faulds, J.E., Mayhew, B., and Mcnamara, D.D., 2016. Analysis of the favorability for geothermal fluid flow in 3D: Astor Pass geothermal prospect, Great Basin, northwestern Nevada, USA. *Geothermics* v. 60, p. 1–12. https://doi.org/10.1016/j.geothermics.2015.11.002

Sladek, C., 2011. Effects on geothermal features following the February 21, 2008 Wells, Nevada earthquake. *In:* dePolo, C.M., and LaPointe, D.D., editors, 2011, The 21 February 2008 M_w 6.0 Wells, Nevada earthquake—a compendium of earthquake-related investigations prepared by the University of Nevada, Reno [online version]: Nevada Bureau of Mines and Geology Special Publication 36, pp. 377-383.

Smith, K., Pechmann, J., Meremonte, M., and Pankow, K., 2011. Preliminary analysis of the Mw 6.0 Wells, Nevada, earthquake sequence. *In:* dePolo, C.M., and LaPointe, D.D., editors, 2011, The 21 February 2008 M_w 6.0 Wells, Nevada earthquake—a compendium of earthquake-related investigations prepared by the University of Nevada, Reno [online version]. Nevada Bureau of Mines and Geology Special Publication 36, pp. 127-145.

Spycher, N., Peiffer, L., Saldi, G., Sonnenthal, E., Reed, M.H., Kennedy, B.M., 2014. Integrated multicomponent solute geothermometry. *Geothermics*, vol. 51, pp. 113–123.

Spycher, N., Peiffer, L., Sonnenthal, E.L., Saldi, G., Reed, M.H., and Kennedy, B.M., 2014. Integrated multicomponent solute geothermometry. *Geothermics*, v. 51, p. 113-123.

Thorman, C.H., and Brooks, W.E., 2011. Bedrock geology of the ranges bounding the Wells earthquake of February 21, 2008. *In:* dePolo, C.M., and LaPointe, D.D., editors, 2011, The 21 February 2008 M_w 6.0 Wells, Nevada earthquake—a compendium of earthquake-related investigations prepared by the University of Nevada, Reno [online version]. Nevada Bureau of Mines and Geology Special Publication 36, pp. 65-78.

Thorman, C.H., and Ketner, K.B., 1979. West-northwest strike-slip faults and other structures in allochthonous rocks in central and eastern Nevada and western Utah. Rocky Mountain Association of Geologists. 1979 Basin and Range Symposium. p. 123-133.

Thorman, C.H., Brooks, W.E., Ketner, K.B., and Dubiel, R.F., 2010. Preliminary geologic map of the Oxley Peak area, Humboldt County, Nevada. Nevada Bureau of Mines and Geology Open-File Report 2003-04.

U.S. Geological Survey, 2006. Quaternary fault and fold database of the United States. website:

WinGEM2 Software Users Guide, 2008. Geophex GEM2 Sensor, Geophex, Ltd.

Won, I.J., Keiswetter, D.A., and Sutton, L.A., 1996. GEM-1: A new multi-frequency electromagnetic sensor. *Journal of Environmental and Engineering Geophysics*, v. 5, n. 2, p. 129-137.

Zehner, R., 2016. Desktop study of geothermal potential in and around the City of Wells. Unpublished report for The City of Wells and Better Cities by Geothermal Development Associates, 9p.

Zehner, R., 2017a. Shallow (2-Meter) temperature survey in and around the City of Wells, Nevada: implications for geothermal exploration. Unpublished report for Elko Heat Company and The City of Wells by Zehner Geological Consulting, LLC, 12p.

Zehner, R., 2017b. Results of Geoprobe survey performed within the thermal anomaly identified by shallow temperature survey near Wells, Nevada. Unpublished report for Elko Heat Company and The City of Wells by Zehner Geological Consulting, LLC, 9p.

Zehner, R.E., Coolbaugh, M.F., and Shevenell, L., 2006. Regional groundwater geochemical trends in the Great Basin: implications for geothermal exploration. *Geothermal Resources Council Transactions*, v. 30, p. 117-124.

Zehner, R.E., Tullar, K.N., and Rutledge, E., 2012. Effectiveness of 2-meter and Geoprobe shallow temperature surveys in early stage geothermal exploration. *Geothermal Resources Council Transactions*, v. 36, p. 835-841.

Zoback, M.D., and Townend, J., 2001. Implications of hydrostatic pore pressures and high crustal strength for the deformation of intraplate lithosphere. *Tectonophysics*, v. 336, p. 19–30. https://doi.org/10.1016/S0040-1951(01)00091-9

Zuza, A.V., 2017. Preliminary geologic map of the southern Snake Mountains near Wells, Nevada. University of Nevada, Reno, Nevada Bureau of Mines and Geology.

APPENDICES

APPENDIX A – ZEHNER (2016) DESKTOP STUDY

APPENDIX B – ZEHNER (2017A) 2-M SURVEY REPORT

APPENDIX C – ZEHNER (2017B) GEOPROBE REPORT

APPENDIX D – ZUZA (2017) GEOLOGIC MAP AND CROSS SECTIONS

APPENDIX E – INTERPRETED NDWR LITHOLOGIC LOGS, LITHOLOGIC CROSS SECTIONS, AND TEMPERATURE PROFILES

APPENDIX F – WATER GEOCHEMICAL DATA COMPILATION FROM OLDER SOURCES

APPENDIX G – NEW WATER GEOCHEMICAL DATA

APPENDIX H – EXPLANATION OF DC RESISTIVITY SURVEY

APPENDIX I – CITY OF WELLS GEOTHERMAL DATA CATALOG

APPENDIX J – MATLAB SCRIPT FOR GENERATING FAULT PLANES IN EARTHVISION

APPENDIX K – GEO#1 GEOTHERMAL EXPLORATION WELL TECHNICAL MEMO

APPENDIX L – GEO#4 GEOTHERMAL EXPLORATION WELL DOCUMENTATION

APPENDIX A – ZEHNER (2016) DESKTOP STUDY

May 10, 2016

To: Layla Walz, City of Wells
Jolene Supp, City of Wells
Kelby Bosshardt, Better Cities

From: Rick Zehner, Geothermal Development Associates

Subject: Desktop Study of Geothermal Potential In and Around the City of Wells

Summary

Hot springs with temperatures up to 60°C (140°F) occur along a range-front fault which forms the western edge of the Snake Range. Geochemistry and field observations from past studies suggest that reservoir temperatures may be considerably hotter, possibly high enough to support a commercial binary power plant. Thermal wells in and around the City of Wells are cooler, and may represent outflow from this system, or may indicate a separate geothermal system located closer to the center of town. Distinguishing the subsurface flow of this system(s) is important in locating sites where thermal waters hot enough to support a district heating system are both close enough to the surface and a short enough distance from the proposed redevelopment area in town to make economic sense. Federal land ownership outside town further constrains the area suitable for short-term geothermal development.

A shallow (2-meter) temperature survey, along with geochemical sampling and down-hole temperature surveys in select areas around Wells are recommended as a first-step program to delineate possible drilling targets. This would be accompanied by an economic analysis that would determine the maximum depths and distances that hot water could be economically drilled and piped, in order to provide preliminary guidance to next-step development.

Introduction

Better City LLC of Ogden, Utah contacted Geothermal Development Associates (GDA) regarding the geothermal potential in and around the City of Wells, Nevada (CW) in January 2016. Better City had identified the thermal springs and wells in the area as being of potential benefit to the Downtown Core Economic Vision it had developed for the CW. In April 2016 CW hired GDA to assist it in evaluating this geothermal potential, and planning an exploration and development program.

This memo is meant to convey results of a desktop study performed by GDA that (1) compiled relevant work and data to date, (2) analyzed that data, (3) noted data gaps and suggest further work to fill those gaps, (4) proposed hypothesis that explain the data, and (5) make preliminary recommendations.

General Geology

Many geothermal systems in the world are associated with volcanoes and buried magmatic intrusions that occur along the Pacific “Ring of Fire”. Here the interaction of tectonic plates creates the conditions for magma generation (subduction zones and spreading centers). However, geothermal systems also form in areas undergoing regional extension, where the crust is being slowly pulled apart. This has the effect of thinning the crust, producing high heat flow as well as opening up near-vertical faults and fractures that serve as conduits for heated groundwater to reach the surface.

Northern Nevada is an area undergoing regional extension, which is associated with the Pacific-North American Plate boundary to the west (Figure 1). This extension has created the northeast-oriented valleys and uplifted mountains so characteristic of the Basin and Range geographic province. Nevada has hundreds of extensional-type hot springs and wells, most of which lie on or adjacent to valley-forming (range front) fault and fracture zones (Penfield et. al, 2010).

These surface thermal manifestations are indicative of subsurface geothermal reservoirs that can be tapped for various uses. A 'geothermal reservoir' is simply a permeable zone (an area of fractured bedrock or a sedimentary aquifer) that contains a large amount of heated water. The temperature and permeability of geothermal reservoirs varies greatly. Many geothermal systems in Nevada are hot enough (say ~130°F) to support direct uses such as greenhouses or district heating; a few are large and hot enough (>275°F) to produce commercial-scale electricity.

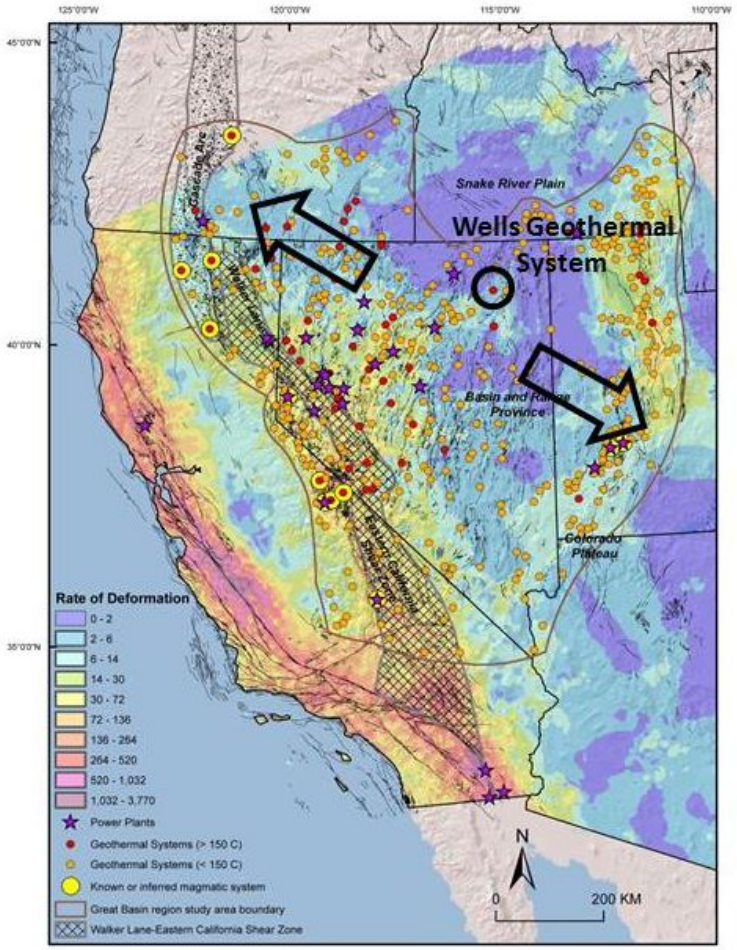

Figure 1. Map of the Great Basin showing the relationship of crustal extension to the location of geothermal systems. Arrows show the extension direction.

Thermal water from geothermal systems doesn't always reach the surface, and when it does, the spring or well is not always immediately above the geothermal reservoir. Sometimes a hot spring travels directly up a fault zone to come out right along the fault trace (the "upflow zone", Figure 2A). Other times the hot water encounters either a permeable horizon or the top of the water table, and moves laterally down the hydrologic gradient (the "outflow zone", Figure 2B). Exploration to target the geothermal reservoir largely involves using various geologic tools (shallow temperature surveys, geophysics, temperature gradient drilling, etc.) to track surface thermal features of outflow and upflow zones to locate the underlying reservoir.

Geology of the Geothermal System(s) In and Around the City of Wells

The area around Wells is underlain by Paleozoic sedimentary rocks, consisting primarily of low-permeability quartzite, limestone, and chert. These are unconformably overlain by Eocene to Recent

volcanic and sedimentary rocks of varying composition and permeability, which are flat lying to gently eastward-dipping in the Snake Range to the north.
Several hot springs occur north of Wells, rising along a range-front fault system that forms the western boundary of the Snake Range (Figure 3). This fault system extends to the south, where it splays to form both the northwest and eastern edges of the East Humboldt Range, and is thought to be the primary conduit where geothermal fluids rise to the surface. The hottest of these is Humboldt Hot Springs, with a measured surface temperature of 60°C (140°F).

Indirect evidence suggests that temperatures of the geothermal reservoir feeding these springs may be considerably higher. Credible geothermometer reservoir temperature estimates from water samples taken from these springs are in the vicinity of 140° - 150°C (285° - 300°F) and range somewhat higher[1]. These temperatures are well within the range required for binary power plants[2] (Table 1). In addition Jewell (1982) reports silicification along strands of the range front fault adjacent to the hot springs, which suggests that the geothermal system at least at one time had temperatures closer to 180°C.

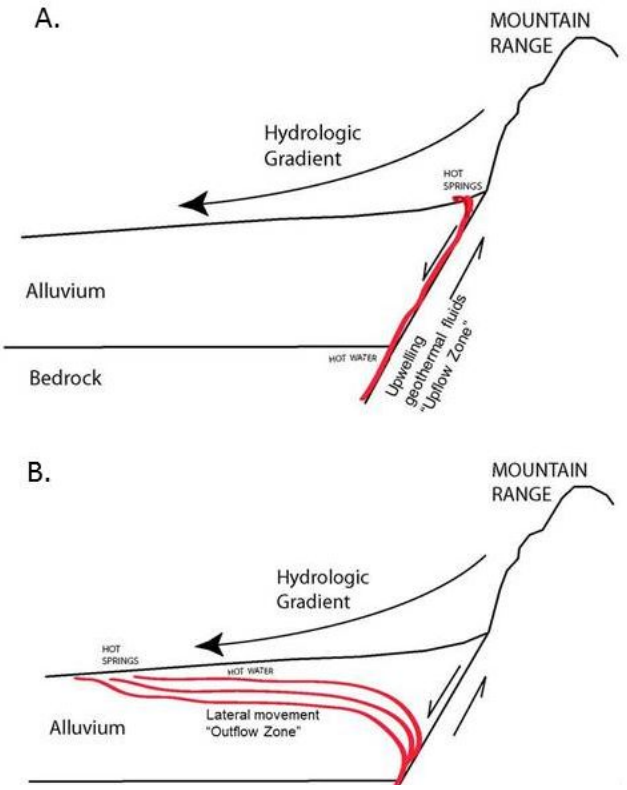

Figure 2. Effect of lateral groundwater flow on geothermal systems. A. Hot spring occurring at surface trace of fault (upflow zone). B. Thermal fluids that have become entrained in lateral groundwater flow may travel miles down-gradient to show up in distal thermal springs or wells (outflow zone).

Figure 4 shows a Piper Diagram, which plots the molar ratios of major cations and anions from the same springs (and one well) listed in Table 1. Several points are worthy of note. First, the geothermal system appears to be primarily of sodium-potassium bicarbonate composition, with low chloride and sulfate. Second, the hot spring samples plot fairly closely together, indicating they probably are sourced by the same geothermal system. Next, the cold springs that occur along the range front fault are considerably higher in calcium and magnesium, than the thermal waters, which is common in Nevada (Ca and Mg have solubilities that increase as temperature decreases). Last, the sample from the Reynolds Well plots intermediate between the hot and cold spring samples, implying some amount of mixing going on between geothermal and non-thermal groundwater.

[1] Data from Great Basin Groundwater Geochemical Database, available at http://www.nbmg.unr.edu/geothermal/GeochemDatabase.html, and Jewell (1982).
[2] Estimated geothermometer temperatures are estimates only, and are based on a number of assumptions, which include: (1) good sample collection and analysis, (2) that the thermal fluids are in equilibrium with rocks in the reservoir, (3) no mixing or dilution with cold groundwater, (4) no precipitation of minerals on the way to the surface.

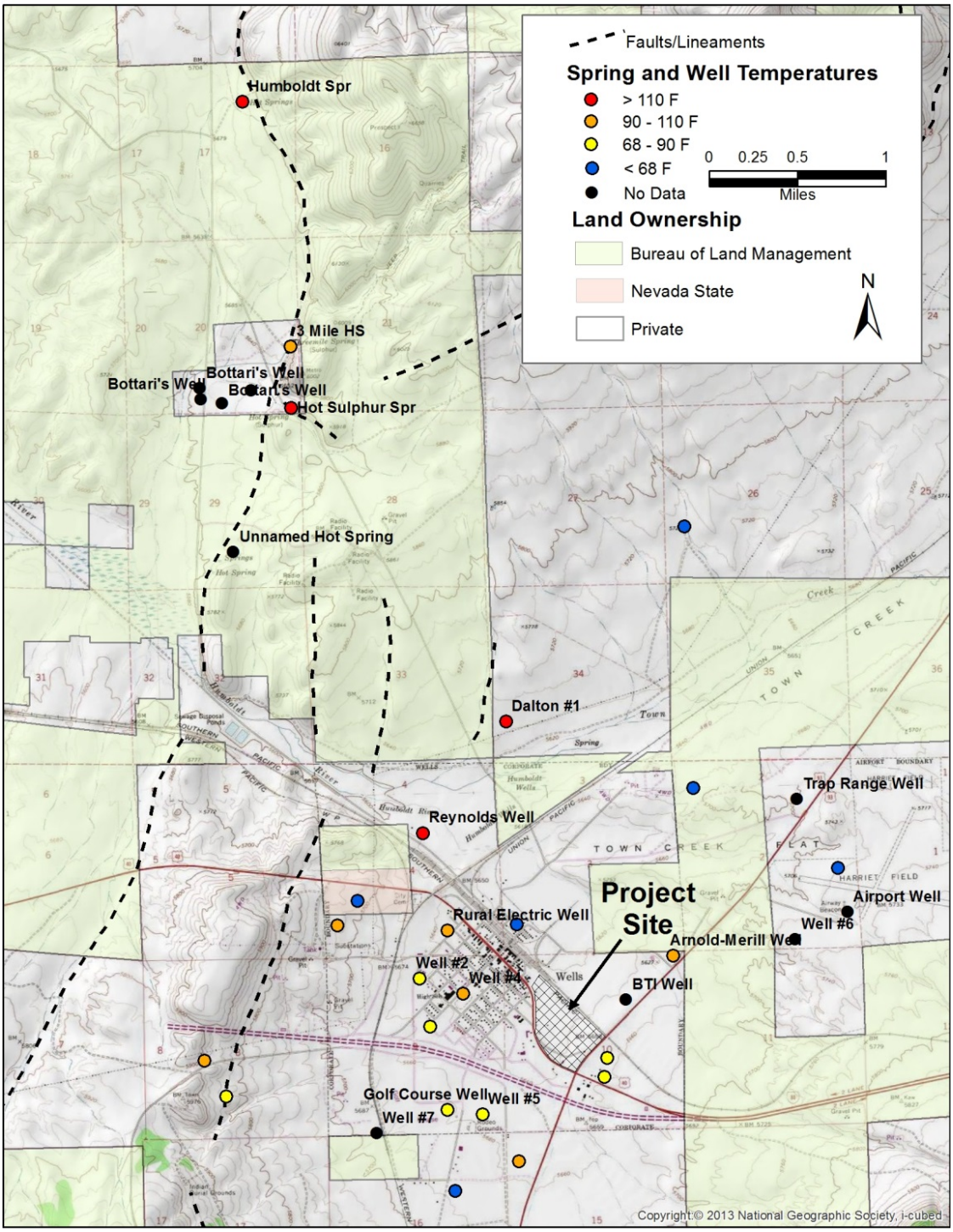

Figure 3. Map showing location of thermal springs and selected wells within the project area. Many cold wells are not shown.

Table 1: Estimated reservoir temperatures of the hot springs north of Wells, using four commonly used geothermometers.

Sample Name	Chalcedony	Quartz	Na-K-Ca	Na-K-Ca-Mg
Cold Spring (NW Sec. 9)	36.9	73.7	35.1	35.1
Humboldt Wells	116.5	137.2	178.6	34.0
Humboldt Wells	144.2	157.7	184.1	183.4
Humboldt Wells	101.4	125.7	199.3	80.4
Humboldt Wells	113.5	135.0	180.7	31.6
Humboldt Wells	104.7	128.3	190.5	72.6
Humboldt Wells	112.8	134.5	185.6	35.5
Reynold's Well	102.7	126.8	228.4	121.5
Threemile Spring	100.0	124.7	190.4	77.1
Threemile Spring	94.2	120.2	187.9	76.1
Threemile Spring	94.2	120.2	187.9	187.9
Threemile Spring	91.1	117.8	193.6	84.9
Twelvemile Spring	60.6	93.4	46.3	46.3

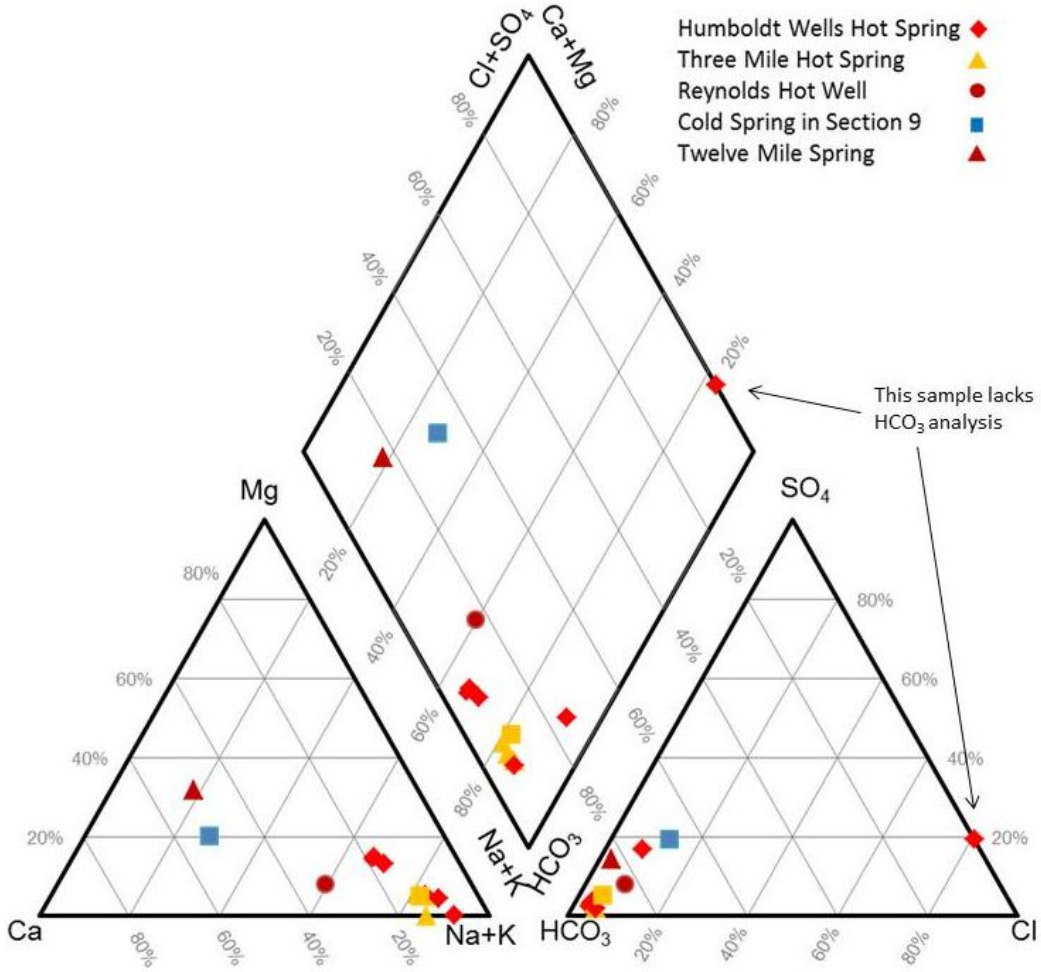

Figure 4. Piper Diagram of thermal and non-thermal springs and Reynold's Well in western Snake Range.

Thermal water has also been encountered in numerous wells in and around town. For example, the Reynolds Well just north of town reportedly has a measured temperature of 120°F, while City Well #4 at Wells High School, at 92°F, has been permitted as a geothermal well. In addition, Nevada Division of Water Resources (NDWR) data indicates that two residential wells off of Nevada Route 231 southwest of town have measured temperatures over 90°F. Shallow (25-30 foot) wells drilled at the Fourway Truck Stop just across Highway 93, close to the proposed redevelopment area are thermal, with measured temperatures of 85°F.

A depth versus temperature graph of wells in and around the CW is shown in Figure 5. This graph suggests that thermal and non-thermal wells are distinct populations; that is to say, encountering hot or cold water in any well is a hit or miss affair. The thermal wells (except the Reynolds Well) seem to show a fairly strong correlation between temperature and depth, on the order of 10°F per 600 feet of depth. If this temperature-depth relationship holds (which it probably does not), then one would have to drill a ~3,000 foot well to encounter a 150°F direct-use resource. Such a thermal gradient would not present an enticing target for drilling. The only well that is off this trend is the Reynolds Well, which has a much higher thermal gradient, and will be discussed in the following section.

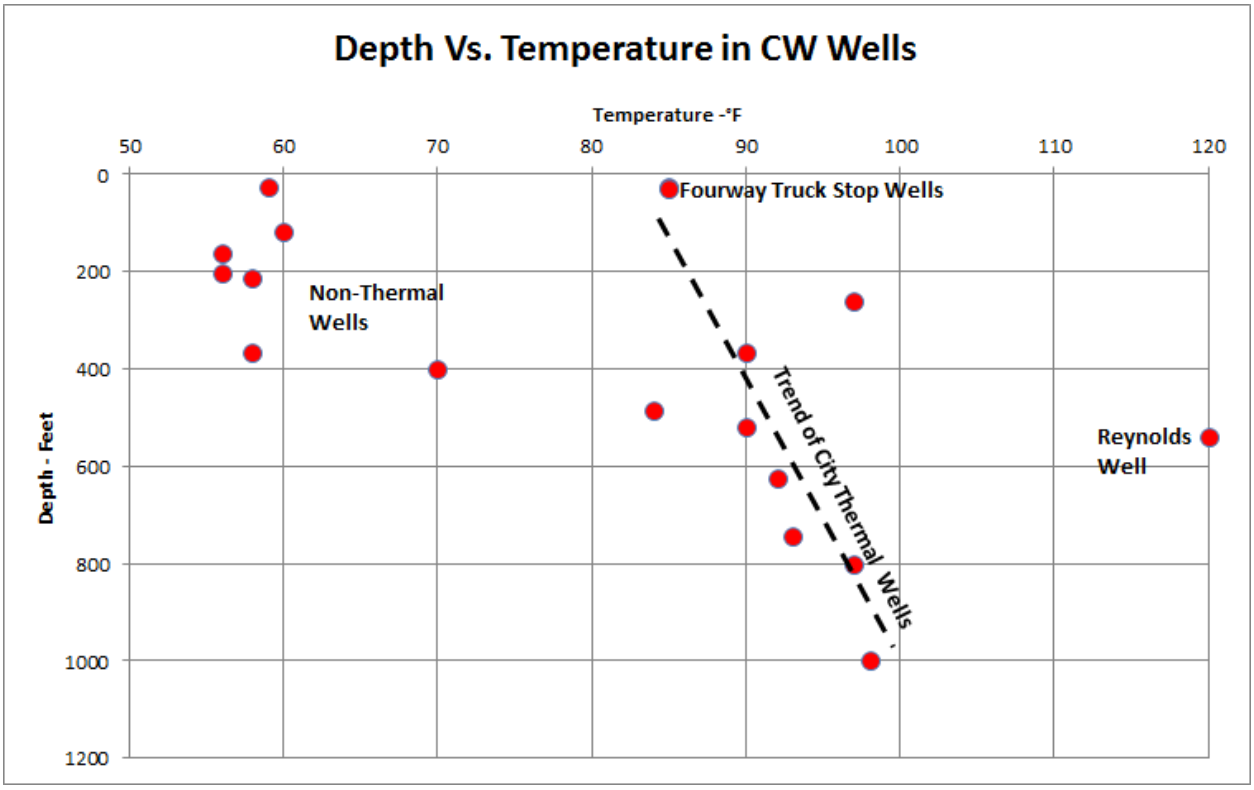

Figure 5. Depth versus temperature for select wells in and around the City of Wells. Many non-thermal wells are not shown.

The overall distribution of thermal springs and wells in and around the CW can be explained by two different scenarios. In Scenario 1, all of the thermal manifestations in and around CW are the result of upflow along the range-front fault system that forms the western boundary of the Snake Range and the northwest boundary of the east Humboldt Range. The warm CW wells are caused by upflowing thermal fluids encountering permeable horizons (sandstones and conglomerates) within the Miocene sedimentary rocks, which then flow eastward, mixing and diluting with cold groundwater (Figure 6A). In

the Scenario 2, the thermal waters in and around the CW are the result of a second “blind” geothermal system whose upflow zone is a near-vertical fault underlying the town somewhere (Figure 6B).

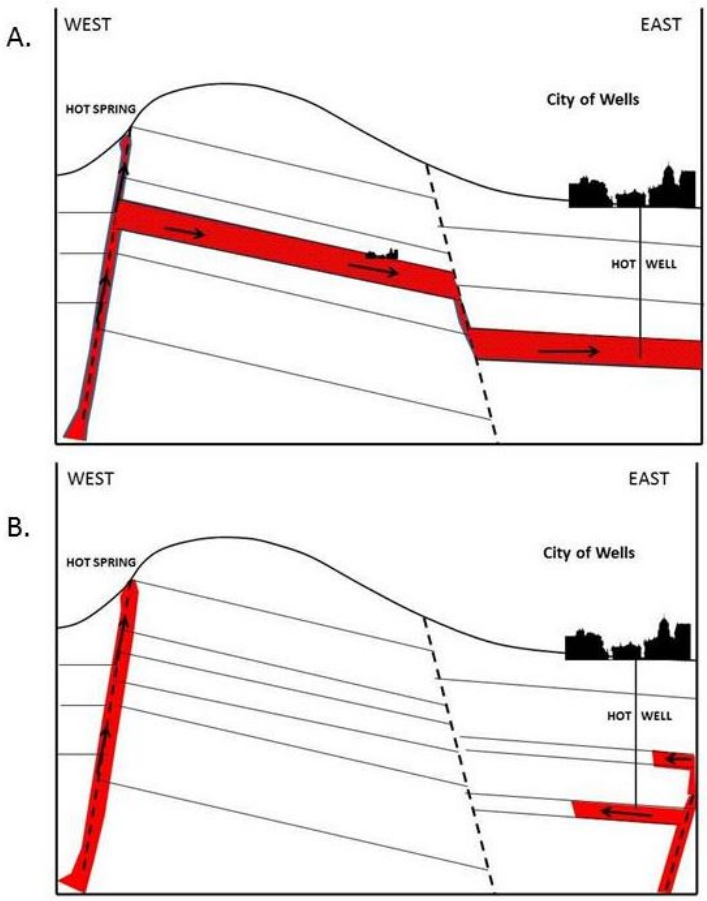

Figure 6. Scenarios that explain the distribution of springs and wells in and around the City of Wells. A: Scenario 1, where upflow and outflow from the range front fault system accounts for all thermal manifestations. B. Scenario B, where a second geothermal system with upflow directly below town accounts for the thermal wells.

A primary goal for future exploration will be to understand which of these two scenarios is actually occurring. If Scenario 1 is correct, then in order to obtain fluids of sufficient temperature for direct use, future exploration would focus on the range front fault system to the west. One could not count on deeper drilling to produce hot enough water. However, if Scenario 2 is correct, then exploration and development drilling could shift eastwards towards the center of town and the redevelopment site. This could result in a potential cost saving through reduced pipeline costs. Still, since Scenario 1 is simpler and requires only one, already-identified geothermal system, it seems the more likely hypothesis.

<u>Discussion and Recommendations</u>

The Better Cities report envisions the CW utilizing its geothermal resource for multiple direct use purposes. This includes district heating of downtown buildings, swimming and soaking pools, and green-housing, which could occur outside of the redevelopment area. To this GDA would like to add the potential for commercial electrical power production. This section will discuss ways in which the CW could potentially move these geothermal development plans forward.

First, as mentioned above, it is apparent that thermal waters are hot enough for direct use at the Humboldt Wells Hot Spring, and probably at some other locations along the range-front fault where thermal fluids are upwelling. Whether fluids hot enough for direct use lie at reasonable depth underneath the City of Wells is debatable. It seems likely that water in CW wells is distal outflow from that fault source; however, if there was evidence pointing to a separate geothermal system underneath Wells, the focus of exploration might shift to the downtown area.

One inexpensive way to test this would be to collect a suite of water samples from CW wells and have them analyzed for major cations and anions, plus some trace elements; currently no such water analyses are available. An aqueous geochemist could use this information to determine if the thermal wells had a

different source than the hot springs. Mixing models could also be employed to determine the amount of mixing of geothermal fluids with each other and/or cold groundwater. If this evidence suggested a different geothermal system underneath the CW, a close-spaced gravity survey could be used to try and identify the presumed source: an upflow structure[3].

This water sampling should be accompanied by down-hole temperature surveys of open wells in the CW that are not currently being pumped. This would allow for measurement of a rough temperature profile that would be helpful in tracking the lateral flow of hot and cold groundwater.

Along these same lines, a shallow temperature survey should also be employed in order to understand the subsurface flow of thermal fluids. The initial survey would be conducted on existing roads on both private and BLM land at an approximate density of 4 per square mile, with higher sampling density along the range-front fault system (Figure 7). Additional sampling would be directed to appropriate areas, once thermal anomalies were identified. This survey would yield an inexpensive reconnaissance view of the temperatures at shallow depth[4], which in turn would suggest where thermal fluids were close to the surface.

At least one field day should be spent examining the geology along the range-front fault, especially around the hot springs. This time would be spent gathering structural (fault & fracture) orientations and mapping areas of hydrothermal alteration as mentioned by Jewell (1982). This would aid in identifying cross-structures and dilatant zones that typically form upflow structures, and (via silica mapping) might help determine the maximum temperature of the reservoir.

Someone familiar with district heating systems should prepare a spreadsheet that calculates the economics of a district heating system, given a set of economic assumptions appropriate for the CW. This would be useful in calculating the maximum distance from source to customer, depths of production wells, and minimum production flows and temperatures needed to make the project economic. This information would then be used as a template to guide exploration. Although GDA has engineers with direct use experience, the Elko Heat Company probably has more immediate experience in an environment very similar to Wells.

Of all the thermal manifestations identified during this desktop study, one area stands out as being particularly prospective for direct use application: the Reynolds Well. This well has a much higher temperature gradient than any well in town (Figure 5), reaching 120°F at 540 foot depth. The well is relatively close (1.5 miles) to the center of the redevelopment area.

One interpretation of the driller's log is that the well intersects alluvial sediments and cold Humboldt River groundwater until it encounters Tertiary volcanic bedrock at 365 feet. The driller reports artesian conditions at this point, and the temperature increasing rapidly from 96°F (at 365 feet) to 120°F at total depth. Thus, in this area hot geothermal fluids are covered by cold groundwater flow at the near-surface. Recall that the geochemical data indicates that the Reynolds Well water is a mixture of geothermal fluids and cold groundwater. This suggests that the well temperature might be higher if it was drilled deeper and/or the well was better cased and cemented. So at first pass this the area around the Reynolds Well should be a primary area for exploration efforts.

[3] This fault would likely uplift higher-density basement rocks on one side of the fault and down-drop them on the other (and be covered by lower density Tertiary rocks). This difference in density would show up as a linear density contrast on a map.

[4] This technique can register thermal anomalies from depths up to several hundred feet, unless covered by cold groundwater.

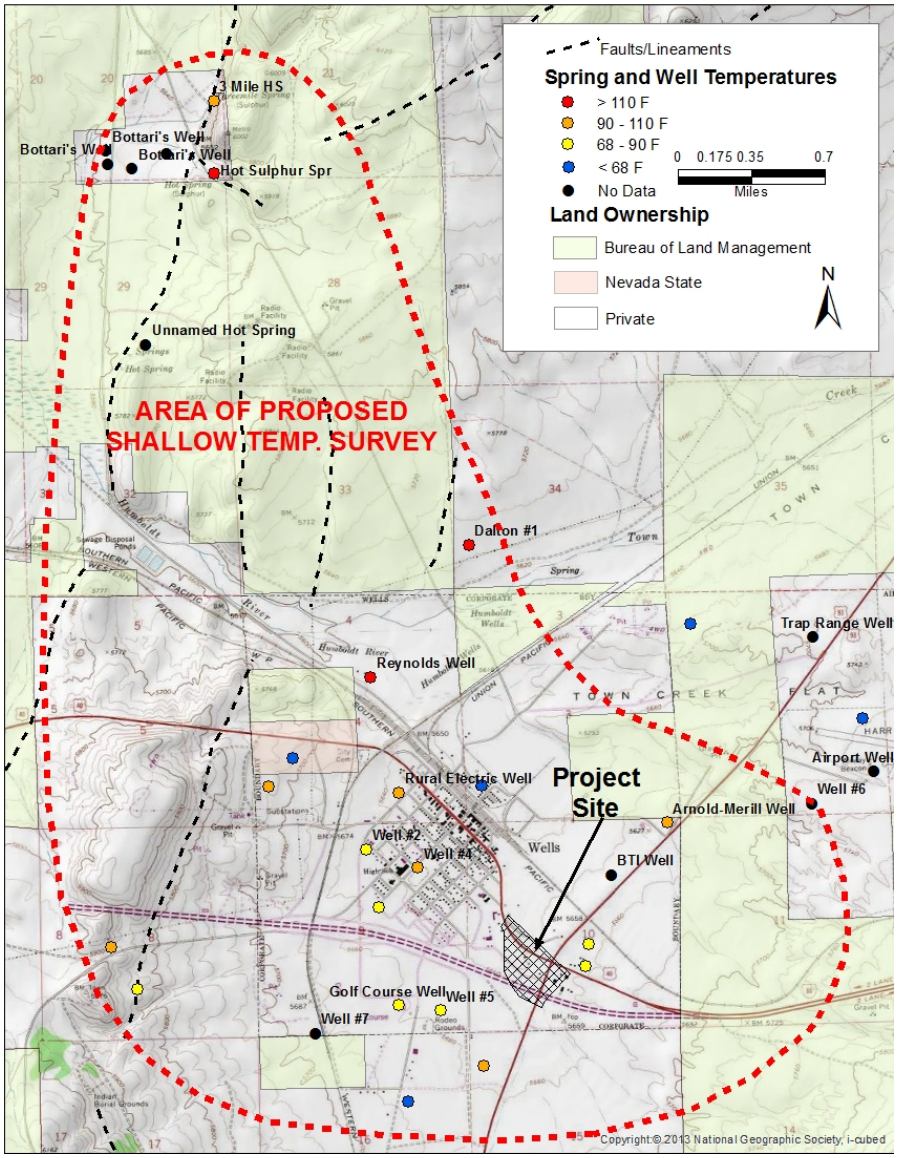

This memo has focused primarily on exploration for a direct-use project located primarily in the downtown and re-development area (the "Project Site" in Figure 7), but mention should be made regarding green-housing and commercial power plant development. Both are potential uses of geothermal fluids, but there are reasons for keeping them separate from the redevelopment area. For example, greenhouses take up lots of room, and power plants can require unsightly piping systems and generate noise as well as electricity. Happily, both uses can benefit from the higher temperatures known to occur outside of town at the hot springs.

Most or all of the recommendations for exploration work outlined above would benefit greenhouse or power development projects. The CW should consider these possible longer-term projects when planning their initial exploration program.

References

Better City, LLC, 2015(?), Downtown Core Economic Vision, Wells Nevada: internal report, 34 p.

Faulds, J.E., Hinz, Nicholas, Kreemer, Corne, and Coolbaugh, Mark, 2012, Regional patterns of geothermal activity in the Great Basin region, western USA: correlation with strain rates: Geothermal Resources Council Transactions, v. 36, p. 897-902.

Jewell, P.W., 1982, Geology and geothermal potential north of Wells, Nevada: University of Utah Research Institute, Earth Science Laboratory Open File Report DOE/ID/12079-83, 38 p.

Penfield, Robin, Shevenell, Lisa, Garside, Gary, and Zehner, Richard, 2010, Nevada geothermal resources: Nevada Bureau of Mines and Geology Map 161.

APPENDIX B – ZEHNER (2017A) 2-M SURVEY REPORT

Shallow (2-Meter) Temperature Survey in and Around the City of Wells, Nevada: Implications for Geothermal Exploration

Submitted to
Elko Heat Company and
The City of Wells

Humboldt Hot Spring Vent

by Zehner Geologic Consulting LLC

January 3, 2017

Summary

A shallow (2-meter) temperature survey was conducted in and around the City of Wells, Nevada, during late November and early December, 2016. Temperatures were measured at 1.0, 1.5, and 2.0 meters below ground level at 73 sites within the project area. Temperatures at 14 of the sites were considered to be at or above background levels (13.0°C, or 55.4°F). Indications of weak, western-directed thermal outflow was detected in sites adjacent to the Snake Mountains range front in the vicinity of the known hot springs. Two sites east of the range front near Sulphur Hot Spring indicate that thermal upflow is occurring on structures inboard of the range front.

The most interesting discovery from a direct-use standpoint was the identification of a strong thermal anomaly along the north edge of the Humboldt River due south of Sulphur Hot Spring. The anomaly is approximately 600 meters long with temperatures reaching 24.5°C (76.1°F) at 2-meter depth. The anomaly is interpreted to represent near-surface thermal outflow from the Three Mile – Hot Sulphur Hot Springs area, and is a probable source of thermal fluids to the Reynolds Well. If confirmed, this outflow represents an exploration target for a City of Wells district heating program.

Introduction

In November, 2016 the City of Wells, Nevada (COW) commissioned Zehner Geologic Consulting LLC (ZGC) to perform a shallow (2-meter) temperature survey in an area in and around the town of Wells (Figure 1). This survey followed recommendations of an earlier desktop study compiled by Geothermal Development Associates (Zehner, 2016).

The survey was conducted between November 29th and December 5th, 2016. A total of 73 shallow temperature stations were made on existing roads within the study area, following closely but not exactly the proposed site locations (Figure 1). Ground conditions prevented placement of rods to their full depth at some localities. Additional rods were placed in other locations as necessary to give a good initial appraisal of subsurface temperatures.

Approximately half the study area occurs on land administered by the U.S. Bureau of Land Management (BLM). Because of this, an application was submitted to the BLM to perform the proposed survey on existing roads, which would reduce potential impacts and expedite permitting. On June 14, 2016, the BLM issued a finding of casual use, but placed restrictions on the timing of the survey, and asked that no sampling occur at four of the proposed locations (Blue dots, Figure 1). Subsequent discussions with Gordon Harley of the BLM reached an agreement for alternative sampling of three of the sites: although the sites were not on BLM land, ZGC agreed to use alternative sites adjacent to the restricted ones.

During the survey, temperatures were measured at each site at 1.0, 1.5, and 2.0-meter depths below ground level and were recorded using an Omega HH804 data logger. The measurements taken at 1.0 and 1.5 meters are useful in obtaining localized gradients to confirm that any thermal anomalies identified in the survey are from a geothermal, rather than a solar source. However, since the survey was carried out in late fall when surface air temperature was consistently below freezing, the effect

of solar ground warming was minimal. The temperatures at 1 meter depth were considerably colder at all sites than at 2-meter depth.

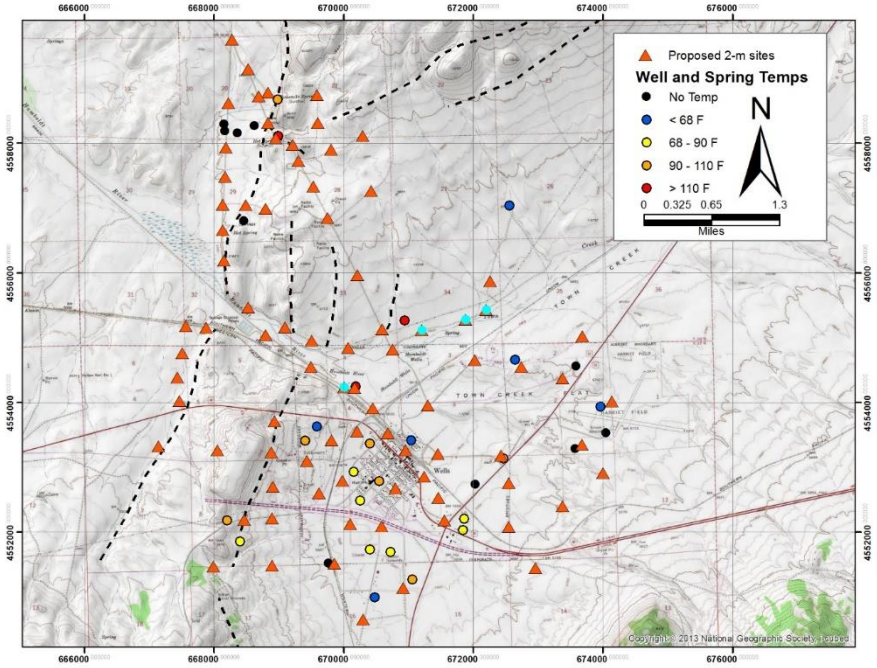

Figure 1. Map showing proposed locations of 2-meter sample sites within the project area. Sites highlighted with blue dots indicate the four sites where the BLM had environmental concerns.

Shallow (2-Meter) Survey Technique and Procedure

The shallow (2-meter) temperature survey method was developed by the Great Basin Center for Geothermal Energy at the University of Nevada at Reno (Coolbaugh et al., 2007; Sladek et al., 2007). It was devised to measure temperature as far below the zone of solar influence as possible, have minimal equilibration time, and yet be portable enough to fit on the back of a pickup truck or all-terrain vehicle.

The method utilizes a direct push technique where 2.3 m long, 1.4 cm outer diameter hollow steel rods are pounded into the ground using a demolition hammer. Resistance temperature devices (RTD's) are then inserted into the rods and allowed to equilibrate for one hour. The temperatures are then recorded, and the rods pulled out of the ground to be re-used at future sites. Usually multiple rods are planted over the course of an hour, and then the sampler returns back to the first station, measures the temperatures, pulls the rods, and so on, to eliminate waiting time. The equipment easily fits into the bed of a pickup truck, making the equipment extremely portable.

The technique does have limitations. Being direct push, the rods cannot penetrate hard substrates such as large cobbles or bedrock. In areas of hard substrates, rods can get stuck, causing delays and reducing the number of rods that can be planted and harvested per day. In addition, the effects of solar heating can be large, and depends on such factors as latitude, albedo, slope, aspect, and elevation. Although the daily effects of solar heating are minimized at 2-m depth, seasonal changes at 2-meter depth approach 10^{o}C in Nevada (Zehner, 2012), and temperature corrections must be made when performing return surveys at the same location, using long-term base station data. Sometimes, when measured temperatures are near the high end of background values, the source (solar or geothermal) of subtle temperature anomalies is difficult to resolve. Thermal anomalies that

are associated with a geothermal system are above background temperatures, and are distinct (i.e., spatially contourable), but remain somewhat qualitative in nature.

Equipment Calibration and Site Variation

The RTD's were given a temperature calibration check in Reno prior to the field work. The RTD's were bunched together and placed into a large bucket of cold water that was equilibrated to outside ambient temperature (Table 1). The RTD's were then placed in the center of a hot tub and temperatures measured. The results indicate that RTD precision is within about 0.1° – 0.2° Celsius. Several informal studies with probes spaced about a meter apart suggest that total temperature variance at a site is slightly higher, on the order of 0.5°C.

Table 1. Results of pre-field temperature calibration check. The blue-shaded area includes measurements (°C) from the bucket of cold water; orange-shaded area indicates samples immersed in the hot tub.

RTD	T 1.0	T 1.5	T 2.0	T 1.0	T 1.5	T 2.0
32	10.1	10.1	10.1	39.2	39.3	39.2
34	10.3	10.1	10.0	39.3	39.3	39.2
35	10.1	10.1	10.2	39.2	39.2	39.3
36	10.1	10.2	10.1	39.3	39.2	39.2
37	10.1	10.3	10.3	39.3	39.4	39.4
39	10.1	10.3	10.3	39.3	39.5	39.5
41	10.3	10.1	10.0	39.4	39.2	39.3
42	10.1	10.2	10.2	39.3	39.4	39.3
Mean	10.15	10.18	10.15	39.29	39.31	39.30
StDev	0.09	0.08	0.12	0.05	0.11	0.10

Anomalous Versus Background Temperature

After a couple of days in the field, it was apparent that background or non-anomalous temperatures at 2-meter depth were somewhere below about 13°-14°C, and that few stations had values above this background value. While plotting data in the field, the breakpoint between background and anomalous temperatures was provisionally set at 13°C. Using this as the dividing point, it became apparent that the shallow temperature survey had detecting a weak, westward-directed outflow zone in the eastern Bishop Flats are just west of the Threemile and Hot Sulphur Springs. Several stronger temperature anomalies occurred east and south of these hot springs and will be discussed in detail below.

A histogram of the data (Figure 2) shows a fairly typical bell-shaped curve with the greatest number of values in the 12° to 13°C range. The curve is steep on its right side, suggesting either that 13°C is too low of a threshold, or that the sample population was not entirely representative. Several of the intermediate-temperature measurements were adjacent to stronger anomalies, which were taken as evidence to indicate that they were also anomalous. This study assumes that the threshold between background and anomalous temperatures at 2-meter depth is within the range of 13.0° - 13.5° C.

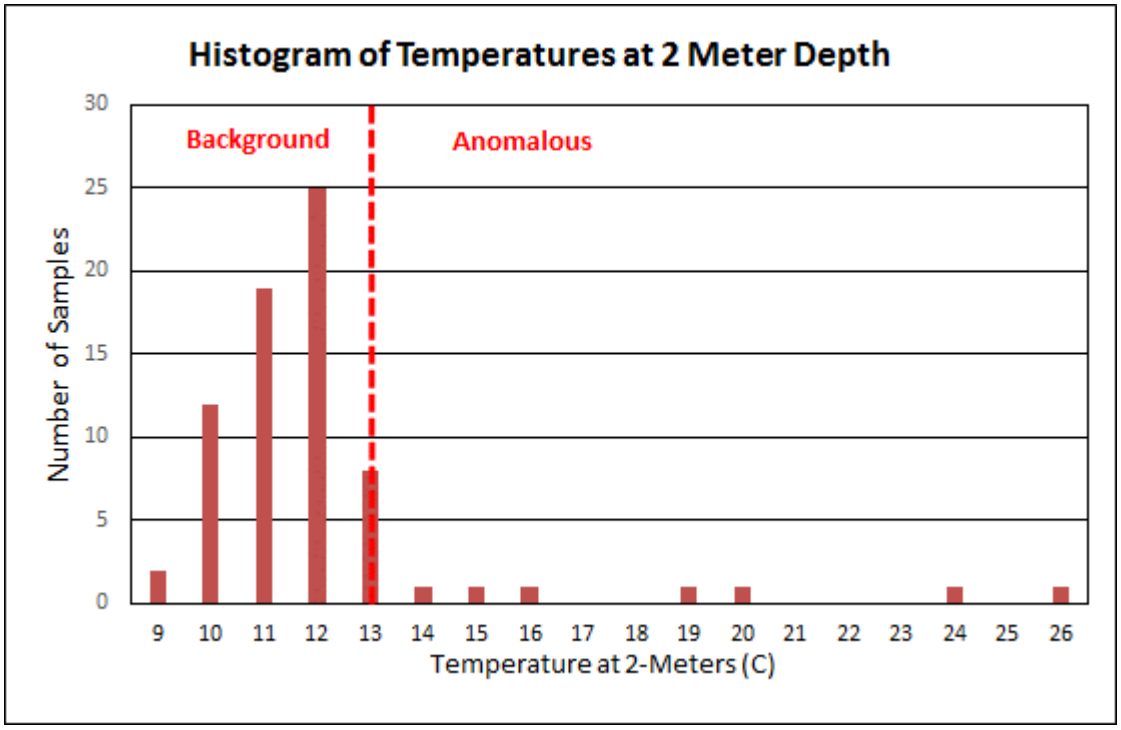

Figure 2. Histogram of measured temperatures from 2-meter depth.

Results and Interpretation of Shallow Temperature Survey

A map showing temperatures at 2-meter depth is shown in Figure 3; the field data are listed in Appendix 1.

Most of the sites appear to reflect normal background temperatures, especially those in the southern half of the study area. Sites adjacent to the thermal wells in and around town did not display anomalous temperatures. This indicates that shallow outflow is not occurring here, and/or that cold groundwater overlies and is masking the thermal waters. Since the City of Wells occupies a topographic low, the water table is close to the surface (typically 10 to 40 feet within town) and could be providing this masking effect.

All the sites with an apparent thermal anomaly occur within a mile or two of the known geothermal area. The site with the highest measured temperature at 2-meter depth (Site 80: 26.1°C) occurs just east and inboard from the range front, close to the reported location of Hot Sulphur Springs. The spring itself was not observed. A site over 300m to the southeast (Site 7: 16.5°C) was also anomalous. The temperature at these sites, east of and above the hydrologic gradient of the springs, seems to suggest the presence of fault structures inboard of the range front that serve as conduits for geothermal fluids.

A weak thermal anomaly in Bishop Flats west of the known hot springs probably represents westward-directed outflow from the geothermal system (area outlined by dashed magenta line in Figure 3). Although the four wells on private land in this area are labeled as having no measured temperature, they are reported to be thermal (Jolene Supp, personal communication).

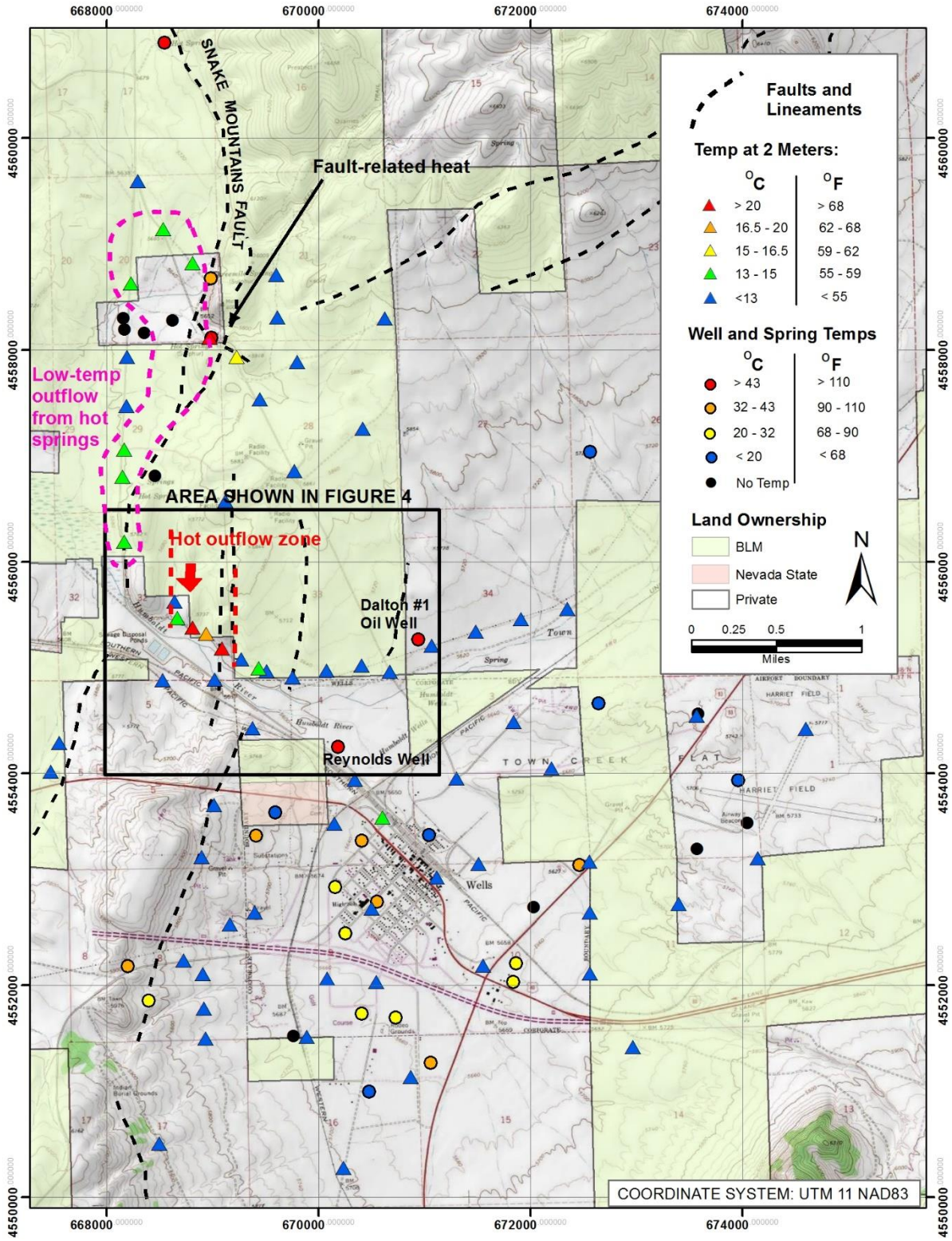

Figure 3: Map showing temperatures at 2-meter depth as measured by the shallow temperature survey.

Probably the most intriguing result of the shallow temperature survey was the identification of a thermal anomaly to the south of the known hot spring area (Figures 3 and 4). This anomaly is approximately 600 meters long, and occurs just north of the Humboldt River, at the southern edge of the hills that rise to form the Snake Mountains. This thermal anomaly is interpreted to represent

shallow, relatively high-temperature geothermal outflow entering the subsurface of the Humboldt River from the north or west.

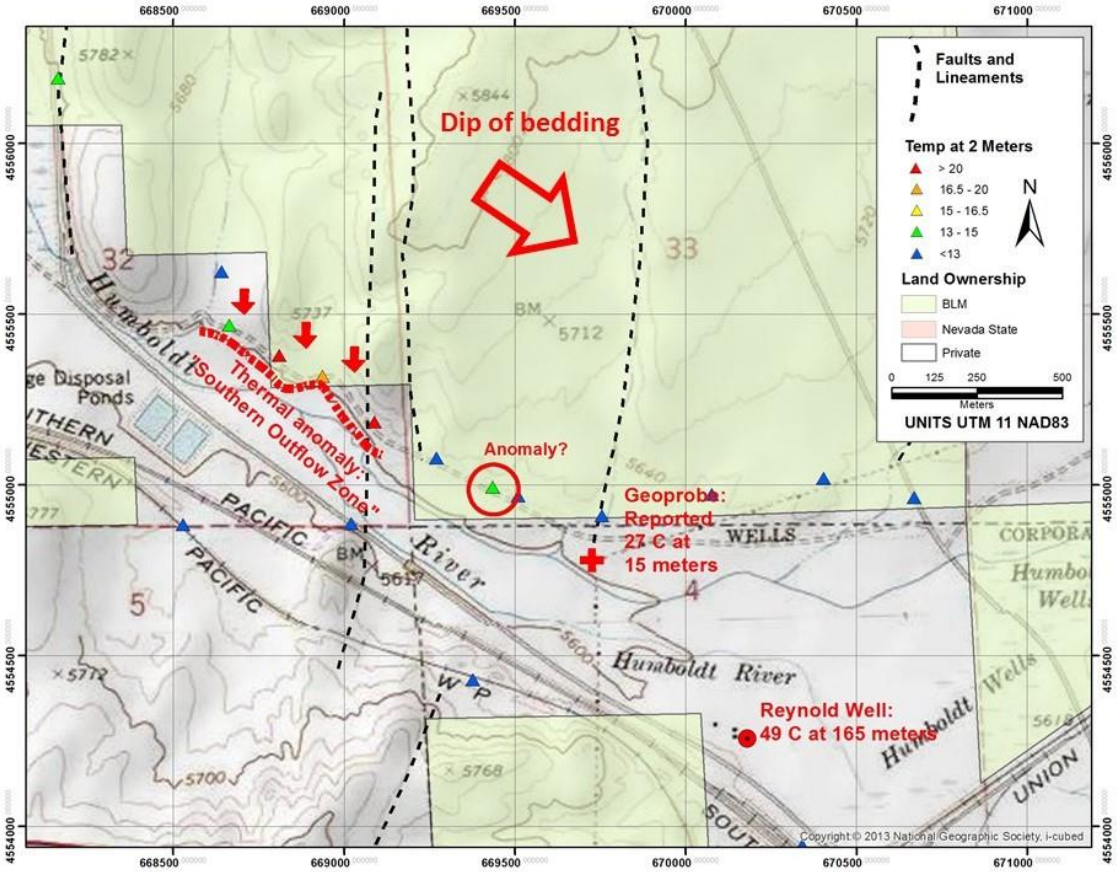

Figure 4. Close-up view of the thermal anomaly adjacent to the Humboldt River, showing both results of the 2-meter survey and the HEAT LLC Geoprobe test.

This probable outflow zone (herein called the 'Southern Outflow Zone', or SOZ) occurs about 1.5 km northwest of the Reynolds geothermal well. Zehner (2016) noted the high depth-to-temperature ratio of the Reynolds Well and speculated that it was being fed by a shallow thermal source coming from somewhere along the range front fault system that forms the western boundary of the Snake Mountains.

Interestingly, Humboldt Environmental Alternative Technologies LLC (HEAT LLC) performed a test Geoprobe hole on August 3rd of this year, at a location approximately halfway between the SOZ and the Reynolds Well (Figure 4). A Geoprobe is another direct-push device that pounds hollow rods into the ground to depths of up to 50 meters, and is used by the environmental industry to collect bottom-hole water samples. It has recently been employed by the geothermal industry to collect water samples and measure bottom-hole temperatures (Zehner et al., 2012). The Geoprobe hole made it down to 15 meters (50 foot) depth where it encountered thermal groundwater reported at 27°C (80°F).

The presence of a thermal anomaly at the Geoprobe site area calls into question the earlier dismissal of a weak thermal anomaly from a 2-meter site located roughly halfway between the Geoprobe site

and the SOZ (circled green triangle in Figure 4). It is possible that some additional outflow might be occurring to the east of the main SOZ.

Influence of Local Geology

Both Jewell (1982) and Thorman et al. (2010) indicate that the Snake Mountains are being uplifted and tilted gently to the east by the range front fault system, herein called the Snake Mountains Fault Zone (SMFZ), that hosts the geothermal system. In the area south of Sulphur Hot Springs and north of the Humboldt River, both authors show that the rocks are tilted approximately 25°to the east or southeast. Jewell's mapping around the SOZ further indicates that some fault-bounded segments have gentler dips or are subhorizontal.

The geologic map by Thorman et al. (2010) divides rocks in the study area into a Miocene formation they call the 'Sedimentary and Volcanic Rocks of Threemile Spring', which is a part of the Humboldt Formation as mentioned by Jewell (1982). The formation approaches 1 km in thickness, as measured from the drill log of the nearby Dalton #1 well (Figure 3; Jewell, 1982). The lowermost unit is a yellowish brown to tan lacustrine and fluvial unit composed of siltstone, sandstone, and conglomerate, which they report crops out in the westernmost railroad cuts. The middle unit is similar to the lower unit, but is characterized by abundant wood fragments and is separated from the lower unit by a coarse conglomerate that is locally silicified. The upper unit is composed of white to greenish vitric airfall tuff that may not crop out in the study area.

Silicification occurs along the SMFZ, as mapped by Jewell (1982). It is most prominent in the vicinity of Threemile and Hot Sulphur Springs, where fault silicification can be traced for 1,300 m (4,300 feet) along strike, and 75 m (250 feet) vertically. The Threemile Spring issues from a northeast-striking fracture in silicified conglomerate at the foot of the main range-front fault. Jewell (1982) also mapped silicification along a north-striking fault that crosses the Humboldt River and bisects the SOZ.

Some time was taken during the shallow temperature survey in order to examine the local geology. The rocks within the area shown in Figure 4 seem to correspond with the lower and middle units of the Threemile Spring formation of Thorman et al. (2010); the upper unit is probably not exposed. Both the lower and middle units consist predominately of poorly consolidated siltstone and lesser fine-grained sandstone that do not form good outcrop. Where they do form outcrop, bedding dips are to the southeast as mapped by Thorman et al. (2010). However, dips might be gentler (i.e. less than 25°) in poor outcrop areas.

Silicification within the faults consists predominately of chalcedony, with textures indicating multiple events of brecciation and re-healing. Silicified fault breccia clasts occur within a matrix composed of either silicified gouge or chalcedony veinlets. Fine-grained euhedral quartz was noted as open-space filling in vugs within the fault breccia.

The coarse conglomerate unit between the lower and middle units of the Threemile Spring formation bears some attention. It consists of one or more conglomerate and sandstone beds with thicknesses in the tens of feet. The unit is strongly silicified adjacent to the SMFZ near Threemile and

Hot Sulphur Springs; silicification appears to decrease downdip to the east and south. Silicification within this unit tends to form resistant dipslopes, such that the outcrop area of this unit is significantly overrepresented relative to its thickness. Limited exposures of the lower and middle siltstone units above and below the conglomerate appear to be unaltered, even a short distance from highly silicified beds. All of these features are suggestive of geothermal fluid flow coming up the SMFZ and moving laterally and downdip through the conglomerate unit, depositing silica as it went.

The silicification mapped by Jewell (1982) along the fault that intersects the Southern Thermal Anomaly appears on cursory inspection to be limited to conglomerate beds which are presumably part of this conglomerate unit. No evidence of fault-hosted silicification was observed at the SOZ, although detailed mapping might prove otherwise. The silicification consists of matrix-filling chalcedony, together with what appears to be white vitreous opal blebs and veinlets in the process of dewatering to chalcedony and/or β-cristobalite.

Jewell (1982) also mapped silicification south of the Humboldt River along the fault that crosses the SOZ. However, a cursory examination of outcrop in this area only identified carbonate cement in the siltstone cropping out along the county road south of the river. No thermal anomaly was detected in the hills south of the river, even with additional rods placed along the railroad tracks south of the county road. This would seem to indicate that fluid flow through the SOZ is coming from the north.

The textures and degree of silicification within the faults and conglomerates in the area between Threemile Hot Spring and the SOZ indicate copious fluid flow in what must have been a very robust early phase of the geothermal system. This phase must have been active prior to latest movement along the SMFZ: the top of the silicified fault ridge and conglomerate beds are some ~75 m (~250 feet) above Bishop Flats. At least the amount of the time it took to uplift the ridge that amount has passed since this phase of the system was active.

Conclusions and Recommendations

The shallow temperature survey identified thermal anomalies only north of the Humboldt River, in the general vicinity of the Threemile and Hot Sulphur springs. As mentioned above, 2-meter sites adjacent to the thermal wells in town did not have anomalous temperatures. Thermal waters must be emitting from sources other than the hot springs area: the Dan Morgan and Kevin Smith wells southwest of town are thermal and are located close to the southern trace of the SMF (no shallow outflow was detected at shallow temperature sites down the hydrologic gradient from them). Although a thermal well hot enough for direct use purposes (>150°F) would be ideally placed south of the river within the City of Wells, exploration in this area would be difficult and expensive.

The Southern Outflow Zone appears to be the one target identified by the shallow temperature survey worthy of follow-up in terms of future geothermal exploration. Its geologic nature is unknown, but it is possible that current geothermal fluid flow is similar to that of the earlier phase of the geothermal activity that deposited the silica that is seen on the surface. That is to say, upflow is occurring along north or northeast-striking vertical structures and outflow is occurring along southeast-dipping permeable beds. Three possible explanations for the origin of the SOZ are:

1. Upflow is occurring along the range front portion of the SMF, and is flowing down southeast-dipping permeable beds and through the SOZ.
2. Upflow is occurring along the range front portion of the SMF, but is somehow influenced by the silicified structure mapped by Jewell (1982) that intersects the SOZ, so that thermal fluids are redirected into the SOZ.
3. Upflow is occurring along the silicified structure mapped by Jewell (1982) that intersects the SOZ .

There is evidence to indicate that outflow from the SOZ continues southeastward underneath the Humboldt River alluvium to reach the Reynolds Well, and possibly continues on in the subsurface underneath the City of Wells. First, water from the Reynolds Well appears to be a mixture of groundwater together with geothermal fluids similar in composition to those of the Threemile and Hot Sulphur Springs (Zehner, 2016). Second, the bottom of the Reynolds Well is on strike and down-dip of a permeable bed that would constitute the SOZ. Third, the presence of a thermal anomaly in HEAT LLC's Geoprobe hole suggests that thermal fluids are present halfway between the SOZ and the Reynolds Well.

Although the SOZ is almost certainly not the only outflow zone around Wells that is potentially hot enough, and close enough, to serve City's direct use needs, it is an identified target worthy of additional exploration work. This work should include:

1. Follow-up Geoprobe holes in and around the SOZ. This should include four sites along the road within the SOZ and additional sites to the north and southeast, if the original four holes are successful.
2. Geochemical sampling of any fluids encountered by the Geoprobe.
3. A down-hole temperature survey of the (flowing) Reynolds Well, in order to measure temperatures below the cold water zone.
4. Geologic and structural mapping of the area from Humboldt Hot Springs south past the Humboldt River, from the range front east approximately two miles.
5. If hot enough fluids are encountered or inferred during the Geoprobe survey, a shallow rotary test well should be drilled.

References

Coolbaugh, M.F., Sladek, C., Faulds, J.E., Zehner, R.E., and Oppliger, G.L., 2007, Use of rapid temperature measurements at a 2-meter depth to augment deeper temperature gradient drilling: Proceedings, 32nd Workshop on Geothermal Reservoir Engineering, Stanford University, Stanford, CA, Jan. 22-24, 2007, p. 109-116.

Jewell, P.W., 1982, Geology and geothermal potential north of Wells, Nevada: University of Utah Research Institute, Earth Science Laboratory Open File Report DOE/ID/12079-83, 38 p.

Sladek, C., Coolbaugh, M., and Zehner, R.E., 2007, Development of shallow 2-meter soil temperature probes and results of temperature survey conducted at Desert Peak, Nevada, U.S.A., Geothermal Resources Council Transactions, v. 31, p. 363-368.

Thorman, C.H., Brooks, W.E., Ketner, K.B., and Dubiel, R.F., 2010, Preliminary geologic map of the Oxley Peak area, Humboldt County, Nevada: Nevada Bureau of Mines and Geology Open-File Report 2003-04.

Zehner, R., 2016, Desktop study of geothermal potential in and around the City of Wells. Unpublished report for The City of Wells and Better Cities by Geothermal Development Associates, 9p.

Zehner, R.E., Tullar, K.N., and Rutledge, E., 2012, Effectiveness of 2-Meter and Geoprobe shallow temperature surveys in early stage geothermal exploration: Geothermal Resources Council Transactions, v. 36, p. 835-841.

Appendix 1. Sample data. Spatial coordinates are in UTM 11, NAD83; temperatures are in Celsius.

Site	Northing	Easting	Date	Time	T1.O	T1.5	T2.0
Site1	4559593.2	668293.4	29-NOV-16	9:21:23	7.1	10.0	11.9
Site2	4559140.7	668534.4	29-NOV-16	12:52:2	8.5	12.4	15.0
Site3	4558820.5	668812.4	29-NOV-16	1:02:07	7.8	11.2	13.2
Site5	4558629.6	668230.2	29-NOV-16	9:42:19	7.9	11.2	13.3
Site7	4557933.3	669226.3	29-NOV-16	2:13:07	9.5	13.6	16.5
Site8	4557531.8	669447.2	30-NOV-16	7:56:39	7.1	12.4	11.7
Site9	4557888.4	669798.6	30-NOV-16	8:08:50	8.1	10.8	11.8
Site10	4558294.7	670624.9	30-NOV-16	8:19:53	7.2	11.0	12.5
Site12	4556854.9	669772.7	30-NOV-16	1:05:25	5.9	9.4	12.2
Site13	4557931.8	668189.7	29-NOV-16	9:51:41	7.3	11.2	12.7
Site14	4557468.7	668183.2	29-NOV-16	10:05:0	8.3	10.9	13.0
Site 15	4557058.0	668167.0	29-NOV-16	10:10	8.4	11.6	13.9
Site19	4554962.2	670670.0	30-NOV-16	1:35:48	6.1	9.0	11.1
Site 25	4556802.0	668146.0	29-NOV-16	10:22	8.3	12.2	13.7
Site26	4556192.0	668162.3	29-NOV-16	10:30:3	8.6	11.9	13.6
site27	4555623.8	668640.3	30-NOV-16	2:22:55	7.7	11.0	12.7
Site28	4555183.7	669089.1	30-NOV-16	2:14:09	16.4	21.4	24.9
Site29	4554966.9	669509.6	30-NOV-16	2:01:43	7.5	10.5	12.7
Site30	4554972.8	670076.9	30-NOV-16	1:46:57	7.2	10.3	12.3
Site34	4554488.1	671840.4	01-DEC-16	9:02:04	5.0	8.6	10.1
Site35	4553954.1	671303.0	01-DEC-16	8:38:47	5.9	10.5	10.0
Site36	4553705.0	669013.3	02-DEC-16	1:55:27	5.7	8.1	10.4
Site37	4553212.7	668896.1	03-DEC-16	10:18:4	6.2	10.0	12.4
Site38	4552575.8	669163.5	03-DEC-16	9:52:38	4.7	9.0	11.5
Site39	4552234.1	668724.0	02-DEC-16	9:24:56	8.7	11.3	12.7
Site40	4551497.7	668933.6	02-DEC-16	8:50:50	5.5	9.2	12.1
Site43	4551513.9	669890.4	05-DEC-16	1:45:40	5.9	8.5	11.5
Site44	4553944.7	670341.9	01-DEC-16	1:59:32	7.4	10.3	11.4
Site46	4553527.6	670148.7	01-DEC-16	2:15:49	7.0	9.8	11.5
Site49	4552063.7	670081.2	01-DEC-16	1:23:59	7.4	10.9	12.5
Site50	4552186.7	671549.9	01-DEC-16	1:43:36	7.6	10.5	12.7
Site52	4553021.3	671115.0	01-DEC-16	1:01:32	8.9	11.3	12.7
Site53	4553150.7	671510.9	01-DEC-16	9:38:37	5.7	8.9	10.0
Site55	4553583.7	670604.2	01-DEC-16	12:44:2	9.6	12.0	13.4
Site56	4552729.5	670501.6	01-DEC-16	1:15:26	5.8	9.1	11.2
Site57	4552031.2	670546.4	01-DEC-16	1:30:10	7.8	9.9	11.3
Site58	4554051.8	672197.8	05-DEC-16	1:27:56	2.1	6.8	9.5
Site59	4554546.3	673566.7	05-DEC-16	8:30:22	5.3	8.0	11.1
Site61	4554425.6	674600.3	05-DEC-16	8:49:45	5.8	9.3	10.8
Site63	4553203.9	674147.0	05-DEC-16	8:57:49	5.7	9.7	10.8
Site64	4552768.1	673398.3	05-DEC-16	9:05:38	5.6	8.8	11.2
Site65	4553169.2	672556.5	01-DEC-16	9:29:04	6.4	9.2	10.8
Site66	4552115.5	672561.7	05-DEC-16	9:29:45	5.2	8.5	10.6
Site67	4552690.5	672562.9	05-DEC-16	9:18:45	6.6	9.2	10.0
Site70	4554019.9	667470.7	03-DEC-16	12:45:2	7.2	10.4	12.4
Site74	4554289.7	667550.9	03-DEC-16	1:00:30	7.9	11.0	12.9

Site	Northing	Easting	Date	Time	T1.O	T1.5	T2.0
Site77	4551137.7	670870.3	05-DEC-16	10:06:2	6.4	9.6	10.8
Site78	4550276.1	670233.7	05-DEC-16	1:56:02	5.3	7.6	10.3
Site79	4551417.7	672967.4	05-DEC-16	9:50:39	5.1	10.0	11.8
Site80	4558113.3	668970.2	29-NOV-16	1:59:25	14.6	21.9	26.1
Site81	4558306.4	669612.6	30-NOV-16	8:47:42	6.9	9.9	11.8
Site82	4558707.5	669599.7	30-NOV-16	8:38:11	7.8	10.9	12.4
Site83	4557255.0	670415.7	30-NOV-16	1:13:34	7.5	10.7	12.2
Rogue1	4555018.7	670404.5	30-NOV-16	1:40:47	7.0	10.2	12.5
Rogue2	4554909.2	669755.8	30-NOV-16	1:53:33	6.7	10.1	12.2
Rogue3	4555206.6	671064.6	01-DEC-16	7:49:58	8.2	10.3	11.2
Rogue4	4555342.1	671481.5	01-DEC-16	7:58:55	6.9	10.7	12.2
Rogue5	4555457.6	671910.8	01-DEC-16	8:06:41	6.6	9.1	11.0
Rogue6	4555552.7	672348.1	01-DEC-16	8:16:58	6.3	9.6	11.1
Rogue7	4550509.4	668493.3	02-DEC-16	8:29:55	6.8	10.3	12.3
Rogue8	4551785.1	668915.4	02-DEC-16	8:56:22	6.8	10.5	12.9
Rogue9	4552108.4	668906.1	02-DEC-16	9:13:43	8.0	10.9	12.8
Rogue10	4552304.7	666829.1	02-DEC-16	9:50:04	7.7	10.5	12.3
Rogue11	4555378.5	668809.7	02-DEC-16	12:43:2	14.2	18.2	20.4
Rogue12	4555318.5	668936.1	02-DEC-16	12:49:2	12.3	16.7	19.4
Rogue13	4555079.0	669271.1	02-DEC-16	12:55:4	8.0	10.8	12.3
Rogue14	4554994.0	669434.9	02-DEC-16	1:11:46	8.0	11.1	13.3
Rogue15	4554886.2	669020.1	02-DEC-16	1:31:59	5.5	8.4	9.7
Rogue16	4552691.5	669399.4	02-DEC-16	2:25:08	5.2	9.5	12.5
Rogue17	4555467.5	668663.7	02-DEC-16	3:11:23	7.6	8.4	14.2
Rogue18	4556571.7	669119.3	03-DEC-16	9:00:50	7.1	10.2	11.9
Rogue19	4554429.0	669377.1	03-DEC-16	10:45:0	5.6	8.8	10.8
Rogue20	4554883.3	668528.9	03-DEC-16	11:16:5	7.0	9.5	11.4

APPENDIX C – ZEHNER (2017B) GEOPROBE REPORT

Results of Geoprobe Survey Performed Within the Thermal Anomaly Identified by Shallow Temperature Survey Near Wells, Nevada

Submitted to
Elko Heat Company and
The City of Wells

Geoprobe "Drilling" of Hole WGP-5

by Richard "Rick" Zehner
Geologic Consulting LLC

May 18, 2017

Summary

A direct-push Geoprobe survey was conducted on April 27, 2017 at a location approximately 2 miles northwest of Wells, Nevada. The survey consisted of eight non-cased holes ranging from 17 to 30 feet (5 to 9 meters) in depth, which explored a thermal anomaly identified by a previous shallow (2-meter) temperature survey. Measured bottom-hole temperatures were between 32.2° and 45.4° C (~90°-114° F), indicative of a very high geothermal gradient. None of the Geoprobe holes penetrated to the water table, so no water samples could be collected for geochemistry.

This gradient is interpreted to indicate the presence of geothermal fluids at a very shallow depth. These hot fluids could result either from upflow along a fault mapped by Zuza (2017), a south-directed outflow zone from the hot springs area to the north, or some combination of the two. This Geoprobe survey essentially verifies the anomaly found by the 2-meter survey and confirms this area as being a worthwhile exploration target for a City of Wells district heating system.

Introduction

The City of Wells (CW), together with the Elko Heat Company (EHC) and Better City LLC (BC), are continuing to explore the City's geothermal resources, as part of its Downtown Core Economic Vision. This report, which outlines the findings of a Geoprobe survey conducted in late April, 2017, is the third in a series of reports to the CW and EHC covering this topic[1].

The Geoprobe survey was conducted April 27, 2017 along a ~650 m long thermal anomaly identified by a shallow temperature survey conducted in late fall of 2016 (Zehner, 2016). This thermal anomaly, located approximately two miles northwest of downtown Wells on the north side of the Humboldt River, was thought to indicate the presence of hot geothermal fluids at relatively shallow depth. The Geoprobe was chosen as an inexpensive follow-up method to measure temperatures and obtain water samples at greater depths.

A Geoprobe uses direct push technology (DP) to advance a small diameter rod to depths up to several hundred feet in unconsolidated substrate (see picture on cover page). Unlike traditional rotary drill rigs, DP minimizes the impact of the drilling site because it creates little to no cuttings. The track-mounted Geoprobe that was used is 14 feet long and 5' 4" wide, utilizing 5-foot rods having a 2 ¼" outer diameter. The subcontractor performing the survey was Zacchary Woodbury of Humboldt Environmental Alternative Technologies Consulting, LLC. (HEATC LLC) with offices located at 1053 Idaho Street in Elko.

Typical Geoprobe methodology involves driving the tool string down until it can't go any further "rejection", then pulling back a few feet to create a "cellar" or void space at the bottom of the hole. After cleaning the inside diameter with water, a plastic tube is inserted down the string to just above the cellar. A resistive temperature device (RTD) can then be lowered to measure the bottom-hole temperature, and if the cellar is below the water table, a water sample can be collected. Temperature equilibration times range from several minutes under wet conditions, to several hours in dry holes. Like the 2-meter sampling technique, the Geoprobe has its drawbacks. Although it has

[1] The first report was a desktop study which described the geology and geochemistry of the thermal springs and wells of the area (Geothermal Development Associates, 2016). The study outlined a plan to explore for direct use resources, and pointed out the potential for power plant development. The second report (Zehner, 2017) described the findings of a shallow (2-meter) temperature survey, which identified (among other things) a shallow temperature anomaly that became the focus for the Geoprobe survey discussed in this report.

much greater “push” than the demolition hammer used in the 2-meter setup, it still cannot penetrate large amounts of the same obstacles, including bedrock.

Permitting Requirements and Issues

The dirt road on which the thermal anomaly was identified crosses both private land and land controlled by the U.S. Bureau of Land Management (BLM). Permission to operate the Geoprobe was acquired by the CW. However, a written request to punch some holes on BLM land turned up several critical issues, even while working on existing roads. This included the need for a reclamation bond, BLM consultation with the Nevada Department of Wildlife regarding sage grouse habitat, and a cultural inventory. Because of these issues, the decision was made to perform at least the initial Geoprobe survey on private land only. This had the effect of removing a ~200 meter (650 foot) section of the anomaly along the road, and two of the originally proposed sites, from being sampled.

Although the situation was easier permitting the Geoprobe on private lands, there were still some issues. Members of the CW, EHC, BC, and Zehner met for a scoping session with the Nevada Division of Minerals in mid-February 2017 to discuss (among other things) the upcoming Geoprobe survey. During this meeting, NDOM’s geothermal lead Lowell Price mentioned that (uncased) Geoprobe holes, under Nevada law, would need to be permitted as (cased) observation wells. Just prior to the survey commencing, when Zehner went to NDOM to file the paperwork, he was told that the Geoprobe holes would be permitted as temperature gradient wells, and as a result needed to be “drilled” by a licensed Nevada well driller. Quick actions on the part of CW and HEAT LLC were necessary to get the Geoprobe survey going on time. As it were, temperature gradient wells numbered WGP-1 through WGP-8 were permitted at eight sites (Figure 1).

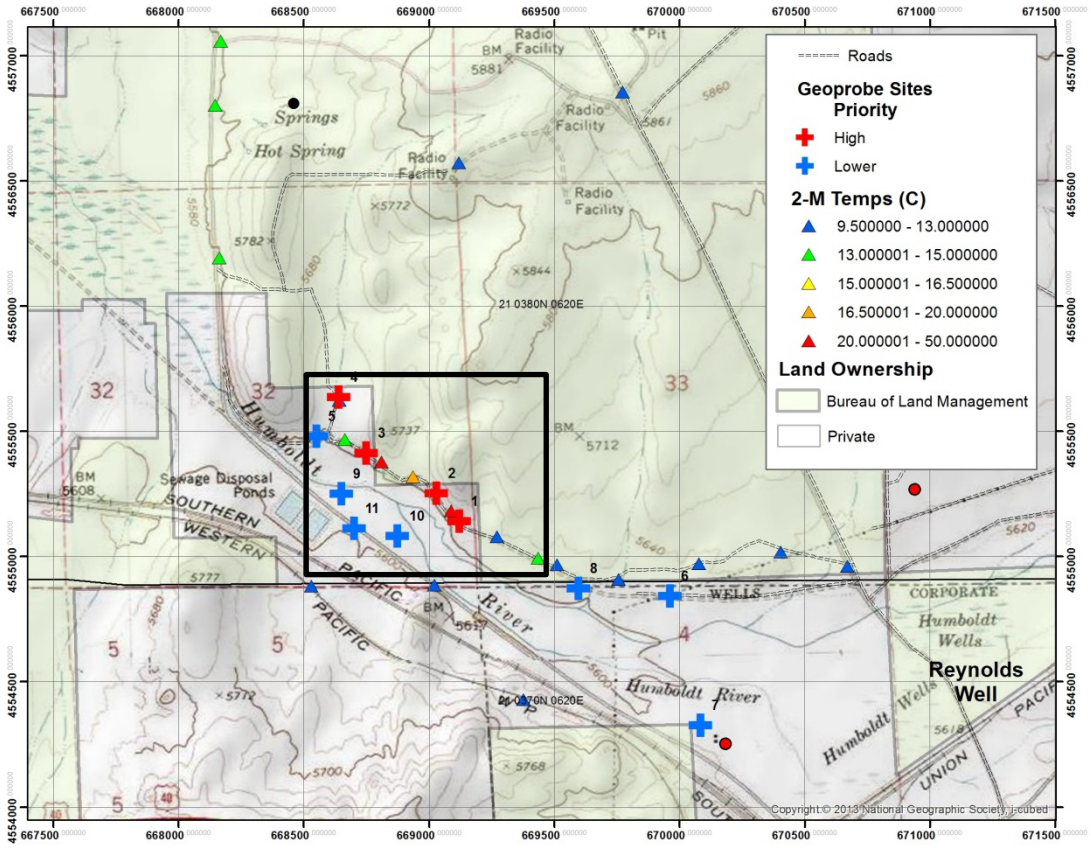

Figure 1: Original locations of Geoprobe sites, as envisioned prior to permitting. Sites 1-4, 6, 7, 8, and 11 were selected and permitted as temperature gradient wells. The final sites were different than this, as described below. Area enclosed in rectangle is shown in Figure 2.

The Geoprobe Survey

The Geoprobe survey started on the morning of April 27, 2017, and was completed by that afternoon. A total of eight holes (or "wells") were punched into the ground. Although the maximum depth reached in any of the holes was 30 feet, bottom-hole temperatures from each hole were well above the normal geothermal gradient (Table 1). The maximum measured temperature of 45.4° C (113.7° F) from hole WGP-5 was warmer than the Threemile Spring to the north and any of the thermal wells from around town to the south and southeast, including the Reynolds Well.

Table 1: Information about the Geoprobe survey. Temperatures are from the bottom of the hole. Location data are in UTM 11, NAD83.

Well	Site	Easting	Northing	Depth Ft	Temp F	Depth M	Temp C
WGP1	WGP1	669,122	4,555,144	23	92.5	7.0	33.6
WGP2	WGP2	669,028	4,555,260	22	112.5	6.7	44.7
WGP3	WGP3	668,746	4,555,424	30	91.9	9.1	33.3
WGP4	WGP9	668,957	4,555,274	23	90.0	7.0	32.2
WGP5	WGP10	668,998	4,555,245	19	113.7	5.8	45.4
WGP6	WGP11	669,071	4,555,176	26	98.1	7.9	36.7
WGP7	WGP12	669,079	4,555,196	17	100.6	5.2	38.1
WGP8	WGP13	669,059	4,555,219	19	104.2	5.8	40.1

During "drilling" of the first three holes, it was noticed that the Geoprobe was encountering a hard substrate that it could not penetrate. Because reaching the water table was of primary importance (both to measure temperatures and for collecting water samples), it was decided to abandon the strategy of sampling according to the original plan with sites outside the thermal anomaly (i.e., Figure 1) and focus on it. As a result, the locations of WGP-4 through WGP-8 were relocated to sites within the thermal anomaly (Figure 2). Unfortunately, none of the later holes hit the water table, either, so no water samples ended up being collected.

Field Work Concurrent with the Geoprobe Survey

During the latter half of April 2017, several other groups were conducting field work for the CW and EHC. As it is presumed that they will issue their own detailed reports, only those portions of their work that is relevant to the Geoprobe survey will be mentioned here.

Andrew Zuza of the Nevada Bureau of Mines and Geology conducted a week-long field mapping exercise focused on the structure and stratigraphy of the Wells geothermal system (Zuza, 2017). A primary goal was to confirm the mapping of Jewell (1982) and Thorman and others (2012), as well as the observations of Zehner (2016). Several points are worthy of note. First, Zuza mapped the conglomerate unit mentioned by the previous workers, both north and south of the Humboldt River. In addition, he identified and mapped an additional white tuff marker bed. Both of these are important in unraveling the stratigraphic and structural history of the area. Next, Zuza mapped several faults that comprise the Snake Mountains range front fault system, including one north-south structure mapped by Jewell (1982) that passes through the thermal anomaly. Last, his mapping confirmed the general model of Zehner (2016), in which geothermal upflow is occurring along the main range-front faults and traveling down-dip in permeable east-dipping beds.

In addition, geochemists from Lawrence Berkeley National Laboratory (Nic Spycher and Markus Bill) and the Great Basin Center for Geothermal Energy (GBCGE; Bridget Ayling) conducted an extensive sampling campaign of springs and wells in and around the City of Wells. When they arrived to sample the Reynolds Well, they found out through the owner that the well is cooler than originally

thought (106° F). They also determined that the well is under considerable hydraulic head, and could not be opened for a down-hole temperature survey. The implications of this finding will be discussed below.

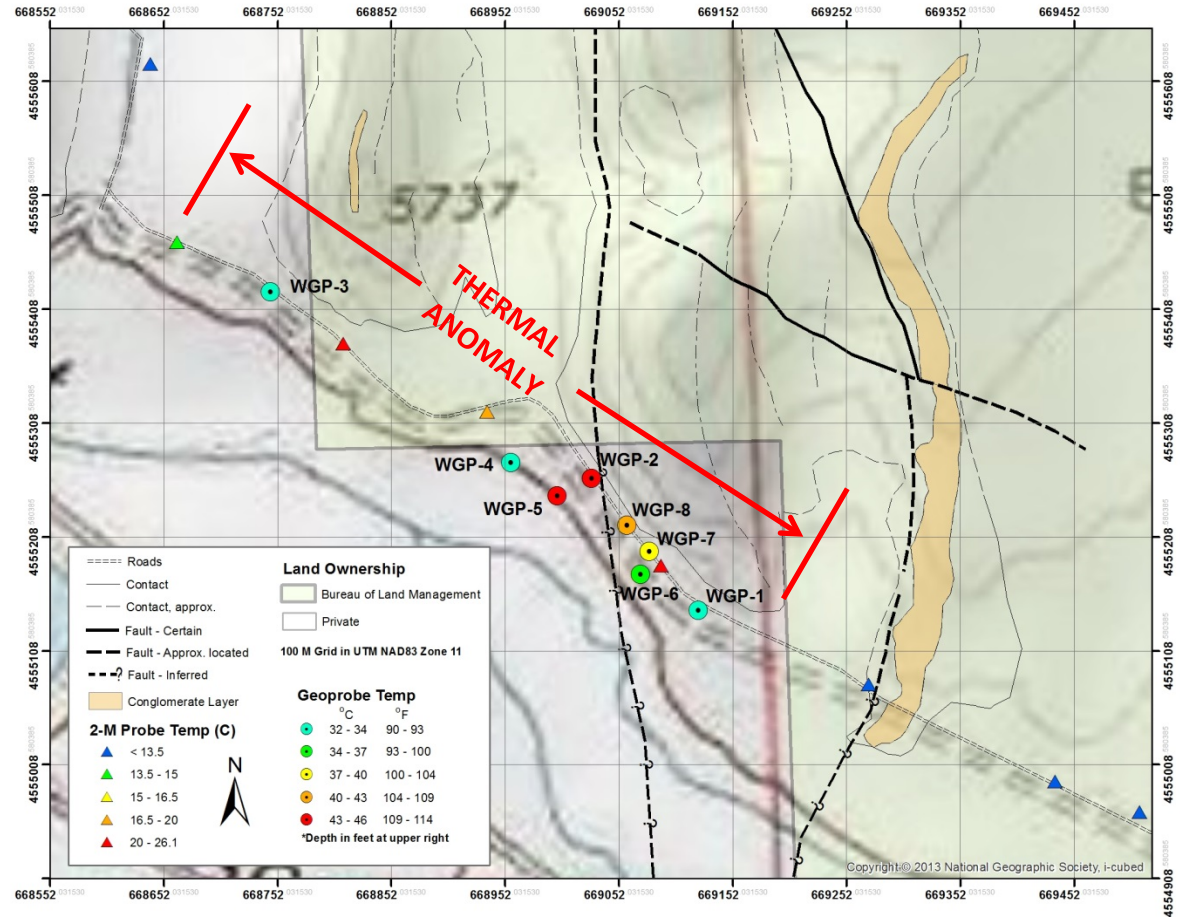

Figure 2: Location and bottom-hole temperatures of the "drilled" Geoprobe holes, along with temperatures from the fall 2016 2-meter survey. Geology from Zuza (2017). Note that no holes could be "drilled" in that part of the anomaly which is on BLM land.

Finally, Zuza recently received a preliminary copy of the LIDAR data from a survey run over the region several years ago. A hillshade model derived from this data tends to confirm many of the faults mapped by previous workers. Of particular note is a short north 70° west-striking lineament that occurs just north of the Humboldt River, adjacent to the thermal anomaly. The implication here is that the hot waters presumably underneath the thermal anomaly may be rising up a structural intersection with the north-striking fault shown on Figures 2 and 3. These data are preliminary.

Discussion

The high bottom-hole temperatures measured by the Geoprobe survey can only be the result of hot geothermal fluids at shallow depth underneath the thermal anomaly. Zehner (2016) proposed that this thermal anomaly could form geologically in one of three ways:

1. Upflow is occurring along the range front portion of the Snake Mountains fault zone to the west, and is flowing down southeast-dipping permeable beds and through the thermal anomaly.
2. Upflow is occurring along the range front portion of the Snake Mountains fault zone, but is somehow influenced by a fault mapped by Jewell (1982) and Zuza (2017) that intersects the thermal anomaly, such that thermal fluids are redirected into it.

3. Upflow is occurring along the fault mapped by Jewell (1982) and Zuza (2017) that intersects the thermal anomaly.

Which hypothesis is closest to the mark is still unknown. However, the hottest part of the thermal anomaly lies square on top of the fault mapped by Zuza (Figure 2), which would seem to favor arguments 2 or 3 above. When it became apparent during "drilling" that the hottest holes were adjacent to this fault, several 2-meter probes were planted south of the Humboldt River so as to intersect its southern projection (Figure 3). Identifying a thermal anomaly to the south would presumably support the third argument, because it would be difficult (but not impossible) for shallow outflow from the hot spring area reaching south of the river. However, none of the 5 2-meter sites south of the river along the fault trace detected any sort of a thermal anomaly at 2-meter depth.

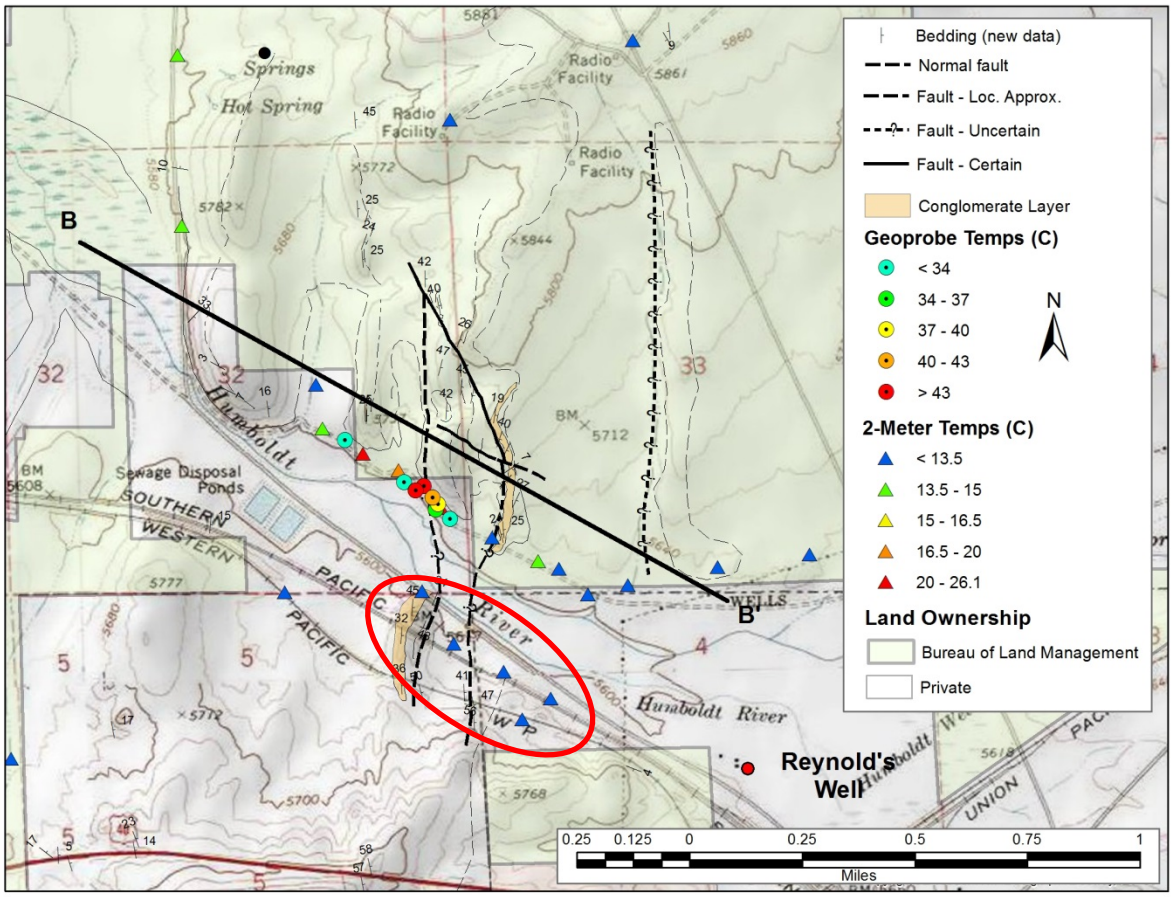

Figure 3: Shallow (2-meter) and Geoprobe temperature data around the faults mapped by Zuza (2017). 2-meter probes of the fault area south of the Humboldt River (red ellipse) are cold. Location of Zuza's B to B' cross section (Figure 4) is shown.

One interesting feature shown in Figures 2 and 3 is the conglomerate bed mapped by Zuza (2017), which is adjacent to the fault both north and south of the river. Previous workers described a similar conglomerate unit that was pervasively silicified where adjacent to the Threemile Hot Springs. The conglomerate unit was postulated as having the highest permeability in the stratigraphic section, and thus served as a conduit for geothermal outflow. Zuza (personal communication) found the conglomerate adjacent to the thermal anomaly to be less silicified than at the Threemile Springs, and the exposure of the conglomerate south of the river to have even less silicification than at the thermal anomaly. Like the 2-meter data, this would seem to indicate that geothermal upflow is not

occurring on this fault, and that the thermal anomaly likely represents outflow coming from a source to the north.

Figure 4 shows a cross section from Zuza (2017), essentially along the line of the thermal anomaly. His analysis was aided by two marker beds (white tuff and conglomerate). According to his cross section, the (here silicified) east-dipping conglomerate bed should be located just below the surface in the area of the thermal anomaly. It is possible that this silicified conglomerate bed might be the hard substrate that the Geoprobe could not penetrate. The initially permeable conglomerate would thus work like an aquifer, but with continued geothermal flow would silicify and self-seal, forming a non-permeable aquiclude. Fluid flow underneath this unit would then behave like a confined aquifer, and could be under pressure.

The very high thermal gradient noted at the thermal anomaly could be explained by a shallow aquiclude separating the surface from hot geothermal fluids. Zehner (2016) postulated that the geothermal fluids in the Reynolds Well might be flowing through the thermal anomaly. Since the Reynolds Well is now known to be under considerable hydrostatic head, it follows that the fluids underneath the thermal anomaly could be pressurized as well. The main point here is that the geothermal fluids underneath the thermal anomaly may well comprise a confined aquifer, and any drill testing of this target should have appropriate equipment to deal with this situation.

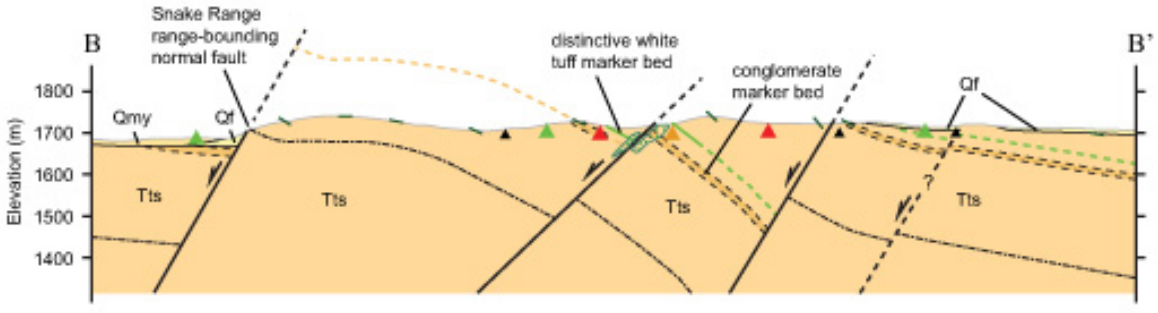

Figure 4: B to B' cross section from Zuza (2017), showing 2-meter temperatures symbolized similar to Figures 2 and 3. The Line of the cross section is shown in Figure 3.

The shallow thermal gradient at the thermal anomaly is substantially higher than some other geothermal systems in Nevada. Figure 5 shows data from Wells compared with two other places where 2-meter and Geoprobe data are available: McGee Mountain in Humboldt County, and Teels Marsh in Mineral County. At Wells the Geoprobe could only reach shallower depths than elsewhere, but by extrapolating the temperatures (dashed yellow lines), one would predict that deeper drilling would encounter boiling water at a depth of perhaps 22 to 30 meters (72 to 98 feet[2]; boiling at the elevation of Wells occurs at 200° F, or 93° C). This clearly presents a direct-use target for the City of Wells, but again argues for cautionary measures to be taken while drilling.

Conclusions and Recommendations

The Geoprobe survey confirmed that the thermal anomaly remains a high-priority target as a source for direct-use geothermal fluids. However, this target would make economic sense only if a well at this location would generate sufficient income to make a project viable. Thermal waters underlie much of the City of Wells; however known temperatures are insufficient for a district heating

[2] The thermal gradients in Figure 5 are shown as a straight line. Actual thermal gradients tend to follow a curve more similar to that shown as Kratt et al (2008).

system. The question becomes one of deciding to allocate future exploration funding towards a known hot water source (i.e., the thermal anomaly) versus finding a "blind" source of hot water closer to the user base in town.

A preliminary economic study is required that would estimate the profitability of a direct use system. From the supply side, this study might evaluate:

- Distance from well to user (e.g. pipeline costs).
- Issues regarding piping geothermal fluids across the Humboldt River drainage.
- Temperatures and flow rates required for various direct use scenarios

Shallow (2-meter) probing south of the Humboldt River did not yield any evidence of a shallow thermal anomaly, even along the southern extension of the north-south fault that passes through the thermal anomaly. Some inexpensive additional surface exploration that might aid in decision making prior to drilling the thermal anomaly might include:

1. The thermal anomaly currently consists of a panel or cross-section along a northwest-striking road. An additional off-road 2-meter survey could be employed in the region just north of the Humboldt River, in order to "see" the anomaly in two dimensions.
2. A close-spaced gravity survey extending from north of the thermal anomaly south into the City of Wells would help delineate fault structures that could help identify targets underneath town.
3. Additional Geoprobe holes, especially when guided by surveys (1) and (2) above, might identify shallow geothermal outflow in the area south of the Humboldt River.
4. The National Energy Technology Laboratory's EM survey should at least in part cover the possible up-dip and down-dip extensions of the thermal anomaly.

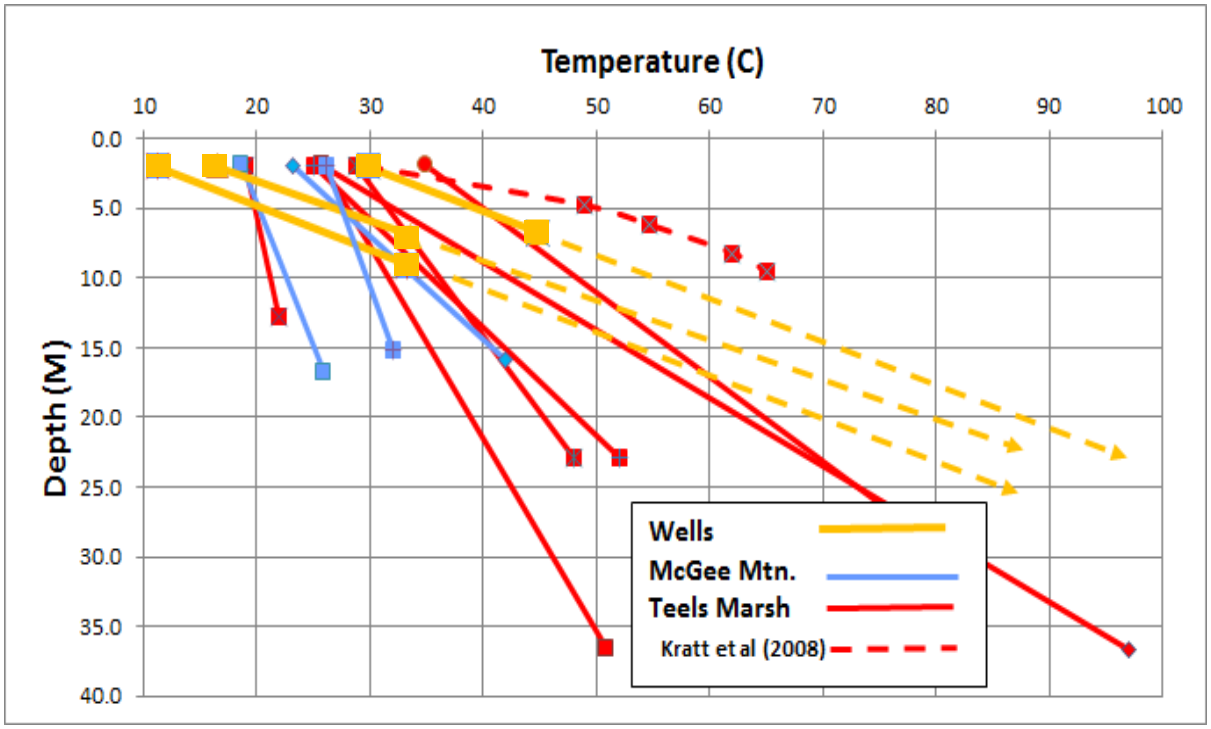

Figure 5: Temperature-depth plot showing 2-meter and Geoprobe samples from the Wells (WGP-1 through WGP-3), McGee Mountain, and Teels Marsh geothermal systems, modified from Zehner et al. (2012). The Wells 2-meter data shown here was collected the same day as the Geoprobe survey and thus constitutes a different dataset than described elsewhere.

It is anticipated that drilling a shallow exploration well within the thermal anomaly would encounter geothermal fluids of sufficient temperature to supply many direct uses, including a district heating system. The available evidence suggests that hot, perhaps boiling water occurs very near the surface, and could be under pressure. For this reason, a qualified engineer should be consulted to advise an appropriate well design. This well could be narrow diameter whose depth need not be greater than 500 feet. Care should be taken to prevent geothermal fluids from entering the Humboldt River. Although these measures will increase the cost of this observation well, these costs are justified, given our present knowledge.

References

Geothermal Development Associates, 2016, Desktop study of geothermal potential in and around the City of Wells. Unpublished report for The City of Wells and Better Cities by Geothermal Development Associates, 9p.

Jewell, P.W., 1982, Geology and geothermal potential north of Wells, Nevada: University of Utah Research Institute, Earth Science Laboratory Open File Report DOE/ID/12079-83, 38 p.

Thorman, C.H., Brooks, W.E., Ketner, K.B., and Dubiel, R.F., 2010, Preliminary geologic map of the Oxley Peak area, Humboldt County, Nevada: Nevada Bureau of Mines and Geology Open-File Report 2003-04.

Zehner, R.E., Tullar, K.N., and Rutledge, E., 2012, Effectiveness of 2-Meter and Geoprobe shallow temperature surveys in early stage geothermal exploration: Geothermal Resources Council Transactions, v. 36, p. 835-841.

Zehner, 2016, Shallow (2-meter) temperature survey in and around the City of Wells, Nevada: implications for geothermal exploration: Unpublished report for The City of Wells and Elko Heat Company, 12 p.

Zuza, A.V., 2017, Preliminary Geologic map of the southern Snake Mountain near Wells, Nevada, scale 1:15,000.

APPENDIX D – ZUZA (2017) GEOLOGIC MAP AND CROSS SECTIONS

Preliminary Geologic Map of the southern Snake Mountains near Wells, Nevada

A.V. Zuza

2017

Units

- Qty — Active tributary stream deposits
- Qmy — Active medial stream deposits
- Qf — Alluvial fan deposits
- Qs — Spring deposits
- Qls — Landslide deposits
- Qfo — Older alluvial fan deposits
- Tts — Sedimentary and volcanic rocks of Threemile Spring (Miocene)
  - ~2-5 m thick conglomerate unit
- Tbc — Boulder conglomerate (upper Miocene?)
- Tvb — Volcaniclastic breccia (Miocene)
- Tro — Rhyolite lava (~15 Ma)
- Try — Rhyolite lava (~13 Ma)
- Silicic alteration

Shallow Temp Survey

- Background tempeartures
- 13-15°C
- 15-16.5°C
- 16.5-20°C
- > 20°C

Spring and Well Temperatures

- No Temp
- < 20°C
- 20 - 32°C
- 32 - 43°C
- > 43°C

Line of cross section

B — B'

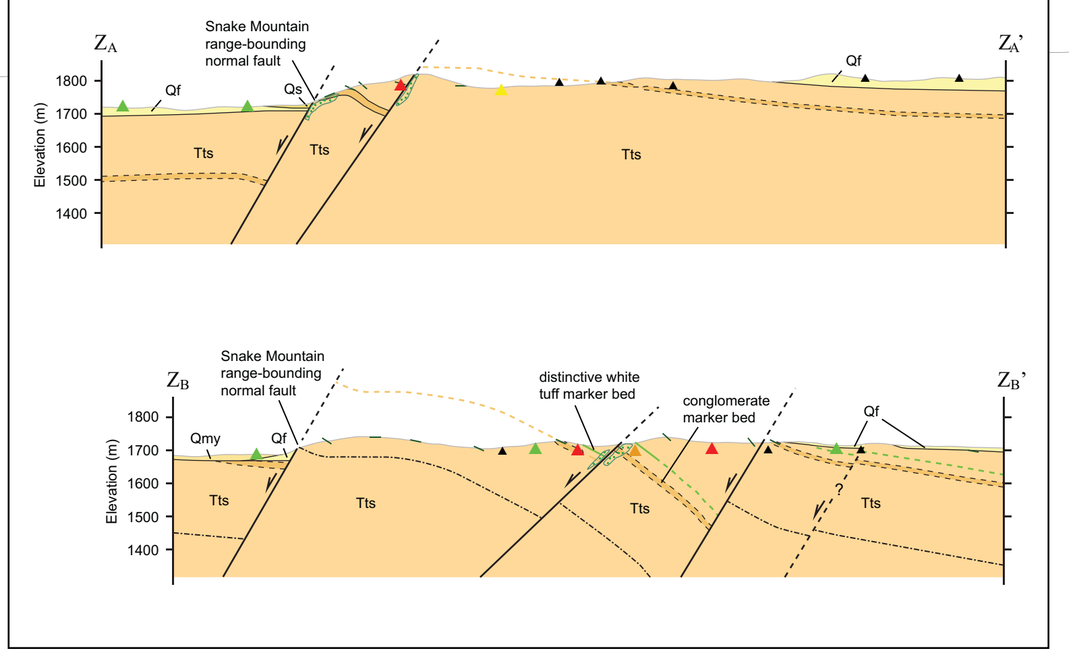

Map compiled from Jewell (1982), Thorman et al. (2010), and Henry and Thorman (2011) with new mapping by Andrew V. Zuza and data from Zehner (2016a, b).

Projection: Universal Transverse Mercator, Zone 11N, North American Datum 1983 (m)

References

Henry, C.D., and Thorman, C.H., 2011, Geologic map of the Wells area, Elko County, Nevada: Nevada Bureau of Mines and Geology Special Publication 36, Appendix A.

Jewell, P.W., 1982, Geology and geothermal potential north of Wells, Nevada: University of Utah Research Institute, Earth Science Laboratory Open File Report DOE/ID/12079-83, 38 p.

Thorman, C.H., Brooks, W.E., Ketner, K.B., and Dubiel, R.F., 2010, Preliminary geologic map of the Oxley Peak area, Humboldt County, Nevada: Nevada Bureau of Mines and Geology Open-File Report 2003-04.

Zehner, R., 2016a, Desktop study of geothermal potential in and around the City of Wells. Unpublished report for The City of Wells and Better Cities by Geothermal Development Associates, 9p.

Zehner, R., 2016b Shallow (2-Meter) Temperature Survey in and Around the City of Wells, Nevada: Implications for Geothermal Exploration. Unpublished report for Elko Heat Company and The City of Wells by Geothermal Development Associates, 12p.

Base maps: U.S. Geological Survey Oxley Peak 7.5' quadrangle (1982), Wells 7.5' quadrangle (1982)

115°1'30"W — 115°0'0"W — 114°58'30"W — 41°11'0"N — 41°10'0"N — 41°9'0"N — 41°8'0"N — 41°7'0"N — 41°6'0"N

Oxley Peak quadrangle

Wells quadrangle

Scale: 1:15,000 Contour Interval: 20 feet

0 0.5 1 km

Contact Dashed where inferred.

Marker beds Shown by dot-dash lines within units.

Fault Showing dip (tick) and trend and plunge of slickenlines (arrow); dashed where inferred; queried where uncertain.

Normal fault Bar and ball on downthrown side; dashed where inferred.

Strike-slip fault Arrows show relative movement; oblique normal motion with bar and ball.

Strike and dip of inclined beds

New attitudes | Jewell (1982) attitudes | Henry and Throman (2011) attitudes

APPENDIX E – INTERPRETED NDWR LITHOLOGIC LOGS, LITHOLOGIC CROSS SECTIONS, AND TEMPERATURE PROFILES

Appendix E:

Appendix E can be found at:
https://edx.netl.doe.gov/dataset/small-business-vouchers-pilot-technical-assistance-from-lbnl-netl-to-elko-and-wells-nevada/resource_download/2c6aac65-690d-4619-8818-428e3a19051b

This Appendix was compiled by researchers at the National Energy Technology Laboratory in Albany, Oregon and includes:

1. 56 graphically illustrated lithologic logs obtained from:
   - 54 well driller's reports from the State of Nevada Division of Water Resources (NDWR) access database
     - Wells L1 – L59
   - 1 geothermal well completion report from the State of Nevada Department of Business and Industry Division of Minerals
     - BTI well
   - 1 geothermal well completion report and technical memorandum from Lumos & Associates
     - GEO#1 well

   For each well log, information was compiled about surface locations and elevations, drilled depths, perforated intervals, water levels, and measured water temperatures. The logs usually indicate the driller's interpretation of lithology (i.e., rock type) and unit thicknesses. Each well was graphically illustrated in Adobe Illustrator CC6 and exported as a high-resolution jpeg image (1000 dpi) for use in subsequent subsurface interpretations. Graphically illustrating the lithologic logs frequently required further geologic interpretation. For example, a unit described as "loam," "sand," or "hard rock" in the lithologic log was displayed as "top soil," "sandstone," or "basement" in the graphical illustration. Refer to **Section 5.2.6** of the main body of the report for more information.

2. An index of wells included in the graphical illustrations included, above.

3. Four cross sections constructed from the graphically illustrated lithologic logs described above (A-A', B-B', C-C', and D-D'). The cross sections cover the southeast region of the study area and follow a zigzag path, rather than a straight-line transect, to maximize the number of lithologic logs in the cross sections. Lithologic logs were selected for inclusion in cross sections based on one or more of the following criteria: depth (>25 m), water level information, measured water temperatures, and the presence of conglomerate and/or basement lithologic units. In some instances, the cross sections transect a fault (or inferred fault). This information is also displayed on the cross sections. Refer to **Section 5.2.6** of the main body of the report for more information.

4. Interpolated temperature profiles extracted from the 3-dimensional conceptual geologic model. These temperature profiles parallel cross sections A-A', B-B', C-C', and D-D' to demonstrate any correlations between the lithologic logs and interpolated subsurface temperatures.

5. An overview map showing the locations of wells contained lithologic logs and the cross section traverses constructed for the study. Refer to **Section 7.2.2** of the main body of the report for more information.

APPENDIX F – WATER GEOCHEMICAL DATA COMPILATION FROM OLDER SOURCES

ID	Assigned Name	Easting UTM	Northing UTM	Notes on location, coordinates
12	Twelvemile Spring	671949	4567732	Spring is 9.8 miles NNE of Wells. Coordinates from GBCGE and Google Earth
1	Cold Spring - 73	669212	4562294	R. Zehner GPS coordinates, very accurate
42	Jewell_15	670181	4561133	Uncertain cold water location listed at sw/nw 9. Here it is digitized from Jewell's map and plots further south in nw/ne 16.
25	Humboldt HS - Sladek_W7	668684	4561033	Assumed to be Spring 1 to NE of terrace.
9	Humboldt HS - GBCGE_82613	668512	4560915	Assumed to be the main spring; R. Zehner GPS coordinates.
8	Humboldt HS - GBCGE_80549	668512	4560915	Assumed to be the main spring; R. Zehner GPS coordinates.
24	Humboldt HS - Sladeck_W6-2	668512	4560915	Assumed to be the main spring; R. Zehner GPS coordinates.
7	Humboldt HS - GBCGE_1413	668512	4560915	Assumed to be the main spring; R. Zehner GPS coordinates.
6	Humboldt HS - GBCGE_1348	668512	4560915	Assumed to be the main spring; R. Zehner GPS coordinates.
44	Humboldt HS - Jewell_17	668512	4560915	Assumed at location of Humbolt HS because it is consistent with Jewell's map, and also listed together with his samples Sec17-1 and Sec17-2 at Humbolt HS.
48	Threemile Spg - Jewell_WE-NV-3	668986	4558659	Jewell lists this point at same location as his sample Sec20-2 at nw/se 20, and the latter matches GBCGE_108 and Sladek W5-3
2	Threemile Spg - GBCGE_83	668986	4558659	R. Zehner GPS coordinates
10	Threemile Spg - GBCGE_82615	668986	4558659	R. Zehner GPS coordinates
22	Threemile Spg -Sladek_W5-2	668986	4558659	Sladek calls it Travertine Spring. Assume same location as other 3mi spg samples
3	Threemile Spg - GBCGE_108	668986	4558659	From R. Zehner GPS coordinates
49	Threemile Spg - Jewell_20	668986	4558659	Jewell lists this point at same location as his sample Sec20-2 at nw/se 20, and the latter matches GBCGE_108 and Sladek W5-3
5	Hot Sulfur Spg -GBCGE_1293**	668985	4558115	GBCGE coordinates. Corresponds to Hot Sulfur Spring 0.5 km South of Threemile spring
23	Hot Sulfur Spg - Sladek_W5-1	668985	4558115	Sladek describes it as 0.5 km south of W5 (and calls W5 Travertine Spring), which corresponds to Hot Sulfur spg.
4	Hot Sulfur Spg - GBCGE_129	668985	4558115	GBCGE coordinates. Same analysis as Sladek listed as 0.5 km South W5, so assume same location

ID	Assigned Name	Easting UTM	Northing UTM	Notes on location, coordinates
47	Hot Sulfur Spg - Jewell_19	668985	4558115	Plots too far South on Jewell's map. He lists this point together with his sample Sec20-1 at se/se 20, which matches the analysis of GBCGE_129, so it was moved to that same location.
53	Jewell_WE-NV-5	674842	4557321	Assumed located at windmill East of location digitized on Jewell's map
50	Jewell_21	670812	4557239	Assumed at nearby windmill North of location digitized from Jewell's map, although his sample list shows a different location (nw/sw 21).
46	Jewell_18	668486	4556810	Jewell lists this point together with WE-NV-4 in sw/se 29. Very likely 'Spring' on topo map in sw/sw 29, thus assumed at this location. Note that there is also a 'Hot Spring' on topo map very close , south of this location.
45	Jewell_WE-NV-4	668486	4556810	Jewell lists this point together with his sample 18 in sw/se 29. Very likely 'Spring' on topo map in sw/sw 29, thus assumed at this location. Note there is also a 'Hot Spring' on topo map very close to this location.
51	Jewell_WE-NV-6	671812	4555047	Listed as in section 34 with no further info. Assumed at spring shown on topo map 1 km S of center of section 34. Jewell lists this point together with his sample 22, however Cl and Na are much higher here (in fact is Cl higher than anywhere else).
52	Jewel 22	671812	4555047	Jewell lists this point below his sample WE-NV-6, but without location information. Assumed same location as WE-NV-6, but Na and Cl concentrations are much lower here.
14	Reynolds Well - Sladek_W2-1	670184	4554253	R. Zehner coordinates, somewhat inaccurate
11	Reynolds Well - Sladek_W2-2	670184	4554253	R. Zehner coordinates, somewhat inaccurate
15	Reynolds Well - Sladek_W2-3	670184	4554253	R. Zehner coordinates, somewhat inaccurate
37	Reynolds Well - Jewell_11	670184	4554253	R. Zehner coordinates, somewhat inaccurate
39	Wells - Jewell_13	670772	4553754	Uncertain location in/near town, listed by Jewell in nw/nw 9. Here it is digitized from Jewell's map and plots inconsistently in ne/se 4.
43	Wells - Jewell_16	670469	4553602	Uncertain location in/near town, listed by Jewell in sw/se 9. Here it is digitized from Jewell's map and plots inconsistently in the middle of se 4.

ID	Assigned Name	Easting UTM	Northing UTM	Notes on location, coordinates
38	Wells - Jewell_12	670120	4553148	Uncertain location in/near town, listed by Jewell in ne/se 4. Here it is digitized from Jewell's map and plots inconsistently at mid boundary between sec 9 and 4.
36	Wells - Jewell_10	671651	4552815	Uncertain location in town, listed by Jewell in sw/ne 16. Here it is digitized from Jewell's map and plots inconsistently ne/nw 10 close to the BTI well, but with different chemistry.
41	WHS - Jewell_14	670549	4552792	Assume same location as WHS as suggested by Jewell's table
40	WHS - Jewell_WHS	670549	4552792	R. Zehner GPS coordinates of Wells High School well #4
13	BTI Well - Sladek_W1	672033	4552739	Accurate location from R. Zehner
35	South Wells - Jewell_9	670272	4551436	Uncertain location south of town, listed by Jewell in sw/ne 16. Here it is digitized from Jewell's map and plots inconsistently in nw/ne 16, very near Reynolds house well.
16	Reynolds House - Sladek_W3-1	671086	4551386	Accurate location of house well from R. Zehner
17	Reynolds House - Sladek_W3-2	671086	4551386	Assumed at Reynolds House; Sladeck mentions it is near house, but it cannot be very far from it.
18	Reynolds House - Sladek_W3-3	671086	4551386	Assumed at Reynolds House; Sladeck mentions it is near house, but it cannot be very far from it.
19	Reynolds House - Sladek_W3-4	671086	4551386	Assumed at Reynolds House; Sladeck mentions it is near house, but it cannot be very far from it.
30	Reynolds House - Jewel_4	671086	4551386	Assumed at Reynolds House. Jewell lists it in nw/nw 15 consistent with this location.
31	Reynolds House - Jewel_5	671086	4551386	Assumed at Reynolds House. Jewell lists it in nw/nw 15 consistent with this location.
32	Reynolds House - Jewel_6	671086	4551386	Assumed at Reynolds House. Jewell lists it in nw/nw 15 consistent with this location.
34	Reynolds House - Jewel_8	671086	4551386	Assumed at Reynolds House. Jewell lists it in nw/nw 15 consistent with this location.
33	South - Jewel_7	670817	4550527	Uncertain location south of town, listed by Jewell in ne/se 16. Here it is digitized from Jewell's map and plots at that general location.

ID	Assigned Name	Easting UTM	Northing UTM	Notes on location, coordinates
29	South - Jewel_3	669332	4550057	Uncertain location south of town, listed by Jewell in se/nw 32. Here it is digitized from Jewell's map and plots inconsistently in se/se 17.
20	SW Spring - Sladek_W4-1	669308	4549243	Assumed at location of spring near road, seems to plot close to digitized location on Sladek's map.
21	SW Spring - Sladek_W4-2	669308	4549243	Assumed at location of spring near road, seems to plot close to digitized location on Sladek's map.
27	South - Jewel_NW-VE-2	668781	4548028	Taken at location of spring on topo map, consistent with listed location at nw/ne 29 and close to digitized location on Jewell's map.
28	South - Jewel_2	668781	4548028	Taken at location of spring on topo map, consistent with listed location at nw/ne 29 and close to digitized location on Jewell's map.
26	South - Jewel_1	668560	4547375	Uncertain location south of town, listed by Jewell in sw/sw 21. Here it is digitized from Jewell's map and plots inconsistently several km further south.
54	Angel Lake - Jewell_23			No precise location for surface water
55	South Fork - Jewell_24			No precise location for surface water
56	Trout Creek - Jewell_25			No precise location for surface water

ID	Assigned Name	Reference	Name in Zehner (2016)	Name in Sladeck (2011)	Name in Jewell (1994)
12	Twelvemile Spring	Zehner 2016	Twelvemile Spring		
1	Cold Spring - 73	Zehner 2016	Cold Spring (LDMW for GT 14, 15, and 16RM 74) - 73		
42	Jewell_15	Jewell 1994			Sample 15
25	Humboldt HS - Sladek_W7	Sladek 2011		W-7, mud slide	
9	Humboldt HS - GBCGE_82613	Zehner 2016	Hot Spring - Humboldt Wells - 82613	W-6 (1st entry), travertine spring area	
8	Humboldt HS - GBCGE_80549	Zehner 2016	Hot Spring - Humboldt Wells - 80549	W-6 (3rd entry), near travernine spring area	
24	Humboldt HS - Sladeck_W6-2	Sladek 2011		W-6 (2nd entry), travertine spg area	
7	Humboldt HS - GBCGE_1413	Sladek 2011	Hot Spring - Humboldt Wells - 1413	W-6 (4th entry), near travertine spring area	Sec17-1
6	Humboldt HS - GBCGE_1348	Zehner 2016	Hot Spring - Humboldt Wells - 1348	W-6 (5th entry), near travertine spring area	Sec17-2
44	Humboldt HS - Jewell_17	Jewell 1994			Sample 17
48	Threemile Spg - Jewell_WE-NV-3	Jewell 1994			WE-NV-3
2	Threemile Spg - GBCGE_83	Zehner 2016	Threemile Spring - Humboldt Wells - 83		
10	Threemile Spg - GBCGE_82615	Sladek 2011	Threemile Spring - Humboldt Wells - 82615	W-5 (1st entry), 3mile spring area	
22	Threemile Spg -Sladek_W5-2	Sladek 2011		W-5 (2nd entry), 3mi spg area	
3	Threemile Spg - GBCGE_108	Zehner 2016	Threemile Spring - Humboldt Wells - 108	W-5 (3rd entry), 3mile spring area	Sec20-2

ID	Assigned Name	Reference	Name in Zehner (2016)	Name in Sladeck (2011)	Name in Jewell (1994)
49	Threemile Spg - Jewell_20				Sample 20
5	Hot Sulfur Spg -GBCGE_1293**	Zehner 2016	Hot Sulphur Springs - Humboldt Wells - 1293		
23	Hot Sulfur Spg - Sladek_W5-1	Sladeck, 2011		Hot spg 0.5 km south of W-5 (1st entry)	
4	Hot Sulfur Spg - GBCGE_129	Zehner 2016	Hot Spring - Humboldt Wells - 129	Hot spg 0.5 km south of W-5 (2nd entry)	Sec20-1
47	Hot Sulfur Spg - Jewell_19	Jewell 1994			Sample 19
53	Jewell_WE-NV-5				WE-NV-5
50	Jewell_21				Sample 21
46	Jewell_18	Jewell 1994			Sample 18
45	Jewell_WE-NV-4	Jewell 1994			WE-NV-4
51	Jewell_WE-NV-6				WE-NV-6
52	Jewel 22				Sample 22
14	Reynolds Well - Sladek_W2-1	Sladek 2011		W-2 (1st entry), Reynolds	

ID	Assigned Name	Reference	Name in Zehner (2016)	Name in Sladeck (2011)	Name in Jewell (1994)
				Ranch Well	
11	Reynolds Well - Sladek_W2-2	Jewell 1994	Reynolds Well	W-2 (2nd entry), Reynolds Ranch Well	NV-WE-1
15	Reynolds Well - Sladek_W2-3	Sladek 2011		W-2 (3rd entry), Reynolds Ranch Well	
37	Reynolds Well - Jewell_11	Jewell 1994			Sample 11
39	Wells - Jewell_13	Jewell 1994			Sample 13
43	Wells - Jewell_16	Jewell 1994			Sample 16
38	Wells - Jewell_12	Jewell 1994			Sample 12
36	Wells - Jewell_10	Jewell 1994			Sample 10
41	WHS - Jewell_14	Jewell 1994			Sample 14
40	WHS - Jewell_WHS	Jewell 1994			WHS
13	BTI Well - Sladek_W1	Sladek 2011		W-1, BTI well	
35	South Wells - Jewell_9	Jewell 1994			Sample 9
16	Reynolds House - Sladek_W3-1	Sladek 2011		W-3 (1st entry), Ray Reynolds Well	
17	Reynolds House - Sladek_W3-2	Sladek 2011		W-3 (2nd entry), Near Ray Reynolds Well	
18	Reynolds House - Sladek_W3-3	Sladek 2011		W-3 (3rd entry), Near Ray Reynolds Well	

ID	Assigned Name	Reference	Name in Zehner (2016)	Name in Sladeck (2011)	Name in Jewell (1994)
19	Reynolds House - Sladek_W3-4	Sladek 2011		W-3 (4th entry), Near Ray Reynolds Well	
30	Reynolds House - Jewel_4	Jewell 1994			Sample 4
31	Reynolds House - Jewel_5	Jewell 1994			Sample 5
32	Reynolds House - Jewel_6	Jewell 1994			Sample 6
34	Reynolds House - Jewel_8	Jewell 1994			Sample 8
33	South - Jewel_7	Jewell 1994			Sample 7
29	South - Jewel_3	Jewell 1994			Sample 3
20	SW Spring - Sladek_W4-1	Sladek 2011		W-4 (1st entry), Spring SW of Wells	
21	SW Spring - Sladek_W4-2	Sladek 2011		W-4 (2nd entry), Spring SW of Wells	
27	South - Jewel_NW-VE-2	Jewell 1994			NV-WE-2
28	South - Jewel_2	Jewell 1994			Sample 2
26	South - Jewel_1	Jewell 1994			Sample 1
54	Angel Lake - Jewell_23	Jewell 1994			Sample 23
55	South Fork - Jewell_24	Jewell 1994			Sample 24
56	Trout Creek - Jewell_25	Jewell 1994			Sample 25

ID	Assigned Name	Type	Temp (°C)	pH_field	pH_lab	Li mg/L	Na mg/L	K mg/L	Ca mg/L	Mg mg/L	SiO2 mg/L
12	Twelvemile Spring	Spring					16.0	5.8	45.3	17.6	39.6
1	Cold Spring - 73	Spring	6.0	7.1		0.01	16.0	2.8	29.0	6.8	23.0
42	Jewell_15	Well	11.5	8.2	7.6		26.0	3.0	28.0	10.0	
25	Humboldt HS - Sladek_W7	Spring	34.2	6.4		0.7	338.0	34.7	78.4	37.1	85.0
9	Humboldt HS - GBCGE_82613	Spring	48.7	6.5		0.4	285.2	31.9	63.4	30.0	103.8
8	Humboldt HS - GBCGE_80549	Spring	54.0	6.0		0.35	386.0	38.8	36.5	11.2	90.9
24	Humboldt HS - Sladeck_W6-2	Spring	46.0	7.7			290.0	10.0	56.0	30.0	
7	Humboldt HS - GBCGE_1413	Spring	61.0	7.3		0.8	300.0	31.0	75.0	37.0	105.0
6	Humboldt HS - GBCGE_1348	Spring	55.0	6.6		1.2	370.0	46.0	48.0	13.0	86.0
44	Humboldt HS - Jewell_17	Spring	46.0	7.0	7.7		275.0	10.0	55.0	30.0	
48	Threemile Spg - Jewell_WE-NV-3	Spring			7.7		303.0	37.0	55.0	12.0	
2	Threemile Spg - GBCGE_83	Spring	36.0	7.0		0.7	390.0	41.0	49.0	13.0	84.0
10	Threemile Spg - GBCGE_82615	Spring	36.6	6.4		0.00	330.0	38.7	48.4	11.4	71.9
22	Threemile Spg -Sladek_W5-2	Spring	35.0	7.7			355.0	31.0	43.0	10.0	
3	Threemile Spg - GBCGE_108	Spring	36.0	6.3		0.65	340.0	36.0	51.0	13.0	76.0
49	Threemile Spg - Jewell_20	Spring	35	6.3	7.7		345	31	40	10	
5	Hot Sulfur Spg -GBCGE_1293**	Spring	60.0	7.3		1.2	160.0	16.0	12.0	0.3	165.0
23	Hot Sulfur Spg - Sladek_W5-1	Spring	45.0	7.8			390.0	35.0	38.0	10.0	

ID	Assigned Name	Type	Temp (°C)	pH_field	pH_lab	Li mg/L	Na mg/L	K mg/L	Ca mg/L	Mg mg/L	SiO2 mg/L
4	Hot Sulfur Spg - GBCGE_129	Spring	60.0	6.6		0.8	300.0	30.0	78.0	36.0	110.0
47	Hot Sulfur Spg - Jewell_19	Spring	45.0	6.1	7.8		375.0	35.0	40.0	10.0	
53	Jewell_WE-NV-5	Well		6.6	7.8		34	9	36	16	
50	Jewell_21	Well	21	7.7	7.7		36	12	13	5	
46	Jewell_18	Spring	9.0	8.4	8.3		455.0	6.0	5.0	5.0	
45	Jewell_WE-NV-4	Spring		7.5	8.4		384.0	12.0	7.0	6.0	
51	Jewell_WE-NV-6	Spring					93	10	68	30	
52	Jewel 22	Spring			7.8		47	9	60	10	
14	Reynolds Well - Sladek_W2-1	Well	40.6	6.9		0.05	53.2	18.3	29.9	5.2	108.5
11	Reynolds Well - Sladek_W2-2	Well	40.0	6.8	8.2		58.0	20.0	33.0	5.0	88.0
15	Reynolds Well - Sladek_W2-3	Well		8.0			51.0	17.0	13.0	4.0	
37	Reynolds Well - Jewell_11	Well			8.0		51.0	17.0	15.0	4.0	
39	Wells - Jewell_13	Well			7.8		37.0	9.0	20.0	18.0	

ID	Assigned Name	Type	Temp (°C)	pH_field	pH_lab	Li mg/L	Na mg/L	K mg/L	Ca mg/L	Mg mg/L	SiO2 mg/L
43	Wells - Jewell_16	Well	34.0	8.1	7.8		32.0	10.0	18.0	4.0	
38	Wells - Jewell_12	Well			7.6		31.0	10.0	21.0	6.0	
36	Wells - Jewell_10	Well			7.9		24.0	9.0	16.0	10.0	
41	WHS - Jewell_14	Well	29.0	8.2	7.9		31.0	8.0	24.0	6.0	
40	WHS - Jewell_WHS	Well					23.0	8.0	38.0	7.0	
13	BTI Well - Sladek_W1	Well	32.8	7.1			92.4	16.4	37.3	9.8	89.7
35	South Wells - Jewell_9	Well			7.8		22.0	4.0	20.0	14.0	
16	Reynolds House - Sladek_W3-1	Well	28.6	7.2		0.00	37.1	7.2	45.4	6.8	54.6
17	Reynolds House - Sladek_W3-2	Well					23.0	4.0	19.0	12.0	
18	Reynolds House - Sladek_W3-3	Well					28.0	6.0	22.0	8.0	
19	Reynolds House - Sladek_W3-4	Well	37.0	8.2			61.0	12.0	25.0	8.0	
30	Reynolds House - Jewel_4	Well			7.8		23.0	4.0	17.0	12.0	
31	Reynolds House - Jewel_5	Well			8.0		28.0	6.0	19.0	8.0	
32	Reynolds House - Jewel_6	Well	37.0		8.2		61.0	12.0	18.0	8.0	

ID	Assigned Name	Type	Temp (°C)	pH_field	pH_lab	Li mg/L	Na mg/L	K mg/L	Ca mg/L	Mg mg/L	SiO2 mg/L
34	Reynolds House - Jewel_8	Well			7.7		25.0	3.0	21.0	11.0	
33	South - Jewel_7	Well			7.7		41.0	3.0	47.0	19.0	
29	South - Jewel_3	Spring	14.0	7.9	7.5		24.0	2.0	30.0	9.0	
20	SW Spring - Sladek_W4-1	Spring	19.3	6.8		0.00	33.6	3.1	50.0	15.1	23.3
21	SW Spring - Sladek_W4-2	Spring	19.5	7.8			38.0	3.0	48.0	13.0	
27	South - Jewel_NW-VE-2	Spring		6.8	8.2		27.0	6.0	48.0	15.0	
28	South - Jewel_2	Spring	22.0	7.5	6.8		39.0	5.0	35.0	14.0	
26	South - Jewel_1	Spring	19.5	7.8	7.9		38.0	3.0	33.0	13.0	
54	Angel Lake - Jewell_23	Stream	4	6.6	7.4		0.8	0.2			
55	South Fork - Jewell_24	Stream	8	8.2	7.8		2.4	22			
56	Trout Creek - Jewell_25	Spring	14.5	7.9	7.9		6	3			

ID	Assigned Name	Cl mg/L	F mg/L	SO4 mg/L	HCO3 mg/L	CO3 mg/L	δ^2H	$\delta^{18}O$	Sampling_Date
12	Twelvemile Spring	4.7		32.2	239.0				
1	Cold Spring - 73	13.0	0.3	26.0	116.0	1.0			
42	Jewell_15	22.0		27.0	159.0		-134.0	-15.1	11/12/1991
25	Humboldt HS - Sladek_W7	21.5	5.5	14.0	1016.0				3/25/2008
9	Humboldt HS - GBCGE_82613	22.0	6.5	30.8	909.6				3/26/2008
8	Humboldt HS - GBCGE_80549	36.6	2.1	18.1	1096.0				6/24/2002
24	Humboldt HS - Sladeck_W6-2	15.0		28.0	950.0				11/12/1991
7	Humboldt HS - GBCGE_1413	27.0	7.2	32.0	1135.0				Mariner et al. 1974
6	Humboldt HS - GBCGE_1348	37.0	7.4	12.0	1230.0				Mariner et al., 1975
44	Humboldt HS - Jewell_17	15.0		28.0	950.0		-137.0	-16.1	11/12/1991
48	Threemile Spg - Jewell_WE-NV-3	35.0		15.0	1170.0				11/16/1991 likely should be 7/10/81
2	Threemile Spg - GBCGE_83	40.0	7.2	18.0	1180.0				
10	Threemile Spg - GBCGE_82615	29.0	6.3	41.0	872.0				3/25/2008
22	Threemile Spg -Sladek_W5-2	20.0		25.0	1000.0				11/16/1991
3	Threemile Spg - GBCGE_108	34.0	7.0	29.0	1150.0	1.0			Mariner et al., 1975
49	Threemile Spg - Jewell_20	20		25	1000		-145.0	-15.2	11/16/1991
5	Hot Sulfur Spg -GBCGE_1293**	22.0	10.0	61.0	345.0				
23	Hot Sulfur Spg - Sladek_W5-1	20.0		12.0	1080.0				11/16/1991
4	Hot Sulfur Spg - GBCGE_129	26.0	6.1	24.0	1210.0	1.0			Mariner et al., 1975

ID	Assigned Name	Cl mg/L	F mg/L	SO4 mg/L	HCO3 mg/L	CO3 mg/L	δ^2H	$\delta^{18}O$	Sampling_Date
47	Hot Sulfur Spg - Jewell_19	20.0		12.0	1080.0		-129.0	-15.5	11/16/1991
53	Jewell_WE-NV-5	17		20	234				7/10/1981
50	Jewell_21	15		27	131		-140.0	-15.9	11/16/1991
46	Jewell_18	18.0		21.0	1090.0		-141.0	-16.5	11/16/1991
45	Jewell_WE-NV-4	29.0		13.0	1040.0				7/10/1981
51	Jewell_WE-NV-6	136		55					7/10/1991 likely should be 7/10/81
52	Jewel 22	22		50	282		-138.0	-16.5	11/16/1991
14	Reynolds Well - Sladek_W2-1	10.6	1.0	22.3	190.0				3/26/2008
11	Reynolds Well - Sladek_W2-2	16.0		20.0	259.0				3/16/1980
15	Reynolds Well - Sladek_W2-3	10.0		24.0	214.0				11/11/1991
37	Reynolds Well - Jewell_11	10.0		24.0	214.0		-136.0	-16.6	11/11/1991
39	Wells - Jewell_13	20.0		44.0	193.0		-130.0	-16.7	11/12/1991
43	Wells - Jewell_16	9.0		18.0	173.0		-137.0	-16.5	11/12/1991

ID	Assigned Name	Cl mg/L	F mg/L	SO4 mg/L	HCO3 mg/L	CO3 mg/L	δ^2H	$\delta^{18}O$	Sampling_Date
38	Wells - Jewell_12	9.0		19.0	172.0		-130.0	-16.2	11/12/1991
36	Wells - Jewell_10	7.0		14.0	173.0				11/11/1991
41	WHS - Jewell_14	10.0		19.0	175.0		-130.0	-16.7	11/12/1991
40	WHS - Jewell_WHS	10.0		16.0	183.0				1/4/1984
13	BTI Well - Sladek_W1	15.3	2.5	30.1	301.0				3/26/2008
35	South Wells - Jewell_9	11.0		22.0	185.0		-139.0	-16.6	11/11/1991
16	Reynolds House - Sladek_W3-1	7.2	1.3	18.8	210.0				3/26/2008
17	Reynolds House - Sladek_W3-2	9.0		17.0	164.0				11/11/1991
18	Reynolds House - Sladek_W3-3	7.0		14.0	177.0				11/11/1991
19	Reynolds House - Sladek_W3-4	14.0		7.0	224.0				11/11/1991
30	Reynolds House - Jewel_4	9.0		17.0	164.0		-130.0	-17.0	11/11/1991
31	Reynolds House - Jewel_5	7.0		14.0	177.0		-130.0	-17.0	11/11/1991
32	Reynolds House - Jewel_6	14.0		7.0	244.0		-147.0	-18.7	11/11/1991
34	Reynolds House - Jewel_8	36.0		20.0	173.0		-131.0	-16.1	11/11/1991
33	South - Jewel_7	26.0		42.0	185.0				11/11/1991

ID	Assigned Name	Cl mg/L	F mg/L	SO4 mg/L	HCO3 mg/L	CO3 mg/L	δ^2H	$\delta^{18}O$	Sampling_Date
29	South - Jewel_3	9.0		23.0	180.0				11/11/1991
20	SW Spring - Sladek_W4-1	18.9	0.7	34.3	197.0				3/27/2008
21	SW Spring - Sladek_W4-2	15.0		30.0	227.0				11/11/1991
27	South - Jewel_NW-VE-2	21.0		27.0	234.0				7/10/1981
28	South - Jewel_2	16.0		30.0	175.0		-134.0	-16.8	11/11/1991
26	South - Jewel_1	15.0		30.0	227.0		-134.0	-17.1	11/11/1991
54	Angel Lake - Jewell_23						-114.0	-15.2	5/9/1992
55	South Fork - Jewell_24						-111.0	-15.6	5/9/1992
56	Trout Creek - Jewell_25						-125.0	-16.1	5/9/1992

** Sample no. 5 was determined to be an outlier – it may have been mislabeled in the original compilation and most likely relates to another Sulfur Spring

Sampling Locations

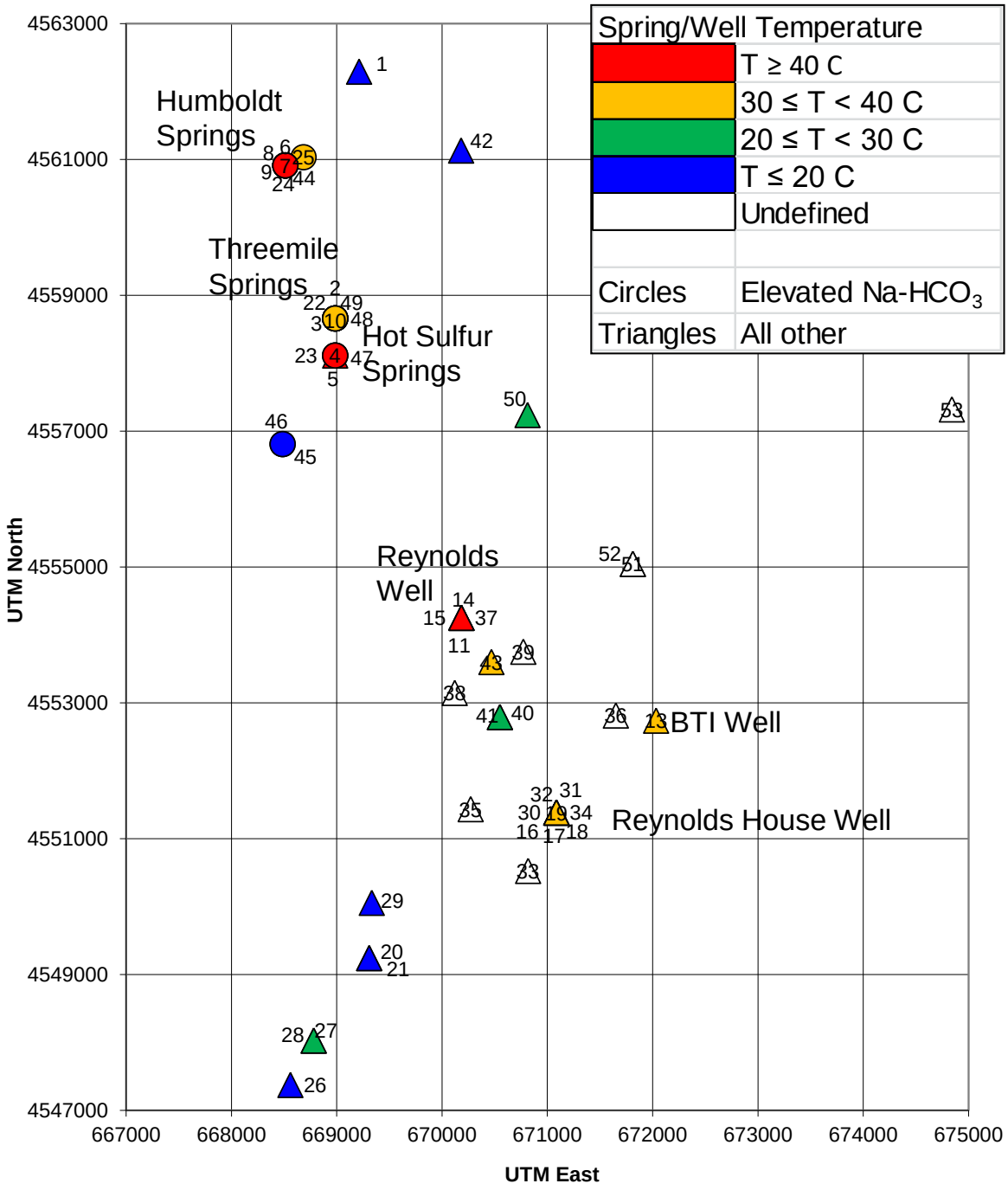

(Map North and East axes are not on the same scale)

APPENDIX G – NEW WATER GEOCHEMICAL DATA

Sampling locations and chemical analyses, City of Wells, 2017
See Section 5.3 of the main report

ID	Name	Type	Well Depth (ft)	Perforated (ft)	Year Drilled	Date Sampled	Time (Approx.)	Easting (m)	Northing (m)	Approx. Elevation (msl)	Approx. Elevation (ft)	Temperature (°C)	Temperature (°F)	Field Cond mS/cm	Field Cl ppm
1	Rural Electric	City Well	795	475-775	1985	4/26/2017	10:50-12:00	670402	4553365	1706	5597	34.6	94.3	333	<30
2	Well #2	City Well	484	153-470	1973	4/26/2017	12:15-12:45	670152	4552927	1692	5551	29.0	84.2	335	<30
3	Well #6	City Well	750	250-350 500-560 600-740	2004	4/26/2017	14:15-15:00	670727	4551696	1732	5683	26.0	78.8	330	<30
4	Golf Course Well	City Well	400	53-400	1975	4/26/2017	15:10-15:45	670407	4551729	1747	5732	23.3	73.9	375	<30
5	Well #7	City Well				4/26/2017	16:00-16:45	669770	4551534	1726	5663	20.9	69.6	443	<30
6	Well #5	City Well				4/26/2017	17:20-17:50	673571	4553291	1742	5716	25.4	77.7	423	<30
7	Airport Well	City Well	539	236-256 539-799	1997	4/26/2017	18:00-18:30	674053	4553531	1737	5699	13.5	56.3	429	<30
8	Reynolds Well	Private Well	540	60-540	1978	4/26/2017	9:30-10:45	670179	4554259	1707	5601	41.0	105.8	433	<30
9	Arnold Merrill Well	Private Well	>55	>55	1995	4/27/2017	9:15-9:50	672254	4552864	1700	5578	20.1	68.2	320	<30
10	BTI Well	Private Well	870	0-50 750-850	2006	4/27/2017	10:15-11:00	671971	4552744	1727	5666	30.5	86.9	630	<30
11	Dan Morgan Well	Private Well	365	205-225 285-305 345-365	2010	4/27/2017	11:20-12:00	668388	4551882	1783	5850	32.0	89.6	630	<30
12	Reynolds House	Private Well	1000	900-1000	1990	4/28/2017	9:15-9:45	671043	4551274	1733	5686	17.7	63.9	460	<30
13	Bottari Well	Private Well	180	160-180	2004	4/28/2017	13:15-14:00	668587	4558251	1718	5637	21.4	70.5	1270	<30
14	Three-mile spg	Spring				4/27/2017	15:20-16:00	668990	4558659	1711	5614	41.6	106.9	1725	30
15	Humboldt spg (lower)	Spring				4/27/2017	16:30-17:30	668512	4560914	1734	5689	53.0	127.4	1545	<30
16	Humboldt spg (upper)	Spring				4/27/2017	18:00-18:45	668692	4561041	1769	5804	44.9	112.8	1300	<30
17	Spring (NID 20)	Spring				4/28/2017	10:15-11:00	669320	4549216	1769	5804	16.2	61.2	510	<30
18	Railroad Spg	Spring				4/28/2017	11:15-12:00	668782	4548025	1770	5807	23.7	74.7	515	<30
19	"Last" Spring	Spring				4/28/2017	16:00-16:45	668174	4556142	1680	5512	15.0	59.0	1615	33
20	Twelve-mile spg (hot)*	Spring				June 2017		671949	4567732						
21	Twelve-mile spg (cold)*	Spring				June 2017		671949	4567732						
22	Trap Range Well*	Private Well	131	111-131	1988	June 2017		673574**	4554566**						
23	Windmill Well*	Private Well				8/30/2017		670805	4557233						
24	Ritchies Well*	Private Well				8/30/2017		670777	4554896						
25	Seep 1*	Seep/spring				Aug. 2017		669562	4554634			17.0	62.6		
26	Seep 2*	Seep/spring				Aug. 2017		669515	4554624			13.5	56.3		
27	Seep 3*	Seep/spring				Aug. 2017		669499	4554658			17.2	63.0		
28	Seep 4*	Seep/spring				Aug. 2017		669472	4554688						
29	Seep 5*	Seep/spring				Aug. 2017		669377	4554761			22.6	72.7		
30	Seep 6*	Seep/spring				Aug. 2017		669245	4554807			18.0	64.4		
31	Seep 7*	Seep/spring				Aug. 2017		669410	4554775			15.9	60.6		
32	Seep 8*	Seep/spring				Aug. 2017		669451	4554785						
33	Seep 9*	Seep/spring				Aug. 2017		669328	4554851			15.4	59.7		
34	Seep 10*	Seep/spring				Aug. 2017		669240	4554871			16.4	61.5		
35	Seep 11*	Seep/spring				Aug. 2017		669260	4554901			16.4	61.5		
36	E. Fork Humboldt River	River				10/1/2017		668167	4555708	1700		8.2	46.8		118
37	E. Fork Humboldt River	River				10/1/2017		668167	4555708	1700		8.2	46.8		118

*Grab samples by in soda bottles

UTM/UPS (11T) ** Approximate, from Google Earth general location

Sampling locations and chemical analyses, City of Wells, 2017
See Section 5.3 of the main report

ID	Name	Type	Field pH	Lab pH	ppm Li	ppm Na	ppm K	ppm Ca	ppm Mg	ppm SiO2	ppm B	mg/L Cl	mg/L F	mg/L SO4	mg/L HCO3***	mg/L NO3
1	Rural Electric	City Well	7.0	7.95	0.029	24.9	11.6	36.5	5.98	93.8	0.0814	4.52	0.402	14.8	171	7.32
2	Well #2	City Well	7.4	7.78	0.021	22.8	9.80	37.7	7.49	81.8	0.0707	10.8	0.312	15.3	179	7.56
3	Well #6	City Well	7.5	8.22	0.026	22.8	7.05	36.4	10.5	61.9	0.0742	8.04	0.371	15.2	187	5.51
4	Golf Course Well	City Well	7.6	7.7	0.014	20.0	5.97	36.6	11.9	61.9	0.058	10.5	0.246	16.0	185	6.21
5	Well #7	City Well	7.8	8.4	0.025	27.5	10.3	36.0	11.3	73.1	0.079	17.7	0.442	18.1	197	4.98
6	Well #5	City Well	7.6	8.15	0.017	34.1	5.99	34.5	11.4	35.5	0.10	16.8	0.130	21.1	210	0.359
7	Airport Well	City Well	7.8	8.01	0.012	16.6	4.65	35.6	17.5	48.9	0.060	31.5	0.204	26.5	147	15.5
8	Reynolds Well	Private Well	7.2	8.1	0.043	51.0	17.4	28.9	4.99	100	0.143	10.3	0.751	20.0	227	4.16
9	Arnold Merrill Well	Private Well	7.6	8.24	0.032	18.1	8.38	30.7	12.5	72.6	0.066	27.7	0.508	13.0	139	3.78
10	BTI Well	Private Well	7.2	7.98	0.124	91.2	16.9	36.5	10.3	95.1	0.200	13.4	2.11	26.7	357	0.437
11	Dan Morgan Well	Private Well	7.7	7.96	0.070	95.7	10.3	24.2	6.14	53.9	0.191	41.1	1.72	86.7	222	0.635
12	Reynolds House	Private Well	7.5	8.02	0.071	38.9	7.15	48.6	7.08	50.2	0.093	7.44	1.36	16.9	260	1.10
13	Bottari Well	Private Well	7.1	7.36	0.217	244	15.5	52.2	7.77	66.1	0.480	15.3	2.00	25.0	819	2.43
14	Three-mile spg	Spring	6.2	6.62	0.597	376	38.3	51.3	11.7	73.1	0.666	32.6	5.78	27.5	1474	0.016
15	Humboldt spg (lower)	Spring	6.4	6.95	0.544	256	27.6	74.4	30.4	91.6	0.573	15.1	3.69	16.9	1188	0.045
16	Humboldt spg (upper)	Spring	6.2	6.61	0.580	281	31.6	68.2	27.0	94.0	0.663	20.5	6.05	20.5	1433	0.0057
17	Spring (NID 20)	Spring	7.6	7.91	0.027	31.4	3.07	47.2	14.5	22.3	0.082	21.4	0.641	32.3	245	4.00
18	Railroad Spg	Spring	7.5	8.04	0.027	33.8	2.78	50.4	14.8	21.8	0.079	21.1	0.629	32.1	239	4.03
19	"Last" Spring	Spring	7.7	8.15	0.364	440	6.73	9.86	3.04	19.8	0.495	36.8	12.6	8.95	1074	0.240
20	Twelve-mile spg (hot)*	Spring		6.92												
21	Twelve-mile spg (cold)*	Spring		6.85												
22	Trap Range Well*	Private Well		7.23												
23	Windmill Well*	Private Well														
24	Ritchies Well*	Private Well														
25	Seep 1*	Seep/spring														
26	Seep 2*	Seep/spring														
27	Seep 3*	Seep/spring														
28	Seep 4*	Seep/spring														
29	Seep 5*	Seep/spring														
30	Seep 6*	Seep/spring														
31	Seep 7*	Seep/spring														
32	Seep 8*	Seep/spring														
33	Seep 9*	Seep/spring														
34	Seep 10*	Seep/spring														
35	Seep 11*	Seep/spring														
36	E. Fork Humboldt River	River	7.5													
37	E. Fork Humboldt River	River	7.5													

*Grab samples by in soda bottles

*** Total Inorganic Carbon as HCO3

Sampling locations and chemical analyses, City of Wells, 2017
See Section 5.3 of the main report

ID	Name	Type	ppm As	ppm Rb	ppm Cs	ppm Sr	ppm Ba	ppm Fe	ppm Mn	ppm Al	ppm P	ppb Be	ppb V	ppb Cr	ppb Se	ppb Ti	ppb Ni
1	Rural Electric	City Well	0.00407	0.0243	0.000097	0.334	0.279	0.084	0.0077	0.064	2.14	0.229	9.83	4.59	1.44	6.62	1.32
2	Well #2	City Well	0.00582	0.0239	0.000048	0.318	0.235	0.013	0.00075	0.059	1.77	0.041	12.2	1.96	0.860	5.70	1.26
3	Well #6	City Well	0.00617	0.0172	0.00026	0.239	0.197	0.010	0.00030	0.053	1.35	N.D	13.3	2.07	0.750	4.28	1.89
4	Golf Course Well	City Well	0.0054	0.013	0.000012	0.232	0.186	0.020	0.00043	0.054	1.34	0.016	14.6	3.77	0.506	4.38	0.967
5	Well #7	City Well	0.0045	0.017	0.000014	0.328	0.172	0.022	0.00079	0.056	1.58	N.D	13.1	2.22	0.823	5.11	0.965
6	Well #5	City Well	0.0035	0.012	0.000055	0.348	0.170	0.125	0.0039	0.053	0.82	N.D	7.79	0.629	0.220	2.23	1.01
7	Airport Well	City Well	0.0050	0.0038	0.0000053	0.264	0.049	0.033	0.0200	0.051	1.09	0.0038	15.7	6.08	0.927	3.21	1.30
8	Reynolds Well	Private Well	0.0060	0.041	0.00048	0.296	0.261	0.015	0.00053	0.055	2.05	N.D	21.5	1.19	0.805	6.35	0.979
9	Arnold Merrill Well	Private Well	0.0058	0.011	0.000019	0.336	0.100	0.020	0.00097	0.058	1.42	N.D	18.7	5.03	0.488	4.41	0.959
10	BTI Well	Private Well	0.0034	0.045	0.00039	0.403	0.184	0.011	0.0058	0.054	1.85	N.D	14.9	0.921	0.293	5.91	1.87
11	Dan Morgan Well	Private Well	0.0061	0.035	0.0012	0.280	0.055	0.018	0.0019	0.055	1.29	N.D	6.10	0.757	2.29	2.93	0.992
12	Reynolds House	Private Well	0.0023	0.0299	0.00046	0.246	0.202	0.017	0.00042	0.054	0.93	N.D	9.39	2.23	0.384	2.75	1.65
13	Bottari Well	Private Well	0.0025	0.057	0.0049	0.441	0.102	0.014	0.00052	0.059	1.25	0.135	8.03	3.16	0.335	4.36	1.32
14	Three-mile spg	Spring	0.00001	0.275	0.053	0.664	0.319	0.014	0.096	0.068	1.37	2.95	0.174	0.842	0.0183	5.69	1.46
15	Humboldt spg (lower)	Spring	0.000099	0.193	0.040	0.518	0.505	0.017	0.0048	0.056	1.69	3.00	0.155	0.866	N.D	6.99	2.07
16	Humboldt spg (upper)	Spring	0.031	0.229	0.041	0.503	0.540	0.212	0.194	0.087	1.73	1.20	0.413	1.01	0.067	7.58	3.11
17	Spring (NID 20)	Spring	0.00090	0.0065	0.00078	0.268	0.083	0.024	0.0013	0.063	0.505	N.D	3.55	1.03	0.592	1.32	1.68
18	Railroad Spg	Spring	0.00083	0.0064	0.00078	0.262	0.082	0.0082	0.00020	0.055	0.503	0.0010	3.44	0.738	0.567	1.13	1.49
19	"Last" Spring	Spring	0.00083	0.035	0.0054	0.243	0.157	0.0740	0.072	0.061	0.371	0.55	0.435	0.752	0.049	1.41	0.434
20	Twelve-mile spg (hot)*	Spring															
21	Twelve-mile spg (cold)*	Spring															
22	Trap Range Well*	Private Well															
23	Windmill Well*	Private Well															
24	Ritchies Well*	Private Well															
25	Seep 1*	Seep/spring															
26	Seep 2*	Seep/spring															
27	Seep 3*	Seep/spring															
28	Seep 4*	Seep/spring															
29	Seep 5*	Seep/spring															
30	Seep 6*	Seep/spring															
31	Seep 7*	Seep/spring															
32	Seep 8*	Seep/spring															
33	Seep 9*	Seep/spring															
34	Seep 10*	Seep/spring															
35	Seep 11*	Seep/spring															
36	E. Fork Humboldt River	River															
37	E. Fork Humboldt River	River															

*Grab samples by in soda bottles

Sampling locations and chemical analyses, City of Wells, 2017
See Section 5.3 of the main report

ID	Name	Type	ppb Co	ppb Cu	ppb Zn	ppb Ge	ppb Rb	ppb Zr	ppb Mo	ppb Ag	ppb Cd	ppb Sn	ppb Sb	ppb Eu	ppb Pb	ppb Th	ppb U
1	Rural Electric	City Well	0.298	1.32	140.3	0.385	24.3	N.D	2.37	0.314	0.120	0.184	0.200	0.077	0.422	0.690	2.34
2	Well #2	City Well	0.111	1.05	72.56	0.299	23.9	N.D	2.13	0.095	0.029	0.091	0.185	0.056	0.217	0.178	2.60
3	Well #6	City Well	0.091	2.92	29.93	0.401	17.2	N.D	2.30	0.050	0.019	0.096	0.103	0.046	0.190	0.073	1.86
4	Golf Course Well	City Well	0.067	1.72	36.88	0.117	12.9	N.D	1.78	0.032	0.011	0.080	0.130	0.038	0.083	0.038	2.42
5	Well #7	City Well	0.063	1.46	45.01	0.145	17.0	N.D	1.87	0.015	0.0082	0.124	0.116	0.040	0.106	0.022	2.18
6	Well #5	City Well	0.051	0.673	33.84	0.095	11.8	N.D	0.974	0.0042	N.D	0.062	0.103	0.031	0.069	0.0081	2.30
7	Airport Well	City Well	0.067	0.637	34.65	N.D	3.76	N.D	1.52	0.0091	0.0026	0.057	0.262	0.0093	0.064	0.0022	1.67
8	Reynolds Well	Private Well	0.055	0.972	12.95	0.438	40.7	N.D	4.13	0.0081	0.012	0.034	0.237	0.057	0.022	N.D	2.40
9	Arnold Merrill Well	Private Well	0.048	0.514	23.86	0.100	11.1	N.D	1.77	0.0021	N.D	0.038	0.163	0.020	0.026	N.D	1.89
10	BTI Well	Private Well	0.072	2.64	52.73	0.692	45.1	N.D	2.35	N.D	0.0014	0.051	0.199	0.044	0.044	N.D	4.25
11	Dan Morgan Well	Private Well	0.039	1.80	31.92	1.14	35.5	N.D	6.69	0.0025	0.011	0.031	0.024	0.011	0.062	N.D	1.29
12	Reynolds House	Private Well	0.057	1.91	28.14	3.10	29.9	N.D	1.41	N.D	0.0013	0.036	0.065	0.046	0.060	N.D	0.682
13	Bottari Well	Private Well	0.059	4.58	32.59	6.51	57.5	N.D	3.38	N.D	0.0077	0.016	0.194	0.026	0.020	N.D	5.07
14	Three-mile spg	Spring	0.065	5.47	18.74	31.7	275	0.021	0.247	N.D	0.00066	0.017	N.D	0.074	0.018	N.D	0.212
15	Humboldt spg (lower)	Spring	0.091	4.12	31.24	18.20	193	N.D	0.083	N.D	N.D	0.024	0.0061	0.122	0.015	N.D	0.033
16	Humboldt spg (upper)	Spring	2.90	7.45	82.43	29.2	229	0.013	2.05	N.D	0.067	0.039	0.223	0.113	0.196	N.D	0.315
17	Spring (NID 20)	Spring	0.070	0.584	20.42	1.41	6.55	N.D	1.07	N.D	N.D	0.011	0.025	0.019	0.014	N.D	2.83
18	Railroad Spg	Spring	0.059	0.820	28.01	1.37	6.43	N.D	1.06	N.D	0.00016	0.021	0.031	0.016	0.0075	N.D	2.83
19	"Last" Spring	Spring	0.081	6.83	15.49	38.1	35.1	0.176	1.58	N.D	N.D	0.018	0.0088	0.037	0.023	N.D	0.083
20	Twelve-mile spg (hot)*	Spring															
21	Twelve-mile spg (cold)*	Spring															
22	Trap Range Well*	Private Well															
23	Windmill Well*	Private Well															
24	Ritchies Well*	Private Well															
25	Seep 1*	Seep/spring															
26	Seep 2*	Seep/spring															
27	Seep 3*	Seep/spring															
28	Seep 4*	Seep/spring															
29	Seep 5*	Seep/spring															
30	Seep 6*	Seep/spring															
31	Seep 7*	Seep/spring															
32	Seep 8*	Seep/spring															
33	Seep 9*	Seep/spring															
34	Seep 10*	Seep/spring															
35	Seep 11*	Seep/spring															
36	E. Fork Humboldt River	River															
37	E. Fork Humboldt River	River															

*Grab samples by in soda bottles

Sampling locations and chemical analyses, City of Wells, 2017
See Section 5.3 of the main report

ID	Name	Date Sampled	Time (Approx.)	Easting (m)	Northing (m)	Approx Elev (m)	Temperature (°C)	δ^2H_{SMOW} (‰)	$\delta^{18}O_{SMOW}$ (‰)	$\delta^{13}C_{PDB}$ (‰)	DIC*** mmol/L C	DIC*** ppm as HCO3
1	Rural Electric	4/26/2017	10:50-12:00	670402	4553365	1706	34.6	-131.074	-17.130	-6.98	2.8	173
2	Well #2	4/26/2017	12:15-12:45	670152	4552927	1692	29.0	-130.087	-16.775	-7.09	3.0	185
3	Well #6	4/26/2017	14:15-15:00	670727	4551696	1732	26.0	-128.728	-16.793	-6.74	3.0	184
4	Golf Course Well	4/26/2017	15:10-15:45	670407	4551729	1747	23.3	-131.096	-17.129	-7.49	2.7	162
5	Well #7	4/26/2017	16:00-16:45	669770	4551534	1726	20.9	-131.437	-17.025	-6.67	3.1	188
6	Well #5	4/26/2017	17:20-17:50	673571	4553291	1742	25.4	-136.868	-17.366	-4.95	3.3	204
7	Airport Well	4/26/2017	18:00-18:30	674053	4553531	1737	13.5	-134.590	-17.142	-5.97	2.4	147
8	Reynolds Well	4/26/2017	9:30-10:45	670179	4554259	1707	41.0	-135.536	-17.620	-4.48	3.8	230
9	Arnold Merrill Well	4/27/2017	9:15-9:50	672254	4552864	1700	20.1	-128.254	-16.660	-6.88	2.8	169
10	BTI Well	4/27/2017	10:15-11:00	671971	4552744	1727	30.5	-132.83	-17.05	-1.75	6.2	376
11	Dan Morgan Well	4/27/2017	11:20-12:00	668388	4551882	1783	32.0	-136.44	-17.23	-3.61	3.2	192
12	Reynolds House	4/28/2017	9:15-9:45	671043	4551274	1733	17.7	-129.25	-16.83	-3.59	4.4	266
13	Bottari Well	4/28/2017	13:15-14:00	668587	4558251	1718	21.4	-132.93	-16.49	0.81	13.1	802
14	Three-mile spg	4/27/2017	15:20-16:00	668990	4558659	1711	41.6	-131.37	-16.02	-1.00	32.0	1955
15	Humboldt spg (lower)	4/27/2017	16:30-17:30	668512	4560914	1734	53.0	-130.59	-16.32	-0.57	34.9	2128
16	Humboldt spg (upper)	4/27/2017	18:00-18:45	668692	4561041	1769	44.9	-129.08	-16.12	-1.06	45.1	2750
17	Spring (NID 20)	4/28/2017	10:15-11:00	669320	4549216	1769	16.2	-130.73	-16.77	-5.19	4.7	289
18	Railroad Spg	4/28/2017	11:15-12:00	668782	4548025	1770	23.7	-131.47	-16.95	-5.71	3.6	218
19	"Last" Spring	4/28/2017	16:00-16:45	668174	4556142	1680	15.0	-137.44	-16.79	0.49	16.4	998
20	Twelve-mile spg (hot)*	June 2017		671949	4567732	NA	NA	-131.15	-17.07	-4.89	5.7	350
21	Twelve-mile spg (cold)*	June 2017		671949	4567732	NA	NA	-129.56	-16.72	-4.87	5.5	333
22	Trap Range Well*	June 2017		673574**	4554566**	NA	NA	-131.53	-16.76	-8.82	3.3	203
23	Windmill Well*	8/30/2017		670777	4554896	NA	NA	-131.20	-16.64	-6.92	2.4	147
24	Ritchies Well*	8/30/2017		670805	4557233	NA	NA	-131.31	-17.05	-8.12	2.8	168
25	Seep 1*	August 2017		669562	4554634	NA	17.0	-126.52	-15.87	-7.79	6.4	391
26	Seep 2*	August 2017		669515	4554624	NA	13.5	-131.16	-16.97	-10.31	4.4	267
27	Seep 3*	August 2017		669499	4554658	NA	17.2	-122.19	-15.05	-6.34	4.0	245
28	Seep 4*	August 2017		669472	4554688	NA	NA	-124.62	-15.89	-11.48	10.4	635
29	Seep 5*	August 2017		669377	4554761	NA	22.6	-131.54	-16.89	-5.85	3.6	220
30	Seep 6*	August 2017		669245	4554807	NA	18.0	-131.59	-16.82	-6.43	3.8	231
31	Seep 7*	August 2017		669410	4554775	NA	15.9	-131.74	-16.69	-8.36	3.3	198
32	Seep 8*	August 2017		669451	4554785	NA	NA	-128.02	-16.00	-8.13	3.9	241
33	Seep 9*	August 2017		669328	4554851	NA	15.4	-133.26	-17.02	-10.06	4.9	299
34	Seep 10*	August 2017		669240	4554871	NA	16.4	-130.90	-16.51	-4.93	3.7	227
35	Seep 11*	August 2017		669260	4554901	NA	16.4	-134.30	-17.13	-6.01	3.3	199
36	E. Fork Humboldt River	10/1/2017		668167	4555708	1700	7.5	-124.36	-15.35			
37	E. Fork Humboldt River	10/1/2017		668167	4555708	1700	7.5	-124.91	-15.44			

*Grab samples by in soda bottles

** Approximate, from Google Earth general location UTM/UPS (11T)

*** Not as precise as TIC analyses for high values

APPENDIX H – EXPLANATION OF DC RESISTIVITY SURVEY

Explanation of DC Resistivity

Resistivity ρ is a constant of proportionality derived from the measurement of resistance (R) along the length of a uniform cylinder and is a physical property of a pure material (Herman, 2001):

$R= \rho(L/A)$ (1)

where L= length and A= area

The total resistance can then be determined by measuring the potential difference throughout a cylinder where a known current is applied in accordance with Ohm's Law:

$R=V/I$ (2)

where V=potential difference and I=transmitted current

One conceptual model for the Earth can be thought of as consisting of a homogeneous and isotropic half-space medium. In this case the potential at any point in that medium may be determined by:

$V=\rho I/2\pi r$

where

V=potential difference (volts),

ρ is the resistivity of the medium,

I is current in amperes,

and r is the distance to the electrode.

Apparent resistivity (ρ) then by substitution and rearrangement,

$\rho=(V/I)\ (A/L) = R_A(K)$ (3)

where

R_A is the apparent resistance and K is referred to as the geometric factor which describes the geometry of the hypothetical cylinder through which the current flows. The geometric factor term K involves the specific geometrical distribution of measurements and are important experimental parameters that have evolved with the technique. Depending on the type of electrode configuration and pattern of current injection and potential measurements, varying geometries can provide enhancement of features in the horizontal or vertical direction. Equation 4 shows the geometric factor (K) for a dipole-dipole array.

$\pi\alpha n(n+1)\ (n+2)$ (4)

Apparent resistivity (ρa) is then calculated from the ratio of current to measured potential according to equation 5.

$\rho a=\pi\alpha n(n+1)\ (n+2)\ (V/I)$ (5)

APPENDIX I – CITY OF WELLS GEOTHERMAL DATA CATALOG

Dataset	Dataset name in database	Description	Category	Spatial extent	Year published or created	Format	# of records	Public or Private
Topographic and Administrative Boundaries								
City of Wells	City of Wells	Areal extent of the City of Wells, digitzed from topo map	Administrative	City of Wells	2017	Feature Class	1	Public
Elko County	Elko County	Areal extent of Elko County, Nevada	Administrative	Elko County	2010	Feature Class	1	Public
Nevada	Nevada	Areal extent of Nevada	Administrative	Nevada	2009	Feature Class	1	Public
LiDAR Elevation	N/A	1m LiDAR elevation data from FEMA. Used for depth calibrations in 3D geologic model	Elevation	City of Wells area	2017	Raster	N/A	Private
LiDAR Hillshade	Wells_LiDAR_DEM_Hillshade	Hillshade created from LiDAR elevation data	Elevation	City of Wells area	2017	Raster	N/A	Public
3D geologic model extent	Geologic 3D Model Extent	Areal extent used for 3D geologic model	Boundary	City of Wells area	2017	Feature Class	1	Public
Geologic and Structural Data								
Aquifers	Aquifers USGS 2005	Aquifers in Elko County	Geology	Elko County	2005	Feature Class	70	Public
Alteration	Alteration_Zuza_2017	Chemical alteration of surface rocks	Geology	City of Wells area	2017	Feature Class	19	Public
Geologic structure- attitudes (Henry and Thorman, 2011)	Attitudes_Henry_and_Thorman_2011	Fault, fold, and other geologic structure data	Geology	City of Wells area	2011	Feature Class	863	Public
Concealed contact faults	Concealed_Contact_Faults_Henry_and_Thorman_2011	Contact faults covered in subsurface	Geology	City of Wells area	2011	Feature Class	254	Public
Contact faults	Contact_Faults_Henry_and_Thorman_2011	Faults which one type of rock contacts a different type	Geology	City of Wells area	2011	Feature Class	1603	Public
Depth to groundwater in Elko County	Depth_to_Groundwater_USGS_2005	Depth to groundwater source	Geology	Elko County	2005	Feature Class	379	Public
Geolines	Geolines Henry and Thorman 2011	A 1:48,000-scale geologic map of the Wells area, in Elko County, Nevada, with descriptions of 54 geologic units, 2 cross-sections, and seismicity data for the preliminary and revised epicenters of the February 21, 2008 magnitude 6.0 earthquake, and its aftershocks.	Geology	City of Wells area	2011	Feature Class	1887	Public
Conglomerate	Conglomerate_Zuza_2017	Location of conglomerate lithologic units at the surface	Geology	City of Wells area	2017	Feature Class	10	Public
Faults and contacts	Faults and contacts Henry and Thorman 2011	A 1:48,000-scale geologic map of the Wells area, in Elko County, Nevada, with descriptions of 54 geologic units	Geology	City of Wells area	2011	Feature Class	109	Public
Faults annotations	Fault Annotations Henry and Thorman 2011	A 1:48,000-scale geologic map of the Wells area, in Elko County, Nevada, with descriptions of 54 geologic units	Geology	City of Wells area	2011	Feature Class	139	Public
Cross section lines (Zuza, 2017)	Cross_Section_Lines_Zuza_2017	Locations for subsurface cross section from Zuza 2017	Geology	City of Wells area	2017	Feature Class	2	Public
Dip, strike, slip, and dilation	Dip Strike Slip and Dilation Tendency Siler 2017	Faults with dip, strike, slip, and dilation information interpreted from Thorman (2011) and Zuza (2017)	Geology	City of Wells area	2017	Feature Class	31461	Public
Folds	Folds_Henry_and_Thorman_2011	Geologic folds	Geology	City of Wells area	2006	Feature Class	35	Public
Surface geology around wells	Geology_Henry_Thorman_2011	A 1:48,000-scale geologic map of the Wells area, in Elko County, Nevada, with descriptions of 54 geologic units	Geology	City of Wells area	2011	Feature Class	1159	Public
Geologic structure- attitudes (Jewell, 1982)	Attitudes_Jewell_1982	Fault, fold, and other geologic structure data from Jewell 1982	Geology	City of Wells area	1982	Feature Class	6	Public
Geologic structure- attitudes (Zuza, 2017)	Attitudes_Zuza_2017	Fault, fold, and other geologic structure data from Zuza 2017	Geology	City of Wells area	2017	Feature Class	90	Public
Slickenlines	Slickenlines Zuza 2017	Shear fractures with polished and/or coated with secondary mineral growths that bear a linear structure	Geology	City of Wells area	2017	Feature Class	3	Public
Young faults in Elko County	Young Faults Dohrenwend 2012	Quarternary faults in Elko County	Geology	Elko County	2012	Feature Class	1121	Public
Depth to groundwater	Depth_to_groundwater_Lopes_et_al_2006	Data set was created as part of an effort to provide statewide information on depth to ground water and water-table levels in Nevada	Geology	Nevada	2006	Raster	1	Public
Depth to Pre-Cenozoic bedrock (basement)	Depth_to_pre_Cenozoic_bedrock_Ponce_and_Damar_2017	This digital raster dataset represents depth to pre-Cenozoic bedrock in northern Nevada	Geology	Northern Nevada	2017	Raster	1	Public
3D geologic model faults	Faults 3D Geologic Model NETL 2017	Compiled and selected faults used in 3D geologic modeling	Geology	City of Wells area	2017	Feature Class	15	Public
Wells with lithologic logs	Wells with lithologic logs NDWR	Locations of wells used to interpret drillers well logs into lithologic logs	Geology	City of Wells area	2017	Feature Class	54	Public
Lithologic cross section lines	Lithologic Cross Sections NETL 2017	2D lines representing geologic cross sections developed from the NDWR well logs	Geology	City of Wells area	2017	Feature Class	4	Public
Geophysical Data								
Earthquakes near Elko County	Earthquakes USGS	Recorded earthquakes in and near Elko County	Geophysical	City of Wells area	2017	Feature Class	122	Public
Apparent conductivity survey-North	N/A	Interpolation for 1530 Hz apparent conductivity (near hot springs)	Geophysical	City of Wells area	2017	Raster	N/A	Private
Apparent conductivity survey-South	N/A	Interpolation for 1530 Hz apparent conductivity (near geoprobes)	Geophysical	City of Wells area	2017	Raster	N/A	Private
Wells with geophysical logs	N/A	Location of IHS Wells with Geophysical Well Logs	Geophysical	City of Wells area	2015	Feature Class	6	Private
Merged electromagnetic survey tracks	N/A	Electromagnetic survey tracks from NETL's 2017 EM survey	Geophysical	City of Wells area	2017	Feature Class	220307	Private
Resistivity line survey	N/A	Line tracks for NETL's 2017 resistivity survey	Geophysical	City of Wells area	2017	Feature Class	3	Private
Subsurface stress data	Stress Data Heidbach et al 2008	Focal mechanism and other structual data	Geophysical	City of Wells area	2012	Feature Class	1	Public
Seismic line	Seismic Line SEI 1976	Seismic line available within the 3D model extent	Geophysical	City of Wells area	1976	Feature Class	1	Public
Geothermal and Geochemical Data								
Geoprobe	N/A	Geoprobe meaurements collected in April 2017	Geothemal	City of Wells area	2017	Feature Class	13	Private
April 2017 Well and spring sampling locations	N/A	Corrected well and spring locations	Geothermal	City of Wells area	2017	Feature Class	19	Private
Shallow temperature points	N/A	Shallow temperature meaurements collected in April 2017 from wells and springs	Geothermal	City of Wells area	2017	Feature Class	73	Private
Spring and well data pre-April 2017	N/A	Spring and well temperature measurements collected before 2017	Geothermal	City of Wells area	2016	Feature Class	37	Private
NDWR Wells with temperature	Wells_with_Temperature_NDWR	Nevada Division of Water Resources groundwater data with temperature. Locations are updated within the vicinity of Wells	Geothermal	City of Wells area	2017	Feature Class	320	Public
Exploration wells	N/A	Location of slimline holes for geothermal exploration	Geothermal	City of Wells area	2017	Feature Class	4	Private
Wells and springs with temperature data (compilation)	N/A	Compilation of existing datasets with robust temperature measurements from wells and springs in the area	Geothermal	City of Wells area	2017	Feature Class	139	Private
Geochemical data	Geochemical_Data_Spycher_and_Zehner_2017	Compiled published water analyses for springs and wells in and around the city of Wells (up to 2011, mostly thermal waters, some cold groundwater wells/springs). The compilation also includes best estimates of sampling locations (UTM coordinates).	Geothermal/Geochemistry	City of Wells area	2017	Feature Class	56	Private
Groundwater samples	Groundwater_Samples_Zehner_et_al_2006	Chemical and temperaure measurements from spring/groundwater samples in the area	Geothermal/Geochemistry	City of Wells area	2006	Feature Class	151	Public
Chemical and isotopic analysis October 2017	Chemical Isotopic Data Spycher 2017	Chemical and Isotopic Analyses of wells, springs, rivers, and seeps from April to October 2017	Geothermal/Geochemistry	City of Wells area	2017	Feature Class	37	Public

Dataset	Available at (link to data source)	Data Source/Owner	Citations (Not all from peer reviewed sources)	Acquired by	Data collected/interpreted for analysis
Topographic and Administrative Boundaries					
City of Wells	https://www.arcgis.com/home/item.html?id=99cd5fbd98934028802b4f797c4b1732	ESRI	ESRI, 2017, World Topographic Map.	National Energy Technology Laboratory	No
Elko County	https://www.arcgis.com/home/item.html?id=a00d6b6149b34ed3b833e10fb72ef47b	ESRI	ArcGIS Content Team, 2010, U.S. Counties (Generalized): ESRI	National Energy Technology Laboratory	No
Nevada	https://www.census.gov/geo/maps-data/data/cbf/cbf_state.html	US Census Bureau	U.S. Census Bureau, Geography Division, 2009, TIGER/Line Shapefile, 2009, nation, U.S., Current State and Equivalent National: U.S. Department of Commerce.	National Energy Technology Laboratory	No
LiDAR Elevation	N/A	Federal Emergency Management Agency	FEMA, 2015, "2015 FEMA REG-Elko, NV-LiDAR-FY15'	National Energy Technology Laboratory	No
LiDAR Hillshade	https://edx.netl.doe.gov/dataset/new_resource/city-of-wells-geothermal-data	Federal Emergency Management Agency (Processed by National Energy Technology Laboratory)	Miller, R., 2017, Hillshade from 2015 FEMA Lidar survey, University of Nevada, Reno: National Energy Technology Laboratory.	National Energy Technology Laboratory	No
3D geologic model extent	https://edx.netl.doe.gov/dataset/new_resource/city-of-wells-geothermal-data	National Energy Technology Laboratory	NETL, 2017, Section 7.2 in report	National Energy Technology Laboratory	Yes
Geologic and Structural Data					
Aquifers	http://www.nbmg.unr.edu/geothermal/Data.html	USGS	USGS, 2005, Great Basin Major Aquifers	Nevada Bureau of Mines and Geology	No
Alteration	https://edx.netl.doe.gov/dataset/new_resource/city-of-wells-geothermal-data	A.V. Zuza	Zuza, A.V., 2017, Preliminary geologic map of the southern Snake Mountains near Wells, Nevada: University of Nevada, Reno, Nevada Bureau of Mines and Geology.	Nevada Bureau of Mines and Geology	Yes
Geologic structure- attitudes (Henry and Thorman, 2011)	http://data.nbmg.unr.edu/Public/freedownloads/sp/sp036/	Nevada Bureau of Mines and Geology	Henry, D.C. and Thorman, C.H., 2011, Geologic map of the Wells area. Elko County, Nevada: Nevada Bureau of Mines and Geology Special Publication 36, Appendix A.	Nevada Bureau of Mines and Geology	No
Concealed contact faults	http://data.nbmg.unr.edu/Public/freedownloads/sp/sp036/	Nevada Bureau of Mines and Geology	Henry, D.C. and Thorman, C.H., 2011, Geologic map of the Wells area. Elko County, Nevada: Nevada Bureau of Mines and Geology Special Publication 36, Appendix A.	Nevada Bureau of Mines and Geology	No
Contact faults	http://data.nbmg.unr.edu/Public/freedownloads/sp/sp036/	Nevada Bureau of Mines and Geology	Henry, D.C. and Thorman, C.H., 2011, Geologic map of the Wells area. Elko County, Nevada: Nevada Bureau of Mines and Geology Special Publication 36, Appendix A.	Nevada Bureau of Mines and Geology	No
Depth to groundwater in Elko County	http://www.nbmg.unr.edu/geothermal/Data.html	United States Geological Survey	U.S. Geological Survey, National Water Information System, 2005, Depth to Groundwater (measured in feet) in Nevada water wells.	Nevada Bureau of Mines and Geology	No
Geolines	http://data.nbmg.unr.edu/public/freedownloads/sp/sp036/	Nevada Bureau of Mines and Geology	Henry, D.C. and Thorman, C.H., 2011, Geologic map of the Wells area. Elko County, Nevada: Nevada Bureau of Mines and Geology Special Publication 36, Appendix A.	Nevada Bureau of Mines and Geology	No
Conglomerate	https://edx.netl.doe.gov/dataset/new_resource/city-of-wells-geothermal-data	A.V. Zuza	Zuza, A.V., 2017, Preliminary geologic map of the southern Snake Mountains near Wells, Nevada: University of Nevada, Reno, Nevada Bureau of Mines and Geology.	Nevada Bureau of Mines and Geology	Yes
Faults and contacts	http://data.nbmg.unr.edu/public/freedownloads/sp/sp036/	Nevada Bureau of Mines and Geology	Henry, D.C. and Thorman, C.H., 2011, Geologic map of the Wells area. Elko County, Nevada: Nevada Bureau of Mines and Geology Special Publication 36, Appendix A.	Nevada Bureau of Mines and Geology	No
Faults annotations	http://data.nbmg.unr.edu/public/freedownloads/sp/sp036/	Nevada Bureau of Mines and Geology	Henry, D.C. and Thorman, C.H., 2011, Geologic map of the Wells area. Elko County, Nevada: Nevada Bureau of Mines and Geology Special Publication 36, Appendix A.	Nevada Bureau of Mines and Geology	No
Cross section lines (Zuza, 2017)	https://edx.netl.doe.gov/dataset/new_resource/city-of-wells-geothermal-data	A.V. Zuza	Zuza, A.V. Preliminary geologic map of the southern Snake Mountains near Wells, Nevada: University of Nevada, Reno, Nevada Bureau of Mines and Geology.	Nevada Bureau of Mines and Geology	Yes
Dip, strike, slip, and dilation	https://edx.netl.doe.gov/dataset/new_resource/city-of-wells-geothermal-data	United States Geological Survey	Siler, D., 2017, Section 7.1 in report	United States Geological Survey	Yes
Folds	https://edx.netl.doe.gov/dataset/city-of-wells-geothermal-project-data	Nevada Bureau of Mines and Geology	Henry, D.C. and Thorman, C.H., 2011, Geologic map of the Wells area. Elko County, Nevada: Nevada Bureau of Mines and Geology Special Publication 36, Appendix A.	Nevada Bureau of Mines and Geology	No
Surface geology around wells	http://data.nbmg.unr.edu/public/freedownloads/sp/sp036/	Nevada Bureau of Mines and Geology	Henry, D.C. and Thorman, C.H., 2011, Geologic map of the Wells area. Elko County, Nevada: Nevada Bureau of Mines and Geology Special Publication 36, Appendix A.	Nevada Bureau of Mines and Geology	No
Geologic structure- attitudes (Jewell, 1982)	https://edx.netl.doe.gov/dataset/new_resource/city-of-wells-geothermal-data	US Department of Energy	Jewell, P.W., 1982, Geology and Geothermal Potential North of Wells, Nevada: University of Utah Research Institute, Earth Science Laboratory Open-File Report DOE/ID/12079-83, 38 p.	Nevada Bureau of Mines and Geology	No
Geologic structure- attitudes (Zuza, 2017)	https://edx.netl.doe.gov/dataset/new_resource/city-of-wells-geothermal-data	A.V. Zuza	Zuza, A.V., 2017, Preliminary geologic map of the southern Snake Mountains near Wells, Nevada: University of Nevada, Reno, Nevada Bureau of Mines and Geology.	Nevada Bureau of Mines and Geology	Yes
Slickenlines	https://edx.netl.doe.gov/dataset/new_resource/city-of-wells-geothermal-data	A.V. Zuza	Zuza, A.V., 2017, Preliminary geologic map of the southern Snake Mountains near Wells, Nevada: University of Nevada, Reno, Nevada Bureau of Mines and Geology.	Nevada Bureau of Mines and Geology	Yes
Young faults in Elko County	http://www.nbmg.unr.edu/geothermal/Data.html	United States Geological Survey	Dohrenwend, J., 2012, Young Faults: U.S. Geological Survey.	Nevada Bureau of Mines and Geology	No
Depth to groundwater	https://pubs.usgs.gov/sir/2006/5100/	United States Geological Survey	Lopes, T.J., Buto, S.G., Smith, J.L., and Welborn, T.L., 2006, Water-table levels and gradients, Nevada, 1947-2004: U.S. Geological Survey Scientific Investigations Report 2006-5100, 27 p.	National Energy Technology Laboratory	No
Depth to Pre-Cenozoic bedrock (basement)	https://www.sciencebase.gov/catalog/item/59b6d705e4b08b1644ddf8dc	United States Geological SurveyBureau of Land Management	Ponce, D.A., and Damar, N.A., 2017, Depth to pre-Cenozoic bedrock in northern Nevada: U.S. Geological Survey data release, https://doi.org/10.5066/F75B01DD.	National Energy Technology Laboratory	No
3D geologic model faults	https://edx.netl.doe.gov/dataset/new_resource/city-of-wells-geothermal-data	National Energy Technology Laboratory	Mark-Moser M., 2017, Section 7.2.1 in report or Appendix J	National Energy Technology Laboratory	Yes
Wells with lithologic logs	http://water.nv.gov/welllogquery.aspx	Nevada Division of Water Resources	DiGiulio, J., 2017, Section 5.2.6 in report or Appendix E	National Energy Technology Laboratory	Yes
Lithologic cross section lines	https://edx.netl.doe.gov/dataset/new_resource/city-of-wells-geothermal-data	Nevada Division of Water Resources	DiGiulio, J., 2017, Section 5.2.6 in report or Appendix E	National Energy Technology Laboratory	Yes
Geophysical Data					
Earthquakes near Elko County	https://earthquake.usgs.gov/earthquakes/search/	United States Geological Survey Northern California Earthquake Data Center	NCEDC, 2016, Northern California Earthquake Data Center. UC Berkeley Seismological Laboratory. Dataset. doi:10.7932/NCEDC.	Nevada Bureau of Mines and Geology	No
Apparent conductivity survey-North	N/A	National Energy Technology Laboratory	NETL, 2017, Section 5.4 in report or Appendix H	National Energy Technology Laboratory	Yes
Apparent conductivity survey-South	N/A	National Energy Technology Laboratory	NETL, 2017, Section 5.4 in report or Appendix H	National Energy Technology Laboratory	Yes
Wells with geophysical logs	N/A	IHS and others	IHS, Inc. and its affiliated and subsidiary companies. 2015, IHS Lognet Database. IHS Enerdeq.	National Energy Technology Laboratory	No
Merged electromagnetic survey tracks	N/A	National Energy Technology Laboratory	NETL, 2017, Section 5.4 in report or Appendix H	National Energy Technology Laboratory	Yes
Resistivity line survey	N/A	National Energy Technology Laboratory	NETL, 2017, Section 5.4 in report or Appendix H	National Energy Technology Laboratory	Yes
Subsurface stress data	https://edx.netl.doe.gov/dataset/new_resource/city-of-wells-geothermal-data	German Research Centre for Geosciences	Heidbach, O., Tingay, M., Barth, A., Reinecker, J., Kurfeß, D., Müller, B., 2008. The World Stress Database Release 2008. sdf. https://doi.org/doi:10.1594/GFZ.WSM.Rel2008	Lawrence Berkeley National Laboratory	Yes
Seismic line	https://edx.netl.doe.gov/dataset/new_resource/city-of-wells-geothermal-data	Seismic Exchange Inc.	Shell (Seismic Exchange, Inc.) 1976, 17-1418-17-02281A.	National Energy Technology Laboratory	No
Geothermal and Geochemical Data					
Geoprobe	N/A	Lumos and Associates	Zehner, R., 2017b, Geoprobe report. See Section 5.1.2 or Appendix C	Lumos and Associates	Yes
April 2017 Well and spring sampling locations	N/A	Lumos and Associates	Spycher, N. and Zehner, R., 2017, . See Section 5.3 or Appendix G	Lumos and Associates	Yes
Shallow temperature points	N/A	Lumos and Associates	Zehner, R., 2017a Shallow (2-Meter) Temperature Survey in and Around the City of Wells, Nevada: Implications for Geothermal Exploration. Unpublished report for Elko Heat Company and The City of Wells by Geothermal Development Associates, 12p	Lumos and Associates	Yes
Spring and well data pre-April 2017	N/A	Lumos and Associates	Zehner, R., 2016, Desktop study of geothermal potential in and around the City of Wells. Unpublished report for The City of Wells and Better Cities by Geothermal Development Associates, 9p.	Lumos and Associates	Yes
NDWR Wells with temperature	http://water.nv.gov/welllogquery.aspx	Nevada Division of Water Resources	NDWR, modified from "Well log data file"	National Energy Technology Laboratory	No
Exploration wells	N/A	City of Wells	Zehner, R. 2017. Section 8.1 in report or Appendix K	City of Wells	Yes
Wells and springs with temperature data (compilation)	https://edx.netl.doe.gov/dataset/new_resource/city-of-wells-geothermal-data	National Energy Technology Laboratory	NETL, 2017, Section 7.2 in report	National Energy Technology Laboratory	Yes
Geochemical data	N/A	Spycher, N. and Zehner, R.	Spycher, N. & Zehner, R. 2017. Chemical data from the Literature and Best Estimate of Location of Springs and Wells in the Vicinity of Wells, Nevada (Elko County).	Spycher, N. and Zehner, R.	No
Groundwater samples	http://www.nbmg.unr.edu/geothermal/Data.html	Nevada Bureau of Mines and Geology	Zehner, R.E., Coolbaugh, M.F., and Shevenell, Lisa, 2006, Regional groundwater geochemical trends in the Great Basin: Implications for Geothermal Exploration, GRC Transactions 2006	Nevada Bureau of Mines and Geology	No
Chemical and isotopic analysis October 2017	https://edx.netl.doe.gov/dataset/new_resource/city-of-wells-geothermal-data	Lawrence Berkeley National Laboratory	Spycher, N., 2017, Section 5.3 or Appendix G	Lawrence Berkely National Laboratory	Yes

APPENDIX J – MATLAB SCRIPT FOR GENERATING FAULT PLANES IN EARTHVISION

Appendix J – MATLAB Script for Generating Fault Planes in EarthVision

The following script generates a .dat file that can be imported into EarthVision (to be gridded into fault planes). The output .dat file contains a 3-D array of points that comprise the inferred fault plane. Fault geometries used in this study are described within Table 1 below.

Fault parameters to be defined by the user:

- "fname": the surface trace of the fault in .dat format. Must have XY location information and elevation (Z)
- "dip": degrees fault dips from horizon
- "max_depth": maximum depth to project surface points
- "resolution": spacing between points
- "numHeaderLines": number of header lines (skips header to XYZ data)

The result is a .dat file of XYZ points used as a direct input for the EarthVision modeling workflow.

```
close all; clear all;

%% DEFINE FILE AND PARAMETERS HERE

fname = 'Fault13_Zuza_Final.shp.dat';
horz_angle = 210; %dip direction
dip = 75; %Cannot be 90; EarthVision will not grid correctly. Use 89 for 90
dip_angle = 90-dip;
max_depth = 0;
resolution = 1; %spacing per point
fid = fopen(fname);
numHeaderLines = 15; %alter per file

%% LOAD SCATTERED DATA FROM EARTHVISION IMPORT

%loop through header lines

for i = 1:numHeaderLines
    [~] = fgetl(fid);
end

%initialize line that will be looked at
thisline = fgetl(fid);
k = 1;

while feof(fid)==0 %loop until end of file
    tmp = textscan(thisline,'%f%f%f');
    x(k) = tmp{1}; %assign first cell value to x
    y(k) = tmp{2}; %to y
    z(k) = tmp{3}; %to z
    thisline = fgetl(fid); %update line that will be looked at
    k = k+1;
 end
```

```
fclose(fid); %close file

%x, y, and z should be the variables you want

figure; hold on
scatter(x,y)

%% find new x,y,z points

surfX = x; surfY = y; surfZ = z;
for i = 1:numel(x)
    count = 1;
    for k = z(i)-1:(-1.*resolution):max_depth %k is depth value, NOT index
        total_depth = z(i)-k;
        hypot(i) = tand(dip_angle).*total_depth;
        xd = sind(horz_angle).*hypot(i);
        yd = cosd(horz_angle).*hypot(i);
        x2(count) = x(i)+xd;
        y2(count) = y(i)+yd;
        z2(count) = k;
        count = count+1;
    end
    surfX = horzcat(surfX,x2);
    surfY = horzcat(surfY,y2);
    surfZ = horzcat(surfZ,z2);

end

figure;
hold on
scatter3(surfX,surfY,surfZ)

%% Write to .dat

all_data = vertcat(surfX,surfY,surfZ);
all_data = all_data';

headera = '# Type: scattered data';
headerb = '# Version: 80';
headerc = '# Format: free';
headerd = '# Field: 1 x meters';
headere = '# Field: 2 y meters';
headerf = '# Field: 3 z';
headerg = '# Coordinate_System_Id: CRD589B1';
headerh = '# Coordinate_System_Name: NAD83 / UTM Zone 11 North';
headeri = '# Projection: Universal Transverse Mercator';
headerj = '# Zone: 11';
headerk = '# Units: meters';
headerl = '# Ellipsoid: GRS 1980/NAD83';
headerm = '# End:';
%header1 = 'X';
%header2 = 'Y';
%header3 = 'Z';
fid=fopen([fname,'_dip.dat'],'wt');
```

```
fprintf(fid, [headera '\n' headerb '\n' headerc '\n' headerd '\n' headere
'\n' headerf '\n' headerg '\n' headerh '\n' headeri '\n' headerj '\n' headerk
'\n' headerl '\n' headerm '\r\n']);
%'\n' header1 ' ' header2 ' ' header3
fprintf(fid, '%f %f %f \r\n', all_data');
fclose(fid);
```

***Table 1**. Inferred fault geometries used to convert the two-dimensional fault traces to three-dimensional faults planes in the EarthVision model.*

Filename (.shp)	Slip	Dip (degrees)	Dip direction (azimuth)
Fault1_Zuza_Final	Normal	60	280
Fault2_Zuza_Final	Normal	60	280
Fault3_Zuza_Final	Normal	60	220
Fault4_Zuza_Final	Normal	60	270
Fault5_Zuza_Final	Normal	60	300
Fault6_Zuza_Final	Normal	60	270
Fault7_Zuza_Final	Strike-slip	85	200
Fault8_Zuza_Final	Strike-slip	85	200
Fault9_Zuza_Final	Normal	60	280
Fault10_Zuza_Final	Normal	60	280
Fault11_Zuza_Final	Normal	60	280
Fault12_Zuza_Final	Normal	75	210
Fault13_Zuza_Final	Normal	75	210
QuatFaultLong	Normal	60	300

APPENDIX K – GEO#1 GEOTHERMAL EXPLORATION WELL TECHNICAL MEMO

TECHNICAL MEMORANDUM

LUMOS & ASSOCIATES

9222 Prototype Drive
Reno, NV 89521
Tel: 775.827.6111
Fax: 775.827.6122
www.lumosinc.com

DATE: November 10, 2017

TO: Jolene Supp, Wells City Manager

FROM: Rick Zehner

CC: Mike Hardy

SUBJECT: Results of Logging Geothermal Well/Hole GEO-1 PN: 9325.000

Project Understanding

The City of Wells (CW) requested assistance from Lumos and Associates (Lumos) with the logging of a geothermal exploration well up to 500 feet deep on CW-owned property north of town. Lumos logged from the bottom of the 60 foot conductor casing to total depth of the borehole. The objective was to collect lithologic samples, describe rock type and alteration, measure drill mud temperatures, and look for evidence of fractures that might control geothermal fluid flow. This Technical Memorandum describes the data logging of the borehole, together with analysis and conclusions.

Introduction and Summary

The planned geothermal observation well[1] was located near the top of a surface thermal anomaly, as detected by 2-meter and Geoprobe surveys (Zehner, 2017A, 2017B). The well was drilled with the intention of answering the following questions:

1. Are the thermal waters that are expected to be encountered moving upwards from a fault or fault intersection, or are they the result of lateral outflow from a permeable sandstone or conglomerate unit?
2. What is the source of the thermal anomaly, and what is the temperature and flow rate of any geothermal fluids?
3. How does the resistivity data obtained by the National Energy Technology Laboratory (NETL) relate to the geology and geothermal waters?

Rosenlund Drilling LLC (Rosenlund) of Ruby Valley, Nevada was contracted by the City of Wells to drill the geothermal observation well. They mobilized a Schramm T685S drilling rig to the project site during the week of October 23-27, 2017. The rig drilled Borehole GEO-1 to 60 feet below ground level (bgl) and installed and cemented a nominal 8-inch steel conductor casing. The driller, Logan Rosenlund, measured drilling mud temperatures at two points within the cased interval, collected lithologic samples at 5-foot intervals, and placed them in standard chip trays.

[1] This exploration hole was originally permitted as a geothermal observation well. Because the borehole was not cased, it is technically not a "well", so it will be referred to as a 'borehole' for the remainder of this memo.

Lumos arrived on site during the afternoon of October 30th to set up the data logging station and discuss drill and safety procedures with Rosenlund. The drilling of the 7 7/8" diameter borehole began the next morning (October 31st). Lumos collected lithologic samples at 5-foot intervals at the discharge port off the conductor casing, described the lithology and hydrothermal alteration, and (like Rosenlund) placed a representative sample in chip trays. Temperature data were also collected at 5-foot intervals, using a resistive temperature device (RTD) attached to an Omega HH804 data logger, having an accuracy of 0.1° C. Lumos also logged the drilling rate and watched for evidence of faulting/fracturing.

Rosenlund drilled to 320 feet below ground level (bgl) by late afternoon on October 31st. The following day, November 1st, the borehole was drilled to 440-foot depth. During drilling, the maximum temperature of the drilling mud reached approximately 22° C (72° F) at the bottom of the borehole. Due to the lower temperature of the drill mud, the decision was made to terminate the borehole at 440 feet bgl and not install the casing.

Borehole Geology and Thermometry

The drill encountered silty clay in the interval from 0-15 feet. The five-foot intervals between 15 to 25 feet contained mostly medium-coarse sand, with minor gravel. Judging from the ratio of clay to sand in these intervals, this unit is estimated to lie between 14 and 24 feet bgl. The interval from 25 feet bgl to the bottom of the borehole at 440 feet consisted of claystone with varying amounts of silt with minor sand

It was noted early in the drilling that the color and grain size of the clay in the zone of oxidation (i.e. above 90 feet) is strikingly similar to the Tertiary claystone found in the small borrow pit about a hundred feet north of the borehole. Many of the clay intervals contained tabular chips strongly suggestive of interbedded silty claystone and clayey siltstone. This caused the clay sand at the top of hole to be reinterpreted as originally lithified claystone and sandstone. The lack of alluvial sediments at the top of the borehole suggests that the rig was sitting on Tertiary "bedrock" and drilled entirely within fine-grained Tertiary sedimentary rocks.

The only zone of probable fracturing noted during drilling occurred in the interval from 170 – 175 feet bgl. During this interval the drill rod was jittering and jumping, and Rosenlund informed Lumos that it had hit a fault or fracture zone. Because there was no change in rock type, and because the small measured temperature drop (0.5° C) could have been sampling error, this fracture is considered to have had minimal influence.

No hydrothermal alteration was noted during the logging of the borehole.

Drilling mud temperatures throughout the borehole were lower than expected. Rosenlund's measured temperatures at 0 and 60 feet were 66° and 68° F (19° and 20° C). Temperatures below the casing ranged from 11.9° C at 60 feet to 22.1° C at 440 feet (53.4° to 71.9° F) rising fairly steadily, with no reversals (Figure 1). Temperatures seemed to rise during the warmer daylight hours and be lowest in the early morning. Temperatures also appeared to rise slightly in response to the drilling rate; that is, the slower the drilling, the higher the temperature.

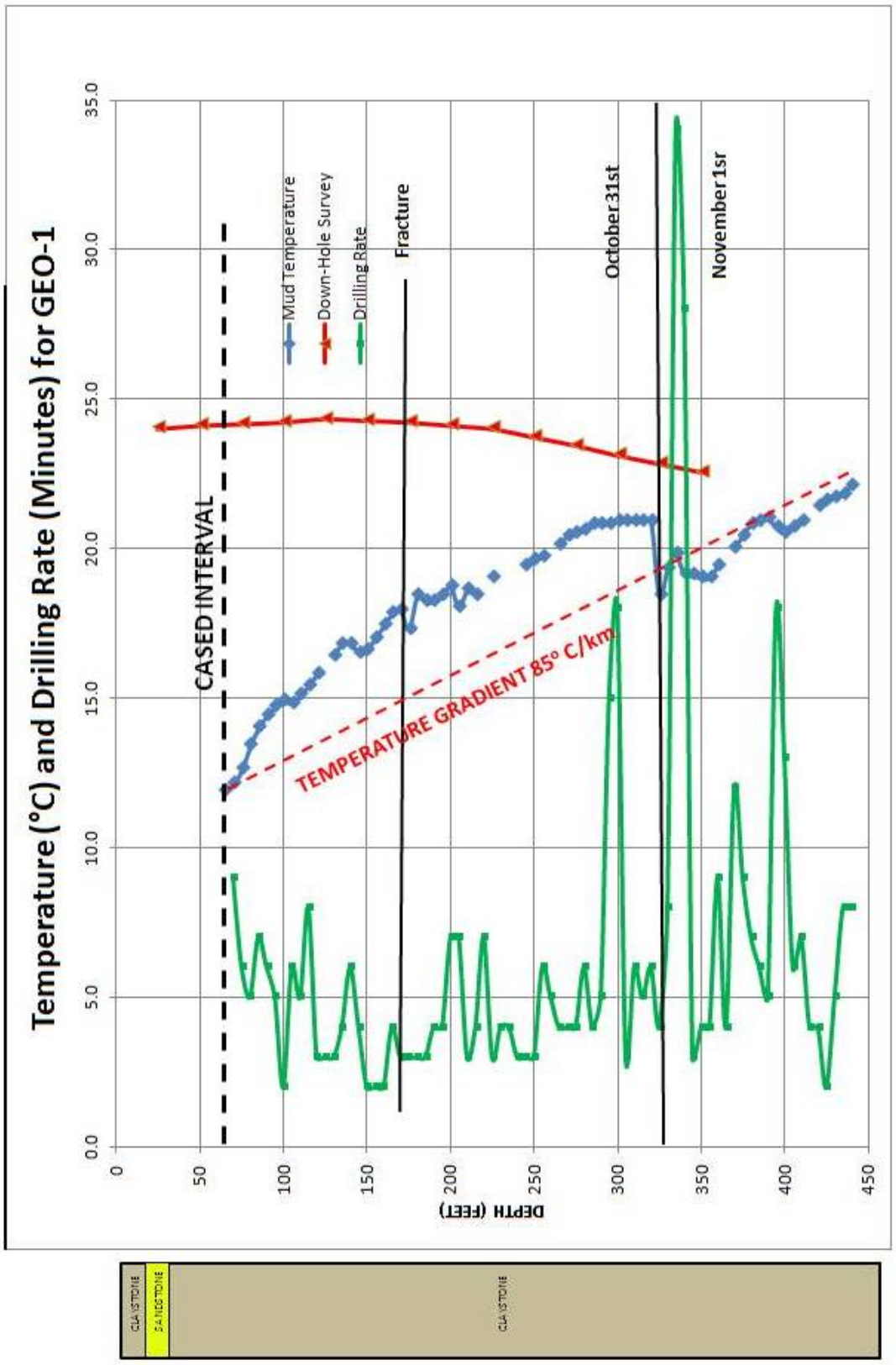

Figure 1. Visual log of Hole GEO-1

Overall, the drilling mud temperatures collected during drilling indicate an average temperature gradient of approximately 85° C/km. This value is typical of conductive temperature gradients in Nevada in places adjacent to geothermal systems, but somewhat distal to convective geothermal flow. Because of the low measured temperatures and geothermal gradient encountered during drilling, the decision was made not to case the borehole.

The CW commissioned Dewey Data, Inc. (Dewey) to perform a down-hole temperature and resistivity survey to 350-foot depth on November 6 (Figure 1). Thus, the drilling mud in the borehole had six days to equilibrate. The temperature profile from this survey bears little resemblance to the measured mud return temperatures, indicating a warmer, more uniform temperature through the interval from 0 – 350 feet. Temperatures vary less than 2° C from a high of 24.3° C (75.8 ° F) at 125 feet to a low of 22.6° C (72.7° F) at 350 feet. This indicates a slightly negative gradient in the lower part of the borehole.

Dewey's resistivity data correlates well with the electromagnetic survey performed by the National Energy Technology Laboratory (NETL). Both show a resistivity high in the upper part of the borehole in the interval 10 – 25 feet. This corresponds to the depth of the sandstone layer, which would be expected to have a higher resistivity than the adjacent clay or claystone. The Dewey log shows a small resistivity high at 170 – 175 feet, the location of the fault/fracture. Other anomalies at 200 – 220 feet and 290 – 340 feet correlate well with the presence of blue-green-gray claystone (as opposed to gray claystone) in the lithologic log.

Analysis of Results

The borehole geology appears to represent a sequence of poorly-lithified lacustrine sedimentary rocks, with a thin sandstone unit near the top of the section. This sequence is likely part of the Miocene Threemile Springs Formation of Thorman et al., 2010. Permeability in these rocks will be low, with the exception of the sandstone layer at the top of the borehole.

Several factors seem to have influenced the drilling mud measured temperatures, in addition to the rock temperature, at a given interval:

1. The cemented casing in the top 60 feet of the borehole has probably obscured any heat contribution from that depth interval.
2. Mud temperatures are obviously affected by daily temperature changes; there is a distinct rise in mud return temperature during October 31st from the beginning of drilling (air temperature -8° C) to mid-afternoon (air temperature ~16° C), with a noticeable overnight drop (Figure 1).
3. Mud return temperature appears to rise with increase in drilling time. This could be the results of either greater equilibration with wall rock temperatures, or (conversely) by additional heat added by the pumping equipment.
4. Cold water was injected at various times during drilling, and it was noticed that mud return temperatures dropped during at least some of these periods. So it must be kept in mind that the actual measured temperature during any interval results from a combination of these factors.

The down-hole temperature data rather unambiguously indicates the lack of any evidence for geothermal upwelling in the vicinity of the borehole. Thus the theory of geothermal heat rising from a fault or fault intersection is probably not true. If this were the case, one would expect to see a strong increase in

temperature with depth. The rather high geothermal gradient (85° C/km) probably indicates that the borehole is situated within the zone of conductive heat adjacent to the geothermal system.

The sandstone layer located between 14 and 24 feet bgl bears close scrutiny. It is the only unit in the lithologic section that appears to have enough permeability to allow the lateral flow of geothermal water. The lower contact of the sandstone corresponds roughly with the maximum depth of penetration of the Geoprobe holes in this area (17 to 30-foot depth). Thus the claystone below the sandstone unit was the harder unit preventing the Geoprobe holes from going any deeper. Temperatures of 32.2° - 45.4° C (90.0° - 113.7° F) were recorded from this depth, far higher than any mud returns measured in Hole GEO-1. Yet this interval is part of the cased interval at the top of the borehole, and Rosenlund's measured temperatures were taken above and below it.

The logical conclusion at this time is that the source of the thermal anomaly, identified by the shallow temperature equipment, is lateral geothermal flow within the sandstone unit. Where it was hoped that the anomaly indicated a hot target at 'depth' (i.e., below a hundred feet), the anomaly is in fact coming from a shallower, cooler resource within the sandstone unit. The thermal anomaly is probably the result of lateral outflow along the only unit capable of transmitting sufficient water to create the anomaly.

The questions raised by this new data can be summarized as follows:

1. Are temperatures within this unit, either proximal or distal to the borehole, of sufficient temperature and flow rate so as to warrant further exploration of this target?
2. If so, then what strategy should be employed to further test this hypothesis?

Since the sandstone unit seems to correlate with zone of higher-resistivity as seen on NETL's cross sections, shallow electromagnetic surveys (EM) could be used to find the location and depth of the sandstone unit. NETL's existing data along their sample line could be used as a starting point. Shallow boreholes (Elko Heat Co. was suggesting auger holes) could be drilled in various spots to determine whether temperature (and possibly flow) increased, thus suggesting a direction to vector future exploration.

References

Thorman, C.H., Brooks, W.E., Ketner, K.B., and Dubiel, R.F., 2010, Preliminary geologic map of the Oxley Peak area, Elko County, Nevada: Nevada Bureau of Mines and Geology Open-File Report 03-4, 2nd ed.

Zehner, R., 2017A, Shallow (2-Meter) Temperature Survey in and Around the City of Wells, Nevada: Implications for Geothermal Exploration. Unpublished report for Elko Heat Company and The City of Wells, Zehner Geologic Consulting LLC, 12p.

Zehner, R., 2017B, Results of Geoprobe survey performed within the thermal anomaly identified by shallow temperature survey near Wells, Nevada: Unpublished report for Elko Heat Company and The City of Wells, Zehner Geologic Consulting LLC, 8p.

Project: City of Wells Geothermal	**Date Logged:** 10/31/17 - Drilled 10/27/17	Sheet "0" of 4
Job No: 9325.000	**Time Boring Started:**	**Boring No.** GEO-1
Client: City of Wells	**Time Boring Ended:**	**Site Elev:**
Location: Cosmopolitan Rd.	**Drill Rig Type:** Schramm T6855	**Total Depth:** 440'
Logged By: R. Zehner SCS	**Drill Method:** Mud rotary	**Water Depth:** 4'
	Drilling Contractor: Rosenlund Drilling	
	Operators: Logar	

Depth in Ft. From	Depth in Ft. To	Drill Rate	Flow Rate (GPM)	Lithological Description & General Notes	TDS (ppm)	Temp. (F)	pH
				This portion of well was drilled to 60 Ft by Logan without geologist present.			
0	5		CL	Off-white clay with sparse rounded granules. Some roots.			
5	10			SAP			
10	15		CL	Light brown clay with rounded sand to 3mm. Mostly clay.			
15	20		SW	Gravelly sand with little to no clay component. Mostly subrounded quartz + rock fragments, but subangular & rounded grains as well. Gravel ~10% by volume, up to 1 cm size.*			
20	25		SW	Gravelly sand as previous, but with light tan silty clay ~15%			
25	30		CL	Light gray silty clay with ~15% rounded sand/gravel clasts to ~7mm			
30	35			SAP - less coarse component			
35	40			Light gray silty clay with gravel to 1 cm (rounded) - not a lot of sand size.			
40	45			SAP			
45	50			SAP - Silty clay but no appreciable sand or gravel component.			
50	55			Creamy white clay			
55	60			Creamy white clay with ~5% rounded rock clasts ~3-4 mm			

Site Condition/Notes:

Note: SAP = "Same as previous" (interval)

* From Logan's description verbally.

LUMOS & ASSOCIATES

Project: City of Wells Geothermal	**Date Logged:** 10/31/17	**Sheet** 1 of	
Job No: 9325.000	**Time Boring Started:** 9:03 AM	**Boring No.** GEO-1	
Client: City of Wells	**Time Boring Ended:**	**Site Elev:**	
Location: Cosmopolitan Rd	**Drill Rig Type:** Schramm T685S	**Total Depth:** 440'	
Logged By: R. Zehner SCS	**Drill Method:** Mud rotary	**Water Depth:** ~4' bgl	
	Drilling Contractor: Rosenlund Drilling LLC		
	Operators: Logan & Kent		

Depth in Ft. From	Depth in Ft. To	Drill Rate	Flow Rate (GPM)	Lithological Description & General Notes	TDS (ppm)	Temp. (F)	pH
				Arrived at site 7:30 to see driller leave to buy ether to start mud pump. Temp -8C			
				This log starts at 60': bottom of cased & cemented interval. 7⅞" hole.			
				SWL 4 ft bgl. Mud starts circulating, 8:55 AM - 9.4°C			
60	65	9	CL	9:03 begin drilling. Mud in 4.9°C. Light tan clay.		11.9	
65	70	6		9:12 Light tan clay - low silt component		12.1	
70	75	5		9:18 " " Can see residual bedding chips		12.6	
75	80	7		9:23 Light tan clay - low silt. End 9:30		13.4	
80	85	7		Start 9:35 SAP 9:37		14.0	
85	90	6		Dark gray clay - sparse silt 9:43		14.4	
90	95	5		SAP		14.7	
95	100	2		Medium gray silty claystone 9:48		14.9	
100	105	6		Start 9:53 Mid-gray silty claystone with some hardened chlorite-green chips		14.8	
105	110	5		Dark gray claystone - less silt.		15.1	
110	115	8		SAP	16.8	15.4	
115	120	3		10:12 Dark gray claystone) End 10:15		15.8	
120	125	3		Start 10:19 SAP - Medium gray, low silt		16.4	
125	130	3		SAP MG, low silt		16.8	
130	135	4		SAP End 10:28			
135	140	6		Medium gray claystone - here clay balls. 10:34	15.6	16.8	
140	145	4		Start 10:44. SAP. Relict bedding 10:45	19.4	16.5	
145	150	2		clearly visible in chips (tabular) 10:50 Medium gray clay and claystone, 10:55 both as clay "balls" and tabular chips from poorly-consolidated rock.		16.6	
150	155	2				17.0	
155	160	2		10:58		17.4	

LUMOS & ASSOCIATES

Site Condition/Notes: Morning temp 20°F; took an hour for the drillers to get water and get the mud pump going.

This has been a sequence of medium-gray claystone, with some silt. The interval 100-105 had some hydrous alt in one chip.

Project: City of Wells GeoThermal	**Date Logged:** 10/31/17	**Sheet** 2 of
Job No: 9325.000	**Time Boring Started:**	**Boring No.** GEO-1
Client: City of Wells	**Time Boring Ended:**	**Site Elev:**
Location:	**Drill Rig Type:**	**Total Depth:**
Logged By: R. Zehrer SCS	**Drill Method:**	**Water Depth:**
	Drilling Contractor: Rosenlund Drilling	
	Operators: Logan	

Depth in Ft. From	Depth in Ft. To	Drill Rate	Flow Rate (GPM)	Lithological Description & General Notes		TDS (ppm)	Temp. (F)	pH
160	165	4	CL	Start 11:01 SAP	11:05		17.8	
165	170	3		SAP - Chips not visible			17.9	
170	175	3		Fracture - bit is chattering Temp went down - could be mistake in temp meas.			17.3	
				Med gray clay and claystone			18.4	
175	180			Start 11:23 Interbedded light and dark			18.2	
180	185	3		clay - siltstone layers				
185	190	4		Light gray clay, - minor silt	11:30		18.2	
190	195	4		SAP	11:34		18.4	
195	200	7		SAP	11:41	16.6	18.7	
200	205	7		Start 11:47 Color change to grey-blue-green: Clay with substantial silt and some sand.	11:51 / 11:54		18.0	
205	210	3		B-gr-gray clay with sparse silt. SAP			18.6	
210	215	4		Tabular chips of med-gray claystone			18.4	
215	220	7		End 12:08 SAP			19.0	
220	225	3		Start 12:12 Med-gray claystone	12:15			} data logger issue
225	230	4		SAP	12:19			
230	235			SAP				
235	240	3		SAP	12:39			
240	245	3		Med gray Claystone with silt and sparse sand.	12:43		19.4	
245	250	3		SAP	12:46		19.6	
250	255	6		SAP	12:51	12.4	19.7	
255	260	5		SAP	12:57			
260	265	4		Start 1:07 Medium gray claystone	13:11		20.1	
265	270	4		SAP, with minor silt and sand.			20.4	
270	275	4		" " "	13:19		20.5	
275	280	6		" " "	13:25		20.6	
280	285	4		Start 1:51. Med-gray clay (stone) with minor silt and sand.			20.8	
285	290	5		Silty clay with some sand. One thin sandstone layer. 288' color change to blue-green-gray clay	2:02		20.8	
290	295	15		Blue-gr-gray clay - sparse silt/sand	2:17		20.8	

LUMOS & ASSOCIATES

Site Condition/Notes:

1:15 Water/rod truck leaves to go get water. No rods to drill at 13:25 until it returns.

2:15 Driller puts more weight on the bit as progress is slowing.

Project: Geothermal City of Wells	**Date Logged:** 10/31/17	Sheet 3 of	
Job No: 9325.000	**Time Boring Started:**	**Boring No.** GEO-1	
Client: City of Wells	**Time Boring Ended:**	**Site Elev:**	
Location: Cosmopolitan Road	**Drill Rig Type:**	**Total Depth:**	
Logged By: R. Zehner SCS	**Drill Method:**	**Water Depth:**	
	Drilling Contractor:		
	Operators: Logan & K		

Depth in Ft. From	Depth in Ft. To	Drill Rate	Flow Rate (GPM)	Lithological Description & General Notes	TDS (ppm)	Temp. (F)	pH
295	300	18	CL	2:17 SAP: Blue-green-gray clay, End 2 some tabular as thin beds. Minor silt and sand (sparse). End 2:35		20.9	
300	305	3		Start 2:39 SAP 2:42			
305	310	6		Blue-green-gray clay with minor silt and sand. 1% oxidized clasts. 2:48		20.9	
310	315	5		SAP 2:53		20.9	
315	320	6		SAP - no visible oxidized clasts. 2:59		20.9	
				End day 3:15 at 320 ft			
				New Day Nov. 1, 2017 Cold but above freezing 3.5°C			
				Static WL 4' BGL Mud initial 17.4°C			
320	325	4		Start 8:13 - 8:15 Blue-green gray clay as tabular chips	17.8	18.4	
325	330	8		SAP. Little/no sand. 8:25		19.3	
330	335	34		Blue-gr-gray clay. Sticky - much less tabular chips. Drilling slow. 8:59		19.8	
335	340	28		Mud in 18.4°C BGG* clay with significant sand component. Not sure if clay-sand interbeds, or uniform. 338-340 End 9:27		19.1	
				has much less sand.			
				Mud not lifting enough clay. Driller pulls rods and flushes out.			
340	345	3		Start 12:52 SAP - Sandy BGG clay (store)		19.1	
345	350	4		SAP - little return into sieve. Gravel		19.0	
350	355	4		Medium-gray clay with silt & sand end 1:01		19.0	
355	360	9		Gray clay with silt and sparse sand. 1:10		19.4	
360	365	4		Start 1:16. Med. gray sandy silty clay. 1:20			
365	370	12		SAP - Drilling slowing down. 1:32	18.8	20.0	
370	375	9		Sandy silty clay (store)		20.4	
375	380	7	↓	SAP - Medium gray. 1:48		20.8	

LUMOS & ASSOCIATES

Site Condition/Notes:

2:50: Driller adds polymer, else (?).
11/1 8:50 AM. More polymer.
BGG = blue-green-gray
Note: There is a subtle color change in clays from BGG at 335 to med. gray at 360?
Note: At 340 much polymer added to break up clay balls.

Project: City of Wells Geothermal	**Date Logged:** 11/1/17	**Sheet** 4 of
Job No: 9325.000	**Time Boring Started:**	**Boring No.** GEO-1
Client: City of Wells	**Time Boring Ended:**	**Site Elev:**
Location:	**Drill Rig Type:**	**Total Depth:** 440'
Logged By: R. Zehner	**Drill Method:**	**Water Depth:** 4'
	Drilling Contractor: Rosenlund Drilling	
	Operators: Logan, Kent	

Depth in Ft. From	Depth in Ft. To	Drill Rate	Flow Rate (GPM)	Lithological Description & General Notes	TDS (ppm)	Temp. (F)	pH
380	385	6	CL	Start 1:55 SAP ☆ Note 2:01		20.9	
385	390	5		Med gray silty clay (stone) Drilling is slow. End 2:24	15.8°C	21.0	
390	395	18				20.7	
395	400	13		Medium gray silty clay (stone) with sparse sand. End 2:37		20.5	
400	405	6		Start 2:44 Med-gray silty clay with sparse sand. End 2:50.		20.7	
405	410	7		SAP 2:57		20.9	
410	415	4		SAP 3:01			
415	420	4		SAP: Sand may be over-represented b/c polymer is removing clay balls. Sand is still insignificant. End ~3:05		21.4	
				Start 3:08			
420	425	2		Medium gray silty mud (stone) w v sparse sand. End 3:10		21.6	
425	430	5		SAP End 3:15		21.7	
430	435	8		SAP. 3:23 - Slightly more sand.		21.8	
435	440			Med gr silty clay - v. sparse sand. End 3:31		22.1	
				3:44 let mud circulate to see if temp would increase, but it dropped. Made decision to terminate and abandon well (hole). TD = 440'		21.7	

LUMOS & ASSOCIATES

Site Condition/Notes:

Note: At 1:59-2:00 the wind gust blew the chip tray off the table; tried to reconstruct.
Also, sample material is sparse b/c of polymer addition.
Ira stops by ~2:10-2:25.
~2:20 water truck arrives and starts adding cold water - temp going down.
410' - Switch to alternate data logger.

APPENDIX L – GEO#4 GEOTHERMAL EXPLORATION WELL DOCUMENTATION

Dewey Data

WELLS GEO # 4

COMPANY	: WELLS GEO # 4			OTHER SERVICES:	
WELL	: WELLS GEO # 4			011218	
LOCATION/FIELD	: WELLS				
COUNTY	: ELKO				
LOCATION	: NV				
SECTION	:	TOWNSHIP	:	RANGE	:
DATE	: 01/12/18	PERMANENT DATUM	: GL		
DEPTH DRILLER	: 600			KB	:
LOG BOTTOM	: 704.4	LOG MEASURED FROM:	GL	DF	:
LOG TOP	: 0	DRL MEASURED FROM:	GL	GL	:
CASING DIAMETER	: 10.	LOGGING UNIT	: 2		
CASING TYPE	:	FIELD OFFICE	: DEWEY DATA		
CASING THICKNESS:		RECORDED BY	: KRW		
BIT SIZE	: 6	BOREHOLE FLUID	: MUD	FILE	: ORIGINAL
MAGNETIC DECL.	: 0	RM	: .179	TYPE	: 8144A
MATRIX DENSITY	: 2.65	RM TEMPERATURE	: 68.5	LGDATE:	01/12/18
NEUTRON MATRIX	: SANDSTONE	MATRIX DELTA T	: 54	LGTIME :	12:36:
				THRESH:	99999

ROSENLUND DRILLING
41.124066N -114.979321W

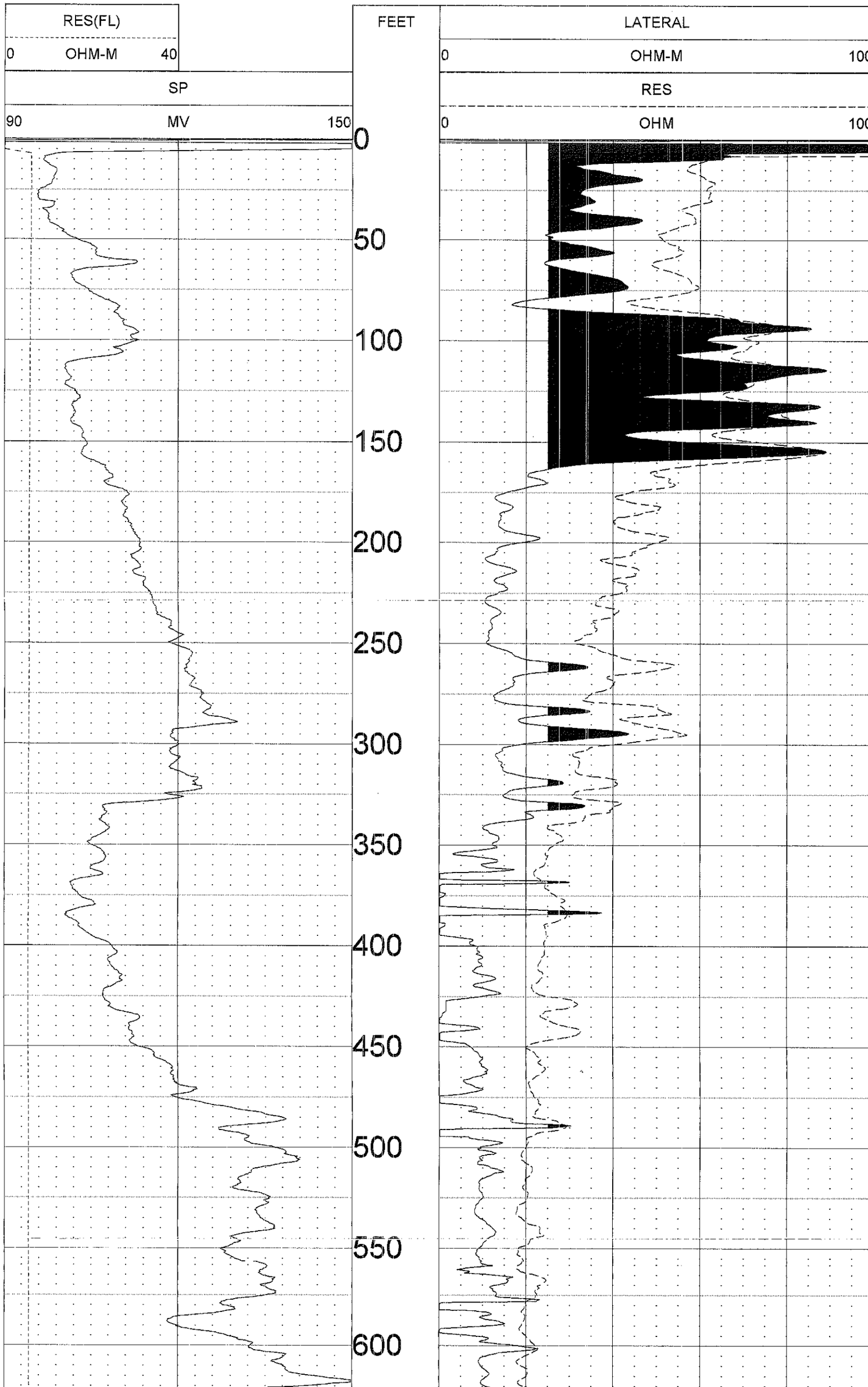
RES(FL)
0
OHM-M
40
SP
90
MV
150
FEET
0
50
100
150
200
250
300
350
400
450
500
550
600
LATERAL
0
OHM-M
100
RES
0
OHM
100

Dewey Data

WELLS GEO # 4

COMPANY	: WELLS GEO # 4				
WELL	: WELLS GEO # 4				
LOCATION/FIELD	: WELLS				
COUNTY	: ELKO				
LOCATION	: NV				
SECTION	:	TOWNSHIP	:	RANGE	:
DATE	: 01/12/18	PERMANENT DATUM	: GL		
DEPTH DRILLER	: 600			KB	:
LOG BOTTOM	: 704.60	LOG MEASURED FROM:	GL	DF	:
LOG TOP	: -0.20	DRL MEASURED FROM:	GL	GL	:
CASING DIAMETER	: 10.	LOGGING UNIT	: 2		
CASING TYPE	:	FIELD OFFICE	: DEWEY DATA		
CASING THICKNESS:		RECORDED BY	: KRW		
BIT SIZE	: 6	BOREHOLE FLUID	: MUD	FILE	: ORIGINAL
MAGNETIC DECL.	: 0	RM	: .179	TYPE	: 8144A
MATRIX DENSITY	: 2.65	RM TEMPERATURE	: 68.5	LGDATE:	01/12/18
NEUTRON MATRIX	: SANDSTONE	MATRIX DELTA T	: 54		
				THRESH:	99999

OTHER SERVICES:
011218

ROSENLUND DRILLING
41.124066N -114.979321W

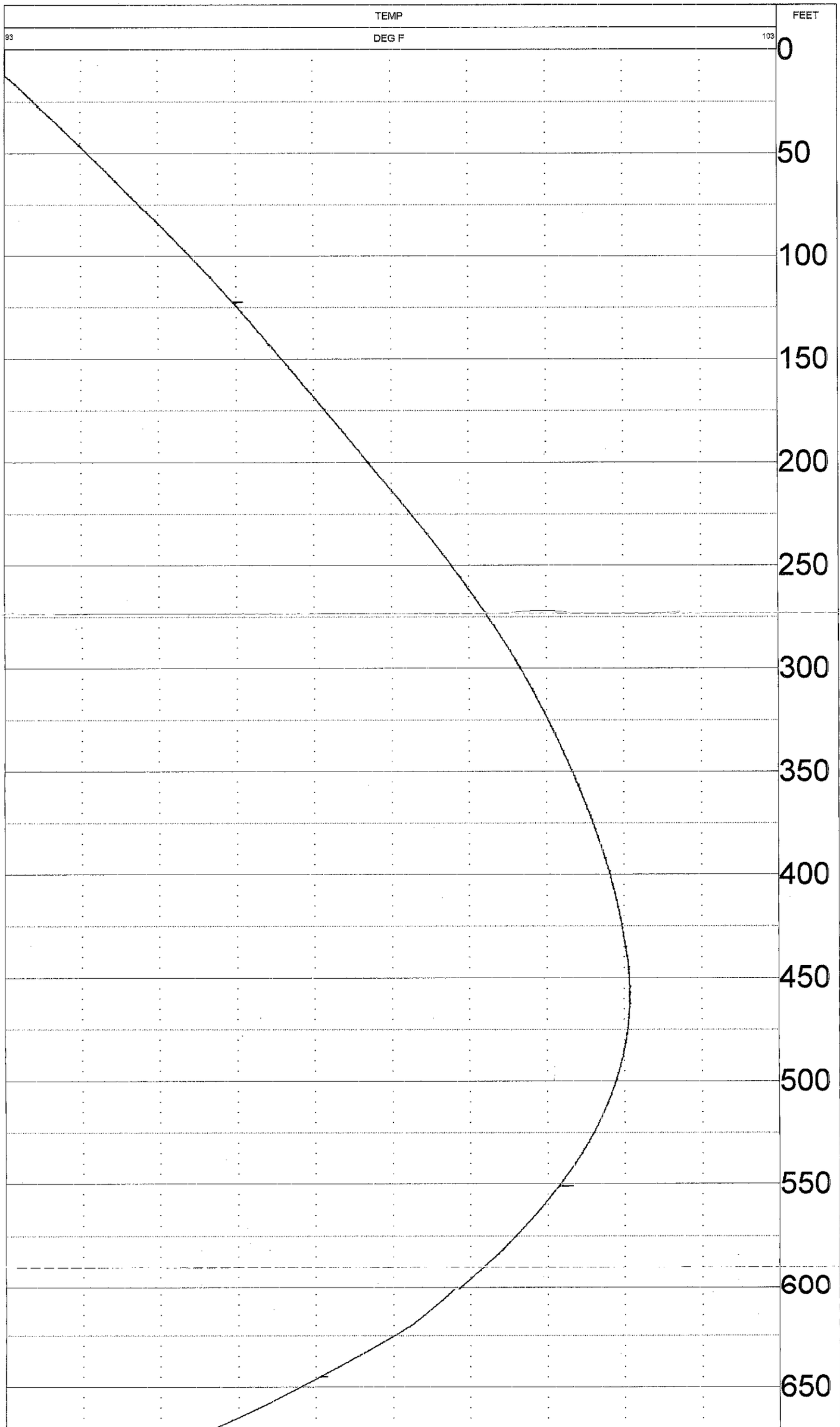
TEMP
FEET
93
DEG F
103
0
50
100
150
200
250
300
350
400
450
500
550
600
650

Sean Plasynski
Executive Director
Technology Development & Integration Center
National Energy Technology Laboratory
U.S. Department of Energy

Bryan Morreale
Executive Director
Research & Innovation Center
National Energy Technology Laboratory
U.S. Department of Energy

Arlene Anderson
Program Manager, Deep Direct Use
Geothermal Technologies Office
U.S. Department of Energy

Josh Mengers
Coordinator
Small Business Vouchers Pilot Program
Geothermal Technologies Office
U.S. Department of Energy

NETL Technical Report Series